CODING OF NATURAL FEATURES BY NEURONAL SYNCHRONIZATION

IN PRIMARY VISUAL CORTEX

By

Melanie Rebecca Bernard

Dissertation

Submitted to the Faculty of the

Graduate School of Vanderbilt University

in partial fulfillment of the requirements

for the degree of

DOCTOR OF PHILOSOPHY

in

Biomedical Engineering

May, 2008

Nashville, Tennessee

Approved:

Professor A. B. Bonds, III

Professor Vivien A. Casagrande

Professor R. Alan Peters, II

Professor Richard G. Shiavi

Professor Adam W. Anderson

ACKNOWLEDGMENTS

TABLE OF CONTENTS

LIST OF TABLES

LIST OF FIGURES

If the brain were so simple we could understand it,
we would be so simple we couldn't.

--Lyall Watson (naturalist and author)

CHAPTER I

INTRODUCTION

Objective

Modern neuroscience seeks to understand the human brain and determine how electrochemical interactions among neurons give rise to perception and behavior. On a molecular level, sensory stimulation induces neurons to relay signals in a stimulus-dependent manner. *Neural coding* describes how these salient stimulus features are represented in neuronal responses. A great deal has been learned about *what* happens in the brain, yet *how* the brain encodes sensory information and provides a direct mapping of stimulus properties to neuronal representations that govern emergent properties like perception or action remain unknown. For practical reasons, most work in the past has focused on the relationship between the stimulus and firing rate patterns of individual neurons. Recent technological developments in multineuron recording have enabled the observation of population behavior as well. One prominent proposal for population-based encoding of information is tight (<10 msec) synchronization in the firing of two or more cells (e.g., Singer et al. 1990; Kohn and Smith 2005). Previous research has found that synchronization of neuronal responses is stimulus-dependent and exists between visual cortical neurons in an amount beyond that predicted by chance (for a review see Singer and Gray 1995). Although synchrony has tremendous potential as a coding mechanism, understanding its relevance is difficult since the techniques to measure and analyze synchrony are relatively new. The work presented here investigates the dynamic associations among small populations of neurons during natural stimulation and seeks the

form of the neural code for representation of visual structures. Microelectrode array technology allows the simultaneous sampling of neurons with a variety of spatiotemporal preferences, which can be used to explore complex intercellular interactions. This recording paradigm and a novel algorithm for quantifying synchrony are used here to study the timing relationships among neurons in the primary visual cortex of cats to evaluate synchrony's role as a possible neural substrate for contour detection.

Specific Aims

Research on neural coding throughout the past several decades has emphasized the study of individual neurons in the visual pathways. The frequency of firing events from a single neuron was found to be stimulus-dependent and reflected the cell's tuning preferences based on its spatiotemporal filter characteristics (Adrian and Zotterman 1926; Hubel and Wiesel 1962). This analysis of average firing rate became the basis of neural coding theories where stimulus properties were thought to be encoded through the spike frequency modulation of independent neurons (Barlow 1972). However, average firing rate of single neurons as a coding mechanism is inefficient and often ambiguous as a foundation for visual perception due to timing constraints and the limited number of neurons in the brain. Alternative theories for the neural representation of stimulus structure involve dynamic assemblies of neurons, which contribute to a population code (Hebb 1949). Due to the dynamic nature of grouping, the combinatorial possibilities of such a scheme offer a vastly increased dimensional magnitude for encoding visual information and also have implications for learning and plasticity. In this manner, visual information would not only be inherent in the activity of individual neurons, but could be extracted from the collective activity of the group as a supplemental code.

2

Until recently, the study of cooperative relationships was mostly confined to interactions among cell pairs because simultaneous recording of the behavior of large populations was impractical. This in turn discouraged the development of analysis techniques for comparing more than two simultaneous neuronal responses. Current approaches quantify synchrony as a relationship between two neurons (Perkel et al. 1967; Aertsen et al. 1989). However, synchrony allows for the formation of transient functional groups which could include tens, hundreds, thousands, or even larger numbers of neurons. Pairwise distance calculations increase exponentially as group size increases and can be computationally exhaustive for large assemblies. As a solution, we have developed a method that detects and quantifies the amount of correlated activity in a neuronal assembly of arbitrary size. Our basic algorithm is designed to reflect the relevance of group synchrony to postsynaptic neurons by modeling the temporal summation of postsynaptic potentials. In this measure, synchrony is computed as a fraction of total activity within an assembly and can be monitored dynamically throughout the stimulus presentation.

Previous research has found that synchrony among pairs of neurons is stimulus-dependent and correlated with the spatial features of simple visual stimuli (Singer and Gray 1995). Our work expands this foundation by exploring how visual information is represented by the cooperative behavior of aggregates of cells in the striate cortex. This research is designed to reveal the role of synchrony as a possible neural substrate for encoding complex contours in natural scenes. When considering theories of neural coding, the transition from the single neuron doctrine to population coding is conceptually grounded, but has not been realized experimentally due to the limited nature of many recording and analysis techniques. Pairwise interactions among cells suggest

3

that synchrony may contribute to a population code, but these theories can only be confirmed if supported by similar findings from larger cell assemblies. For each experiment, we used a 10x10 microelectrode array to acquire simultaneous recordings from dozens of discrete neurons in the striate cortex of paralyzed and anesthetized cats. To investigate synchrony as an encoding strategy, we have posed the following three aims:

Aim 1. To determine the spatial and temporal evolution of synchronous activity throughout the stimulus presentation. Previous studies using simple stimuli have shown that synchrony and oscillations of firing rate in the gamma frequency range rapidly decrease with increasing cortical distance (Nowak et al. 1995; Frien and Eckhorn 2000; Maldonado et al. 2000). Moreover, many laboratories report a higher probability of measuring synchrony between pairs of neurons with similar orientation preferences (Gray et al. 1989; Eckhorn et al. 1988). Often, this quantity is a normalized value corrected by an estimate of the firing rate-induced modulation of synchrony caused by the stimulus. Using natural stimulation, we will document the magnitude of synchrony within assemblies of arbitrary size as a function of cortical distance and orientation. We will disambiguate the dynamic components of raw cooperation into those elements attributed to normalized synchrony and stimulus-locked activity and will also measure the temporal aspects of synchrony to determine the time windows of highest cooperation. These results will provide insight into the cortical mechanisms responsible for the generation and propagation of synchrony.

Aim 2. To determine the role of synchrony in signaling higher-order visual structure by analyzing responses to natural images. Previous studies of cooperative neuronal activity have focused on experiments utilizing artificial stimulation to

systematically investigate the effects of altering various spatial properties such as orientation, spatial frequency, and contrast. However, the importance of synchrony in the process of natural vision remains unknown. Although the statistics of natural scenes are far too complex to manipulate systematically, using a broad selection of natural images offers an efficient approach for analyzing the complex spatial organization of larger assemblies, which have the potential to encode increasingly complex higher-order features not present in artificial stimuli. We will present a large sequence of natural stimuli and identify the appearance of repeatable and reliable cooperative interactions within the neuronal population. Using concepts from the association field theory (Field et al. 1993), we will quantitatively correlate these interactions with unique visual features in the scene and determine how synchrony is governed by the specific association among cells. We will also measure synchrony between assemblies to determine how different features may be related.

Aim 3. To quantify the selectivity of synchrony in larger assemblies in the context of sparse coding. In a sparse coding scheme, input features are represented by activation of a subset of the cell population. Therefore, encoding relies more on the identity of the active membership than on the amount of activation within the assembly. Numerous theoretical and computational studies have shown that neural networks employing sparse coding strategies have exhibited increased efficiency and decreased metabolic demand for visual coding of high dimensionality (Hyvarinen and Hoyer 2001). However, current models of sparse coding in the visual cortex are based on the average firing rate of independent neurons (Field 1994). We will explore the extent to which synchrony supports sparse coding by measuring the sparseness of neuronal response distributions

and the dispersal of responses across the population and set of images. Finally, we will compare the results with firing rate-based coding strategies.

Collectively, these aims provide a comprehensive investigation of synchronous activity within neural assemblies. Aim 1 examines the spatial and temporal factors influencing synchrony, which provides an indirect look at the underlying anatomical mechanisms involved. Aim 2 investigates the specific relationships between assembly receptive field filter characteristics and incoming visual information that induce synchronous activity. Correlated stimulus content is measured across repeatable presentations, isolated, and quantified to determine the explicit visual structures encoded by synchrony. Finally, the research in Aim 3 mathematically describes synchrony as a viable coding strategy employed by the visual cortex. All aims focus on emergent properties examining synchrony in a capacity that is independent of firing rate modulations. In addition to disambiguating the effects of synchrony and firing rate, this work explores new frontiers in synchrony research by quantitatively analyzing the cooperation of multiple single-units and incorporating techniques to systematically study responses to natural stimulation.

Significance

This research will provide fundamental knowledge about how dynamic cell assemblies contribute to visual perception. Neither the properties of single neurons nor pairs of neurons can explain the behavioral and perceptual repertoire of the brain. Understanding the functional interactions and emergent properties of larger neural networks is crucial to linking neurophysiology and perception. We cannot grasp the foundations of perception without exploring how cells work together in local networks to

describe the visual environment. While the focus of this research is rooted in vision, the concept of synchronous neuronal activity as a substrate to encode stimulus features may very well transfer to other sensory modalities and in fact be a general cortical encoding mechanism. Synchrony has been measured within and between other cortical regions (Engel et al. 1991; Roelfsema et al. 1997), but its functional significance is still largely unknown. This research may lead to the discovery of the strategy by which information is assembled by groups of cells, which is critical to understanding the overall function of the brain. By studying small populations of neurons, we are providing a crucial bridge between single unit and global population (EEG, fMRI) studies. Finally, knowledge of normal synchronous behavior has numerous clinical applications such as vision prosthetics and understanding and treating certain visual pathologies.

Background

Introduction

The brain, as the control center of the body, interprets sensory information and creates a perception and/or behavioral response appropriate to the environment. For instance, the visual system is able to integrate the senses, separate figure from ground, perform invariant recognition, complete partially occluded objects, and recognize shape from coherent motion. Information from the visual field is mapped onto the retina, relayed through the lateral geniculate nucleus of the thalamus, and directed through the primary visual cortex before the rest of the visual pathways. Neurons in the primary visual cortex filter incoming information and generate precisely-timed spike trains that transmit this message to higher processing centers. How information is transformed and

multiplexed in a neuronal spike train or distributed across the responses of multiple neurons is unknown. Current research in the field seeks to determine the form of the neural code produced in relation to certain visual structures as a next step in understanding the metaphorical black box of the brain.

The focus of these experiments is on the synchronization of neuronal responses and how these interactions might combine to yield percepts of unique visual features. In the literature, however, the term *synchrony* has been used to describe several quantities that do not reflect our intended use of the term. To avoid any misunderstandings, we provide the following definitions: *stimulus synchrony* refers to stimulus presentations in psychophysical experiments where manipulation of the timing of the stimulus results in motion-induced boundaries between figure and ground elements; *oscillation* refers to the fluctuations in potential from unresolved multi-unit activity due to the covariation of firing rate amongst the neurons (gamma oscillation specifically refers to the fluctuations that occur in the gamma frequency range, 30-70 Hz); *synchronous oscillations* occur when oscillations from two or more multi-unit recording sites are in phase; the term *synchrony* will be used to describe neuronal synchronization where responses (i.e. action potentials or spikes) from two or more neurons (or neuron clusters) occur within some small window of time, usually 10 ms.

Although opinions on the abilities of synchrony differ, it has garnered the attention of researchers in a wide range of fields, from neurophysiologists studying neuronal communication on a cellular level to psychophysicists exploring figure-ground segregation on a perceptual level. In this chapter, we will summarize the accomplishments concerning synchrony and neural coding from many different laboratories. First, we will give a brief overview of the visual system and review the two

prevailing theories on the role of individual neurons in the primary visual cortex. Then, we will introduce the single-unit coding theory and discuss how the shortcomings of that theory have lead others to postulate about multi-unit coding theories and dynamic population codes as a basis for complex feature representation. Next, we will introduce temporal coding via average firing rate and synchronization of neuronal responses. Then, we will describe the binding problem, discuss synchrony as a binding solution, and mention two studies with opposing viewpoints. Finally, we will describe one of our previous experiments that inspired this research by suggesting that synchrony may be a plausible neural substrate for detecting higher-order correlations.

Overview of the Visual System

As an animal roams through its environment, it will encounter a diverse abundance of objects that change shape, follow complicated trajectories, or hide amongst the shadows. Survival depends on the ability to detect and discriminate items of beneficial importance as well as avoid potential sources of danger. The mammalian visual system is adapted to process this wide assortment of visual information to build a representation of the surrounding world. Size, location, and texture are only a few of the many characteristics of objects that can be gauged by the visual system. Depending on their surface properties, objects reflect different amounts of electromagnetic radiation, the visible portion of which can be detected by the eyes. Even though eyes shift and the time of day offers widely varying light conditions, the brain can interpret this dynamic pattern of light to produce a psychological manifestation of the information in the visual field. The animal's perception of the environment is then used to judge the next appropriate course of action to be followed.

The process of vision (Figure 1.1A) begins when light rays enter the structures of the eye and are focused onto the retina. Photons are absorbed by photoreceptors in the posterior portion of the retina and are converted via the process of phototransduction into an electrochemical signal received by the interneurons (bipolar, horizontal, and amacrine cells). Horizontal and amacrine cells facilitate lateral connections in the outer and inner plexiform layers, respectively, while bipolar cells transmit localized graded potentials to the ganglion cells in the anterior portion of the retina. Ganglion cells are neurons whose dendrites integrate graded potentials from bipolar cells to generate action potentials. The axons of ganglion cells form the optic nerve and exit the eye through the optic disc. The optic tracts from each eye separate and the medial portions cross at the optic chiasm such that the axons fed by the left visual hemifield project to the right cerebral hemisphere and the axons fed by the right visual hemifield project to the left cerebral hemisphere (Figure 1.1B). Ganglion cells synapse onto neurons in the lateral geniculate nucleus (LGN) of the thalamus, which eventually sends projections to the primary visual cortex.

In the visual cortex, Korbinian Brodmann named different regions according to histological criteria such as cyto- and myeloarchitecture and primary visual cortex was designated Area 17, also anatomically known as striate cortex. Alternatively, electrophysiological mapping criteria can also be used to define regions and Area 17 contains a complete retinotopic representation of the visual field that is known as V1 (the fovea is on the most posterior end of the occipital lobe while the periphery is represented towards the anterior). All of these terms (Area 17, striate cortex, V1) are used interchangeably to refer to primary visual cortex. In the early stages of visual processing, all stimulus information necessary for analysis in subsequent parts of the cortical hierarchy must be represented. V1 achieves this by organizing input and output

A.
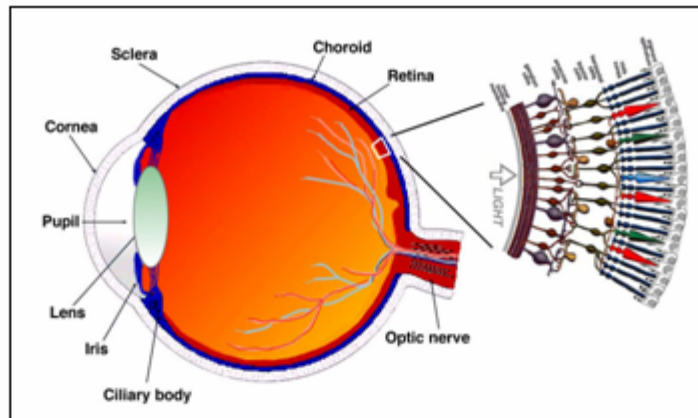
B.
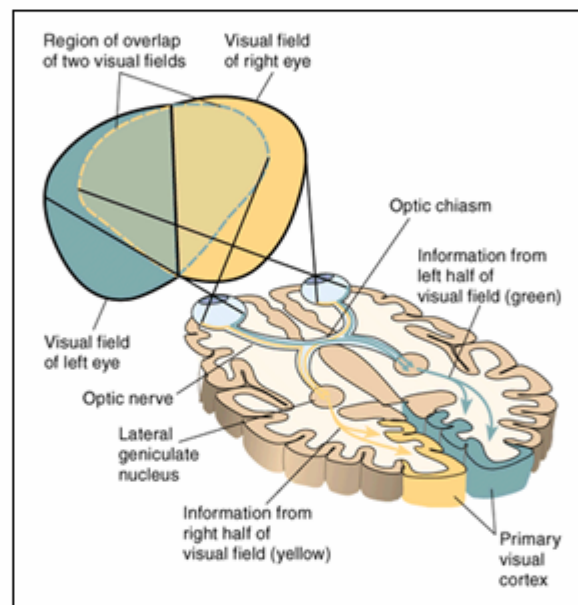
C.
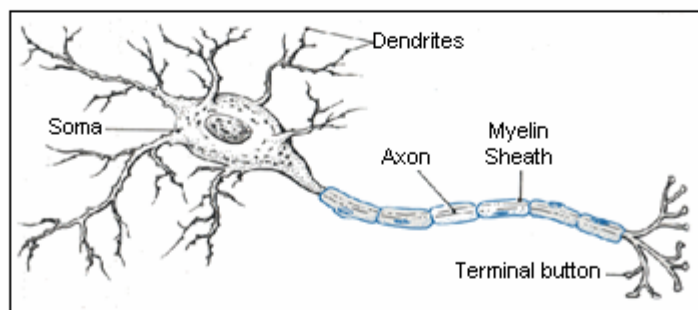
Figure 1.1. Visual system overview. (A) Structures in the eye including layers of the retina (webvision.med.utah.edu/imagesvv/Sagschem.jpeg). (B) Flow of information through the early visual system (homepage.psy.utexas.edu/home page/class/Psy332/Salinas/Origins/visualsystem.gif). (C) Neuron morphology (www.mindcreators.com/Images/NB_Neuron.gif).

connections into six different layers and segregating stimulus features into different iterated modules within each layer. The majority of input from the LGN to the primary visual cortex terminates within layer IV. The superficial layers (I, II, and especially III) output to extrastriate cortical areas such as V2 and V5 (MT) while layers V and VI output to subcortical areas such as the superior colliculus and send feedback projections to the LGN. Hubel and Wiesel (1962) proposed the idea of a hypercolumn to explain columnar and modular organization in V1. In this model, there are orientation columns, ocular dominance columns, and cytochrome oxidase blob modules for each region of visual space so that different stimulus attributes are represented in an iterated fashion across V1 and all properties are represented in each visuotopic location without holes in the visual field.

In their initial investigation of the primary visual cortex, Hubel and Wiesel (1962) noted that not all cortical cells behaved similarly to flashing hand-held light stimuli used to categorize the location and extent of receptive fields. Two different categories of cells seemed to emerge: simple and complex. The receptive fields of simple cells were defined as follows: 1) there were distinct excitatory and inhibitory subregions, 2) there was quasi-linear spatial summation within each excitatory or inhibitory region, 3) there was antagonism between the regions, and 4) responses to simple stimuli could be predicted from a map of the excitatory and inhibitory regions. A receptive field that did not satisfy all of these requirements was classified as complex. In their study of areas 18 (V2) and 19 (V3), Hubel and Wiesel (1965) introduced a new cell type, coined hypercomplex, which had fields similar to complex cells, but exhibited an end-stopping property. The further refinement of stimulus features led Hubel and Wiesel to postulate on a hierarchical connection between areas 17, 18, and 19 and a serial connection of

visual processing through geniculate, simple, complex, and hypercomplex cells. However, doubts arose about the uniqueness of hypercomplex cells and studies providing evidence against a strict serial processing route between areas 17, 18, and 19 are numerous (Dreher and Cottee 1975, Ferster 1981, Singer et al. 1975, Movshon 1975, Orban 1984).

A general rule of most cells in the visual cortex is that they are more selective for the kind of stimulus that will drive them as compared to cells in the earlier stages of visual processing. Both types of cortical cells exhibit an enhanced specialization by responding selectively to stimulus parameters such as spatial frequency, orientation, direction, and disparity. In the case of spatial frequency, some cells may be more selective for sharp edges or fine details while others prefer a stimulus that changes more slowly across space. Cortical cells exhibit tuning to the orientation of an elongated stimulus in their receptive fields and also show preference to the direction of motion orthogonal to stimulus orientation. Finally, primary visual cortex is the first region in which there is excitatory combination of binocular signals. Each cerebral hemisphere contains a map of the opposite visual hemifield and each optic radiation contains axonal projections from both eyes. Therefore, cortical cells can selectively represent stereo information in a visual scene.

Although the receptive field properties of simple and complex cells represent a behavioral dichotomy, there are no morphological differences between the two cell types. Each neuron consists of three main components (Figure 1.1C): dendrites, a soma, and an axon. Dendrites are the branched projections that receive electrochemical stimulation from other cells and function to conduct graded potentials towards the base of the cell soma. The soma is the central cell body and houses the nucleus, organelles, and internal

13

machinery for protein synthesis. At the base of the soma, the axon hillock gives way to the axon and is the region of the cell with the highest density of voltage-dependent sodium channels. This area is the most sensitive to changes in potential and has the ability to integrate graded potentials from different incoming regions on the dendrites. If the summation of these potentials surpasses the action potential threshold, then a single spike is initiated and propagated unidirectionally down the axon. The axon is a cable-like projection that carries nerve impulses away from the soma and branches into numerous axon terminals that synapse onto other target cells. Axon terminals are specialized regions that contain neurotransmitters for release into the synaptic cleft for communication with nearby cells. Action potentials are identical events and restabilization of the electrochemical gradient across the neuronal membrane contributes to the shape of an action potential, which has a rising (depolarization) phase, peak, falling (repolarization) phase, undershoot, and refractory period. Action potentials are the fundamental units of information transmission, but researchers are still unable to forge a unified link between the temporal properties of spike trains and the structure in the visual environment.

The Role of Cortical Cells

In order to unlock the secrets of visual processing, the bottom-up approach attempts to understand the role of individual neurons in terms of how they transform the afferent geniculate input. As mentioned in the previous section, visual cortical cells respond selectively to stimulus parameters such as orientation, spatial frequency, direction, and disparity. Two interpretations for this selectivity and precise stimulus

requirements are that cells behave as feature detectors or spatiotemporal filters (Figure 1.2).

Cortical cells that function as feature detectors (Figure 1.2A) parse out visual images into tangible components, or features, such as lines, bars, curves, and edges. A single cell responds maximally to one specific feature and transmission of this information signals the existence of this certain feature. Simple features are detected in earlier stages of visual processing while more complex objects are detected in higher processing centers. Feature detection theory evolved from the initial descriptions of cortical receptive fields given by Hubel and Wiesel (1962, 1965). Hubel and Wiesel speculated on a serial processing connection between simple, complex, and hypercomplex cells in which each cell required a subsequent refinement of stimulus features or input configurations to generate a response. However, as cells become more specific for stimulus features, they also become progressively more general or invariant to properties like scale and position in the visual field. As one ascends the cortical hierarchy, extrapolation of this theory would yield a neuron, often referred to as a grandmother cell, whose activity would be so specific that it responds to only one object, yet so general it responds to this object anywhere in the visual field (Orban 1984).

Numerous problems arise with feature detection theory in that the number of hypothetical grandmother cells needed to signal the amount of objects one may come across in a lifetime overwhelms the actual number of neurons in the visual cortex. In addition, loss of any single cell would mean the corresponding object could not be recognized. Furthermore, experimental evidence does not generally support this theory. Many experiments recording neuronal responses from animals have shown that a single neuron is not activated uniquely by one specific complicated or simple stimulus (Abeles

A. Feature Detection

Bill

Tail

Foot

B. Spatiotemporal Filtering

Spatial
Frequency

Disparity

Direction

Orientation
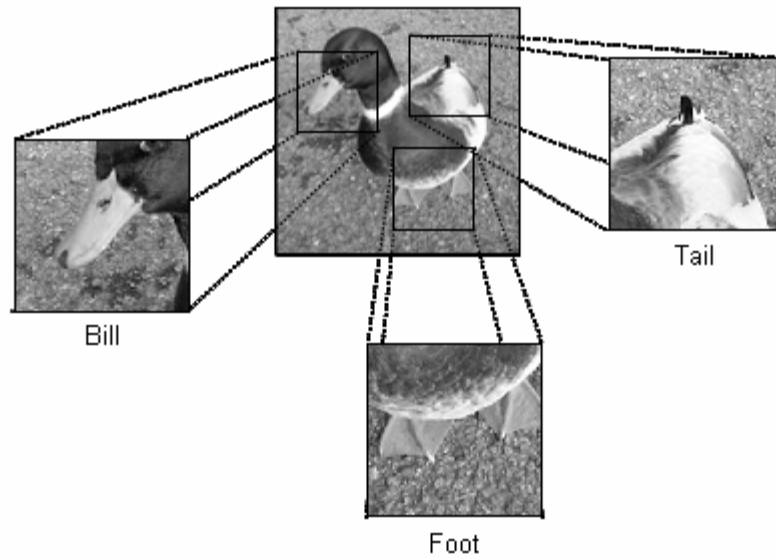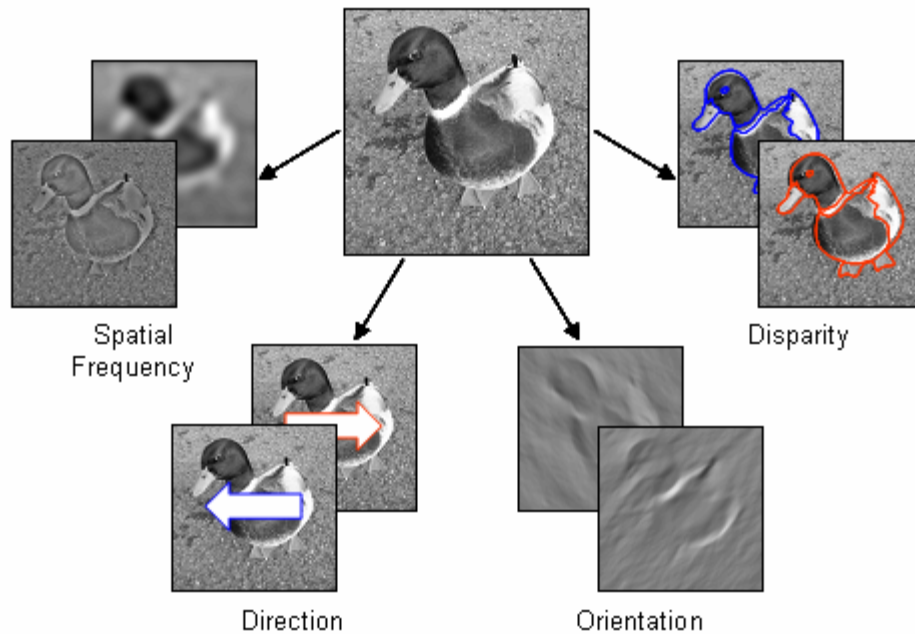
Figure 1.2. Two theories of visual cortical cell function. (A) In feature detection theory, cells respond maximally to one feature and more complex objects are detected via convergence up the cortical hierarchy. In the most extreme case, there is one cell for each unique feature in the world. (B) Similar to Fourier analysis, spatiotemporal filters respond to a limited range of spatial and temporal information in the visual field; cells behave as filters for different stimulus dimensions such as spatial frequency, direction, orientation, and disparity. This theory requires only simple feature detection (e.g. edges) and allows neurons at higher processing centers to respond to multiple objects.

16

and Gerstein 1988, Braitenberg 1977). Even the famous "face" neurons in the temporal

cortex do not respond to single unique faces, to several faces, or to several features

comprising the several faces (Young and Yamane 1992). Conceptually, there is no

generally agreed-upon set of features that can be used to construct the percept of a visual

stimulus. Although Bell and Sejnowski (1997) identified the independent components of

natural scenes as edges, other studies have shown that perceived structure can be derived

simply from temporal coherence of random dot patterns (Peterhans et al. 2005). The term

"feature detection" implies that cells detect some sort of tangible element that has spatial

frequencies. However, cells can detect illusory contours based on temporal properties of

the stimulus (like motion coherency) in the absence of tangible elements. Based on these

arguments, neural coding via feature detection is inefficient, inflexible, impractical,

conceptually flawed, and not supported by current experimental findings.

An alternative proposal for the role of cortical cells is derived from theories which

describe the visual system as performing a Fourier-like analysis of the visual field

(Maffei and Fiorentini 1973). In 1822, Jean Baptiste Joseph Fourier introduced the

concept of linear systems analysis where he demonstrated the mathematical foundations

underlying the idea that any real world signal can be synthesized from the linear sum of

sinusoids with appropriate frequencies, amplitudes, and phases. For the visual system,

real world signals are natural scenes that extend the input to two dimensions. Parameter

specificities allow cells to act as spatiotemporal filters by responding to a limited range of

spatial and temporal information in the visual field. By sampling a continuum of spatial

frequency, orientation, direction, and/or disparity, visual cortical cells behave as filters

for different stimulus dimensions (Figure 1.2B). And because these cells cover the range

of parameter values to which the visual system is sensitive, their activity is sufficient to encode each stimulus attribute.

A spatiotemporal filter approach can explain the detection of illusory contours derived from coherent motion since each cell is responsive to the temporal component of the stimulus. Furthermore, any tangible features detected by neurons often result from their spatiotemporal preferences. For instance, neurons in cat primary visual cortex will respond optimally to bars in their receptive fields as long as the bars match their preferred spatial and temporal frequencies, orientations, and directions (Hubel and Wiesel 1962). However, as mentioned above, these same neurons do not respond uniquely to bars; they also respond to sinewave gratings and objects in natural scenes. Spatiotemporal filtering encompasses simple feature detection, but still allows for the detection of structure in the absence of tangible features using cues like motion. Also, imbedded in this theory is the notion that objects are recognized through the collective activity of a population of cells instead of through the activity of a single cell (the problems with which are described in the arguments concerning grandmother cells above). However, exactly how object binding and figure/ground segregation are accomplished by the distribution of population activity is unknown (theories for which are described in the next section). Nevertheless, when only considering an individual cortical cell, its role is more consistent with spatiotemporal filtering than feature detection.

Neural Coding by Independent Cells vs. Neural Assemblies

For decades, the precise form of the neural code employed in the visual cortex has been hotly debated. Whether cells behave as feature detectors or spatiotemporal filters (Figure 1.2), the exact correspondence between stimulus input and response output is

poorly understood. This is due in part to the ambiguous nature of a neuronal spike train because the neural end-product of visual stimulation upon the retina is, in a certain sense, always the same. After the intricacies of retinal processing (phototransduction, lateral and inhibitory interactions from horizontal and amacrine cells, and the integration of graded potentials via ganglion cell dendrites), the only information left to inform our visual perception is the constantly changing stream of nerve impulses propagating along ganglion cell axons. Determining how a string of action potentials is interpreted by an upstream neuron or network of neurons to induce the full range of visual percepts that can possibly be experienced is a daunting challenge. The neural code underlying visual perception may lie within a single cell or involve any number of dynamically interacting neurons that employ any number of strategies to multiplex visual information within the temporal properties of their spike trains.

To address the relationship between the firing of single neurons and perceptual experience, Barlow (1972) proposed a single-neuron doctrine emphasizing the role of independent cells as stimulus-encoding mechanisms. His classic view of the cardinal cell holds that individual neurons, each responsive to a particular set of local features, modulate their firing rates to reflect salient information in the visual field. The most complex features are detected via convergence up the cortical hierarchy. As this hypothesis echoes feature detection theory, these ideas surrender to the same pitfalls. However, the theory of individual cells as lone information encoders still fails to find a foundation even when cells are considered as spatiotemporal filters. For example, orientation discrimination in the cat has shown that the information conveyed by a single cell is limited. The average visual cortical cell has a broad orientation bandwidth with half-width at half-height of 25.6 degrees while the narrowest orientation tuning is

approximately 5 or 6 degrees (Orban 1984). However, the comparable behavioral thresholds for orientation discrimination in the cat are 2.9 degrees for horizontal and vertical orientations and 4.7 degrees for oblique orientations (Vandenbussche and Orban 1983). Hence, the performance of the whole visual system does not reflect that of a single cell.

Alternative theories for the neural representation of structure involve dynamic assemblies of neurons, which contribute to a population code. Due to the dynamic nature of grouping, the combinatorial possibilities of such a scheme offer a vastly increased dimensional magnitude for encoding visual information and also have implications for learning and plasticity. In 1941, Sherrington proposed that groups of neurons may cooperate synergistically such that the whole is more than the sum of its parts. Hebb (1949) and Hayek (1952) expanded on this theory and suggested that groups of cells could form dynamic regional circuits or spatiotemporal assemblies to represent structures in a visual scene. Indeed, they hypothesized that connections and interactions between neurons, defining a neural network architecture, were more functionally significant than the individual properties of the neurons themselves. In this manner, visual information would not only be inherent in the activity of individual neurons, but could be extracted from the collective activity of the group.

Originally, Hebb (1949) and Hayak (1952) proposed that cooperative relationships in cell assemblies were formed based on anatomical connections, perhaps defined by plasticity during brain development. However, noting the adaptive nature of the brain, Hayak (1952) also suggested that the formation of cell assemblies could result from short-term enhancement of synaptic effectiveness initiated by changes in the temporal structure of spike trains (becoming effectively connected) instead of requiring

actual anatomical changes in synaptic connections. In this manner, groups of cells could

assemble and disassemble during certain tasks and individual cells could belong to more

than one functional group. Furthermore, uncorrelated groups could coexist without

interference.

Temporal Coding

At the turn of the 20th century, the study of individual neurons in the brain became

a reality through the anatomical works of Ramon y Cajal and Golgi. The field of

neurophysiology was pioneered with a novel experimental protocol and recording

technique introduced by Adrian and Zotterman (1926). Using a capillary electrometer

and three-stage amplifier, Adrian and Zotterman recorded the impulses produced in the

plantar digital nerves of a cat when stimulated by contact or pressure. They noted that

the frequency of the impulses (action currents – related to action potentials through

Ohm's Law) varied with the intensity of the stimulus, but the magnitude of individual

impulses did not. These results supported an all-or-none relationship between stimulus

and nerve impulses.

A binary, all-or-none response to a stimulus could signal the presence or absence

of the stimulus, but what property of a cellular response represents stimulus intensity?

Since action potentials are indistinguishable events, the strength of a stimulus cannot be

reflected in the shape or size of an impulse and therefore must be reflected in the

temporal characteristics of the neuronal spike train, such as average firing rate, spike

count, spike patterns, interspike intervals, or precise spike arrival times (Figure 1.3). For

instance, Strehler and Lestienne (1986) found distinct patterns in individual spike trains

that occurred more often than chance with submillisecond precision. Also, Victor (2000)
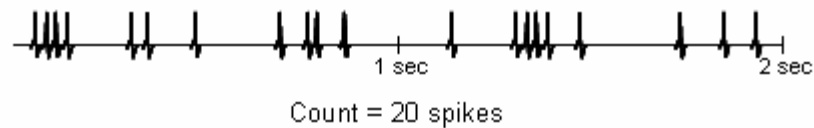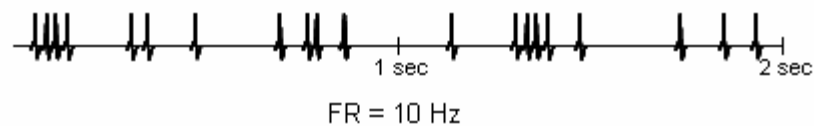
21
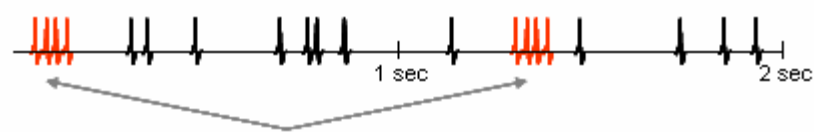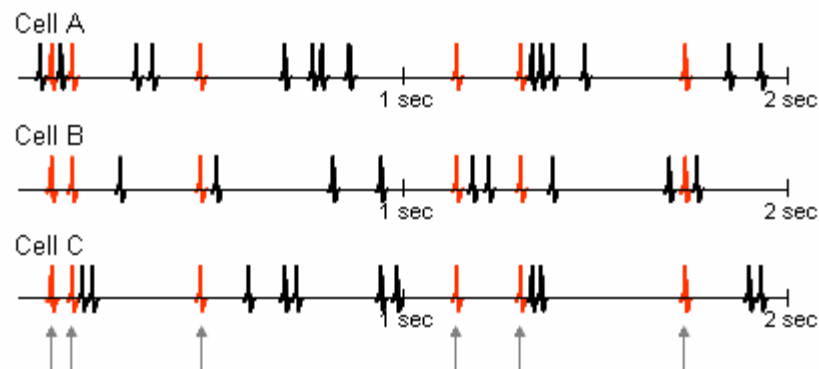
Figure 1.3. Examples of temporal codes. Stimulus information must be reflected in the temporal characteristics of a neuronal spike train. (A) Spike count. The number of action potentials is counted. (B) Average firing rate. The spike count is divided by time to produce a rate. (C) Spike patterns. Similar groups of action potentials appear throughout the time period. (D) Interspike intervals. The time delay between each spike and all other spikes is measured. (E) Precise spike arrival times. The timing of synchrony and number of synchronous episodes (action potentials from two or more cells occurring within a 10 ms integration window) have been shown to be stimulus-dependent.

22

showed that different stimulus features (contrast, orientation, spatial frequency) could be represented at different temporal resolutions of interspike interval histograms. In this manner, stimulus features can be multiplexed in a spike train.

While temporal properties like spike patterns or interspike intervals have gained some support in the field as a means to encode stimulus information, the relationship between stimulus intensity and firing frequency described by Adrian and Zotterman remains central to our understanding of information transmission in the cortex. In a population code, one possible way to associate cells of a common assembly is to consider their correlated relative firing rates (oscillation). When stimulated with visual information, the enhanced specialization of cells in the primary visual cortex ensures that only a small fraction of the neuronal population will have receptive field preferences akin to the presented stimulus features and respond with increased firing probability. These cells are grouped as members of the same neural assembly and their combination reflects a specific structure in the visual field.

However, simply identifying an associated response characteristic across a subpopulation of cells does not give insight into how that characteristic is used to transmit visual information. Now that the members are known, how are they combined? The average firing rate responses from each cell in the assembly could be averaged (weighted or unweighted), considered by absolute or relative standards, or involved in a winner-take-all scheme. Another disadvantage of firing rate-based neural coding is that individual response gradations are limited by an action potential's refractory period. A cell therefore has a maximum firing rate, which imposes a limit on the dynamic range for encoding stimulus intensity. Furthermore, average firing rate is highly variable across stimulus repetitions, so reliable responses must be obtained by averaging across repeated

stimulus presentations (Gershon et al. 1998). From a biological perspective, this cannot

happen as the brain usually recognizes objects with a single viewing. Finally, the

integration of firing rate must take place over some finite time and given the required

broad temporal resolution distinct populations can become confounded.

On the other hand, synchronization of spike arrival times is believed to be more

effective than elevation of firing rates (Abeles 1991; Azouz and Gray 2003) in

forwarding information because the transmission efficiency in the cortex is generally low

(Nicoll and Blakemore 1993; Thomson and West 1993). The precise timing of

synchronization allows expression of unambiguous relationships between cells in an

assembly. Simulations suggest that the effective summation interval based on the

postsynaptic cell membrane time constant is less than 10 ms (Softky and Koch 1993),

permitting rapid and dynamic assembly and disassembly as well as the coexistence of

numbers of independent groups.

The biological consequence of neuronal synchronization can be viewed as an

efficient means of information propagation. Upon external stimulation, simultaneous

activation of voltage-gated sodium and potassium channels induce an action potential, the

wave of which perpetuates and travels down the axon. Once in the presynaptic axon

terminal, depolarization of the membrane by the nerve impulse opens voltage-gated

calcium channels and releases an influx of calcium ions which signals the exocytotic

release of a neurotransmitter (e.g. glutamate, for excitatory neurons) into the synaptic

cleft. The neurotransmitter then binds to ligand-gated channels on the dendrites of a

postsynaptic neuron and the resulting influx of sodium ions produces a graded potential

that propagates down the dendrites to the axon hillock. Each graded potential is

subthreshold and must rely on the temporal and spatial summation of other graded

24

potentials to reach threshold and induce an action potential in the postsynaptic neuron. The process theoretically requires fewer synchronized spikes to reach threshold and synchrony, therefore, transmits information more efficiently than when relying on the spatiotemporal summation of a comparable number of asynchronous spikes.

As a hypothetical neural substrate for encoding salient stimulus properties, synchrony enhances the probability of eliciting postsynaptic action potentials, thus ensuring propagation of this information to subsequent levels of the cortical hierarchy. As an efficient information transmission mechanism, synchronization of neuronal responses is an attractive candidate to play a role in generating perception. Synchrony exists between visual cortical neurons, but its functional significance is largely unknown. Critics and longtime supporters of firing rate-based coding strategies argue that synchronous activity may be artifactual and result trivially from lateral or feedback connections present throughout the visual pathways. Although the exact mechanism generating synchrony is unknown, an overwhelming amount of evidence suggests that synchrony, independent of firing rate-induced modulation of synchrony, is stimulus-dependent. Conceptually, a coding strategy involving dynamic synchronization of neuronal responses offers tremendous advantages in terms of coding capacity and efficiency. The physical mechanism underlying synchrony would allow for neurons to be "effectively" connected and form dynamic regional circuits to reliably and efficiently transmit information throughout the cortex while minimizing metabolic demands.

The Role of Synchrony

Synchronization of precise spike arrival times is an attractive candidate to play a role in encoding objects in the visual field because it seems to solve the binding problem.

25

The surrounding environment is full of complex objects that are characterized by numerous properties such as shape, motion, color, and location. Property binding involves associating stimulus properties with the features they describe. Part binding involves associating the parts of the same object together, sometimes across discontinuities resulting from partial occlusion (Treisman 1996). Therefore, object recognition not only depends on the ability to identify all the parts of an object, but also how those features are combined to reflect a coherent percept. For instance, when viewing a face, it is not only important to identify two eyes, a nose, and a mouth, but also recognize their correct facial locations. Furthermore, the face must be recognized as separate from other faces and objects occupying the scene and also must be segregated from the background.

The temporal binding theory (Milner 1974; von der Malsburg 1981) postulates that dynamic assembly formation is the physical basis for certain perceptual phenomena such as shape perception, figure-ground separation, long and short-term plasticity, and memory. According to this theory, perceptually-related features are linked through correlated firing among subpopulations of cells. Grouping into subpopulations is defined by perceptually-based relationships, e.g. feature proximity, similarity, or motion coherency. In this scheme, only simple feature detectors are required and complex features are extracted through the activities of multiple assemblies.

Experimental support for the temporal binding theory was provided independently by Eckhorn et al. (1988) and Gray et al. (1989) using anesthetized cats. In both studies synchrony and oscillation between cell pairs was found to depend on the orientation and coherence of the visual stimulus. Gray et al. (1989) used multiple electrodes to record the activity of neurons in the primary visual cortex of anesthetized cats to bar stimuli

(Figure 1.4A). Using cross correlation analysis, they examined the correlated timing of

firing between pairs of neurons when stimulated with 1) two light bars moving in

opposite directions; 2) two light bars moving in the same direction; and 3) a long light bar

moving across the receptive fields instead of two short light bars. In the first case, the

two light bars were perceived as two independent objects and the firing of both neurons

was not synchronized. In the second case, however, the two light bars moving in the

same direction was perceived as a single object and the firing of both neurons was

synchronized. Furthermore, when a long light bar was used to stimulate the receptive

fields, the magnitude of synchrony observed was higher. These results suggested that the

magnitude of synchrony was related to object coherence and could be involved in the

binding process.

Following this pioneering experimental study, there have been numerous

neurophysiological studies investigating synchrony as a binding mechanism (i.e., Engel

et al. 1991a, 1991b; Gray et al. 1992; Eckhorn et al. 1989; Eckhorn and Schanze 1991).

More recently, several laboratories have been unable to find unambiguous relationships

between synchrony and specific visual tasks designed around segmentation or

figure/ground discrimination (Lamme and Spekreijse 1998, Thiele and Stoner 2003,

Roelfsema et al. 2004, Palanca and DeAngelis 2005). For instance, Roelfsema et al.

(2004) recorded activity from multiple neurons in the primary visual cortex of macaque

monkeys engaged in a contour-grouping task (Figure 1.4B). Each monkey was required

to locate a fixation point and then make an eye movement to a red target circle connected

to the fixation point by a curved line without being distracted by a separate curve with its

own red circle. Successful completion of the task involved the correct binding of all

contour segments from the target curve. Cross-correlation analysis was used to measure
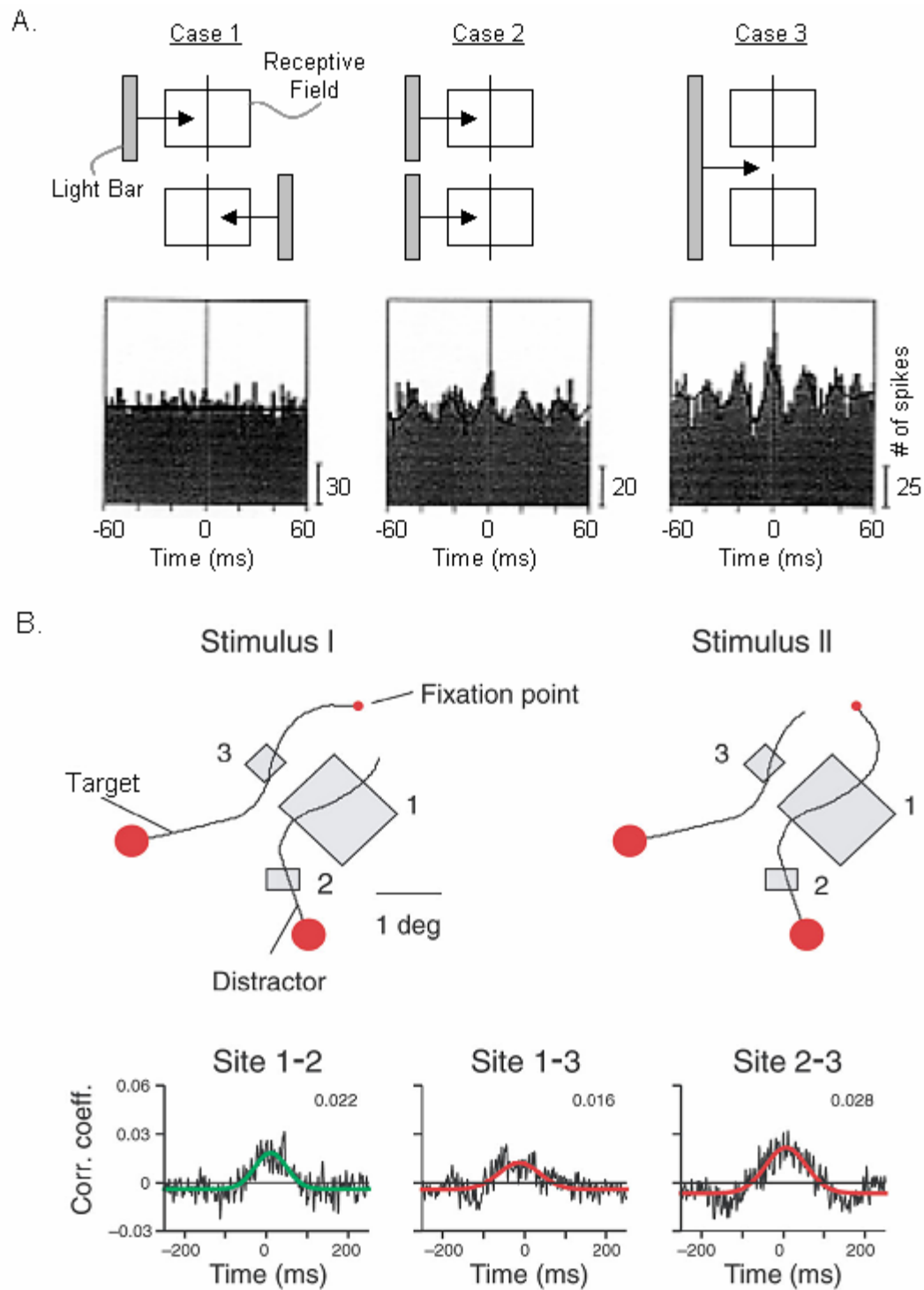
Figure 1.4. Previous evidence about synchrony's role in contour binding is contradictive. (A) In anesthetized cats, Gray et al. (1989) showed that the magnitude of synchrony between two neuronal clusters was greater for a single light bar stimulating two collinear receptive fields than two coherent light bars. (B) In awake monkeys, Roelfsema et al. (2004) showed that the magnitude of synchrony did not predict whether cells were on the same or different contours.

the amount of synchrony between groups of neurons with receptive fields on the same and different contours. They found that the correlation between sites did not depend on object coherence and concluded that the strength of synchrony was unrelated to contour grouping. However, this study examined correlations 200-600 ms after the stimulus onset and their wide cross-correlation functions may be indicative of firing rate artifact and does not necessarily reflect coupling on a millisecond timescale.

In another context, some psychophysical studies with human subjects have indirectly supported the synchrony-for-binding mechanism. These experimental paradigms were designed on the assumption that the manipulation of stimulus timing will affect neuronal synchronization. The idea is that if figures are represented through neuronal synchrony and that synchronous stimuli upon the retina induce internal synchrony in the cortex, then features presented simultaneously will be more easily perceived as a single object that features that are presented asynchronously. Fahle (1993) used visual stimuli consisting of dots to show that a figural region cannot be detected from the background when the difference in temporal phase of the regions was zero, but could emerge with the desynchronization of figural elements from their background by as little as 5-7ms. However, other psychophysical studies using texture segregation tasks (Kiper et al. 1996), Kanizsa triangles (Fahle and Koch 1995), and tasks with multiple presented objects (Keele et al. 1988) have failed to confirm that stimulus synchrony affects perceptual grouping. Although synchrony has been considered as a promising neural mechanism in feature binding, we cannot say simply that synchrony is stimulus-induced and thus a solution to the binding problem. If fact, binding can occur for objects separated in time (Treisman 1996) and also does not occur for all features presented simultaneously.

Synchrony Encodes Collinear and Cocircular Contours

As mentioned above, the first neurophysiological experiments linking synchrony and feature integration used drifting light bars (Eckhorn et al. 1988; Gray et al. 1989). This type of coherent collinear stimulation yielded synchrony between pairs of neuron clusters with similar orientation preferences and collinear receptive fields. These findings led to speculation that synchrony could be facilitated through (or a result of) direct anatomical connections between orientation columns. In this approach, horizontal connections were thought to play a critical role in contour integration since 60-70% of all horizontal connections are between columns with similar orientation preferences in the primary visual cortex (Bosking et al. 1997; Malach et al. 1993; Lund et al. 2003; Stettler et al. 2002). However, after transecting horizontal connections throughout V1 in cats, Sperry et al. (1955) found no difference in performance when discriminating global contours and patterns.

If synchrony is involved in feature integration, but does not rely on horizontal connections as a critical avenue, then it might be observed between cells with different orientation preferences given the appropriate stimulation. In fact, collinearity among receptive fields is a special case of the more general property of cocircularity (Parent and Zucker 1989) in which receptive fields have orientation preferences that are tangent to the same circle. Cocircular structures are ubiquitous in natural scenes (Geisler et al. 2001; Sigman et al. 2001; Elder and Goldberg 2002) and the predictable relationship between cocircular segments has been proposed as the foundation of contour integration (Field et al. 1993). Inspired by psychophysical studies, Field et al. (1993) introduced the *association field* framework which describes the perception of contours and continuity. In this paradigm, contour segments are grouped depending on proximity and the

similarity of their orientations. Applying these concepts to neurophysiology, association field theory predicts linking between orientation-tuned cells that is dependent on their joint relative orientation and spatial position.

By using an experimental protocol consisting of drifting sinusoidal gratings and concentric rings, we tested synchrony's adherence to association field rules by seeing if it predictably existed for pairs of cells with different orientation preferences, but whose receptive fields still had cocircular alignments (Samonds et al. 2006). Using a 10x10 microelectrode array, we simultaneously recorded from multiple single-units in areas 17 and 18 of anesthetized cats and found that neuron pairs synchronized based on an appropriate match between stimulus curvature and receptive field configuration. Furthermore, synchronous responses were more reliable than changes in average firing rate in discriminating between concentric ring and grating stimuli (Figure 1.5). Group membership was found to be dynamic in that individual cells could belong to more than one functional group, which assembled based on the spatiotemporal properties of the stimulus.

Analyses of electrode distance, receptive field overlap, and synchronous lag times show that the magnitude and probability of observing synchrony among cell pairs matched the fundamental prediction of the association field theory. Extending collinear synchrony results (Eckhorn et al. 1988; Gray et al. 1989) to cells with cocircular receptive field properties is vital in establishing synchrony's role in complex feature detection. The fact that synchrony was stimulus-dependent and observed between cells with different orientation preferences undermines a direct causal link between synchrony and anatomy (e.g., horizontal connections) per se and counters the notion that synchronous activity may be an artefact of cortical connections. Instead, these findings
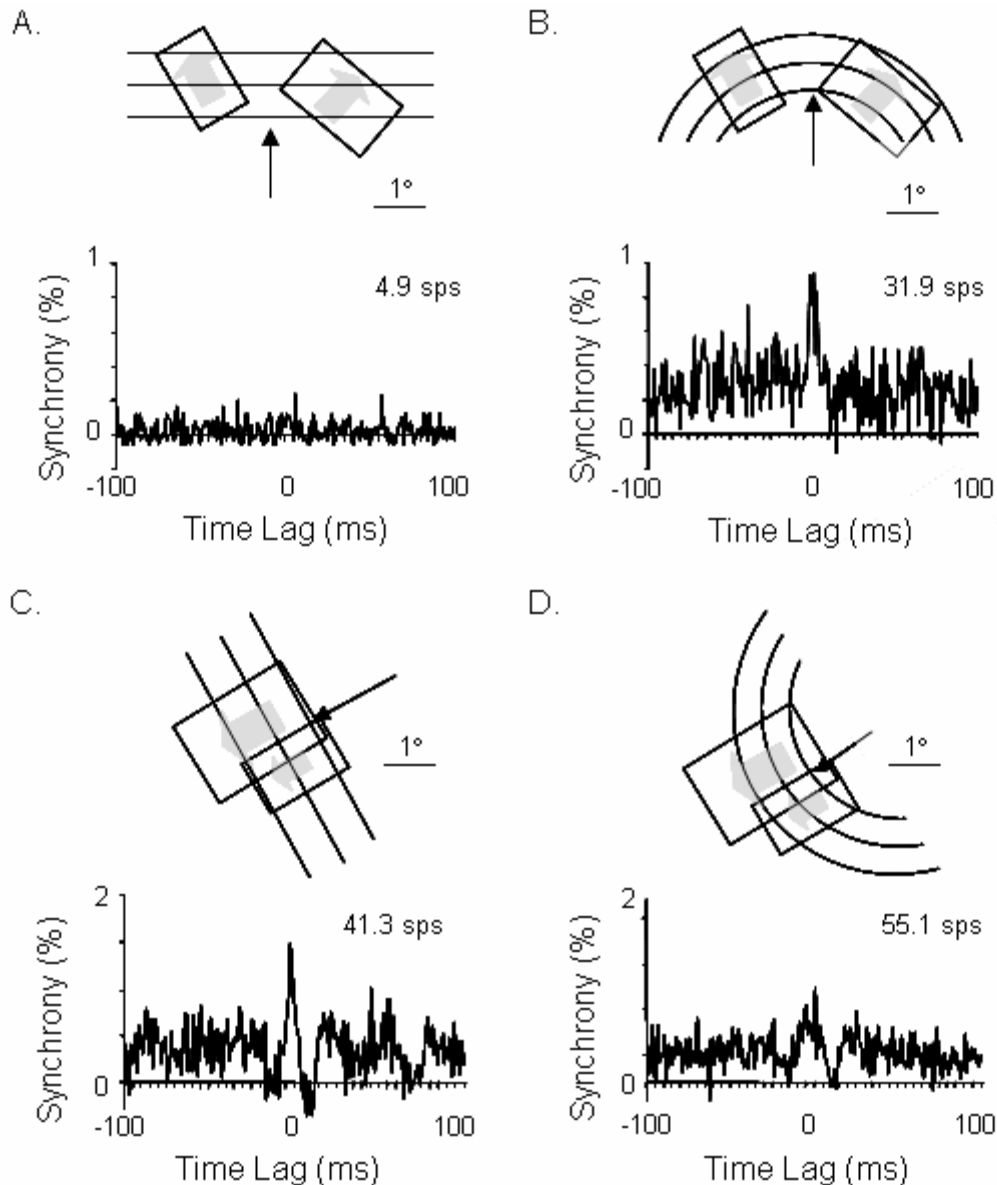
Figure 1.5. Synchrony encodes collinear and co-circular contours. Example cross-correlograms (CCGs) for (A)-(B) a pair of cells whose orientation preferences and receptive field locations are consistent with concentric ring stimulation and (C)-(D) a pair of cells whose receptive field configurations are consistent with grating stimulation. The average total firing rate of each pair is noted in the upper-right corner for each stimulus condition. (A) CCG for a co-circular pair of cells driven by gratings. (B) CCG for a co-circular pair of cells driven by rings. For this pair, both synchrony and firing rate correctly indicated that the ring stimulus drove the cells better than gratings, as predicted by their receptive field organizations. (C) CCG for a collinear pair of cells driven by gratings. (D) CCG for a collinear pair of cells driven by rings. For this pair, synchrony, but not firing rate, correctly indicated that the grating stimulus drove the cells better than rings. From Samonds et al. (2006).

suggest a more global and purposeful function in which synchrony detects related contour segments, which have the ability to be integrated at higher processing centers throughout the visual system.

Chapter Overview

The work presented here supports synchrony as a possible neural mechanism involved in contour detection. Collectively, these results provide a comprehensive investigation of synchronous activity within neural assemblies to natural stimulation by studying the spatiotemporal factors influencing synchrony (Aim 1), the specific relationships between receptive field configuration and stimulus structure conducive to synchrony (Aim 2), and the efficiency of coding (Aim 3). The next six chapters are organized as follows: Chapter 2 describes the experimental setup, procedures, neural recording equipment, and general data processing methods used in all experiments. Chapter 3 speaks to Aim 1 by characterizing the spatial relationships of synchronous assemblies across the cortex and examining the temporal dynamics of synchrony throughout the stimulus presentation. Chapter 4 begins to answer the questions laid out in Aim 2 by showing that synchronous activity is affected by structural modifications in natural images. The specific relationships between local stimulus structure and assembly receptive field organization are defined in Chapter 5 where we determine synchrony's consistency with the association field model in the context of natural stimulation. Chapter 6 expands on Aim 3 to mathematically describe synchrony's ability as a sparse coding mechanism. Finally, we summarize the results from each paper in Chapter 7 and discuss the future directions of this research.

References

Abeles M. *Corticonics: Neural Circuits of the Cerebral Cortex*. Cambridge University Press, New York, 1991.

Abeles M and Gerstein GL. Detecting spatiotemporal firing patterns among simultaneously recorded single neurons. *J Neurophysiol*. Sep;60(3):909-24, 1988.

Adrian ED and Zotterman Y. The impulses produced by sensory nerve endings, Pt. 3: Impulses set up by touch and pressure. *J. Physiol. (Lond)*, 61:465-493, 1926.

Aertsen AMHJ, Gerstein GL, Habib MK, and Palm G. Dynamics of neuronal firing correlation: Modulation of "effective connectivity". *J. Neurophysiol.*, 61:900-917, 1989.

Azouz R and Gray CM. Adaptive coincidence detection and dynamic gain control in visual cortical neurons in vivo. *Neuron,* 37:513-523, 2003.

Barlow HB. Single units and sensation: a neuron doctrine for perceptual psychology? *Perception*, 1:371-394, 1972.

Bell AJ and Sejnowski TJ. The "independent components" of natural scenes are edge filters. *Vision Res*. Dec; 37(23): 3327-38. 1997.

Bosking WH, Zhang Y, Schofield B, and Fitzpatrick D. Orientation selectivity and the arrangement of horizontal connections in tree shrew. *J Neurosci* 17: 2112–2127, 1997.

Braitenberg V. The concept of symmetry in neuroanatomy. *Ann N Y Acad Sci*. Sep 30;299:186-96, 1977.

Dreher B and Cottee LJ. Visual receptive-field properties of cells in area 18 of cat's cerebral cortex before and after acute lesions in area 17. *J Neurophysiol.* Jul;38(4):735-50, 1975.

Eckhorn R, Bauer R, and Reitbock HJ. Discontinuities in visual cortex and possible functional implications: relating cortical structure and function with multielectrode/correlation techniques. In Basa E, Bullock TH eds. Springer series in brain dynamics 2. Springer-Verlag, Berlin, 267-278, 1989.

Eckhorn R, Bauer R, Jordan W, Brosch M, Kruse W, Munk M, and Reitboeck HJ. Coherent Oscillations: A mechanism of Feature Linking in the Visual Cortex? *Biol. Cybern.*, 60:121-130, 1988.

Eckhorn R. and Schanze. Possible neural mechanisms of feature linking in the visual system: stimulus-locked and stimulus-induced synchronizations. In Babloyantz A ed. Self-organization, emerging properties and learning. Plenum Press, New York, 63-80, 1991.

Elder JH and Goldberg RM. Ecological statistics of Gestalt laws for the perceptual organization of contours. *J. Vis.* 2:324-353, 2002.

Engel AK, König P, Kreiter AK, and Singer W. Interhemispheric synchronization of oscillatory neuronal responses in cat visual cortex. *Science*, 252:1177-1179, 1991a.

Engel AK, Kreiter AK, König P, and Singer W. Synchronization of oscillatory neuronal responses between striate and extrastriate visual cortical areas of the cat. *Proc. Nat. Acad. Sci. USA,* 88:6048-6052, 1991b.

Fahle M. Figure-ground discrimination from temporal information. *Proc Biol Sci.* Dec 22;254(1341):199-203, 1993.

Fahle M and Koch C. Spatial displacement, but not temporal asynchrony, destroys figural binding. *Vision Res.* Feb;35(4):491-4, 1995

Ferster D. A comparison of binocular depth mechanisms in areas 17 and 18 of the cat visual cortex. *J Physiol.* Feb;311:623-55, 1981.

Field DJ. What is the goal of sensory coding? *Neural Comp.* 6:559-601, 1994.

Field DJ, Hayes A, and Hess RF. Contour integration by the human visual system: evidence for a local "association field". *Vision Res.* 33:173-193, 1993.

Frien A and Eckhorn R. Functional coupling shows stronger stimulus dependency for fast oscillations than for low-frequency components in striate cortex of awake monkey. *Eur J Neurosci.* Apr;12(4):1466-78, 2000.

Geisler WS, Perry JS, Super BJ, and Gallogly DP. Edge co-occurrence in natural images predicts contour grouping performance. *Vision Res.* 41:711-724, 2001.

Gershon ED, Weiner MC, Lathan PE, and Richmond BJ. Coding strategies in monkey V1 and inferior temporal cortices. *J. Neurophysiol.* 79:1135-1144, 1998.

Gray CM, Engel AK, Konig P, and Singer W. Synchronization of oscillatory neuronal responses in cat striate cortex: temporal properties. *Vis Neurosci.* Apr;8(4):337-47, 1992.

Gray CM, Konig P, Engel AK, and Singer W. Oscillatory responses in cat visual cortex exhibit inter-columnar synchronization which reflects global stimulus properties. *Nature*, 338:334-337, 1989.

Hayek FA. *The Sensory Order.* Chicago: University of Chicago Press, 1952.

Hebb DO. *The Organization of Behavior: a Neuropsychological Theory.* New York: Wiley, 1949.

Hubel DH and Wiesel TN. Receptive fields and funcitonal architecture in two nonstriate visual areas (18 and 19) of the cat. *J Neurophysiol.* Mar;28:229-89, 1965.

Hubel DH and Wiesel TN. Receptive fields, binocular interaction and functional architecture in the cat's visual cortex. *J Physiol* 160: 106–154, 1962.

Hyvarinen A and Hoyer PO. A sparse coding model learns simple and complex receptive fields and topography from natural images. *Vision Res*. Aug;41(18):2413-23, 2001.

Keele SW, Cohen A, Ivry R, Liotti M, and Yee P. Tests of a temporal theory of attentional binding. *J Exp Psychol Hum Percept Perform.* Aug;14(3):444-52, 1988.

Kiper DC, Gegenfurtner KR, and Movshon JA. Cortical oscillatory responses do not affect visual segmentation. *Vision Res*. Feb;36(4):539-44, 1996.

Kohn A and Smith MA. Stimulus dependence of neuronal correlation in primary visual cortex of the macaque. *J Neurosci.* Apr 6;25(14):3661-73, 2005.

Lamme VAF and Spekreijse H. Neural synchrony does not represent texture segregation. *Nature*, 396:362-366, 1998.

Lund JS, Angelucci A, and Bressloff PC. Anatomical substrates for functional columns in macaque monkey primary visual cortex. *Cereb Cortex* 13: 15–24, 2003.

Maffei L and Fiorentini A. The visual cortex as a spatial frequency analyser. *Vision Res*. Jul;13(7):1255-67, 1973.

Malach R, Amir Y, Harel M, and Grinvald A. Relationship between intrinsic connections and functional architecture revealed by optical imaging and in vivo targeted biocytin injections in primate striate cortex. *Proc Nat Acad Sci USA* 90: 10469–10473, 1993.

Maldonado PE, Friedman-Hill S, and Gray CM. Dynamics of striate cortical activity in the alert macaque: II. Fast time scale synchronization. *Cereb Cortex.* Nov;10(11):1117-31, 2000.

Milner P. A model for visual shape recognition. *Psychol. Rev.,* 81: 521-535, 1974.

Movshon JA. The velocity tuning of single units in cat striate cortex. *J Physiol*. Aug;249(3):445-68, 1975.

Nowak LG, Munk MH, Nelson JI, James AC, and Bullier J. Structural basis of cortical synchronization. I. Three types of interhemispheric coupling. *J Neurophysiol.* Dec;74(6):2379-400, 1995.

Nicoll A and Blakemore C. Patterns of local connectivity in the neocortex. *Neural Comp.* 5:665-680, 1993.

Orban GA. Studies of brain function vol 11: neuronal operationsin the visual cortex. Springer-Verlag, Berlin, 1984.

Palanca BJ and DeAngelis GC. Does neuronal synchrony underlie visual feature grouping? *Neuron.* 46:333-346, 2005.

Parent P and Zucker SW. Trace inference, curvature consistency, and curve detection. *IEEE Trans Pattern Anal Machine Intell* 11:823-839, 1989

Perkel DH, Gerstein GL, and Moore GP. Neuronal spike trains and stochastic point processes, II. Simultaneous spike trains. *Biophys. J.* 7:419-440, 1967.

Peterhans E, Heider B, and Baumann R. Neurons in monkey visual cortex detect lines defined by coherent motion of dots. *Eur J Neurosci.* Feb;21(4):1091-100, 2005.

Roelfsema PR, Lamme VA, and Spekreijse H. Synchrony and covariation of firing rates in the primary visual cortex during contour grouping. *Nat. Neurosci.* 7:982-991, 2004.

Roelfsema PR, Engel AK, König P, and Singer W. Visuomotor integration is associated with zero time-lag synchronization among cortical areas. *Nature.* Jan 9;385(6612):157-61, 1997.

Samonds JM, Zhou Z, Bernard MR, and Bonds AB. Synchronous Activity in Cat Visual Cortex Encodes Collinear and Cocircular Contours. *J. Neurophysiol.* 95:2602-2616, 2006.

Sherrington C.S. *Man on His Nature*. London: Cambridge University Press, 1941.

Sigman M, Cecchi GA, Gilbert CD, and Magnasco MO. On a common circle: natural scenes and Gestalt rules. *Proc. Natl. Acad. Sci. USA*. 98:1935-1940, 2001.

Singer W and Gray CM. Visual feature integration and the temporal correlation hypothesis. *Annu. Rev. Neurosci.*, 18:555-586, 1995.

Singer W, Gray CM, Engel A, König P, Artola A, and Bröcher S. Formation of cortical cell assemblies. *Cold Spring Harb Symp Quant Biol*.;55:939-52, 1990.

Singer W, Tretter F, and Cynader M. Organization of cat striate cortex: a correlation of receptive-field properties with afferent and efferent connections. *J Neurophysiol.* Sep;38(5):1080-98, 1975.

Softky WR and Koch C. The highly irregular firing of cortical cells is inconsistent with temporal integration of random EPSPs. *J. Neurosci.,* 13: 334-350, 1993.

Sperry RW, Miner N, and Myers RE. Visual pattern perception following subpial slicing and tantalum wire implantations in the visual cortex. *J Comp Physiol Psychol* 48: 50–58, 1955.

Stettler DD, Das A, Bennett J, and Gilbert CD. Lateral connectivity and contextual interactions in macaque primary visual cortex. *Neuron* 36: 739–750, 2002.

Strehler BL and Lestienne R. Evidence of precise time-coded symbols and memory of patterns in monkey cortical neuronal spike trains. *Proc. Nat. Acad. Sci*. USA, 83:9812-9816, 1986.

Thiele A and Stoner G. Neural synchrony does not correlate with motion coherence in cortical area MT. *Nature*, 421:366-370, 2003.

Thomson AM and West DC. Fluctuations in pyramid-pyramid excitatory postsynaptic potentials modified by presynaptic firing pattern and postsynaptic membrane potential using paired intracellular recordings in rat neocortex. *Neuroscience,* 54:329-46, 1993.

Treisman A. The binding problem. *Curr Opin Neurobiol*. Apr;6(2):171-8, 1996.

Vandenbussche E and Orban GA. Meridional variations in the line orientation discrimination of the cat. *Behav Brain Res*. Aug;9(2):237-55, 1983.

Victor JD. How the brain uses time to represent and process visual information. *Brain Res.*, 886:33-46, 2000.

von der Malsburg C. The correlation theory of brain function. *Internal Report, Max-Planck Institute for Biophysical Chemistry*. Goettingen, Germany, 1981.

Young MP and Yamane S. Sparse population coding of faces in the inferotemporal cortex. *Science* 256:1327-1331, 1992.

CHAPTER II

EXPERIMENTAL PROCEDURES AND DATA PROCESSING

Overview

By the mid-1960's, automatic data processing for neurophysiological experiments

was widely available and enabled researchers to record the precise timing of single cell

spike events over long periods. In 1967, Perkel et al. introduced a variety of statistical

techniques for the analysis of neuronal spike trains. Mathematical descriptions of output

behavior could in turn be used to make inferences about input or cell processing

behavior. Perkel and his colleagues operated under the assumption that details about the

nervous system are inherent in the structure of a neuronal spike train. Since action

potentials are essentially identical, all-or-none events, only the timing of such events

could relay information about the processes which lead to their generation. Speculation

on the precise form of the neural code for representation of visual structures suggested

that perceptual phenomena like contour integration, figure-ground separation, and object

recognition were encoded by the collective activity of multiple neurons (Hebb 1949;

Hayek 1952), which were organized into dynamic spatiotemporal assemblies by the

precise synchronization of cell responses on a millisecond timescale (Milner 1974; von

der Malsburg 1981). However, confirmation of these theories proved difficult because of

the inability to record from multiple neurons while understanding the significance of joint

activity. Over the next few decades, there were numerous advances in the areas of

microelectrode and tetrode arrays (Pouget et al. 2000; Milton and Mackey 2000; Buzsaki

2004), but analysis techniques for these population recordings were limited. Using

39

microelectrode array technology to record from dozens of neurons simultaneously, we demonstrate how to quantify the amount of synchronous activity in an assembly of arbitrary size with the PSP Method.

Experimental Procedures

Preparation and Experiment Setup

Ten adult cats (2.3-4.0 kg) were prepared for electrophysiological recordings in the primary visual cortex (left hemisphere). All procedures were performed in accordance with guidelines set forth by the American Physiological Society and the Institutional Animal Care and Use Committee at Vanderbilt University. Prior to surgery, each cat received intramuscular injections of 0.5 ml acepromazine maleate (10 mg/ml), 0.5 ml atropine sulfate (0.4 mg/ml), and 0.25 ml dexamethasone sodium phosphate (4 mg/ml). Anesthesia was induced with 5% halothane in O_2 and maintained with intravenous injection of Propofol (0.3 mg/kg hr). Two forelimb veins and the trachea were cannulated and the animal was positioned in a stereotaxic device where a small craniotomy was performed over V1 according to Horsley-Clark coordinates. The dura was excised, the electrode array implanted, and the opening was covered with agar and mammalian Ringer's solution, which was refreshed approximately every four hours.

During recording, paralysis was induced with 6 mg pancuronium bromide and maintained through intravenous injection (Pavulon; 0.3 mg/kg hr). Health and effective anesthesia were maintained by monitoring the electrocardiogram and electroencephalogram and administering bolus injections of propofol when necessary. Cats were artificially ventilated with a mixture of N_2O, O_2, and CO_2 (75:23.5:1.5) to hold

expired pCO_2 at 3.9%. Rectal temperature was maintained at 37.5° C with a servo-controlled heating pad. The nictitating membranes were retracted and the natural pupils dilated by instillation of phenylephrine HCl 10% and atropine sulfate 1% in the conjunctival sacs. Contact lenses with 4 mm pupils were placed on the corneas and auxiliary spectacle lenses were added as dictated by direct ophthalmoscopy to render the retinae conjugate with the stimulus plane 57 cm away. At this distance, a visual angle of 1° is equivalent to 1 cm on the screen.

The experiment setup is illustrated in Figure 2.1. Each subject is situated on a table with its head placed in a stereotaxic apparatus to aid in mapping the location of V1 during surgery and ensures fixed eye positions during stimulation and recording. The subject's body is wrapped with a heating pad to preserve physiological temperatures after paralysis is induced. Cardiac and neural activities are displayed on an oscilloscope and pump rates for the paralytic and anesthetic agents are adjusted throughout the experiment to maintain consistent health and effective anesthesia. During receptive field mapping, a plotting table is used to project spots or bars of light for manual recording of receptive field location and extent. The table uses a reflecting surface which splits light into beams projected to the animal as well as to the plotting surface. For drifting sinusoidal grating and natural image stimulation, a mirror is used to direct the subject's gaze to a gamma-corrected (to control for overall brightness and contrast modulation) monitor at a distance of 57 cm. The output from the array is passed through a multichannel amplifier and sent to the Cyberkinetics recording and acquisition system on a personal computer. Binary NEV files from the computer are uploaded to other personal computers for spike sorting and the resulting waveforms are stored for later analysis with MATLAB-based programs.
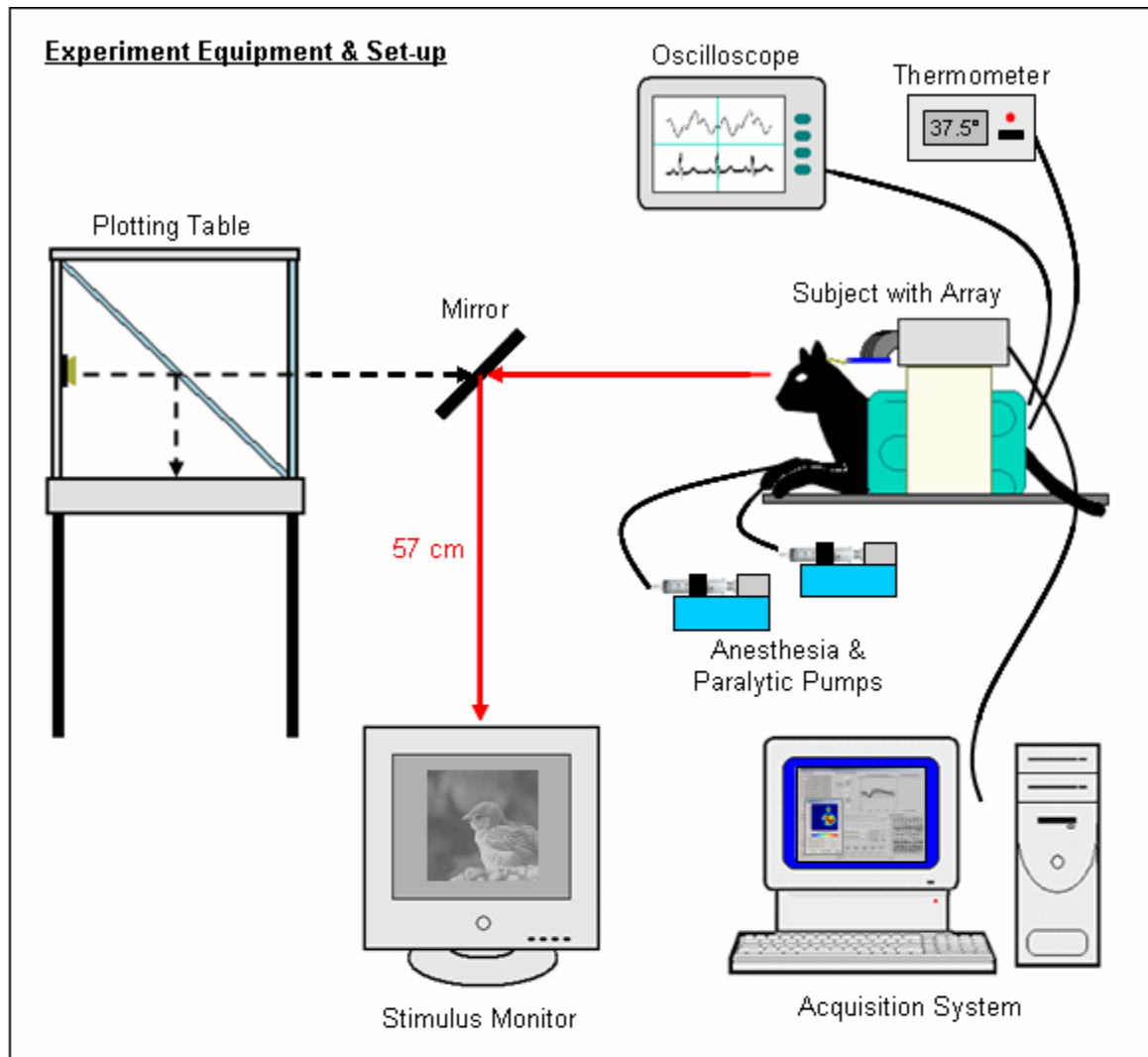
Figure 2.1. Preparation and experimental setup. Each subject is situated in a stereotaxic apparatus and wrapped with a servo-controlled heating pad. Health and effective anesthesia are maintained by monitoring the electrocardiogram and electroencephalogram on an oscilloscope and adjusting the pump rates as necessary. During receptive field mapping, a plotting table is used to project spots or bars of light for manual recording of receptive field location and extent. For drifting sinusoidal grating and natural image presentations, a mirror is used to direct the subject's gaze to a gamma-corrected (to control for overall brightness) monitor at a distance of 57 cm. At this distance, 1 cm on the screen is equivalent to 1 visual degree. The microelectrode array is inserted into layers II/III of the primary visual cortex and stabilized with agar and mammalian Ringer's solution. The output from the array is passed through an amplifier and sent to the Cyberkinetics recording and acquisition system on a personal computer. Binary NEV files from the computer are uploaded to other personal computers for spike sorting and the resulting waveforms are stored for later analysis with MATLAB-based programs.

Data Recording and Acquisition

Simultaneous single-unit recordings are made from cells in the visual cortex via the Utah Intracortical Electrode Array (UIEA; Cyberkinetics Neurotechnology Systems, Foxborough, MA). The UIEA recordings have good signal to noise ratios and have been shown to have qualities comparable to those from single-electrode recordings (Kelly et al. 2007). The implant is a square 10x10 (100 total) silicon array (Figure 2.2A) on 400 micron centers (4x4 mm footprint). The electrodes have a length of 1.0 mm and are inserted to a depth of 0.6 mm with a pneumatic implantation tool (Figure 2.2B; Rousche and Normann 1992) that minimizes tissue damage (Schmidt et al. 1993; Rousche and Normann 1998). The insertion depth concentrates the electrodes in layers II/III and avoids impact to the cortical surface by the electrode base. The wires from the array to the amplifier are flexible, which enhances stability and allows for reliable recording sessions of more than thirty hours. The impedance of each electrode is $50 - 300$ kΩ and the signal on each channel is amplified by 5000 and band-limited between 250 Hz and 7.5 kHz. Thresholds are dynamic and set to 3.25x the mean activity on each electrode and waveforms are sampled at 30 kHz for 1.5 ms windows. Recordings are displayed in real time (Figure 2.2C,D) and the waveform of each neural event is stored for later analysis by a comprehensive software system from Cyberkinetics.

When the array is inserted, not every channel records reliable neural activity. Inevitably, the size of the array coupled with the curvature of the brain places some electrodes over a blood vessel or sulcus. However, the majority of electrodes do record neural activity and these channels are processed with a MATLAB-based spike-sorting program to remove noise and artifact (Shoham et al 2003). The program implements a mixture decomposition algorithm based on the Expectation-Maximization (EM)

A.

B.

C.

D.
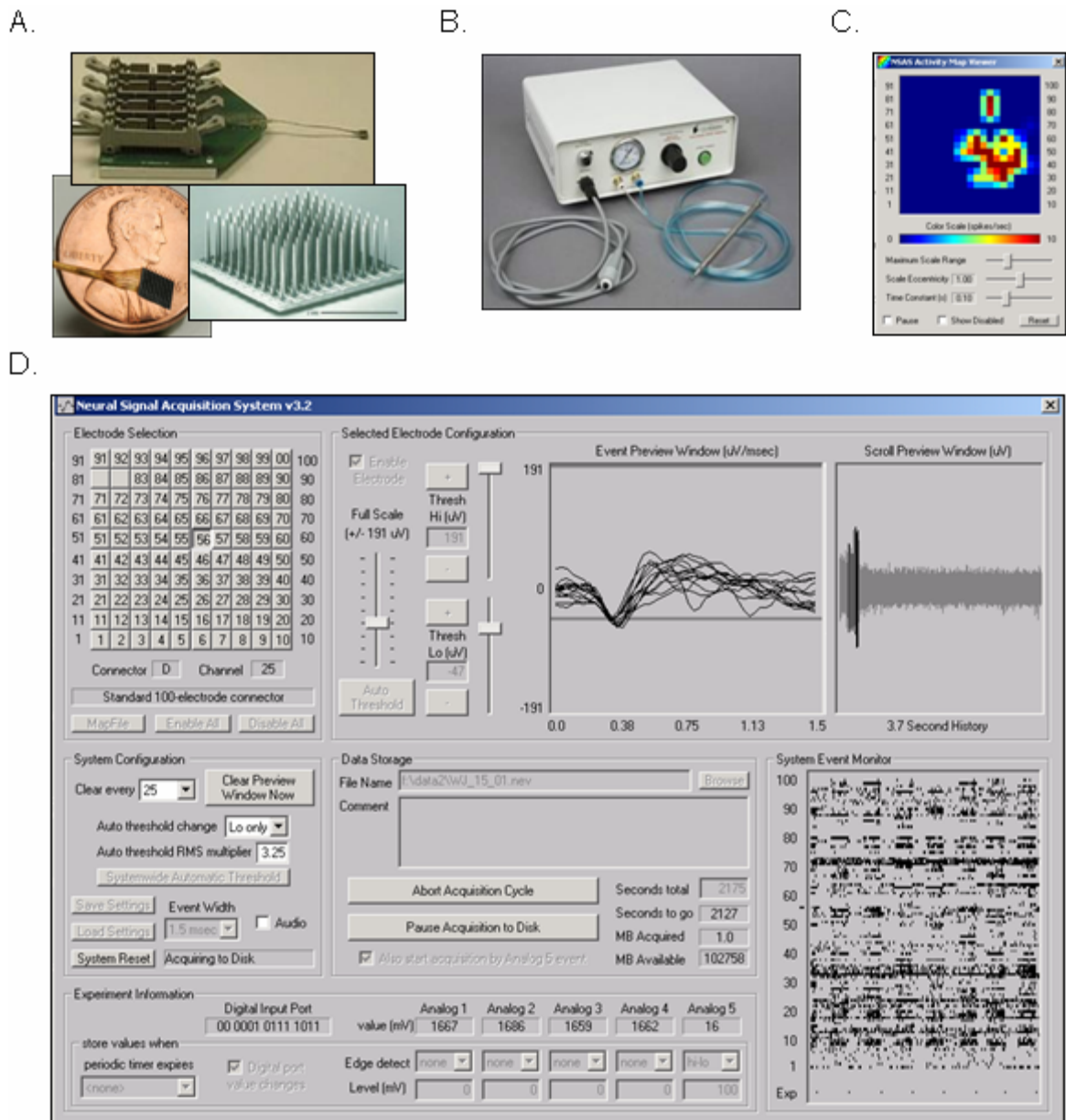
Figure 2.2. Components of the data recording and acquisition system. (A) Images of the 10x10 microelectrode array. (B) Pneumatic implantation tool. (C) Neural Activity Map displaying the spatial layout and magnitude of spiking activity from individual channels in the array. (D) Screen capture of the Neural Signal Acquisition System graphical user interface. A schematic of the array is located in the upper-left corner of the interface and individual channels can be disabled or selected for display in the event and scroll preview windows (upper-right). A graph in the lower-right corner shows a rastor plot of spike activity over time from all channels and also includes markers for stimulus presentations. This image was captured during drifting grating stimulation and note that the rastor plot shows the array activity is stimulus-locked as expected since V1 cells demonstrate orientation selectivity. (A) and (B) from www.cyberkineticsinc.com.

algorithm. Principle component analysis is used to generate a reduced feature set for each waveform and the distribution of waveforms from each source is modeled by a multivariate t-distribution (which utilizes the Mahalanobis metric for distance calculations). An EM algorithm is used to estimate the parameters of mixtures of multivariate t-distributions and clustering is optimized through the competitive elimination of components. We did not include multiple units that were recorded and resolved from a single channel. Approximately 5% of channels showed multi-unit activity and were discarded. Channels with isolated single-unit activity were used only if the activity was ≥ 5 spikes per second and showed clear orientation tuning (signal to noise ≥ 2:1) when viewing drifting sinusoidal gratings (Figure 2.3).

Determining Receptive Field Properties

In order to estimate receptive field properties during the experiment (as most of our analysis is offline), we used a short grating stimulation protocol to reveal orientation tuning preferences (Nishimoto et al. 2005), which were subsequently used during manual mapping of receptive field extent and location. Drifting sinusoidal gratings of varying orientation were presented in random order at 50% contrast, 0.5 cycles/° spatial frequency, and 2 Hz temporal frequency. An 18°x18° field was sufficient to drive all recorded cells simultaneously. We used 36 (18) drifting directions in 10° (20°) increments and 2 (1) blank presentations. Each stimulus was displayed through a circular aperture and presented for 2 seconds followed by 1 second of mean luminance background. We repeated the presentations 25 times and computed the average response properties offline. We then utilized a stimulator that projects spots or bars of light onto a large tangent screen for rapid manual characterization of classical receptive field size and
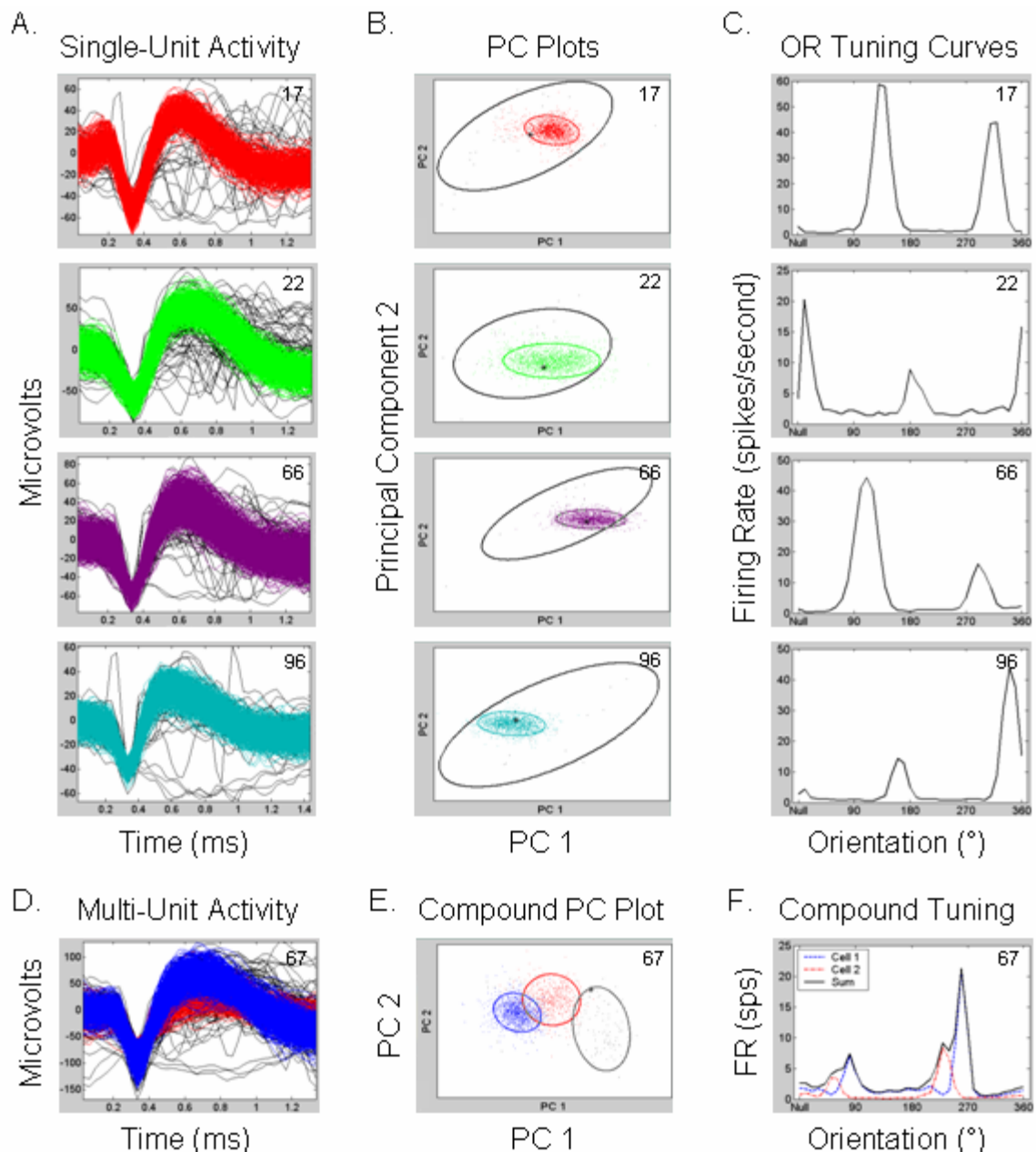
Figure 2.3. Examples of channel activity from the Utah Intracortical Electrode Array in response to sinusoidal grating stimulation. (A) Spike waveforms (color) and noise (black) from 5 typical channels (channel number denoted in upper-right corner). (B) Principal component plots for waveforms depicted in (A). (C) Orientation tuning curves derived from the waveforms in (A). These plots demonstrate good single unit isolation and tuning. (D) Example of a channel with multi-unit activity (in this case, waveforms from 2 cells were recorded on the same electrode). (E) Principal component plot for the waveforms in (D). (F) Compound tuning curve resulting from both cells in (D). Although it is possible to resolve single units on this channel (red and blue), we did not use any channels with multi-unit activity in our analysis.

location. The center of the aggregate receptive field was determined and used to align the stimuli to maximize neuronal responses from the majority of the recorded population. A longer grating experiment was performed after mapping for validation. Gratings were displayed for 2 (0.5) seconds followed by a 1 (0.5) second mean luminance interval and repeated 50, 100, or 150 times for reliability.

Most of the channels contained isolated complex cells from area 17. Although histology was not performed, the response properties, receptive field sizes, Horsley-Clark coordinates, and curvature of the brain suggest that most cells were from area 17 (and are consistent with similar experiments in the past in which histology was performed). The lateral portion of the array most likely enters area 18, but these channels account for less than 8% of the channel activity recorded (Samonds et al. 2006) and even less of the total number of cells actually used for analysis. Table 2.1 summarizes the number of cells analyzed from each experiment. Most cells are complex as determined by their relative modulation, F_1/F_0 (Hubel and Weisel 1962; Skottun et al. 1991).

Stimulation

We tested three different types of stimuli: drifting sinusoidal gratings, individual natural images, and natural image sequences. As mentioned above, gratings were used to estimate neuronal tuning properties. All stimuli were displayed on a gamma-corrected SONY Trinitron 21" monitor with a resolution of 800 x 600 pixels (22.6 pixels per visual degree) driven either by a Cambridge Research Systems VSG2/3F controller board (for gratings) or a video controller using the WinVis software package (for natural images and sequences). Displays were refreshed at 120 Hz, which avoided spike entrainment artifact at the cortical level (Wollman and Palmer 1995; Snider et al. 1996). We projected retinal

Table 2.1. Summary of each experiment. The weight of each subject and number of single units isolated and used for analysis are listed next to each experiment. The cells were classified as simple or complex based on their relative modulation, F_1/F_0 (Hubel and Weisel 1962; Skottun et al. 1991). The median relative modulation for each experiment is also listed.

Experiment	Weight (kg)	Isolated Single Units	Complex Cells	Simple Cells	Median Relative Modulation
MB_01	2.6	37	34	3	0.41
MB_02	2.4	34	31	3	0.17
MB_03	2.6	39	39	0	0.04
MB_04	2.3	42	41	1	0.21
MB_05	2.5	39	36	3	0.05
MB_06	2.8	18	18	0	0.06
MB_07	3.3	32	30	2	0.03
MB_08	4.0	45	41	4	0.11
MB_09	2.7	30	29	1	0.12
MB_10	2.3	47	42	5	0.15

features onto the tangent screen with a reversible ophthalmoscope to ensure all stimuli were displayed in reference to the area centralis. All stimuli spanned 18°x18° and appeared against a mean luminance background (73 cd/m^2). In each experiment, we also showed null stimuli which consisted of only the mean luminance background. All natural images were obtained from www.imageafter.com, converted to grayscale, and scaled to have a global contrast of 0.32 (see Touryan et al. 2005). All stimulus presentations were randomly interleaved.

Data Processing: Quantifying Synchrony

Microelectrode array technology allows for the simultaneous single-unit recording of dozens of neurons, but current analysis methods are unsuitable to accurately and completely describe cooperative population activity (Table 2.2). Perkel et al. (1967) introduced the cross-correlogram (CCG) to quantify cooperative relationships between pairs of neurons. However, CCGs and other techniques such as the Joint Peri-Stimulus Time Histogram (JPSTH; Aertsen et al. 1989) cannot characterize the synchrony between more than two cells. The CCG has been extended to include cooperation among three cells (Gerstein and Perkel 1972; Perkel et al. 1975; Abeles and Goldstein 1977), but the resulting display is limited to triangular coordinates and cannot be applied practically to larger assemblies. Other techniques such as gravitational clustering (Gerstein and Aertsen 1985; Gerstein et al. 1985) identify cells that fire together, but the results are qualitative, do not allow for dynamic grouping, and are still based on pair-wise distance calculations. Therefore, development of a new method was imperative to understand how synchrony and assembly formation contribute to the perception of our environment.

49

Table 2.2. Comparison of synchrony metrics: CCH (Perkel et al. 1967), JPSTH (Aertsen et al. 1989), gravitational clustering (Gerstein et al. 1985), information theory (Johnson et al. 2001), synchrony map (Samonds and Bonds 2004), and the PSP algorithm.

	CCH	JPSTH	Gravitational Clustering	Information Theory	Synchrony Map	PSP Method
Can be used for dynamic grouping?	✗	✗		✗	✗	✗
Quantitative?	✗	✗		✗		✗
Simple significance test?	✗			✗		✗
Reveals temporal dynamics?		✗	✗		✗	✗
Can be used for groups ≥ 2?			✗	✗	✗	✗
No binning?			✗			✗
Does not require pairwise calculations?					✗	✗

Current approaches quantify synchrony in the form of a relationship between two neurons. However, synchrony allows for the formation of transient functional groups which could include tens, hundreds, thousands, or even larger numbers of neurons so long as they fired simultaneously within some narrow time window. Pair-wise distance calculations increase exponentially as group size increases and can be computationally exhaustive for large assemblies. As a solution, we have developed a method that detects and quantifies the amount of correlated activity in a neuronal assembly of arbitrary size. As a hypothetical neural substrate for encoding salient stimulus properties, synchrony enhances the probability of eliciting postsynaptic action potentials (PSPs) when neurons behave as coincident detectors (Azouz and Gray 2003). This enhances propagation of the information to subsequent levels of the cortical hierarchy. Our basic algorithm is designed to reflect the relevance of group synchrony to postsynaptic neurons by modeling the temporal summation of postsynaptic potentials. In this measure, synchrony is computed as a fraction of total activity within an assembly and can be monitored dynamically throughout the stimulus presentation. The purpose of this method is to measure the timing similarity between neuronal spike trains. Neurons with similarly-timed events are considered synchronous and the magnitude of synchrony depends on the degree of similarity.

<u>*Step 1*</u>*: Convert spike waveforms (W_i) to point-process spike trains (C_i)*

If we assume that action potentials are instantaneous and indistinguishable, then only the timing of such events is sufficient to describe visual information. The activities recorded simultaneously from all neurons in a target assembly (N neurons with N_{TS} total spikes and N_{CS} coincident spikes, where coincident spikes

are defined as events that occur within the integration time period, 10 ms) are preprocessed to retain only spike initiation times, creating point-event spike trains ($C_i(t)$ is the spike train from neuron i). Spike trains for a given evaluation must have the same duration, L_S. Note that this does not imply that all spike trains have the same number of spikes. Stimulus repetitions are concatenated to form one long spike train which ensures that sweeps with firing activity, but no synchrony, effectively contribute a zero while sweeps without spikes (firing rate = 0 for all cells) are effectively skipped.
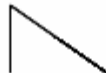
Step 2: Convolve point-process spike trains (C_i) with an alpha function to create PSP trains (P_i)

The comparison of simultaneous spike trains requires deriving a similarity measure that is conscious of time. This can be accomplished by convolving a point-event spike train, $C_i(t)$, with a PSP waveform, $W(t)$, that has area A.

$$P_i(t) = C_i(t) * W(t) = \int_t C_i(\tau)W(t-\tau)d\tau \qquad (2.1)$$

This yields a PSP train, $P_i(t)$. A PSP waveform is often approximated using an alpha function, but any waveform can essentially be chosen based on its desired Weight Function (see Table 2.3). For instance, an alpha waveform nonlinearly weights events so that spikes occurring closely in time are weighted more than those occurring towards the end of the integration time period. Alternatively, waveforms can be chosen to reflect linear or constant weighting schemes. For example, the JPSTH method (Aertsen et al. 1989) effectively uses a constant weighting scheme by binning. For all subsequent illustrations and analysis, a truncated (10 ms) alpha function will be used ($\tau = 1$ ms).

Table 2.3. This table shows different functions used to approximate a PSP waveform. The two-dimensional weight function (for pairs of spikes) for each waveform is shown in the last column, which is created by convolving two PSP waveforms. The alpha function uses a nonlinear weighting scheme that enhances the response of spikes occurring more closely together within the integration time period. Binning produces a constant weight function, which gives equal weight to all spikes within the integration time period. In this case, synchrony can be computed as the product of the number of coincident waveforms in an assembly multiplied by a constant weight.

Function	Waveform	Weight Function	Function	Waveform	Weight Function
Alpha Function $W(t) = A t e^{t/\tau}$			Exponential Function $W(t) = e^{-t}$		
Gaussian Function $W(t) = \dfrac{1}{\sigma \sqrt{2\pi}} e^{\frac{-(t-o)^2}{2\sigma^2}}$			Bartlett Function $W(t) = 1 - \dfrac{|t|}{A}$		
Step Function $W(t) = A u(t) - A u(t - \tau)$			Welch Function $W(t) = 1 - \dfrac{t^2}{A^2}$		
N_{CS}*Constant	N/A		Ramp Function $W(t) = -At + b$		

Step 3: Determine the time windows (t_s) during which all PSP trains (P_i) exhibit activity

Determine the timing of coincident events by noting the time periods (t_s) in which *all* trains exhibit spiking activity, i.e., intervals in which all PSP trains have a value greater than zero.

Step 4: Sum PSP trains (P_i) from all cells to get PSP activity for the entire assembly

To visualize the total amount of activity within an assembly, add PSP trains from all neurons.

$$Assembly\ Activity = \sum_i P_i \qquad (2.2)$$

Step 5: Integrate the assembly activity over t_s and t then divide to compute the Raw Score

The Raw Score is computed as the ratio of the area under the overlapped portion of coincident waveforms to the total area under all waveforms in the assembly. The total area is found by summing all PSP trains and then integrating the resulting waveform over all time (t). The synchronous area results from integration of the summed trains over just the time periods found in Step 3 (t_s). The Raw Score is the ratio of synchronous area to total area and represents the percentage of assembly activity that is synchronous. Alternatively, the total area can be computed by multiplying the area under one waveform, A, and the total number of spikes in the assembly, N_{TS}. The Raw Score is a number between 0 and 1. An assembly with a large Raw Score is comprised of neurons whose responses occur at similar times and are thus very synchronous.

$$Raw\ Score = \frac{\sum_{t_s} Assembly\ Activity}{\sum_t Assembly\ Activity} = \frac{\sum_{t_s} Assembly\ Activity}{AN_{TS}} \qquad (2.3)$$

Step 6: Compute Chance Score by shifting 1 or more stimulus periods and repeating Steps 1-5

The Chance Score is the percentage of waveforms expected to overlap by chance under the null hypothesis that all neurons in the assembly are firing independently. This value can be estimated by calculating the shift predictor (Perkel et al. 1967). Successive trials of stimulus presentations are shifted in time, which destroys any temporal relationships and preserves order-independent statistics. The Chance Score is computed by completing Steps 1-5 with spike trains that are shifted in time by the length of at least one stimulus trial compared to all other trains. This was found to be not significantly different (t-test, p > 0.05) than averaging the scores from all possible shift combinations in assemblies where $N = 2$. However, it is beneficial to perform this step a number of times with different shift combinations to build a distribution with which to statistically compare the Raw Score.

Step 7: Compute statistical significance and normalize the magnitude of synchrony

We use a one-tailed student's t-test ($\alpha = 0.01$) to compare the Raw and Chance Scores. A Normalized Score can be computed by subtracting the Chance Score from the Raw Score and renormalizing the resulting value so that Chance is assigned a value of 0 and synchrony among identical spike trains has a value of 1. A Normalized Score is independent of firing rate and scores greater than zeros represent the percentage of waveforms that are synchronous, but not due to chance from firing rate-induced modulation of synchrony. For instance, a Normalized Score of 0.5 means 50% of waveforms are synchronous beyond that expected by chance. Renormalizing the score ensures that assemblies with

55

different spike counts and Chance Scores can be compared and assemblies with identical spike trains have a Normalized Score of 1.

$$Normalized\ Score = \frac{Raw\ Score - Chance\ Score}{1 - Chance\ Score} \qquad (2.4)$$

Figure 2.4 depicts a graphical representation of the steps in quantifying the magnitude of synchrony. Although this method was developed to measure the temporal similarity of spike trains within an assembly and not to determine underlying functional anatomy (e.g. like the JPSTH, Aertsen et al. 1989), this method can reveal some aspects of effective connectivity. Individual Scores can be calculated by integrating each individual PSP train over t_s and dividing by the Raw Score. The resulting values represent individual contributions to the collective group synchrony. When using an asymmetric waveform like an alpha function in the PSP trains, this information can reveal whether some neurons tend to fire before or after others. Neurons with similar contributions reflect a shared input while uneven contributions reflect direct interactions. Although there are no assumptions about the underlying configuration of the network, these results can be compared to those from a known network configuration to determine whether they are consistent with a certain neuronal architecture.

$$Individual\ Score_i = \frac{\sum_{t_s} P_i}{\sum_t Assembly\ Activity} = \frac{\sum_{t_s} P_i}{AN_{TS}} \qquad (2.5)$$

The magnitude of synchronous activity is normalized so that a neural assembly with identical spike trains will yield a value of unity. Therefore, this quantity is a percentage of its maximum synchrony potential. Note that maximum potential is a conceptual, mathematical quantity and may not be possible to achieve in every assembly. The maximum synchrony potential occurs when all spikes within an assembly are

56
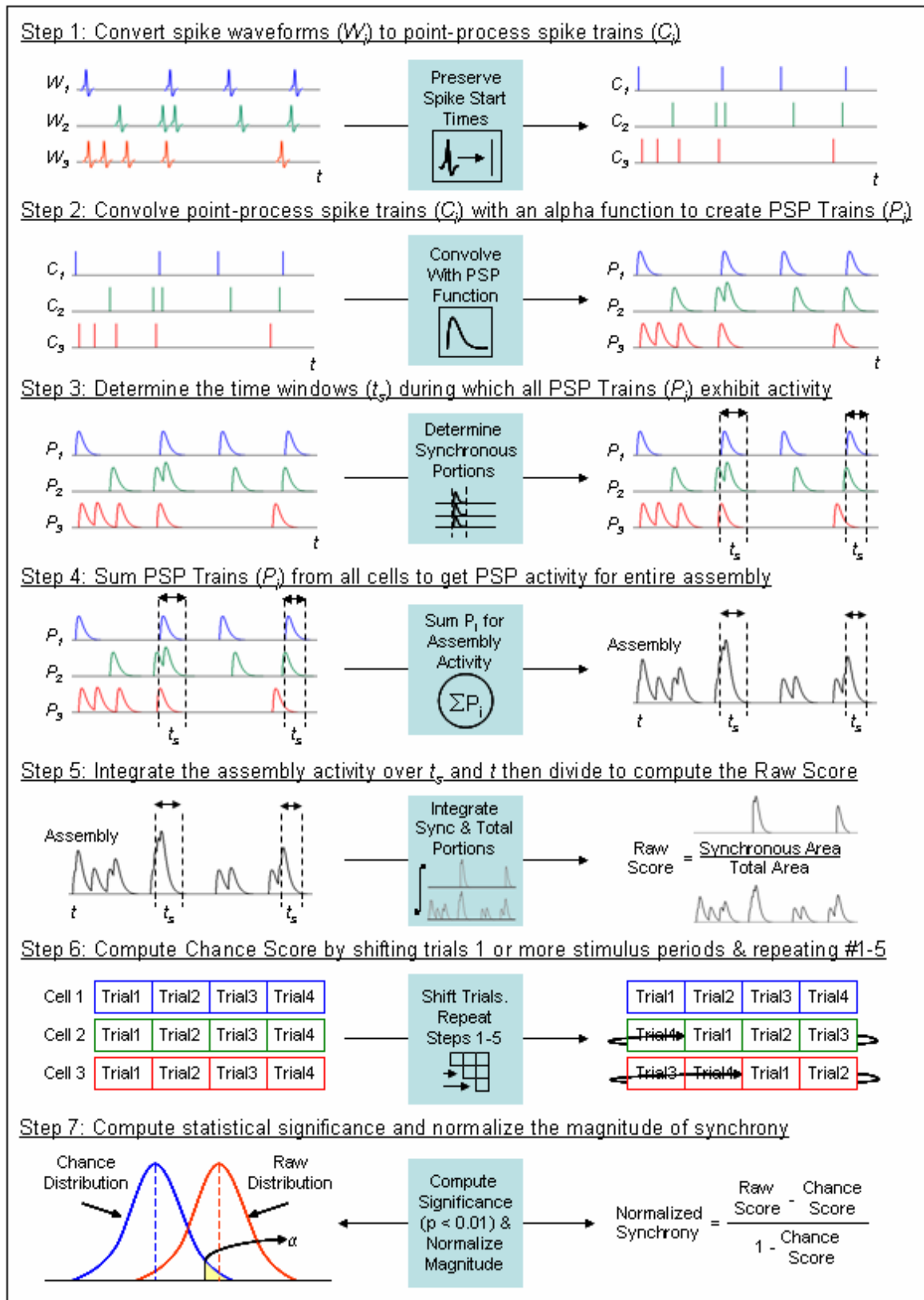
Figure 2.4. Steps in the PSP Method. We demonstrate with 3 neurons, but any number of cells (≥2) can be substituted. Multiple stimulus trials are concatenated.

completely synchronized. However, this may not be realistic if for instance, one non-bursting cell (A) has 25 spikes and another non-bursting cell (B) has 75 spikes (N = 2). This pair cannot achieve their maximum potential to obtain a score of 1 (100 spikes synchronized). Therefore, their highest score (with 50 synchronized spikes – 25 from each cell) is a fraction of their maximum potential (50/100 or 0.5). (Note that bursting could increase the score since two partially overlapping spikes from cell B could coincide with one spike from cell A.)

Figure 2.5 shows the PSP algorithm as it unfolds for an assembly of four cells. While viewing a 260° drifting sinusoidal grating (Figure 2.5A), 4 cells (preferred orientations: 260°, 260°, 260°, and 240°) synchronized their responses. Their individual scores (Figure 2.5B) show a distributed level of synchronization implying a common input triggered by the spatial coherence of the stimulus. The time course of the response for each cell is illustrated in Figure 2.5D. The top four plots are the PSP trains for each neuron followed by the raw (0.0348), chance (0.0061), and normalized synchrony (0.0289) plots extracted from those trains. As demonstrated in this example, the amount of correlation estimated from firing rate effects is small and becomes negligible for larger assemblies.

Discussion

By convolving a point-event spike train with a truncated (10 ms) alpha waveform, we derive a similarity measure that is conscious of time. PSP trains for a group of cells can be summed and compared to identify spike times that are coincident. The magnitude of synchrony is computed as the ratio of the area under coincident waveforms to the total area under all waveforms in the assembly. Unlike other approaches, this can be applied
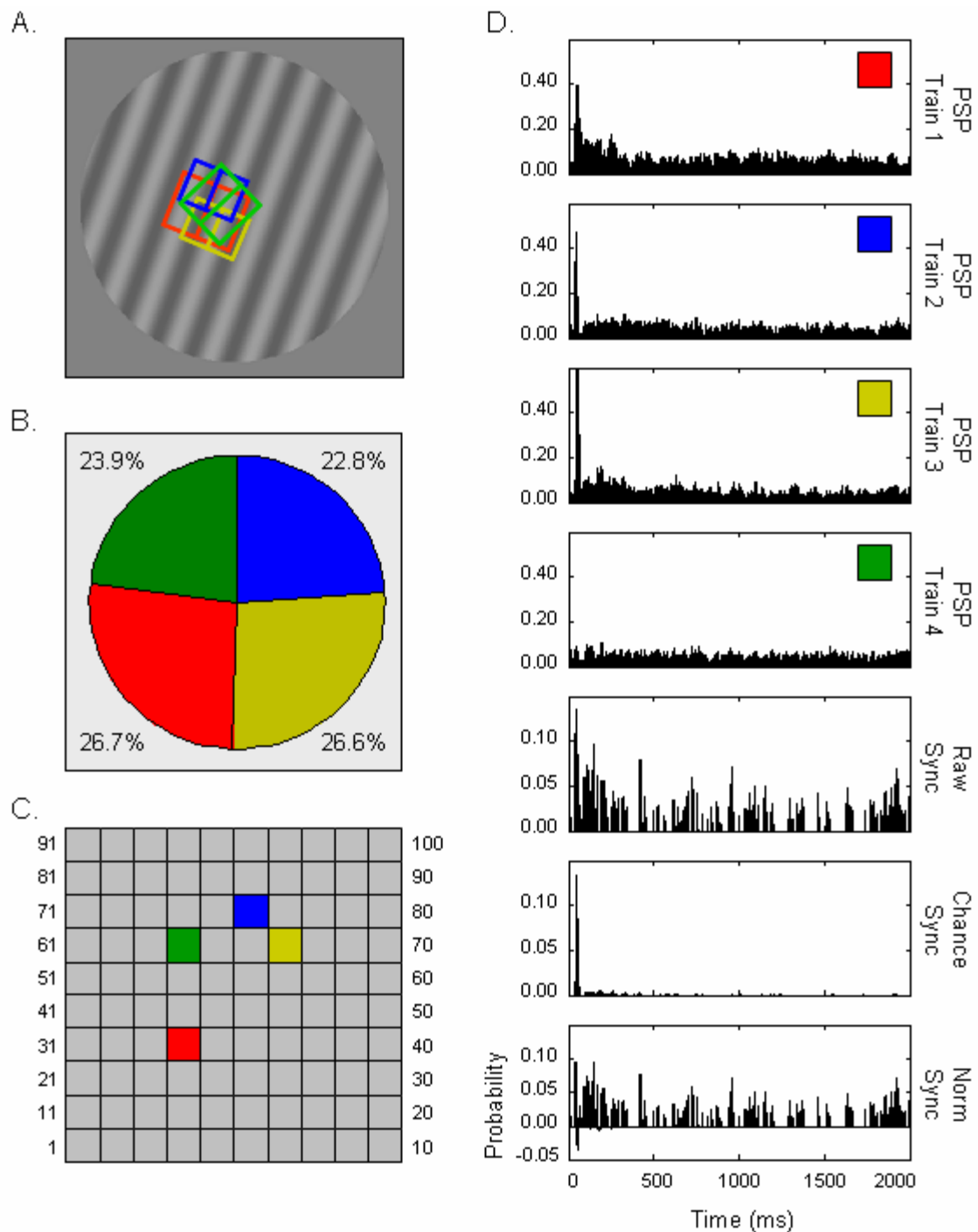
Figure 2.5. Example illustration of temporal dynamics for an assembly of 4 neurons. (A) Each cell's receptive field and preferred orientation are superimposed on the stimulus, a 260° grating. (B) Position of each cell on the microelectrode array with each color corresponding to the same color cell in (A). (C) Individual contributions to synchrony for each cell. (D) Time course of the response for each cell during the stimulus presentation. The top four plots are the PSP trains for each neuron followed by the raw, chance, and normalized synchrony plots extracted from those trains.

to neural assemblies of arbitrary size, not just pairs. This algorithm also selectively emphasizes spikes that occur closely in time instead of treating all spikes within the integration time period as equally important events. By using the shift predictor (Perkel et al 1967), we can resolve and separate sources of synchrony in order to normalize our results for the effects of firing rate. The uncertainties of normalization and firing rate dependence are minimized due to the very large ratios seen between chance and observed probabilities of synchrony as group sizes grow.

This method is advantageous because: (1) it can be applied to an arbitrary number of cells and computation time increases linearly with the number of cells involved; (2) waveform parameters like PSP amplitude, integration time and threshold are adjustable; (3) the temporal dynamics of synchrony can be monitored throughout the stimulus presentation; (4) we can normalize synchrony scores by subtracting the shift predictor to associate coordinated events with specific sources of synchrony (For instance, firing rate effects can be removed and the analysis can focus on synchrony from only endogenous sources.); (5) members of large groups can be predicted from the scores of smaller groups, thus drastically reducing the number of assembly permutations that need to be computed; (6) no binning or smoothing techniques are required; (7) this method is based on biological principles and the results are physically meaningful (i.e., a raw score of 0.15 means that 15% of all waveforms in an assembly were coincident). The flexibility of this approach allows us to investigate the effects of increased/decreased integration times, examine group characteristics, and decipher trends correlated with group size. In order to understand group dynamics and document rules governing group membership, we can use this method to measure collective responses and explore temporal characteristics of neural assemblies. And although we are investigating synchronous

activity in the visual system, this method can be applied to other sensory modalities in any creature in which more than one neuronal spike train is recorded. Synchrony has been observed in the olfactory, auditory, and somatosensory systems and is found in the hippocampus, frontal cortex, and motor system (for review see Engel et al. 1999).

References

Abeles M. and Goldstein M. Jr. Multiple spike train analysis. *Proc. IEEE*, 65:762 -773, 1977.

Aertsen AMHJ, Gerstein GL, Habib MK, and Palm G. Dynamics of neuronal firing correlation: Modulation of "effective connectivity". *J. Neurophysiol.*, 61:900-917, 1989.

Azouz R and Gray CM. Adaptive coincidence detection and dynamic gain control in visual cortical neurons in vivo. *Neuron,* 37:513-523, 2003.

Buzsaki G. Large-scale recording of neuronal ensembles. *Nat Neurosci.* May;7(5):446-51, 2004.

Engel AK, Fries P, Konig P, Brecht M, and Singer W. Temporal binding, binocular rivalry, and consciousness. *Conscious Cogn.* 8:128-151, 1999.

Gerstein GL and Aertsen AMHJ. Representation of cooperative firing activity among simultaneously recorded neurons. *J. Neurophysiol*. 54:1513-1528, 1985.

Gerstein GL, Perkel DH, and Dayhoff JE Cooperative firing activity in simultaneously recorded populations of neurons: Detection and measurement. *J. Neurosci.*, 5:881-889, 1985.

Gerstein GL and Perkel DH Mutual temporal relationships among neuronal spike trains. Statistical techniques for display and analysis. *Biophys. J.* 12:453-473, 1972.

Hayek FA. *The Sensory Order*. Chicago: University of Chicago Press, 1952.

Hebb DO. *The Organization of Behavior: a Neuropsychological Theory.* New York: Wiley, 1949.

Hubel DH and Wiesel TN. Receptive fields, binocular interaction and functional architecture in the cat's visual cortex. *J Physiol* 160: 106–154, 1962.

Kelly RC, Smith MA, Samonds JM, Kohn A, Bonds AB, Movshon JA, and Lee TS. Comparison of recordings from microelectrode arrays and single electrodes in the visual cortex. *J Neurosci.* Jan 10;27(2):261-4, 2007.

Milner P. A model for visual shape recognition. *Psychol. Rev.,* 81: 521-535, 1974.

Milton JG and Mackey MC. Neural ensemble coding and statistical periodicity: speculations on the operation of the mind's eye. *J Physiol Paris.* Sep-Dec;94(5-6):489-503, 2000.

Nishimoto S, Arai M, and Ohzawa I. Accuracy of subspace mapping of spatiotemporal frequency domain visual receptive fields. *J Neurophysiol.* 93:3524-3536, 2005.

Perkel DH, Gerstein GL, and Moore GP. Neuronal spike trains and stochastic point processes, II. Simultaneous spike trains. *Biophys. J.* 7:419-440, 1967.

Perkel DH, Gerstein GL, Smith MS, and Tatton WG. Nerve-impulse patterns: a quantitative display technique for three neurons. *Brain Res.* 100:271-296, 1975.

Pouget A, Dayan P, and Zemel R. Information processing with population codes. *Nat Rev Neurosci.* Nov;1(2):125-32, 2000.

Rousche PJ and Normann RA. Chronic recording capability of the Utah Intracortical Electrode Array in cat sensory cortex. *J. Neurosci. Methods* 82:1-15, 1998.

Rousche PJ and Normann RA. A method for pneumatically inserting an array of penetrating electrodes into cortical tissue. *Annals of Biomed. Eng.*, 20:413-422, 1992.

Samonds JM, Zhou Z, Bernard MR, and Bonds AB. Synchronous Activity in Cat Visual Cortex Encodes Collinear and Cocircular Contours. *J. Neurophysiol.* 95:2602-2616, 2006.

Schmidt S, Horch K, and Normann RA, Biocompatibility of silicon-based electrode arrays implanted in feline cortical tissue. *J. Biomed. Mater. Res.* 27:1393-1399, 1993.

Shoham S, Fellows MR, and Normann RA. Robust, automatic spike sorting using mixtures of multivariate t-distributions. *J Neurosci Methods.* 127:111-122, 2003.

Skottun BC, De Valois RL, Grosof DH, Movshon JA, Albrecht DG, and Bonds AB. Classifying simple and complex cells on the basis of response modulation. *Vision Res.* 31(7-8):1079-86, 1991.

Snider RK, Kabara, JF, Roig BR, and Bonds AB. Synchronous entrainment of cat striate cortical neurons to display refresh rates. *Invest. Ophth. and Vis. Sci.* Suppl. 37, #2187, 1996.

Touryan J, Felsen G, and Dan Y. Spatial structure of complex cell receptive fields measured with natural images. *Neuron*. Mar 3;45(5):781-91, 2005.

von der Malsburg C. The correlation theory of brain function. *Internal Report, Max-Planck Institute for Biophysical Chemistry*. Goettingen, Germany, 1981.

Wollman DE and Palmer LA. Phase locking of neuronal responses to the vertical refresh of computer display monitors in cat lateral geniculate nucleus and striate cortex. *J. Neurosci. Methods* 60:107-113, 1995.

CHAPTER III

EVOLUTION OF NEURONAL SYNCHRONIZATION ACROSS
CORTICAL SPACE AND TIME

Introduction

Neurons in the striate cortex exhibit an enhanced specialization beyond that found in earlier visual areas by responding selectively to stimulus parameters such as spatial frequency, orientation, direction, and disparity. This selectivity allows cells to behave as filters for different stimulus dimensions and since these cells cover the range of parameter values to which the visual system is sensitive, their activity is sufficient to encode each stimulus attribute. Relative to behavioral visual performance, each cell is broadly tuned and tasks such as contour integration and object recognition undoubtedly involve the cooperation of numerous cells with various spatiotemporal filter characteristics. One way to assemble these simple feature detectors is through the precise firing of action potentials on a millisecond timescale (Singer and Gray 1995), which can be discriminated by target cells acting as coincident detectors (Azouz and Gray 2003; Bruno and Sakmann 2006). As a distributed population code, synchrony momentarily enhances the transmission probability of an assembly and this linking is strengthened by repetitions throughout the stimulus duration. Synchrony allows for neurons to be effectively connected into a functional unit and the combinatorial possibilities offer tremendous stimulus-encoding capabilities.

Unfortunately, the term *synchrony* in this context has been interpreted to mean a number of different neurophysiological phenomena. Synchrony has been referred to as the 0 ms correlation between two single-unit responses (e.g. Samonds et al. 2006), two

64

multi-unit responses (e.g. Roelfsema et al. 2004), or the coherence of firing rate

oscillations in single units (e.g. Zhou et al. 2008) or multiple units (e.g. Womelsdorf et al.

2007). Depending on the electrophysiological recording method, oscillations and their

synchrony can be studied at different levels of brain organization (Ford et al. 2007): (1) in

single-unit recordings, continuous firing in a spike train can be resolved into a component

frequency; (2) in multi-unit recordings; (3) in recordings of local field potential; and (4)

in electroencephalogram recordings. With the covariation of firing rates, synchrony can

be measured as the height of a cross-correlation histogram peak among cell responses

regardless of oscillation frequency or refer to the degree to which responses are in phase.

Furthermore, the term *synchronization* has also been used to describe neuronal responses

that are stimulus-locked and modulate with changing stimulus conditions.

Most of what we know about "synchrony" is from research on multi-unit activity

or oscillations of multi-unit activity. Synchrony and oscillations have been postulated as

neural encoding mechanisms because they are stimulus-dependent (Singer and Gray

1995; Neuenschwander and Singer 1996; de Charms and Merzenich 1996) or depend on

the behavioral state of the animal (Abeles et al. 1993; Murthy and Fetz 1992). However,

little has been done to disambiguate synchronization and oscillations although the two are

inherently different and have independent origins (Samonds and Bonds 2005; Roelfsema

et al. 2004). Samonds and Bonds (2005) showed that oscillations in the gamma

frequency range are not needed to generate synchrony between pairs of cells, but can help

strengthen and sustain it.

The goal of this paper is to provide information on the characteristics of neuronal

synchronization between isolated single-units and to specifically illustrate the evolution

of synchrony across cortical space and time. Previously, this kind of effort would have

been impractical due to the immaturity of the field with regard to measuring and analyzing multiple simultaneous responses from single-units. There have been no adequate metrics developed that monitor the temporal dynamics of synchrony in large assemblies throughout an entire stimulus presentation. Modern microelectrode array technology now allows us to study the spatial extent of synchrony by sampling simultaneous spike trains from different areas of cortex within V1. To move beyond pairwise comparisons and take advantage of our recording capabilities, we developed an algorithm for quantifying the amount of synchrony in a neural assembly of arbitrary size. This data processing method measures the raw and firing rate-induced components of synchrony and can be used to document synchronous interactions over time.

We used these measurement and analysis tools to study the synchrony and average firing rate responses of assemblies of up to six cells in paralyzed and anesthetized cats during stimulation with natural images. Synchrony between pairs of cells decreased linearly with distance across the striate cortex, but still existed in significant amounts for cells that were separated by up to 3 mm. The average amount of synchrony declined as the difference in orientation between cells increased, but could still be found between cells with wholly different orientation preferences (< 80°). We investigated the effects of stimulus presentation style and found that jittering stimuli in random directions about the origin produced the same amount of synchrony as that obtained during the most generous drift direction and that moderate amounts of synchrony were still observed during presentation of static stimuli. The temporal analysis showed that most synchrony is generated during the onset transient and reaches a stable value after approximately 800 ms. Finally, an assessment of normalizing synchrony responses to eliminate firing rate effects reveals that the correction is moot for

assemblies with four or more cells. These results provide insight into the underlying

mechanisms of synchrony and suggest that precise timing within assemblies could serve

as a practical platform for contour detection and transmission of salient information.

Materials and Methods

Preparation

Two adult cats were prepared for electrophysiological recordings in V1. All

procedures were performed in accordance with guidelines set forth by the American

Physiological Society and the Institutional Animal Care and Use Committee at

Vanderbilt University. Prior to surgery, each cat received intramuscular injections of 0.5

ml acepromazine maleate (10 mg/ml), 0.5 ml atropine sulfate (0.4 mg/ml), and 0.25 ml

dexamethasone sodium phosphate (4 mg/ml). Anesthesia was induced with 5%

halothane in O_2 and maintained with intravenous injection of Propofol (0.3 mg/kg hr).

During recording, paralysis was induced with 6 mg pancuronium bromide and maintained

through intravenous injection (Pavulon; 0.3 mg/kg hr). The cats were artificially

ventilated with a mixture of N_2O, O_2, and CO_2 (75:23.5:1.5) to hold expired pCO_2 at

3.9%. Rectal temperature was maintained at 37.5° C with a servo-controlled heating pad.

Data Recording and Acquisition

Simultaneous single-unit recordings were made from cells in the striate cortex via

the Utah Intracortical Electrode Array (UIEA; Cyberkinetics Neurotechnology Systems,

Foxborough, MA). The UIEA recordings have good signal to noise ratios and have been

shown to have qualities comparable to those from single-electrode recordings (Kelly et

al. 2007). The implant is a square 10x10 silicon array on 400 micron centers. The electrodes have a length of 1.0 mm and were inserted to a depth of 0.6 mm with a pneumatic implantation tool (Rousche and Normann, 1992). The insertion depth concentrated the electrodes in layers II/III and avoided impact to the cortical surface by the electrode base. Thresholds were dynamic and set to 3.25x the mean activity on each electrode and waveforms were sampled at 30 kHz for 1.5 ms windows. A MATLAB-based spike-sorting program was used to remove noise and artifact from each channel (Shoham et al. 2003). We did not include multiple units that were recorded and resolved from a single channel. Channels with multi-unit activity were discarded. Channels with single-unit activity were used only if the activity was $\geq$ 5 spikes per second and showed clear orientation tuning when viewing drifting sinusoidal gratings (Figure 3.1A).

Stimulation

We tested two different types of stimuli: drifting sinusoidal gratings and individual natural images. Gratings were used to estimate neuronal tuning properties. All stimuli were displayed on a gamma-corrected SONY Trinitron 21" monitor driven either by a Cambridge Research Systems VSG2/3F controller board (for gratings) or a video controller using the WinVis software package (for natural images). Displays were refreshed at 120 Hz, which avoided entrainment artifact (Wollman and Palmer, 1995; Snider et al. 1996). All stimuli spanned 18°x18° to ensure stimulation of both classical and non-classical receptive fields of the entire recorded population and appeared against a mean luminance background (73 cd/m^2). Each stimulus was presented for 2 seconds followed by a 1 second delay in which only the mean luminance background was shown.

68
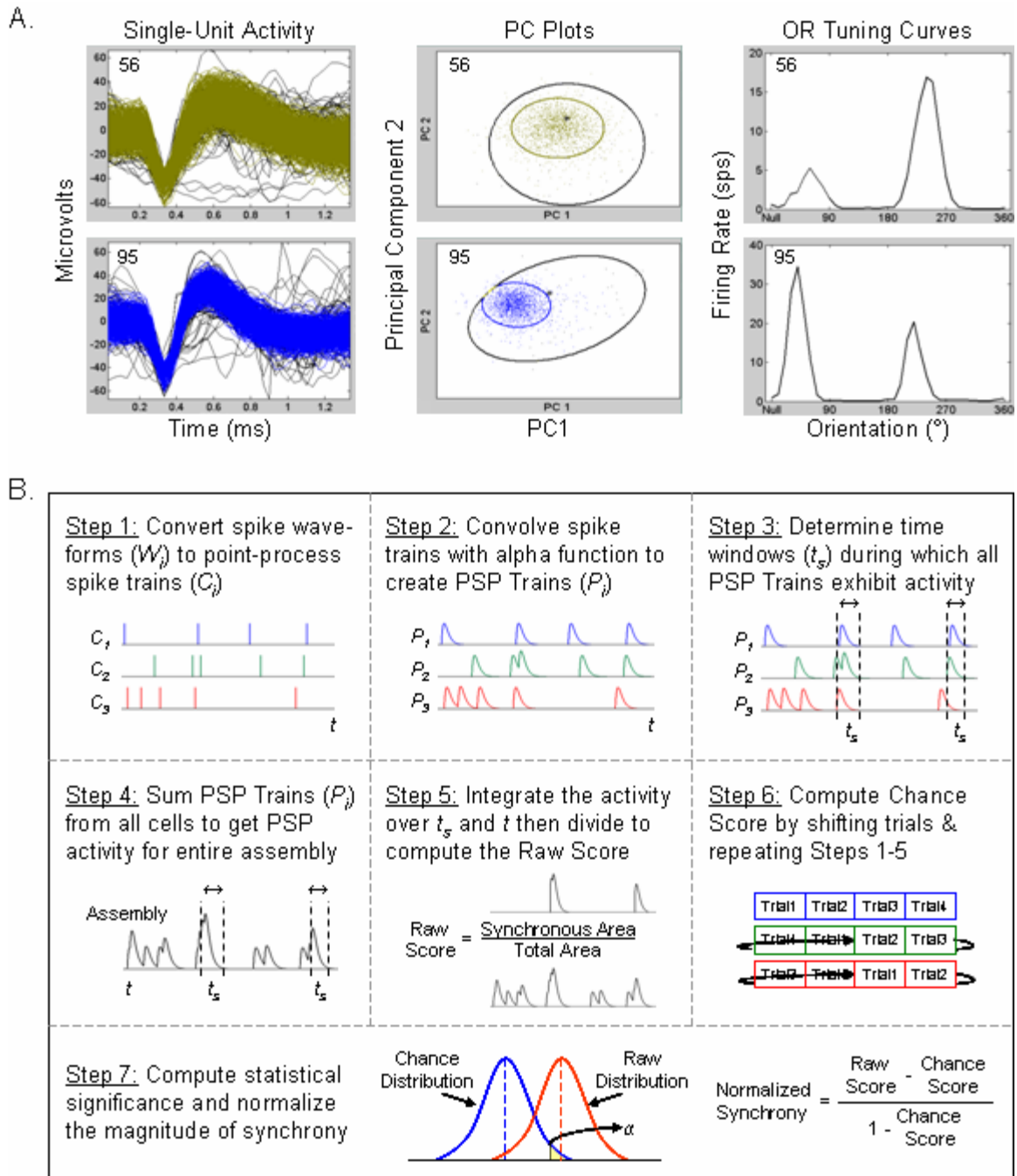
Figure 3.1. Quantification of synchrony. (A) Analysis was only performed on channels that exhibited good single-unit isolation and clear orientation tuning to drifting sinusoidal gratings. *Left*: waveforms (color) and noise (black) from two channels. *Middle*: principal component plots generated by the spike-sorting algorithm. *Right*: orientation tuning curves. (B) Steps in the PSP Method. Synchrony is defined as the ratio of overlapping activity among all cells to the total activity in the assembly. The contribution of synchrony due to firing rate effects is estimated with the Shift Predictor and subtracted from the Raw measure. Stimulus trials are concatenated to form one long initial spike train.

In each experiment, we also showed null stimuli which consisted of only the mean luminance background.

The stimulus protocol contained two natural grayscale images (Image 1: Fungus and Image 2: Leaf) from www.imageafter.com that were scaled to have a global contrast of 0.32 (see Touryan et al. 2005). We investigated four different presentation styles: drift (20° to 360° in 20° increments at a speed of 2°/s), random jitter in a web pattern (60 Hz), random jitter in a star pattern (like an asterisk, 60 Hz), and stationary (Figure 3.3A). The direction of jitter step in a web pattern is random and the step size and therefore speed are not constant. In a star pattern, the direction of jitter step is also random, but followed by the opposite step to place the image back at the origin. In this pattern, jitter step and speed are constant. For both jitter motions, we also varied the size of the jitter step 3 to 9 pixels (< 0.4°). All presentations were randomly interleaved and repeated 100 times for reliability.

Data Processing

To quantify cooperation within multi-cell assemblies, we used the PSP Method as described in the previous chapter. By convolving a point-event spike train with a truncated (10 ms) alpha waveform (yielding a PSP train), we derived a similarity measure that is conscious of time. PSP trains for a group of cells were summed and filtered to identify spike times that were coincident. The magnitude of synchrony was computed as the ratio of the area under coincident waveforms to the total area under all waveforms in the assembly. The use of an alpha function selectively emphasizes spikes that occur closely in time instead of treating all spikes within the integration time period as equally important events. By using the shift predictor (Perkel et al. 1967), we resolved and

separated sources of synchrony in order to normalize our results for the effects of firing rate. The uncertainties of normalization and firing rate dependence were minimized due to the very large ratios seen between chance and observed probabilities of synchrony as group size grows.

Our basic algorithm reflects the relevance of group synchrony to postsynaptic neurons by modeling the temporal summation of PSPs.   Neurons with similarly-timed events are considered synchronous and the magnitude of synchrony depends on the degree of similarity. The steps in this algorithm are as follows (Figure 3.1B):

Step 1: Preprocess data to convert spike waveforms to trains of point events

Step 2: Convolve with PSP waveform to generate PSP trains

Step 3: Determine synchronous portions of PSP trains

Step 4: Obtain assembly activity by summing PSP trains

Step 5: Calculate Raw Score

Step 6: Use Shift Predictor to calculate the Chance Score

Step 7: Compute Normalized Score and determine significance

We computed the statistical significance between the Raw and Chance distributions using a 1-tailed student's t-test with $\alpha = 0.01$.

Results

We used a 10x10 microelectrode array and the PSP algorithm to record from and subsequently analyze the responses of cell assemblies in the striate cortex of two paralyzed and anesthetized cats during natural stimulation. We quantified the amount of synchronous activity generated during different stimulus presentation styles (drift, jitter web, jitter star, and static) and compared the temporal dynamics of each assembly's

71

response to determine the influence of various motions. The preferred orientation pairings were tabulated across all stimulus conditions and the spatial extent of synchrony was mapped across the array. We also conducted a window analysis of synchrony to determine the time windows of greatest synchrony production and stability for all conditions. Finally, we resolved the observed raw synchrony into stimulus-locked and internally-generated components to compare the effects of normalization across assembly size.

We simultaneously recorded single-unit activity from 39 and 47 cells in two cats. The PSP algorithm quantifies the amount of synchrony in assemblies of arbitrary size, but requires the identification of all cells in the group so that specific spike train responses can be compared. Our previous studies with analytical stimuli suggest that cells with similar orientations and extensive receptive field overlap are likely to synchronize, but without precise knowledge of the relationship between stimulus and assembly response, there are no straightforward ways to extract functional groups for testing with the algorithm. Due to the high combinatorial dimensionality of cells from the population, there are endless membership possibilities. Assuming that only a small fraction of subsets in the population will synchronize to any given stimulus, then the probability of randomly testing combinations of cells and finding a significant assembly is very low. Fortunately, we can take advantage of our definition of synchrony to test small groups of cells and effectively build larger assemblies from these. Our definition of synchrony requires participation from all cells in a selected group so all subsets of cells from that group must also synchronize. Essentially, members from larger assemblies can be predicted based on the Normalized Scores from smaller assemblies. We can compute a relatively low number of small assembly scores and progressively cluster cells that

synchronize well to create an assembly of arbitrary size that has a high probability of synchronizing. However, only the members are predicted, not their assembly behavior (Score). These large assemblies can then be entered into the PSP algorithm to determine if, in fact, their grouping is significant (to build larger assemblies from smaller ones, synchrony must exist *between* groups as well as *within* groups).

We used the PSP algorithm to compute the amount of synchronous activity among all pair-wise combinations of cells (N = 1822; 741 pairs from cat 1 and 1081 pairs from cat 2) and used those results to cluster cells into larger assemblies. We found a total of 282 pairs that had significant activity ($\alpha = 0.01$) during at least one condition for Image 1 and 338 pairs for Image 2. These pairs were clustered to suggest larger assemblies (n = 3, 4, 5, and 6) which were then tested with the PSP algorithm to determine statistical significance. We found N = 613 groups of 3, 584 groups of 4, 487 groups of 5, and 533 groups of 6 cells. These groups do not comprise the entire population of synchronous assemblies, but do represent an adequate sample. Groups of 6 cells or less provided ample activity and consistency to study trends during the analysis of temporal dynamics,

Spatial Evolution of Synchrony

Previous studies using simple stimuli have shown that synchrony and oscillations of firing rate in the gamma frequency range rapidly decrease with increasing cortical distance between electrodes (Das and Gilbert 1999; Nowak et al. 1995; Frien and Eckhorn 2000; Maldonado et al. 2000). These studies report a higher probability of measuring synchrony between pairs of neurons or recording sites with overlapping receptive fields and/or similar orientation preferences. Similarly, the first neurophysiological experiments linking synchrony and feature integration used drifting

73

light bars (Eckhorn et al. 1988; Gray et al. 1989). This type of coherent collinear stimulation yielded synchrony between pairs of neuron clusters with similar orientation preferences and collinear receptive fields. Whether this pattern of cooperation was inherent to synchrony (e.g. due to anatomical connections) or was a direct consequence of the spatial organization of the stimulus was unknown. Since collinearity is a special case of the more general property of cocircularity (Parent and Zucker 1989), we used drifting concentric rings to see if synchrony predictably existed for pairs of cells with different orientation preferences, but whose receptive fields still had cocircular alignments (Samonds et al. 2006). A positive finding would be consistent with the association field framework (Field et al. 1993; Hess et al. 2003), which predicts linking between orientation-tuned cells that is dependent on their joint relative orientation and spatial position. We found that neuron pairs synchronized based on an appropriate match between stimulus curvature and receptive field configuration despite wholly different preferences in orientation.

Studies using collinear stimulation restricted the type of cell pairings among which synchronous activity was observed. Our cocircular study (Samonds et al. 2006) expanded this result to additional cellular interactions and although cocircular structures are ubiquitous in natural scenes (Geisler et al., 2001; Sigman et al., 2001; Elder and Goldberg, 2002), drifting sinusoidal concentric rings only represent a limited class of visual structures. To extend these findings further yet, we measured the preferred orientation pairings and spatial extent of synchrony across the striate cortex in response to natural stimulation (Figure 3.2). (How synchrony depends on receptive field proximity, receptive field overlap, and curvature is described in Chapter 5.)

For each channel in the microelectrode array with isolated single-unit activity, we
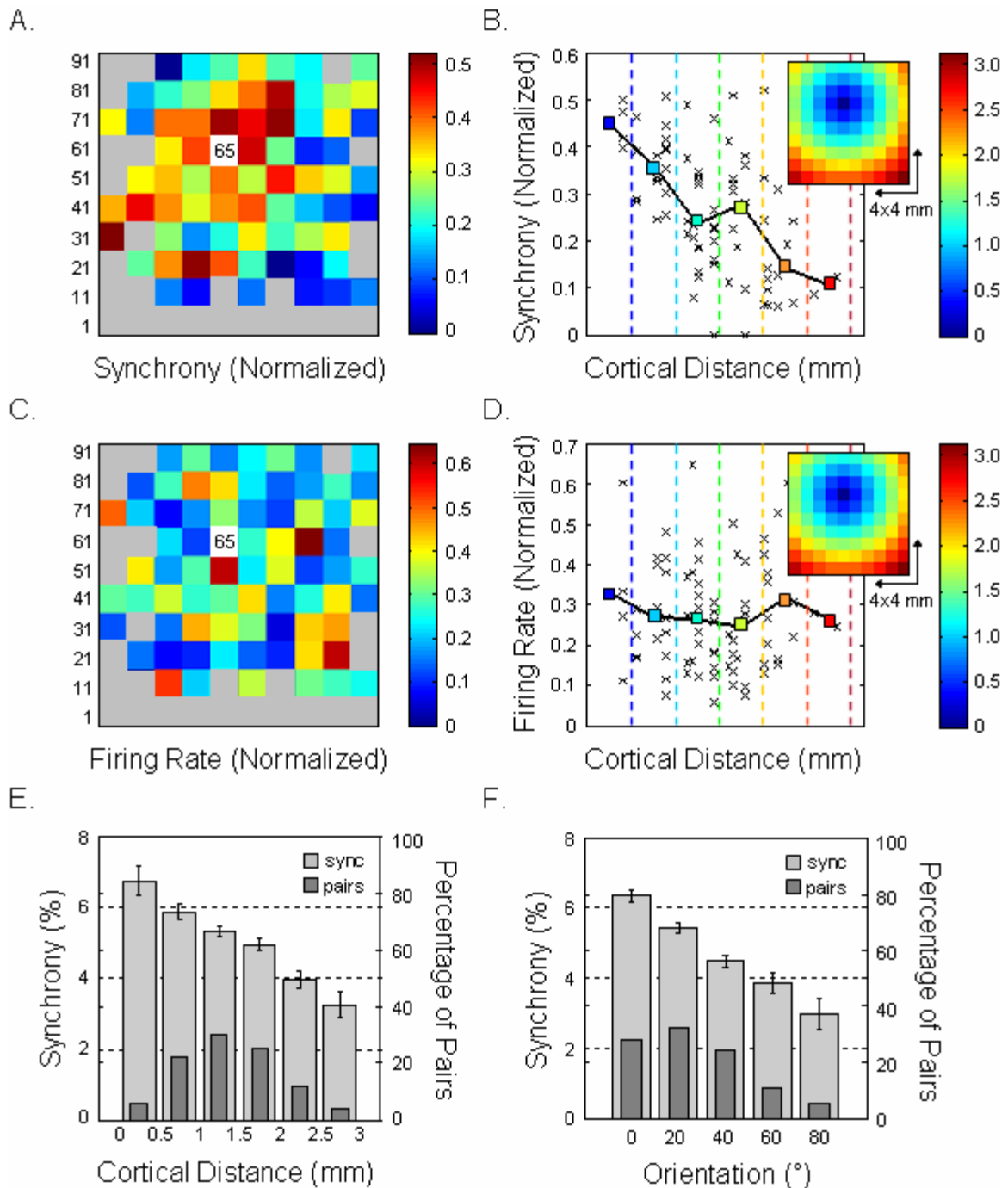
Figure 3.2. Spatial evolution of synchrony. (A) Synchronous pairings for channel 65 across the array. (B) Individual synchrony values from (A) and their means plotted against cortical distance (Euclidean distance between electrodes). Significant scores were extracted from all stimuli and averaged for each pair. We combined array plots from 2 experiments (normalized to the max in each case) to visualize coverage of the cortex. (C) Average firing rate for individual neurons. (D) Values from (C) plotted against cortical distance. (E) Synchrony and number of pairs vs. cortical distance and (F) orientation for N = 620 pairs (SE bars).

75

measured all pairwise interactions in which significant synchrony was observed. These values were averaged and mapped onto the array to visualize the extent of synchronization across the cortex. Figure 3.2A shows the pairings for channel 65 across the array. The synchrony between channel 65 and all other channels was calculated with the PSP algorithm and significant scores were averaged across all conditions from both images over both experiments. For example, if responses from channels 65 and 66 generated synchrony beyond that estimated by stimulus-induced firing rate effects in 10 conditions, these scores are averaged and placed in box 66. This map was unfolded radially to show the correlation between the strength of synchrony and Euclidean distance between electrode centers (Figure 3.2B). Synchrony scores were normalized to the maximum value for each experiment before being combined. For a comparison, average firing rates for each cell were plotted in the array (Figure 3.2C) and against distance (Figure 3.2D). This evaluation demonstrates that our synchrony measure has been normalized for firing rate effects and the largest synchrony scores are not necessarily generated among neurons with the highest firing rates. Again, firing rates were normalized to the maximum value for each experiment before being combined.

The average amount of synchrony measured across all pairs ($N = 620$) and the distribution of pairs are plotted against cortical distance in Figure 3.2E. The strength of synchrony decreased linearly over the extent of the microelectrode array, but significant synchrony was still measured between cells separated by up to 3 mm. The mode separation distance was 1.0-1.5 mm. Synchrony was plotted against the difference in preferred orientation among the pairs and also found to decrease linearly with greater angular differences (Figure 3.2F), but could be supported between cells aligned as much as 80° apart. The mode orientation difference in the population was 20°. These results

76

are similar to those obtained with cocircular stimulation (Samonds et al. 2006) and

support a neurophysiological correlate of the association field model (Field et al. 1993;

Hess et al. 2003).

Although a pairwise analysis was completed, a reasonable question would be to

inquire how these results would change for larger assemblies. One possibility is that

larger assemblies are fickle and require a more rigid relationship among members for

continued cooperation. In this case, perhaps assemblies would only synchronize for cells

with similar orientation preferences in closer proximities. However, the opposite was

found to be true. Synchrony can support larger assemblies over greater distances and

orientation preferences as long as the aggregate receptive field is stimulus-appropriate.

Larger assemblies still show this inverse relationship with synchrony across cortical

distance and orientation. Our pairwise analysis is for comparison with previous studies

and is easily illustrated on a two-dimensional map, but represents the building-block

relationships for larger assemblies. The orientation plot in Figure 3.2F shows the

difference in preferred orientation between pairs, but can also be interpreted as the

maximum preference difference in a large assembly (the plots are similar). The average

orientation difference in an assembly is an indication of the degree of curvature, which is

discussed in Chapter 5.

Stimulus Presentation Style

In their initial investigation of area 17, Hubel and Wiesel (1962) noted that a

moving stimulus was a powerful stimulus and some cells gave no response to a stationary

stimulus. Our subjects are paralyzed and anesthetized, so stimuli require motion for

neurons in the primary visual cortex to avoid adaptation and maintain their responses for

the entire stimulus duration. For artificial stimuli like gratings and concentric rings, unidirectional drift orthogonal to the axis of preferred orientation is commonly used. However, creating motion for discrete natural images is less straightforward. Drifting images causes features to pass through receptive fields, confounding the correlation between stimulus and neuronal response. Solutions to this problem include using a shorter stimulus duration or slower speed, both of which can be drawbacks. Also, since neurons in the striate cortex prefer motion in the direction perpendicular to their preferred orientation (Hubel and Weisel 1962), choosing a drift direction for gratings or bars is relatively simple. A natural image contains novel features that vary in their spatial properties making it difficult to determine the direction of optimal stimulation. Therefore, the image must be drifted in every direction to ensure optimal stimulation of the majority of cells in the population. Using multiple drift directions to find the best one can be time-consuming.

We wanted to see how synchrony and average firing rate compared when generated by drifting or jittering images. Jitter offers two main advantages over drift in that presentation times are drastically reduced and features are anchored within local receptive fields. And although the move towards conducting more neuroethological experiments is imperative to understanding the true neural basis of behavior, using natural or simulated natural movement is often impractical and some laboratory conditions or stimulation equipment limit the type of stimuli available for study. For instance, memory requirements in our computers and stimulator software package limit the presentation of large sequences of images to static displays. Therefore, we also studied the implications of using static stimuli for relatively short durations.

78

We measured the synchrony and average firing rate among assemblies of cells while viewing two natural images undergoing four different types of motion: drift (in 20° increments at a speed of 2°/s), random jitter in a web pattern, random jitter in a star pattern, and stationary (Figure 3.3A). The direction of jitter step in a web pattern is random and the step size and therefore speed are not constant. In a star pattern, the direction of jitter step is also random, but followed by the opposite step to place the image back at the origin. In this pattern, jitter step and speed are constant. For both jitter motions, we varied the size of the jitter step up to 9 pixels or 0.4° (step sizes of zero pixels were used as stationary stimuli). These results were tested in striate cortex and the jitter step size was appropriate relative to the typical receptive field extent, but this step may not be effective in higher visual areas where the receptive fields are larger.

Typical average firing rate (Figure 3.3B) and synchrony (Figure 3.3C) responses for two cells (with receptive fields and orientation preferences as indicated) are displayed across all motion conditions. For the drifting stimuli, each cell shows a tuning preference for 200°, which corresponds to the dominant features in the image. For both types of jitter motion, firing rate increases with jitter step size. For drift conditions, synchrony within this pair of cells shows a similar tuning preference and has a maximum value at 200° as expected. On the other hand, synchrony is relatively constant for jitter step size and appears more stable during the jitter star conditions. Synchrony during the optimal drift direction is similar to that obtained on average over the jitter conditions. In fact, a survey of all pairs (N = 620) shows this trend (Figure 3.3D). The average jitter synchrony is similar to the maximum drift synchrony. This also holds true for larger assembly sizes in which each group had significant synchrony during at least one condition (see groups of 2-4 in Figure 3.3D). More groups are revealed with the use of

79
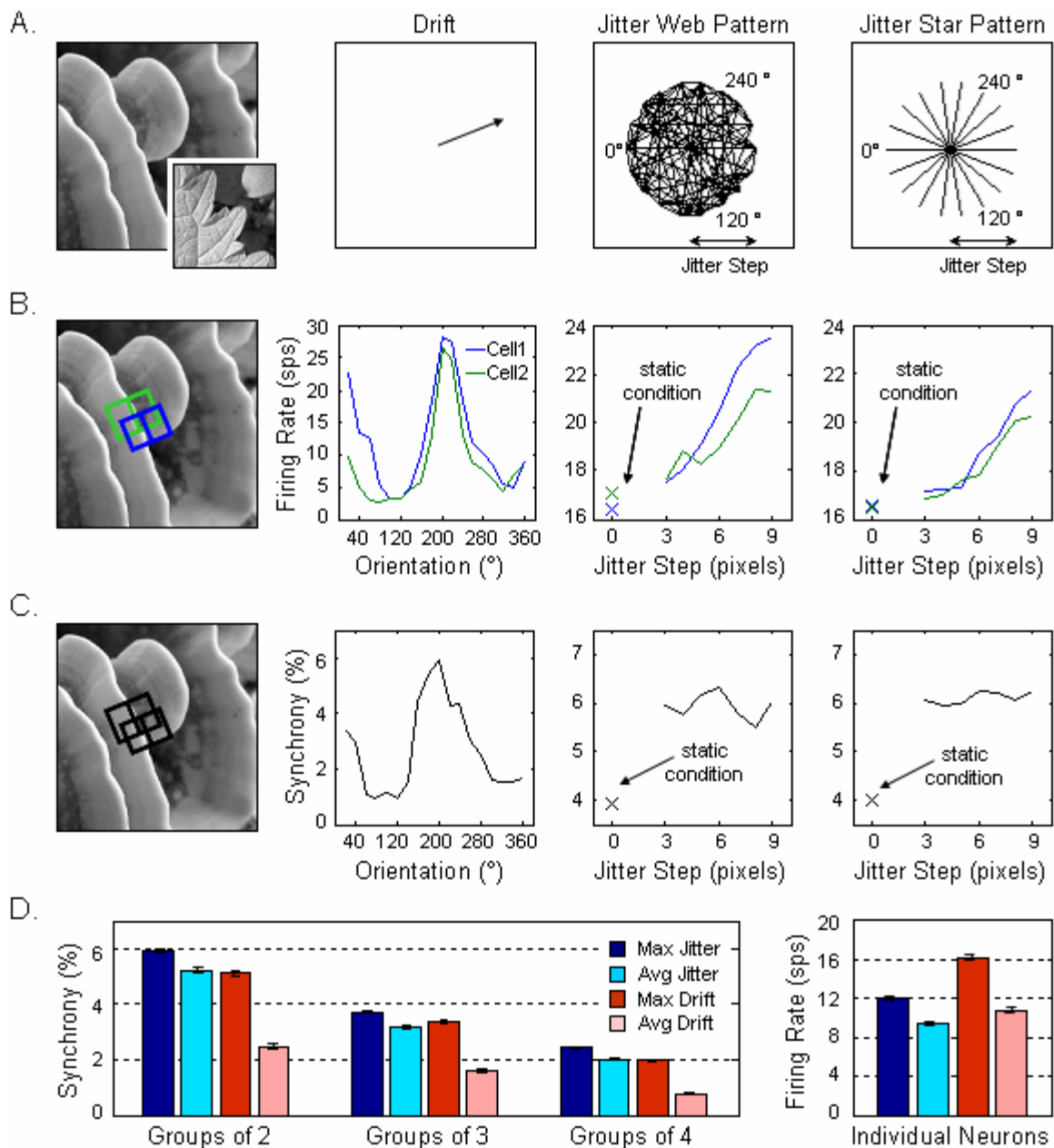
Figure 3.3. Analysis of stimulus presentation style. (A) Two natural images (left) were drifted and jittered in web and star patterns. The jitter step size is indicated with an arrow (0 pixels = static). (B) Firing rate for an example pair (whose receptive field and orientation preferences are displayed on the image) plotted against all stimulus conditions. (C) Synchrony between the pair in (B) for all stimulus conditions. (D) (Left) The maximum and average synchrony (SE bars) generated during all jitter and drift conditions plotted for 620 pairs, 613 groups of 3 cells, and 584 groups of 4 for the images in (A). Each assembly had significant synchrony during at least one condition. (Right) The maximum and average firing rate (SE bars) generated during all jitter and drift stimuli plotted for 86 neurons viewing both images in (A).

jitter, which corresponds to the presentation of the stimuli over all drift directions. Thus

for natural images, a sampling of all drift directions can be replaced by one jitter

condition, which drastically reduces the duration of the experiment or increases the

number of stimuli that can be tested.

These results suggest that synchrony is independent of jitter step size (< 0.4°) and

firing rate. Synchrony seems to be constant for features anchored within their receptive

fields despite temporal variations which affect the firing rate. Compared to the static

conditions, jittering an image by 5 pixels increased the firing rate by 74.2% while a step

of 5 pixels generated only 28.8% more synchrony. These results support our hypothesis

that synchrony is mainly generated from the spatial configuration of the stimulus. Using

jitter, synchrony is generated with a lower overall firing rate, which maintains the

signaling of structural salience while reducing metabolic demand.

Time Course Analysis

Over the past several decades, researchers have developed numerous methods to

quantify the interactions between neurons. Cross-correlation histograms (Perkel et al.

1967) have provided insight into the effective underlying neuronal architecture, but must

represent an average over many stimulus repetitions and the temporal dynamics the

cellular interaction cannot be resolved. To examine the temporal dynamics of neuronal

firing correlation, the idea of a joint peri-stimulus time (JPST) scatter diagram was

introduced (Gerstein and Perkel 1969; 1972). Aertsen et al. (1989) developed methods to

quantify and normalize the JPST scatter diagram. These new procedures allowed the

separation of raw correlation into correlation caused by direct stimulus effects and

correlation caused by interaction between the two neurons. Unfortunately, this procedure

is designed to measure interactions between pairs and cannot be applied practically to larger assemblies. In order to investigate the cooperative activity of assemblies with more than two neurons, the gravitational clustering algorithm was introduced, which characterizes the time-varying organization and extent of neural assemblies (Gerstein et al. 1985; Gerstein and Aertsen 1985; Aertsen et al. 1986). The gravitational clustering algorithm relates the activity of neurons to the motion of particles in a multidimensional Euclidean space. Although each relationship is based on a quantitative measure of attraction, there is no quantitative description of the cooperation in an entire assembly. Furthermore, this algorithm does not readily identify cells that belong to more than one functional group or subsets of cells within larger functional groups.

The PSP Method quantifies the magnitude of synchronous activity within assemblies of arbitrary size. Although each score is computed as an average over multiple stimulus trials, the temporal layout of each sweep can be visualized by extracting the PSP Trains during Step 4 of the algorithm. Furthermore, correlation caused by direct stimulus effects can be estimated using the average Shift Predictor (Perkel et al. 1967) from Step 6. Similar firing rate statistics across trials allow the Shift Predictor to estimate chance synchronous events since the interactions between neurons happen on a smaller time scale than one stimulus period and are destroyed after shifting. This allows us to decompose the raw synchrony observed into correlations caused by direct stimulus effects and internal interactions.

We used the PSP algorithm to document the evolution of synchrony throughout each stimulus presentation. Figure 3.4A shows the post-stimulus time histograms (PSTHs) for the cell pair in Figure 3.3B for the best drift direction, jittering 5 pixels for the web and star patterns, and the best static stimulus (of 2). Each PSTH is computed for

82
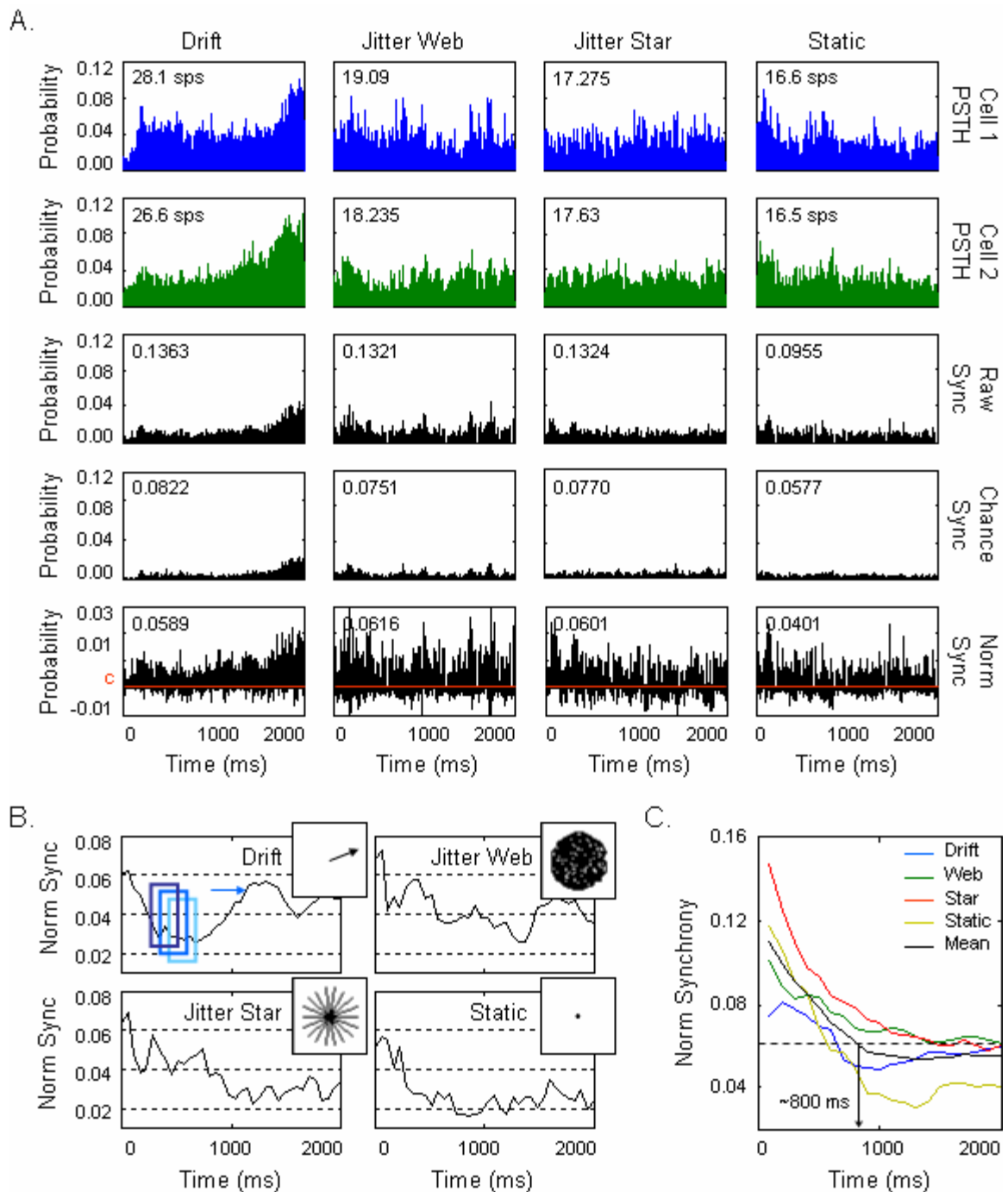
Figure 3.4. Temporal analysis. (A) PSTHs (firing rate, raw, chance, and normalized synchrony) for the pair of cells depicted in Figure 3.3 for the best drift direction, jittering 5 pixels for the web and star patterns, and the best static stimulus (of 2). (B) Sliding window analysis of normalized synchrony for each condition in (A) using a 250 ms window in 50 ms increments. (C) Cumulative analysis of the conditions in (A) using 100 ms increments (100, 200, …, 2000 ms). The mean is plotted in black and the dotted line represents when synchrony is within 10% of its final value (~800 ms).

1 ms bins using spike trains convolved with temporal kernels (PSP Trains) and normalized by the kernel area. The panels in one column depict the time course of each cell's response, the raw synchrony measured from both trains, the chance synchrony estimated with the Shift Predictor, and the normalized synchrony computed by subtracting the raw and chance scores bin by bin and normalizing by *1-chance*. For the drift panels, the PSTH from each cell shows a standard stimulus onset response transient followed by steady firing until an increase in firing rate at the end of the stimulus presentation. The enhanced response towards the end of the presentation is most likely due to the presence of another feature entering the assembly receptive fields. The raw, chance, and normalized synchrony all show this similar time course. Drifting for two seconds causes features in the image to displace 4°, which can be larger than the typical receptive field and highlights the drawbacks of this type of motion. On the other hand, jitter causes features to stay anchored within the receptive field. The responses during the web conditions also depict an onset response, but subsequent firing is more erratic due to the random speeds of each jitter increment. The jitter star conditions have steady increments and result in constant firing patterns while the static stimuli produce pronounced onset responses which decay slightly during the rest of the presentation.

We performed a sliding window analysis of normalized synchrony for each condition in Figure 3.4A using a 250 ms window in 50 ms increments (Figure 3.4B). The raw synchrony in each window was integrated, divided by the total activity measured from each cell's response, then normalized by the corresponding calculation from the chance estimate. During all conditions, the highest synchrony scores were generated within the first 100 ms after the stimulus onset. This may seem surprising for the drift condition since a large peak in the raw synchrony plot occurs during the end of the

84

stimulus period. However, recall that a synchrony score is computed as a ratio of synchronous spikes to total spikes and the new feature also generated a greater proportion of asynchronous spikes during that period as compared to the response onset. We also conducted a cumulative analysis (Figure 3.4C) of the normalized synchrony conditions in Figure 3.4A. Synchrony was computed as in Figure 3.4B for successively larger windows from the stimulus onset in 100 ms increments (100 ms, 200 ms, …, 2000ms). Again, each condition showed a large ratio of synchronous events after the stimulus onset and this value decreased steadily for successive time windows. Synchrony scores were stabilized within 10% of their final value after approximately 800 ms, after which the proportion of synchronous spikes to total spikes remained constant. Across assembly size, group responses displayed a similar pattern in which the maximum synchrony score was almost always generated during the stimulus onset response transient.

Normalization

The temporal binding theory (Milner 1974; von der Malsburg 1981) postulates that dynamic assembly formation is the physical basis for certain perceptual phenomena such as shape perception and figure-ground separation According to this theory, perceptually-related features are linked through correlated firing among subpopulations of cells. The introduction of correlated visual information motivates the generation of precisely-time spike events in the striate cortex. Feature encoding is determined by the reverse correlation of neuronal responses to specific stimulus attributes. However, the exact correspondence between visual structure and response requires knowledge of the induced events that are stimulus-dependent and not a trivial result of firing rate effects. When cells fire action potentials over time, the probability of spikes from two or more

cells being within the same time window increases with higher firing rates. One way to correct for this is to measure all synchronous events and subtract an estimate of the chance events. For cross-correlation histograms (CCH; Perkel et al. 1967), a shift predictor is used to estimate chance synchronous events based on similar firing rate statistics measured across repeated stimulus trials. Similarly, the joint peri-stimulus time histogram (JPSTH; Aertsen et al. 1989) is corrected using an estimate based on the cross-product of both PSTHs. However, application of these estimators for studying correlated neural responses has been criticized by the notion that peaks in the CCH may be induced by trial to trial latency and nonstationarity (Brody 1999a,b), which confound the estimation of synchrony. Ito and Tsuji (2000) have claimed that normalization of the JPSTH is inadequate, especially when cells exhibit higher firing rates. Others suggest the predictors underestimate salient effects by overcorrecting for chance events (Eggermont and Smith 1996) by assuming linearity when disambiguating sources of correlation.

We used the PSP Method to measure the raw synchrony, stimulus-locked synchrony due to modulation of the firing rate, and resulting internally-generated synchrony for assemblies of two to six cells (Figure 3.5). The signal to noise ratios increase exponentially across assembly size from 1.82 in pairs of cells to over 1400 for groups of six cells (Figure 3.5A). For large assemblies, random correlations among all members are exceedingly rare and the probability of chance collisions approaches zero. As a result, the amount of synchrony subtracted as a correction is negligible and the normalized estimate approaches the raw estimate for assemblies with four or more neurons (Figure 3.5B). As processes like contour integration and object recognition undoubtedly involve large numbers of neurons, the effects of normalization become insignificant.
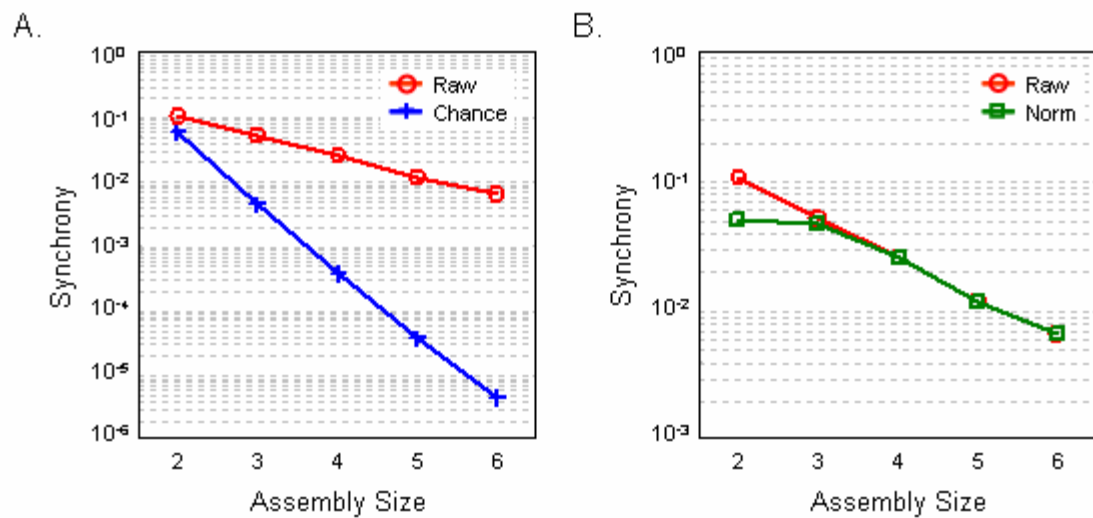
Figure 3.5. Normalizing synchrony scores. (A) Average raw synchrony and chance synchrony scores plotted against assembly size (N = 620 pairs, 613 groups of 3, 584 groups of 4, 487 groups of 5, and 533 groups of 6 cells). The signal to noise ratios (Raw:Chance) are: 1.82, 11.8, 70.4, 316.2, and 1417.4 for successive assembly sizes. (B) Raw synchrony and normalized synchrony scores plotted versus assembly size. The normalized estimate approaches the raw estimate for assemblies ≥ 4 neurons.

Discussion

In this paper, we measured the synchrony and average firing rate responses of assemblies with up to six cells during natural image stimulation undergoing various kinds of motion. We found that synchrony between pairs of cells decreased linearly as a function of electrode separation, but was still observed for cells spanning up to 3 mm. Similarly, the amount of synchrony decreased linearly as a function of increased orientation misalignment, but could be measured in between cells with up to 80° in angular difference. The effects of drifting and jittering stimuli were compared and we found that jittering stimuli in small increments about the origin generated the same magnitude of synchrony as that observed during the most bountiful drift direction. Furthermore, static stimuli still generated about 71.2% of the synchrony seen during jitter conditions. The time course analysis revealed that the greatest proportion of synchronous events was generated during the stimulus onset response transient and achieves stability after approximately 800 ms. Finally, the amount of synchrony due to stimulus-induced modulation of firing rate was found to be negligible for assemblies with four or more neurons, rendering the issue of normalization insignificant for large assemblies.

The Spatial Extent of Synchrony

The spatial analysis of synchrony gives us a topographic map of cooperation, which benefits future studies by identifying areas of high probability of finding synchronous cells or members of a large synchronous assembly. Analyses of electrode distance and orientation preference showed that the magnitude and probability of observing synchrony among cell pairs matched the fundamental prediction of the association field theory. Synchrony existed between cells with closer proximities and

similar orientations despite viewing images with a variety of structural information. The frequent existence of synchronous interactions among cells with similar orientation preferences in the absence of strictly collinear stimulation could reflect a neurophysiological correlate of the association field model and play an important role in encoding contour information. Extending collinear (Eckhorn et al. 1988; Gray et al. 1989) and cocircular synchrony results (Samonds et al. 2006) to natural stimulation is vital in establishing synchrony's role in complex feature integration. The fact that synchrony was stimulus-dependent and observed between cells with different orientations undermines a direct causal link between synchrony and anatomy (e.g. horizontal connections) per se and counters the notion that synchrony may be an artifact of cortical connections. Instead, these findings suggest a more global and purposeful function in which synchrony identifies related contour segments, which have the ability to be integrated at higher processing centers throughout the visual system.

Stimulus Features and Motion

Although natural images provide the best variety of visual information to stimulate an army of cells with different spatiotemporal filter characteristics, they are also fundamentally necessary for understanding the functional role of synchrony. Unfortunately, complex images as opposed to simple analytical stimuli are difficult to manipulate systematically and introduce the additional challenge of optimizing responses from the population of recorded neurons. Based on drifting grating experiments, we knew that motion provided a constant platform for neuronal responses throughout the entire stimulus duration. However, the appropriate direction of drift for natural images is not straightforward because of complex geometries and angle content. Since the drift

speed is 2 °/s, the image will move 4° during the stimulus presentation and any target image features may well be outside a cell's receptive field by the end of the trial. This may cause changes in firing rate and/or synchrony. We tried to circumvent this by using images with large and repeatable features. We also measured the maximum drift response to compare with the jitter results.

Alternatively, we used jitter motion as a different approach to provide constant stimulation. An important result is to find out whether jittering is effective in generating synchrony across the population, and if so, what affect the motion has on the synchrony observed. We found that random jitter around the origin provided as much stimulation as all combined drift directions and that normalized synchrony was independent of jitter style, jitter step size (under 0.4°), and firing rate. Since we are investigating how synchronous cortical activity correlates with structure in the visual scene, we must parse out any portion of synchrony attributed to the temporal aspects of the stimulus. We found that jittering induces 28.8% more synchrony compared to the static condition. These results suggest that synchrony is relatively constant for features anchored within their receptive fields despite temporal variations. This supports our hypothesis that synchrony is mainly generated from the spatial layout of the stimulus.

The Origins of Synchrony

By examining the time course of synchrony, we were able to show that the greatest proportion of synchronous activity was generated during the stimulus onset response transient suggesting that cells may be synchronized by the time of their first spikes (Samonds and Bonds 2005). This synchrony levels off after approximately 800 ms and subsequent synchronous spikes are in constant relation to the total activity

generated. These results are similar to those obtained among pairs of cells viewing simple collinear stimuli. In a separate experiment, we added noise to systematically deconstruct the spatial integrity of drifting sinusoidal gratings in order to disambiguate the effects of spatial and temporal stimulus properties on synchrony and oscillations of firing rate (Zhou et al. 2008). Using cross-correlation and coherence analyses to examine the temporal dynamics of synchronization in the time and frequency domains, we found that synchrony reaches its highest magnitude right after the stimulus onset and stabilizes to within 20% of its final value after 700 ms. Coherence between frequency-specific oscillatory components in the gamma range is apparent after the stimulus onset, but doesn't reach its maximum potential until approximately 900 ms later. We know that gamma oscillation is not needed to generate synchrony (Samonds and Bonds 2005), but coincidence in timing between synchrony stabilization (800 ms) and maximum oscillation coherence (900 ms) may actually reflect the mechanism that contributes to stabilization since oscillations then maintain synchrony at a constant pace.

Our results suggest that spike timing synchronization is initiated by coherent stimulus structure whereas the organization of firing rate oscillations develops as a product of slower acting network interactions. Previous analyses of electrode distance, receptive field overlap, and synchronous lag times suggest that synchrony can be explained by common and synchronous input from earlier stages of visual processing (Samonds et al. 2006) perhaps triggered by visual information falling on the retina. The bottom-up synchronous integration resulting from converging and diverging anatomical connections from previous levels of the visual system may underlie contour integration (Alonso et al. 1996; Usrey and Reid 1999) in which the synchronization of orientation-selective neurons in the striate cortex guide the detection of related contour segments.

A Word on Normalization

The PSP method gives us the advantage of separating raw synchrony into stimulus-locked and internally-generated synchrony by subtraction of the shift predictor (Perkel et al. 1967). We investigated how each component affects the dynamic pathway of synchrony and determined the validity of using normalization methods in our analysis of larger neural assemblies. We found that groups of four neurons had a signal to noise ratio of 70.4 while six neurons generated more than 1400 times the amount of synchrony predicted by chance. Normalizing raw measurements for assemblies with four or more neurons becomes insignificant as the probability of spurious synchrony due to firing rate becomes negligible. Furthermore, the act of normalization is a conceptual tool and in general is irrelevant since the brain provides no such function on incoming visual information. If synchronous activity encodes salient stimulus information, neuronal responses must deviate from independence. An upstream neuron or network of neurons can do little beyond applying thresholds to "normalize" synchrony and does not decipher which events were caused by common input or increased excitability. While deciphering the origins of these sources may lead to important discoveries of the neural mechanism underlying synchrony, our primary focus is on the stimulus-dependence and dynamic behavior of synchrony.

References

Abeles M, Bergman H, Margalit E and Vaadia E. Spatiotemporal firing patterns in the frontal cortex of behaving monkeys. *J. Neurophysiol.* 70, 1629–1638, 1993.

Aertsen AMHJ, Gerstein GL, Habib MK, and Palm G. Dynamics of neuronal firing correlation: Modulation of "effective connectivity". *J. Neurophysiol.*, 61:900-917, 1989.

Aertsen A, Diesmann M, and Gewaltig MO. Propagation of synchronous spiking activity in feedforward neural networks. *J Physiol Paris*. 90(3-4):243-7. 1996.

Alonso JM, Usrey WM, and Reid RC. Precisely correlated firing in cells of the lateral geniculate nucleus. *Nature*, 383:815-819, 1996.

Azouz R and Gray CM. Adaptive coincidence detection and dynamic gain control in visual cortical neurons in vivo. *Neuron,* 37:513-523, 2003.

Brody CD. Disambiguating different covariation types. *Neural Comp. 11*, 1527-1535, 1999a.

Brody CD. Correlations without synchrony. *Neural Comp. 11*, 1537-1551, 1999b.

Bruno RM and Sakmann B. Cortex is driven by weak but synchronously active thalamocortical synapses. *Science*. Jun 16;312(5780):1622-7, 2006.

Das A and Gilbert CD. Topography of contextual modulations mediated by short-range interactions in primary visual cortex. *Nature* 399: 655–661, 1999.

deCharms RC and Merzenich MM. Primary cortical representation of sounds by the coordination of action-potential timing. *Nature* 381, 610–613, 1996.

Eckhorn R, Bauer R, Jordan W, Brosch M, Kruse W, Munk M, and Reitboeck HJ. Coherent Oscillations: A mechanism of feature linking in the visual cortex? *Biol. Cybern.*, 60:121-130, 1988.

Eggermont JJ and Smith GM. Neural connectivity only accounts for a small part of neural correlation in auditory cortex. Exp. Brain Res. *110*, 379-391, 1996.

Elder JH and Goldberg RM. Ecological statistics of Gestalt laws for the perceptual organization of contours. *J. Vis*. 2:324-353, 2002.

Field DJ, Hayes A, and Hess RF. Contour integration by the human visual system: evidence for a local "association field". *Vision Res*. 33:173-193, 1993.

Frien A and Eckhorn R. Functional coupling shows stronger stimulus dependency for fast oscillations than for low-frequency components in striate cortex of awake monkey. *Eur J Neurosci.* Apr;12(4):1466-78, 2000.

Ford JM, Krystal JH, Mathalon DH. Neural synchrony in schizophrenia: from networks to new treatments. *Schizophr Bull*. Jul;33(4):848-52, 2007.

Geisler WS, Perry JS, Super BJ, and Gallogly DP. Edge co-occurrence in natural images predicts contour grouping performance. *Vision Res*. 41:711-724, 2001.

Gerstein GL and Aertsen AMHJ. Representation of cooperative firing activity among simultaneously recorded neurons. *J. Neurophysiol*. 54:1513-1528, 1985.

Gerstein GL, Perkel DH, and Dayhoff JE Cooperative firing activity in simultaneously recorded populations of neurons: Detection measurement. *J. Neurosci.*, 5:881-889, 1985.

Gerstein GL and Perkel DH. Mutual temporal relationships among neuronal spike trains. Statistical techniques for display and analysis. *Biophys. J.* 12:453-473, 1972.

Gray CM, Konig P, Engel AK, and Singer W. Oscillatory responses in cat visual cortex exhibit inter-columnar synchronization which reflects global stimulus properties. *Nature*, 338:334-337, 1989.

Hess RF, Barnes G, Dumoulin SO, and Dakin SC. How many positions can we perceptually encode, one or many? *Vision Res*. Jun;43(14):1575-87, 2003.

Hubel DH and Wiesel TN. Receptive fields, binocular interaction and functional architecture in the cat's visual cortex. *J Physiol* 160: 106–154, 1962.

Ito H and Tsuji S. Model dependence in quantification of spike interdependence by joint peri-stimulus time histogram. *Neural Comp. 12*, 195-217, 2000.

Kelly RC, Smith MA, Samonds JM, Kohn A, Bonds AB, Movshon JA, and Lee TS. Comparison of recordings from microelectrode arrays and single electrodes in the visual cortex. *J Neurosci.* Jan 10;27(2):261-4, 2007.

Maldonado PE, Friedman-Hill S, and Gray CM. Dynamics of striate activity in the alert macaque: II. Fast time scale synchronization. *Cereb Cortex.* Nov;10(11):1117-31, 2000.

Milner P. A model for visual shape recognition. *Psychol. Rev.,* 81: 521-535, 1974.

Murthy VN and Fetz EE. Coherent 25- to 35-Hz oscillations in the sensorimotor cortex of awake behaving monkeys. *Proc. Natl Acad. Sci. USA*. 89, 5670–5674, 1992.

Neuenschwander S and Singer W. Long-range synchronization of oscillatory light responses in the cat retina and lateral geniculate nucleus. *Nature* 379, 728–732, 1996.

Nowak LG, Munk MH, Nelson JI, James AC, and Bullier J. Structural basis of cortical synchronization. I. Three types of interhemispheric coupling. *J Neurophysiol.* Dec;74(6):2379-400, 1995.

Parent P and Zucker SW. Trace inference, curvature consistency, and curve detection. *IEEE Trans Pattern Anal Machine Intell* 11:823-839, 1989.

Perkel DH, Gerstein GL, and Moore GP. Neuronal spike trains and stochastic point processes, II. Simultaneous spike trains. *Biophys. J.* 7:419-440, 1967.

Roelfsema PR, Lamme VA, and Spekreijse H. Synchrony and covariation of firing rates in the primary visual cortex during contour grouping. *Nat. Neurosci.* 7:982-991, 2004.

Rousche PJ and Normann RA. A method for pneumatically inserting an array of penetrating electrodes into cortical tissue. *Annals of Biomed. Eng.*, 20:413-422, 1992.

Samonds JM, Zhou Z, Bernard MR, and Bonds AB. Synchronous Activity in Cat Visual Cortex Encodes Collinear and Cocircular Contours. *J. Neurophysiol.* 95:2602-2616, 2006.

Samonds JM and Bonds AB. Gamma oscillation maintains stimulus structure-dependent synchronization in cat visual cortex. J. Neurophysiol. *93*, 223-236, 2005.

Shoham S, Fellows MR, and Normann RA. Robust, automatic spike sorting using mixtures of multivariate t-distributions. *J Neurosci Methods*. 127:111-122, 2003.

Sigman M, Cecchi GA, Gilbert CD, and Magnasco MO. On a common circle: natural scenes and Gestalt rules. *Proc. Natl. Acad. Sci. USA*. 98:1935-1940, 2001.

Singer W and Gray CM. Visual feature integration and the temporal correlation hypothesis. *Annu. Rev. Neurosci*. 18, 555–586, 1995.

Snider RK, Kabara, JF, Roig BR, and Bonds AB. Synchronous entrainment of cat striate neurons to display refresh rates. *Invest. Ophth. and Vis. Sci.* Suppl. 37, #2187, 1996.

Touryan J, Felsen G, and Dan Y. Spatial structure of complex cell receptive fields measured with natural images. *Neuron*. Mar 3;45(5):781-91, 2005.

Usrey WM and Reid RC. Synchronous activity in the visual system. *Ann. Rev. Physiol.*, 61:435-56, 1999.

von der Malsburg C. The correlation theory of brain function. *Internal Report, Max-Planck Institute for Biophysical Chemistry*. Goettingen, Germany, 1981.

Wollman DE and Palmer LA. Phase locking of neuronal responses to the vertical refresh of computer display monitors in cat lateral geniculate nucleus and striate cortex. *J. Neurosci. Methods* 60:107-113, 1995.

Womelsdorf T, Schoffelen JM, Oostenveld R, Singer W, Desimone R, Engel AK, and Fries P. Modulation of neuronal interactions through neuronal synchronization. Science. Jun 15;316(5831):1609-12, 2007.

Zhou Z. Spatial characteristics of cooperative interactions in the striate cortex. Ph.D. dissertation. Vanderbilt University, 2008.

CHAPTER IV

SYNCHRONOUS ACTIVITY IN CAT VISUAL CORTEX DETECTS STRUCTURAL
MODIFICATIONS IN NATURAL IMAGES

Introduction

The relationship between stimulus intensity and firing frequency remains central

to our understanding of information transmission in the cortex (e.g., Barlow 1972),

although temporal properties like spike patterns or interspike intervals have gained some

attention as a means to encode stimulus information (e.g., Strehler and Lestienne 1986;

Victor 2000). Another alternative for the representation of information is encoding

inherent in the coordinated activity of populations of cells. Although the stimulus

dependence of average firing rate is unambiguous for a single cell in the primary visual

cortex, generalized firing activity considered across a group of cells is not easily defined,

since the integration of firing rate must take place over some finite time period and the

required broad temporal resolution can confound the definition of populations. On the

other hand, brief synchronization of spike times expresses unambiguous relationships

between cells in an assembly. This may serve as a supplemental coding strategy in which

neurons can be effectively connected and form dynamic regional circuits to reliably and

efficiently transmit information throughout the cortex while minimizing metabolic

demands. In this manner, visual information would not only be inherent in the activity of

individual neurons, but could be extracted from the collective activity of the group. Due

to the dynamic nature of grouping, the combinatorial possibilities offer a vastly increased

dimensional magnitude for encoding visual information.

The grouping of neurons responding to perceptually-related features into subpopulations defined by synchrony has been postulated as a neural mechanism underlying feature integration and object binding (Singer and Gray 1995; von der Malsburg 1999; but see also Shadlen and Movshon 1999). For example, Gray et al. (1989) found using cross-correlation analysis that the magnitude of synchrony between pairs of cells with similar orientation preferences and collinear receptive fields was larger when stimulated with a long light bar across the receptive fields than with two shorter light bars over each receptive field. However, these results and others (Eckhorn et al. 1988; Ts'o et al. 1986) only examined synchrony in the context of collinear stimulation.

To generalize the role of synchrony as a substrate for detection of nonlinear contours, we expanded the stimulation protocol to include cocircular figures (Samonds et al. 2006). We found that neuron pairs with receptive field alignments tangent to annular rings would synchronize their responses (as measured by the rate-normalized cross-correlation histogram described by Aertsen et al. 1989), despite wholly different orientation preferences. Synchrony predictably existed between pairs of neurons as long as their receptive fields followed cocircularity and association field rules (Field et al. 1993), and synchronous responses were more reliable than changes in average firing rate in discriminating between concentric ring and grating stimuli. Group membership was dynamic, in that individual cells could belong to more than one functional group, which assembled based on the relationship between the spatial properties of the stimulus and the organization of the receptive fields.

Since synchrony appears to be triggered by spatial coherence, we wish to determine whether synchronous activity between larger groups of cells can serve as a general substrate for detection of contour structure. The receptive fields of single cells

are suitable for analysis with one-dimensional analytical stimuli, but the collective receptive fields of larger cell assemblies generally extend to two dimensions, which markedly expands the space of appropriate test stimuli (e.g., Vinje and Gallant 2000). Pairs of cells can be analyzed with simple curvatures (Samonds et al. 2006), but larger groups may require shapes of arbitrary complexity. We therefore chose to sample this dimensionality with natural images.

Here we explored the dependence of synchrony on structural integrity by using natural images that were modified with various methods and degrees of degradation. We implanted a 10x10 microelectrode array into the visual cortex of two paralyzed and anesthetized cats to record from dozens of neurons simultaneously. Assemblies of up to six cells were analyzed using a novel metric that detects and quantifies the amount of synchronous activity in a neural assembly of arbitrary size. We found that image degradation reduces synchrony more strongly than firing rate and that, unlike firing rate, synchrony is sensitive to the degree of degradation. The decrease in synchrony across different conditions reflected a reduction in the number of synchronous events. A quantitative analysis of receptive field layout showed that assemblies with good associations as described by association field rules (similar preferred orientations and close receptive field proximity) tended to generate more synchrony than those with poor associations. Overall, these results suggest that synchrony signals the presence of contour structure in natural images. We propose that synchrony can overcome the ambiguity of firing rate to identify contour structure, which then is integrated to convey information on complex curvatures and shapes at subsequent sites in the extrastriate hierarchy.

Materials and Methods

Preparation

Two adult cats (2.3 and 2.6 kg) were prepared for electrophysiological recordings in V1. All procedures were performed in accordance with guidelines set forth by the American Physiological Society and the Institutional Animal Care and Use Committee at Vanderbilt University. Prior to surgery, each cat received intramuscular injections of 0.5 ml acepromazine maleate (10 mg/ml), 0.5 ml atropine sulfate (0.4 mg/ml), and 0.25 ml dexamethasone sodium phosphate (4 mg/ml). Anesthesia was induced with 5% halothane in O_2 and maintained with intravenous injection of Propofol (0.3 mg/kg hr). Two forelimb veins and the trachea were cannulated and the animal was positioned in a stereotaxic device where a craniotomy (6x6 mm) was performed over V1. After the dura was excised, the electrode array was implanted and the opening was covered with a mixture of agar and mammalian Ringer's solution.

During recording, paralysis was induced with 6 mg pancuronium bromide and maintained through intravenous injection (Pavulon; 0.3 mg/kg hr). Health and effective anesthesia were maintained by monitoring the EEG and ECG and administering bolus injections of propofol when necessary. Cats were artificially ventilated with a mixture of N_2O, O_2, and CO_2 (75:23.5:1.5) to hold expired pCO_2 at 3.9%. Rectal temperature was maintained at 37.5° C with a heating pad. The nictitating membranes were retracted and the natural pupils dilated by instillation of phenylephrine HCl 10% and atropine sulfate 1% in the conjunctival sacs. Contact lenses with 4 mm pupils were placed on the corneas and auxiliary spectacle lenses were added as dictated by direct ophthalmoscopy to render the retinae conjugate with the stimulus plane at a distance of 57 cm.

Data Recording and Acquisition

Simultaneous single-unit recordings were made from cells in the visual cortex via the Utah Intracortical Electrode Array (UIEA; Cyberkinetics Neurotechnology Systems, Foxborough, MA). The UIEA recordings have good signal to noise ratios and have been shown to have qualities comparable to those from single-electrode recordings (Kelly et al. 2007). Details of the array are described in Chapter 2. The signal on each channel was amplified by 5000 and band-limited between 250 Hz and 7.5 kHz. Thresholds were dynamic and set to 3.25x the mean activity on each electrode. Waveforms were sampled at 30 kHz and preserved in 1.5 ms windows. Channels with single-unit activity were used only if the activity was ≥ 5 spikes per second *and* showed clear orientation tuning (signal to noise ratio ≥ 2:1) while viewing drifting sinusoidal gratings. In the end, we recorded from 81 single units, 79 of which were complex cells (Hubel and Weisel 1962; Skottun et al. 1991) with a mean relative modulation, *F1/F0,* of 0.23±0.17 (n = 79 cells). Unless otherwise stated, all cells were used for analysis.

Stimulation

All stimuli were displayed on a gamma-corrected SONY Trinitron 21" monitor driven either by a Cambridge Research Systems VSG2/3F controller board (for gratings) or a video controller using the WinVis software package (for natural images). The monitor resolution was 800 x 600 pixels (22.6 pixels per visual degree) and displays were refreshed at 120 Hz. All stimuli spanned 18°x18° and appeared against a mean luminance background (73 cd/m^2). The stimulus protocol contained natural, grayscale images from www.imageafter.com with three modifications (contrast reversal, noise addition, and frequency filtering; see Figure 4.1) presented for 2 seconds. Grayscale

noise (3x3 pixels, 0.13°) was added to cover 20%, 30%, 40%, 50%, or 100% of the image. Images were restricted in frequency content with the smooth sinusoidal-edged low-pass filter (extended to two dimensions) in Figure 4.1B, which reduces filtering artifact, where $f_c = 0.44$ and 0.88 cycle/° and $\omega = 0.275$ cycle/°. (High-passed images used the reverse filter.) Images were jittered 5 pixels (0.22°) in a random fashion (like an asterisk, returning to the origin) at 60 Hz to provide motion (Figure 4.1C). This generates as much synchrony as drift (next paragraph), but anchors features within local receptive fields. We did not see 60 Hz entrainment reflected in the power spectra of the neuronal responses and speculate that the use of random jitter directions reduced any 60 Hz transients to the level of noise. There was a 1 second delay between each image, during which only the mean luminance was shown. Each picture spanned 18°x18° to ensure stimulation of both classical and non-classical receptive fields of the entire recorded sample. All presentations were randomly interleaved and repeated 100 times for reliability. Three natural images (referred to as Image 1, Image 2, and Image 3; see Figure 4.1A) and their subsequent modifications were investigated. All images were scaled to have a global contrast of 0.32 (see Touryan et al. 2005), but since the original image in each protocol served as a control, it was not necessary to normalize the images for other spectral content.

While gratings have an inherent drift direction that is orthogonal to their orientation, natural images do not. In a pilot experiment, we measured the amount of average firing rate (n = 47 cells) and synchrony between pairs of isolated single units (n = 338 pairs with significant activity during one or more condition) viewing drifting or jittering natural images and found that average jitter synchrony, independent of jitter style (returning to origin or not), was statistically the same as synchrony generated during the
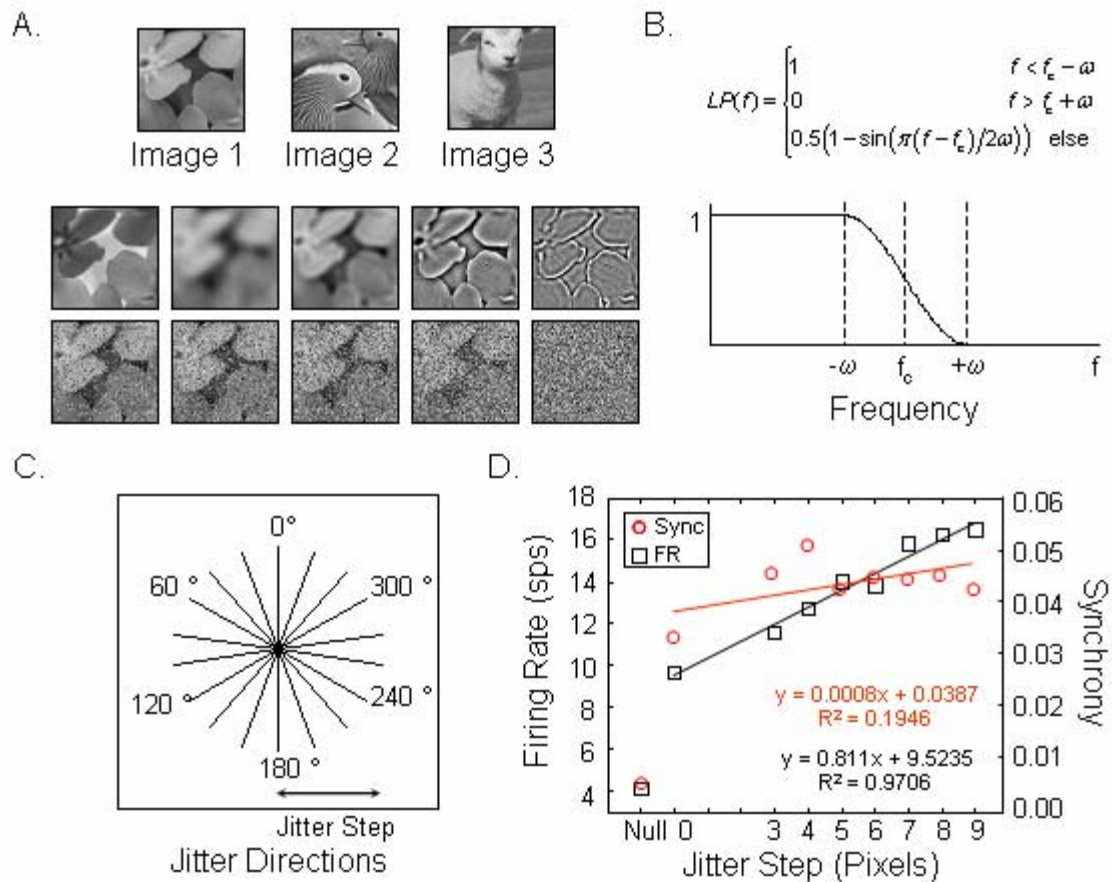
Figure 4.1. Example stimuli. (A) Original images and modifications of Image 1: (top row) polarity-reversal, two degrees of low-pass filtering, two degrees of high-pass filtering, and (bottom row) noise addition with progressively larger areas (20%, 30%, 40%, 50%, and 100%) of the image covered by grayscale noise pixels. (B) Equation and plot of smooth low-pass filter in one dimension (high-pass filter is reverse of low-pass filter). The sinusoidal edge reduces rippling artifact. (C) Schematic of the random jitter motion provided for each stimulus with the size of jitter step indicated with an arrow. The stimulus returns to the center after each excursion. (D) We conducted a separate pilot experiment where average firing rate (n = 47 cells) and synchrony (n = 338 pairs with significant activity during one or more condition) were measured in response to a natural image jittered by 0 (static), 3, 4, 5, 6, 7, 8, or 9 pixels (1 pixel = 0.044°). Firing rate increased linearly with jitter step size and a step of 5 pixels generated 71.0% more spikes than the static condition. On the other hand, synchrony is relatively independent of jitter step size (> 0) and a step of 5 pixels generated on average 27.1% more synchronous events than the static condition.

optimal drift direction. Furthermore, normalized synchrony was independent of jitter

step size (Figure 4.1D; we tested up to 9 pixels or 0.4 °) and firing rate. Firing rate

increased linearly with jitter step size and a step of 5 pixels generated 71.0% more spikes

than the static condition. On the other hand, synchrony is relatively independent of jitter

step size (> 0) and a step of 5 pixels generated on average 27.1% more synchronous

events than the static condition. These results suggest that synchrony is constant for

features anchored within their receptive fields despite temporal variations. This is

optimistic since we propose that synchrony is mainly generated from the spatial

configuration of the stimulus. Using jitter, synchrony is generated with a lower overall

firing rate, which maintains the signaling of structural salience while reducing metabolic

demand.

Data Processing

We have developed a method that detects and quantifies the amount of correlated

activity in a neuronal assembly of arbitrary size. Synchrony enhances the probability of

eliciting postsynaptic action potentials (PSPs) when neurons behave as coincident

detectors (Azouz and Gray 2003). This encourages selective propagation of

synchronously-coded information to subsequent levels of the cortical hierarchy. Our

basic algorithm reflects the relevance of group synchrony to postsynaptic neurons by

modeling the temporal summation of PSPs.   Neurons with similarly-timed events are

considered synchronous and the magnitude of synchrony depends on the degree of

similarity. The steps in this algorithm are discussed in Chapter 2.

Due to the combinatorial arrangement of cells from the population, there are a

very large number of potential inputs (identified groups) to the PSP algorithm. If we

assume that only a small fraction of subsets in the population will synchronize to any given stimulus, then the probability of randomly testing combinations of cells and finding a significant assembly is very low. Fortunately, we have found that members of larger assemblies can, in general, be predicted based on Normalized Scores from smaller assemblies. This is because our definition of synchrony requires participation from all cells so large assemblies with significant synchrony must contain subsets of cells that synchronize. This rule is used to suggest likely members of larger assemblies, but cannot predict assembly behavior, i.e. Normalized Scores from smaller assemblies cannot be combined in some way to produce a Normalized Score from a larger assembly. We can compute a relatively low number of small assembly scores and progressively cluster cells that synchronize well to create an assembly of arbitrary size that has a high probability of synchronizing. For instance, in a population of cells [A B C D], if pairs [AC AD CD] synchronize often and [AB BC BD] do not, a likely group of three cells to input into the algorithm is [ACD] as opposed to [ABC BCD]. (Note that cells are "clustered with replacement" so they can belong to more than one assembly.) These large assemblies can then be entered into the PSP algorithm to determine if, in fact, their grouping is significant (to build larger assemblies from smaller ones, synchrony must exist *between* groups as well as *within* groups).

To establish our algorithm as a viable method for quantifying synchrony, we compared it to the Joint Peri-Stimulus Time Histogram method (JPSTH, Aertsen et al., 1989). The JPSTH can only quantify synchrony among pairs of neurons, so we focused on assemblies of size 2. We found that the PSP method identified the same significant neuron pairs as the JPSTH, and cross-correlograms (CCGs) for a significant neuron pair derived from each method were qualitatively similar (Figure 4.2A). The CCG from the

PSP Method was generated by shifting one spike train relative to the other and calculating the magnitude of synchrony at each lag from -100 ms to 100 ms. Relative magnitudes of synchrony between assemblies differed between the methods due to the non-linear weighting scheme employed by the PSP Method compared to the constant (via binning) weighting scheme employed by the JPSTH. As seen in Figure 4.2A, both CCGs have large central peaks indicating significant synchrony and periodic side lobes resembling oscillation. The smooth appearance of the top graph is most likely due to the graded values available in the PSP Method as opposed to discrete spike counts in the JPSTH method.

In larger groups, the uncertainties of normalization and firing rate dependence are minimized due to the very large ratios seen between chance and observed probabilities of synchrony as group size grows (Figure 4.2B). Observed synchrony was calculated by averaging raw scores for 39 significant assemblies per size group during natural image stimulation. Chance synchrony was calculated by averaging shift predictors computed for 200 randomly chosen assemblies in each size group (each shift predictor was computed as the mean of 100 different shift combinations for each assembly). On average, significant assemblies of 2 cells contain twice the amount of synchrony expected by chance and assemblies of 6 cells contain 1500x more synchrony than expected when cells are firing independently (see also Schneidman et al. 2006).

Results

We used a 10x10 microelectrode array and the PSP algorithm to record from and analyze the responses of cell assemblies in the visual cortex of two paralyzed and anesthetized cats during presentation of three natural images that were systematically
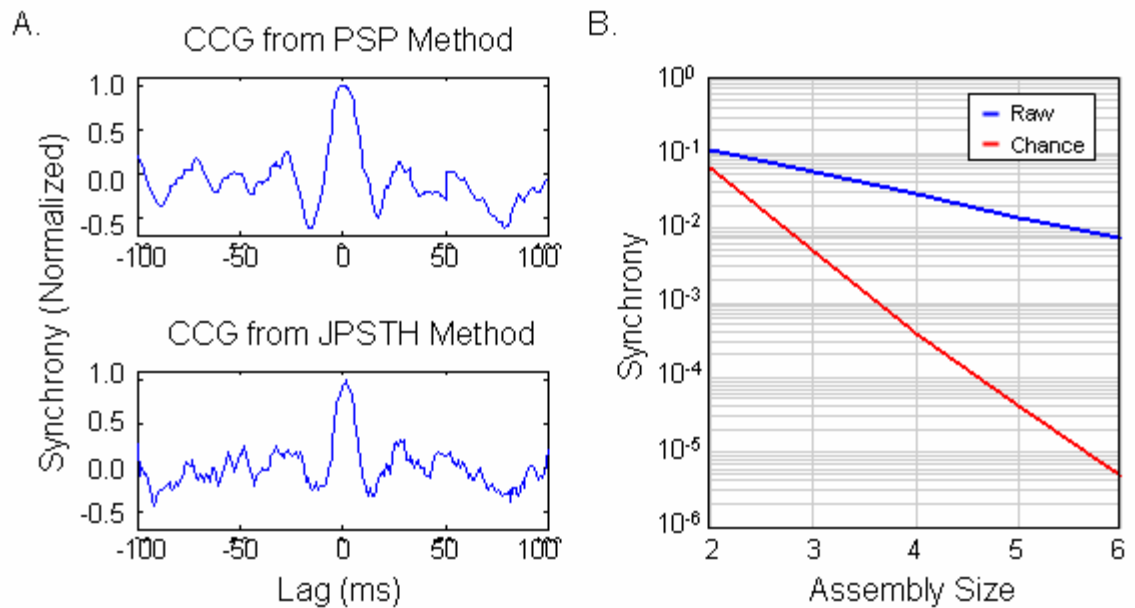
Figure 4.2. Example results from the PSP Method. (A) Comparison of cross-correlograms (CCGs) constructed via the PSP and Joint Peri-Stimulus Time Histogram (JPSTH; Aertsen et al., 1989) methods (smoothed with a 5-point moving average filter). The peaks in each graph are normalized to unity. Each graph contains a large peak at 0 ms lag indicating significant synchrony. The CCG derived from the JPSTH method is noisier due to the discrete spike counts in each histogram bin as opposed to graded synchrony values at each lag in the PSP method. (B) Magnitudes of raw synchrony and chance synchrony plotted against assembly size for neurons stimulated with a natural image. Observed synchrony was calculated by averaging raw scores for 39 significant assemblies per size group. Chance synchrony was calculated by averaging shift predictors computed for 200 randomly chosen assemblies in each size group (each shift predictor was computed as the mean of 100 different shift combinations for each assembly).

modified with noise, blur, and polarity-reversal. We quantified the amount of synchronous activity generated during each modification and compared it to the average firing rate of each neuron. (Note that these quantities are different and this comparison is methodologically difficult. Results derived independently for each response type are qualitatively compared.) The PSP algorithm was also used to explore the temporal dynamics of synchrony throughout the stimulus duration as well as to explore the mechanisms causing decreased cooperation with loss of structural integrity. Finally, we quantitatively examined the receptive field organizations of three-cell assemblies and measured the synchronous activity generated as a function of relative orientation and receptive field overlap.

We simultaneously recorded single-unit activity from 39 and 42 cells in two cats. Unfortunately, analysis of assembly constituents is not straightforward as each of these populations contains trillions of possible inputs to the PSP algorithm. Evaluating the efforts of subgroups of cells leads to a combinatorial explosion of grouping possibilities and requires the identification of assemblies with significant cooperative activity. Especially during the initial response to stimulus onset, large numbers of cells organize cooperatively by responding within a short period of time. Although the amount of raw synchronous activity in an assembly can be computed quickly, the Raw Score is not necessarily a good indication of significance since neurons with high firing rates tend to have more chance synchrony events that artificially inflate the Raw Score. Therefore, Normalized Scores must be computed and analyzed instead. Determining which assemblies have significant cooperation beyond that expected by chance requires statistical calculations that can be cumbersome for large numbers of assemblies. For instance, approximately 68%, or 76,112 groups, out of all possible four-cell assemblies

were active in the visual cortex of cat 2 during the presentation of Image 1. Fortunately, we found that the members of larger assemblies with significant activity can in general be predicted by the Normalized Scores from smaller assemblies. This procedure is helpful to pinpoint larger assemblies of interest although not necessary if promising groups can be identified through other means, e.g., receptive field analysis.

We used the PSP algorithm to compute the amount of synchronous activity among all pair-wise combinations of cells (N = 1602; 741 pairs from cat 1 and 861 pairs from cat 2) and used those results to cluster cells into larger assemblies. This shortcut is justified since our definition of synchrony requires that all cells in a selected assembly participate in overlapping events and, hence, all subsets of that assembly must synchronize as well. We found a total of 266 pairs that had significant activity ($\alpha = 0.01$) for Image 1, 275 pairs for Image 2, and 214 pairs for Image 3. These pairs were clustered to suggest larger assemblies (n = 3, 4, 5, and 6) which were then tested with the PSP algorithm to determine statistical significance until 50 assemblies of each size were identified. Although even larger (n > 6) assemblies were identified (for instance, an assembly of 20 cells synchronized for 4 ms during the onset transient of one stimulus presentation), groups of 6 cells or less provided ample activity and consistency to study trends during the temporal dynamic analysis.

Differential Measurements of Structural Degradation

One challenge in analyzing synchronous responses to natural stimuli lies in pairing the responses to a specific stimulus attribute. Spatial, temporal, and luminance properties may combine in any number of ways to elicit a given response. To investigate the specific properties of natural stimuli that encourage assembly formation, we used

differential measurements, as commonly used in fMRI studies. Our general strategy was to measure a response to a control image and then systematically vary the properties of that image. Cooperative responses were compared to those elicited from the original image and the difference represented the consequences of the imposed modification.

We used three different natural images and measured the effects of noise addition, frequency filtering, and polarity-reversal on the amount of firing rate and synchrony generated in assemblies of size 2, 3, 4, 5, and 6 cells. We found that the average synchrony among each size group is reduced much more strongly than average firing rate across noise and low-passed conditions, yet remained the same for high-passed conditions. We found no significant change in either response property for contrast reversal, indicating that synchrony is independent of luminance levels and, like firing rate, shows non-linear rectification in complex cells. Average firing rate did not change significantly during any modification except the 100% white noise stimulus. Average firing rate was compared on an individual cell basis with a paired t-test, not computed as an average over the entire assembly. Since individual firing rates did not change significantly, it did not matter if we used the sum or product of firing rates across all members.

Figure 4.3 shows the relative change in synchrony and firing rate across each modification for Image 3. For the noise conditions (Figure 4.3A), average synchrony in two-cell assemblies (n = 214) decreased by 33.9% (p < 0.00013) with 50% added noise and synchrony in six-cell assemblies (n = 50) decreased by 44.0% (p < 0.00002). Average firing rate (n = 42) only dropped by 3.7% (p > 0.3). However, total elimination of stimulus structure was followed by a 79.0% reduction of synchrony among cell pairs and a 93.0% reduction among groups of six. Average firing rate dropped significantly by
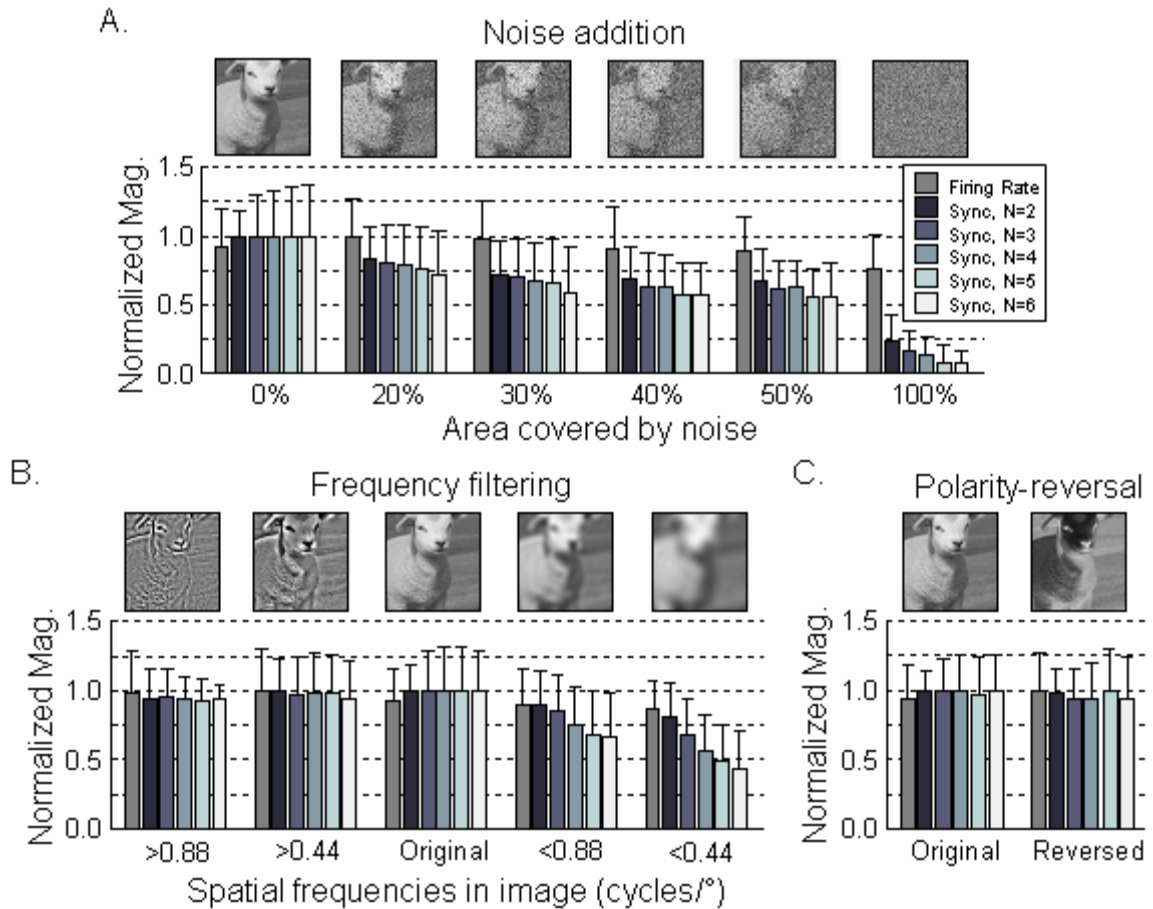
Figure 4.3. Image modification results for Image 3. (A) Synchrony and average firing rate versus noise level. The bar graph shows the changes in average firing rate (n = 42 cells) and synchrony (n = 214 two-cell assemblies, n = 50 for each of three-, four-, five-, and six-cell assemblies). Average firing rate and synchrony within each size group are normalized to the maximum value across all conditions. (B) Synchrony and average firing rate versus frequency filter. Images were filtered with a smooth, sinusoidal-edged filter (see Figure 2C). (C) Synchrony and average firing rate versus polarity. The contrast of the original image was reversed. Again, normalized magnitudes are plotted so that average firing rate and synchrony are both normalized to the maximum score.

15.8% (p < 0.004). For the spectrally-filtered conditions (Figure 4.3B), although synchrony decreased slightly for the high-passed images, there was no significant change across assembly size. However, synchrony was measurably smaller across all sizes for the low-passed modifications (decreased by 11.4% and 44.7% for two cells and six cells, respectively, when frequencies above 0.88 cycles/° were removed; 20.0% and 57.5% for two cells and six cells, respectively, when frequencies above 0.44 cycles/° were removed). Average firing rate was not significantly affected by removing specific frequency bands. Finally, synchrony decreased slightly for all assembly sizes when viewing the contrast-reversed image (Figure 4.3C), but, like firing rate, there was no significant difference when compared to the original (p > 0.6 for synchrony in two-cell assemblies, p > 0.05 for firing rate).

Temporal Dynamics

In the previous section, we showed that progressive structural degradation destroyed synchronous neuronal interactions while preserving firing rate statistics for the most part. Here, we examine the temporal dynamics underlying synchrony and firing rate responses to the noise conditions. In Figure 4.4A, we show an example post-stimulus time histogram (PSTH) for a typical cell averaged over the presentations of Image 3. The PSTH for each condition is computed for 1 ms bins using spike trains convolved with temporal kernels (PSP Trains) and normalized by the kernel area. The maintenance of firing rate after structural degradation is shown over a 250 ms sliding window in 50 ms increments in Figure 4.4B and only for the complete loss of structure does firing rate show a pronounced decrease in spiking activity after the onset transient. However, even during the 100% noise image, 84.2% of the original firing rate is
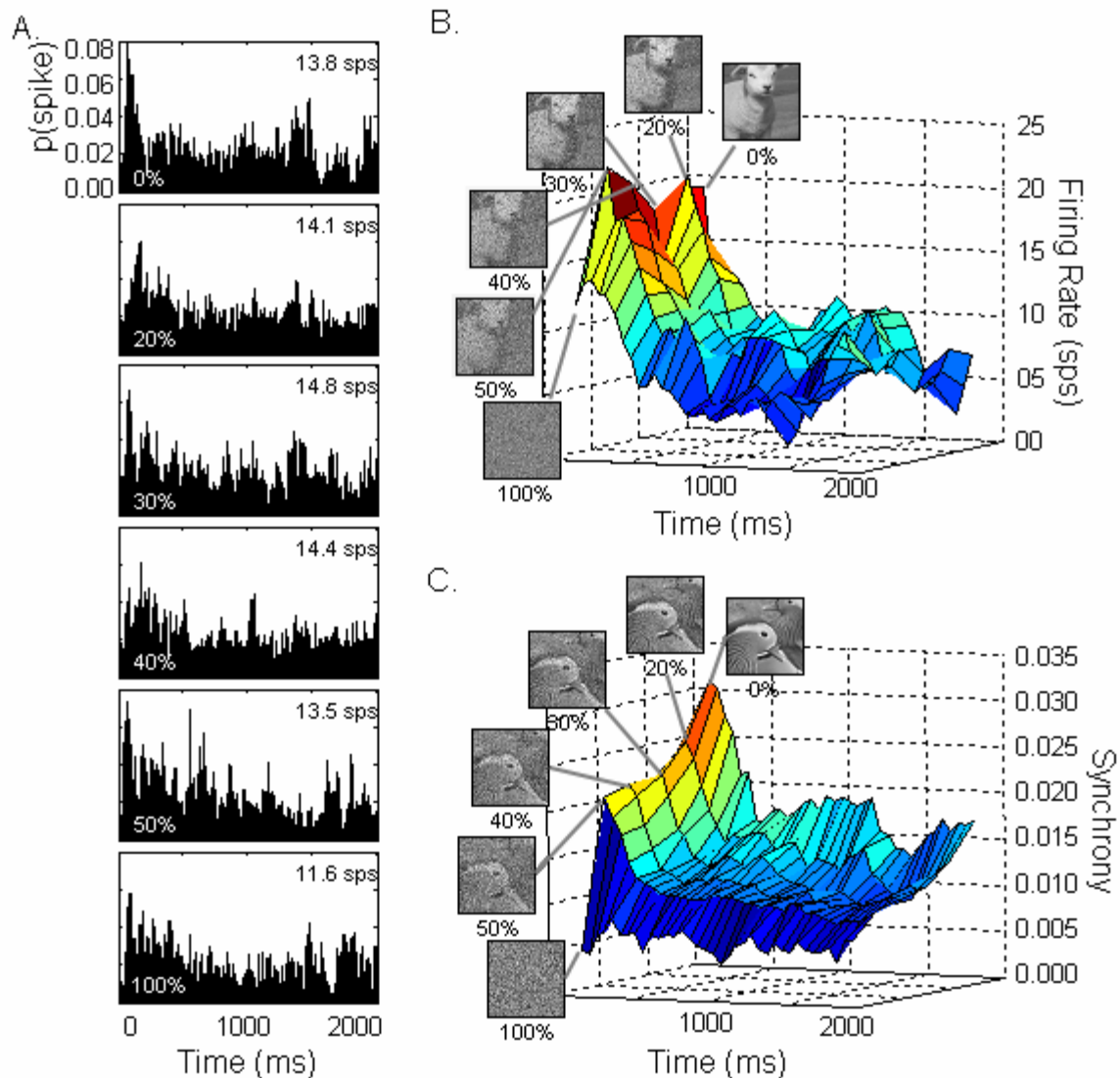
Figure 4.4. Time course analysis. (A) Example Post-Stimulus Time Histogram (PSTH) in response to the noise conditions for Image 3 (see (B)). The average firing rate for this cell is denoted in the upper-right corner for each condition. Each PSTH is computed for 1 ms bins using spike trains convolved with temporal kernels (PSP Trains) and normalized by the kernel area. (B) The mean firing rate for n = 42 cells is calculated over a sliding window of 250 ms in increments of 50 ms for Image 3 and five noise conditions pictured (20%, 30%, 40%, 50%, and 100%). (C) An example time course of synchrony is plotted over the stimulus duration. Synchrony is calculated between three cells, over a sliding window of 250 ms in increments of 50 ms for Image 2 and five noise conditions pictured (20%, 30%, 40%, 50%, and 100%). These three cells generated significant synchrony during stimulation with Image 2 (p < 0.003) and show behavior typical of the population of three-cell assemblies presented in Figure 5A.

maintained and may be accounted for by the extra spikes induced while the stimulus underwent jitter motion (refer to Figure 4.1C,D). The pilot experiment predicted a jitter-induced spiking percentage increase of 71.0%.

In order to investigate the amount of synchrony generated throughout the stimulus presentation, we used the PSP algorithm to calculate Normalized Scores in a 250 ms sliding window moved in 50 ms increments (this window size was necessary to contain enough spikes for a reliable estimate). This was applied to Image 2 and its five noise conditions (20%, 30%, 40%, 50%, and 100%). The time course for one assembly with significant synchrony ($p < 0.003$) during the original image is mapped over all conditions in Figure 4.4C. The introduction of noise reduced the amount of synchrony generated during the onset transient and throughout the stimulus duration until 100% noise completely destroyed the local structure and there was a substantial decrease in synchrony during the onset transient. Similar to firing rate, synchrony is not completely gone during presentation of the white noise stimulus and the 21.0% that remains, on average, among pairs is well predicted by the 27.1% estimated to exist based on the motion-induced activity from stimulus jitter (refer to Figure 4.1C,D).

In Figures 4.3, 4.4, and 4.5, image degradation by noise addition and low-pass filtering caused a reduction in the average amount of synchrony generated. We concentrated on the responses of 50 four-cell assemblies to presentations of Image 1 and its low-passed modifications to determine what firing characteristics contributed to this reduction in synchrony (Figure 4.5A). The factors influencing total synchrony are the number of spikes produced and the duration of synchronous episodes (Figure 4.5B). However, since the average firing rate of each cell was not reduced by image degradation (see Figure 4.5B), reduced synchrony must have resulted from a decrease in the amount
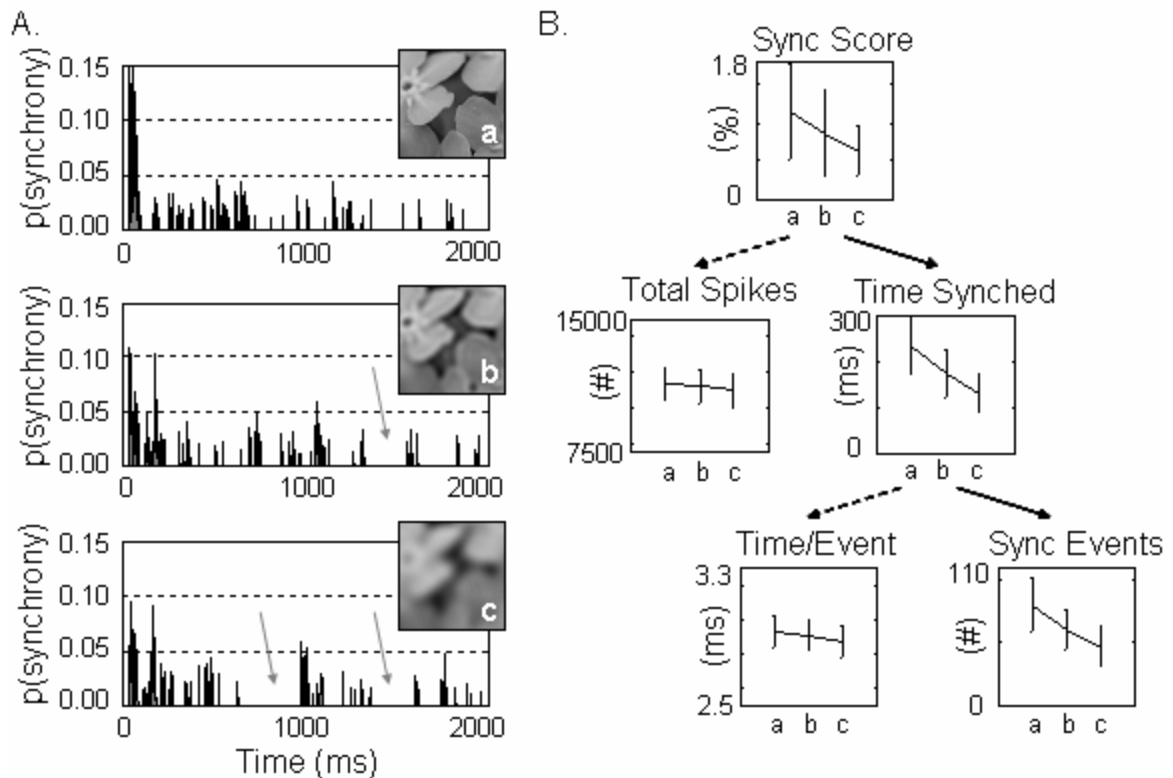
Figure 4.5. Factors that contribute to synchrony reduction. (A) Post-stimulus time plots for the synchrony generated within a four-cell assembly while viewing Image 1 and its low-passed modifications (denoted a, b, and c). The number of synchronous events decreases with increased degradation (see arrows). (B) Synchrony was quantified across the three conditions (a, b, and c) for 50 four-cell assemblies. Reduction in the synchrony score was attributed to a decrease in the amount of time spent synchronizing since the total spikes produced did not change (see Figure 5B). A decline in the number of synchronous events, and not the duration of synchronization during each episode was found. Each plot shows the mean and error bars representing ± 1 standard deviation.

of time spent cooperating. This component in turn can be divided into two quantities: the number of synchronous events and the total time window over which synchrony occurs during each event (by definition, maximum = 10 ms). We found that on average, four-cell assemblies spent approximately 2.9 ms firing together during each synchronous event and this value did not change across the different conditions. However, the number of synchronous events did decline significantly, from 80 to 60 in the first low-passed condition and 60 to 46 in the second, more extreme, low-passed condition. The reduction in synchrony by structural degradation thus results from a decrease in the number of synchronous events. This reduced the proportion of synchronous spikes versus asynchronous spikes, which is our definition of synchrony for the PSP algorithm.

Receptive Field Analysis

Unlike simple stimuli, natural scenes have complex high-order spatial correlations (Field et al. 1993; Schwartz and Simoncelli, 2001). Neighboring locations have similar color and intensity values and line segments are predominantly linear with a decreasing probability of greater curvature (Geisler et al. 2001; Sigman et al. 2001; Elder and Goldberg 2002). Field et al. (1993) found that perceptual integration of oriented Gabor elements depended on their joint relative orientation and spatial position, which resembled the relationship of contour segments in natural scenes. Like similar studies that suggest the structure and function of the visual system reflects the statistics found in nature (Barlow 1961; Kersten 1987; Field 1987; Simoncelli 2003), their concept of an association field (Field et al. 1993; Hess et al. 2003) was proposed as a behavioral correlate with specialized filter cells in the visual cortex. Association field theory predicts linking between orientation-tuned cells that depends on the extent to which

115

receptive fields are aligned on notional contours. Using cocircular stimulation, we found that synchronous activity in V1 tends to follow the predictions made by the association field in that synchrony was generated between pairs of cells with similar relative orientation and closer receptive field proximity (Samonds et al. 2006).

Here we examine the properties of receptive field configurations which generate significant amounts of synchrony in assemblies with more than two members. We found that assemblies with large amounts of synchronous activity tended to be arranged such that all receptive fields followed the association field rules of alignment and spatial proximity (Field et al. 1993). Alignment was computed as the maximum preferred orientation difference among all cells in the assembly. Receptive field overlap was used as a measure of proximity and was computed as the ratio of overlapping area among individual fields to the total area subtended by the compound assembly receptive field (Figure 4.6C). Since this measure is a percentage, it is normalized for receptive field size and eccentricity. In addition, these measures can be calculated for larger assemblies without considering an increasing number of pair-wise combinations.

Figure 4.6A shows the receptive fields and orientation preferences of 3 three-cell assemblies on Image 1 and these groups were chosen for demonstration based on their matching firing rates. For these three assemblies, we measured their average synchrony, average firing rate (computed as the mean over each cell's individual firing rates after subtraction of the baseline activity measured during the null stimulus), maximum orientation difference in the group, and receptive field overlap (see Figure 4.6B). Firing rates did not differ among the groups, and an increase in synchrony seen from Assembly 1 to Assembly 3 corresponded to a decrease in the relative orientation preference between cells and an increase in receptive field overlap. In fact, we measured these two
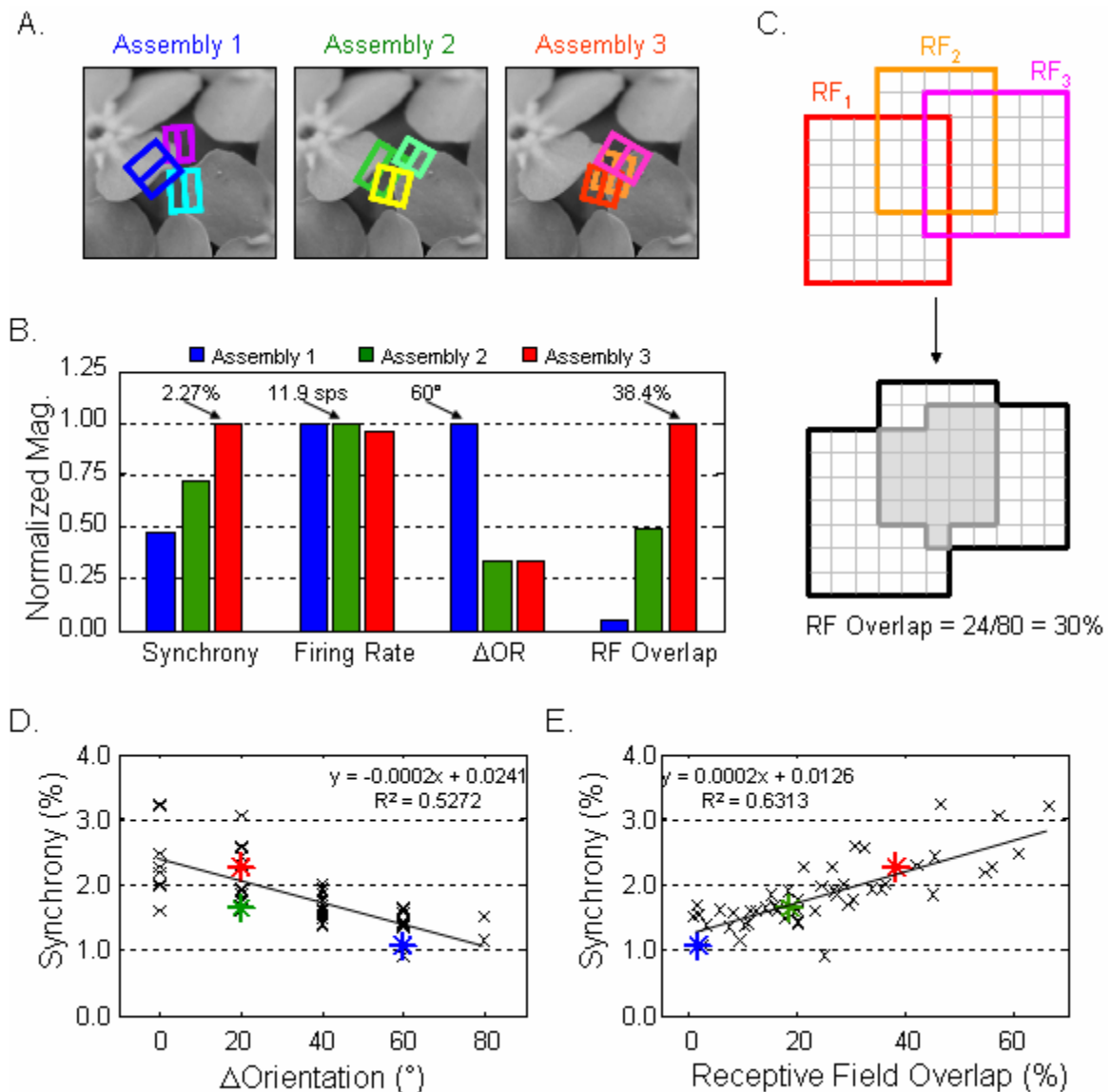
Figure 4.6. Receptive field analysis. (A) The receptive fields of three 3-cell assemblies are displayed with their orientation preferences on Image 1. These assemblies have similar average firing rates (see (B)). (B) Bar graph of synchrony, firing rate, maximum orientation difference, and receptive field overlap (normalized to the maximum in each case, which is displayed above the tallest bar) for the assemblies shown in (A). (C) Schematic of receptive field overlap calculation. Overlap is computed as the ratio of overlapping area among individual fields to the total area subtended by the compound assembly receptive field. Since this measure is a ratio, it is normalized for receptive field size and therefore corrected for eccentricity. (D) Synchrony plotted against maximum orientation difference for n = 50 three-cell assemblies. The data points for the assemblies in (A) are plotted with asterisks. (E) Synchrony plotted against receptive field overlap for n = 50 three-cell assemblies. Again, the assemblies in (A) are marked with asterisks.

parameters across our population of 50 three-cell assemblies (Figure 4.6D,E) and found moderately strong correlations between them and synchrony ($R^2 = 0.53$ for orientation and $R^2 = 0.63$ for receptive field overlap).

Discussion

Using a novel analytical tool, we studied the responses of synchrony-defined neural assemblies to three natural images that had been modified with noise addition, frequency filtering, and contrast reversal. For both noise addition and low-pass filtering, synchrony is reduced much more strongly than firing rate, and synchrony is sensitive to the degree of modification, unlike firing rate. This reduction in the amount of synchrony was related to a decrease in the amount of total time spent in synchrony due to a decline in the number of synchronous events. We found no significant change in either response property for contrast reversal, indicating that synchrony, like firing rate, shows luminance invariance and non-linear rectification in complex cells.

When analyzing the evolution of synchrony over time we found that the largest amount of synchrony occurs during the onset response transient, even after normalization to compensate for chance synchronous events due to an increase in firing rate. However, this quantity decreases with progressive structural degradation. Similar to firing rate, the residual responses observed for synchrony during the white noise stimulus can be approximately accounted for by motion effects in which jitter motion during the stimulus presentation induced activity.

Finally, we analyzed receptive field properties and found that the degree of neuronal synchronization correlates with receptive field configurations exhibiting good alignment and proximity, which suggests that the underlying local stimulus structure to

118

which the assembly is responding is configured with similar alignment and close proximity (e.g., like a continuous, well-defined contour). In the examples from Figure 4.6A, each assembly had a similar firing rate which indicates a sort of equal driving effectiveness between assembly and local image structure. However, the differences reflected in the magnitudes of synchrony could be related to the different arrangements of local structure, specifically how well associated the structure is within the compound receptive field. Orientation and proximity are hallmark properties of the association field (Field et al. 1993), which is based on the perception of contours and continuity. Similar relative orientations contribute to axial alignment, or continuity, which is important since the responses of V1 cells are enhanced when co-aligned structure is presented outside the classical receptive field (Kapadia et al. 1995), but inhibited with co-oriented (parallel) stimulation in the non-classical periphery (Born and Tootell 1991).

Supporting the notion that synchrony appears to encode contours that follow the association field rules is the observation that synchrony was not altered during presentation of high-pass filtered images. In natural scenes, contours and edges are represented by high spatial frequencies that are retained after filtering. From these preliminary observations we hypothesize that while firing rate signals the fundamental structure of the image, synchrony transfers information on fine detail, which is disrupted either by noise or low-pass filtering. This is consistent with our earlier finding that synchrony signals fine, but not coarse, changes in orientation (Samonds et al. 2003).

Implications for Contour Integration

While the spatiotemporal filter design of neurons in the primary visual cortex is sufficient to represent the local contrast of edges within an individual receptive field

(Hubel and Wiesel 1962; Maffei and Fiorentini 1973), edges and contours that extend beyond the scope of one neuronal filter require the organized influence of other neurons for integration. Several neuroanatomical and neurophysiological studies have proposed that contour integration is initiated by linking between orientation-tuned cells in the primary visual cortex (Hess, Hayes, & Field, 2003). However, the mode and source (i.e., feedforward, feedback, lateral projections) of integration information is unknown, although V1 horizontal connections project primarily to orientation columns with similar orientation preferences (Malach et al. 1993; Bosking et al. 1997) and there are longer connections between axially aligned cells (Bosking et al. 1997).

Synchronization of neural responses appears to link cells with similar orientation preferences (Eckhorn et al. 1988; Gray et al. 1989), and our previous study demonstrated that synchrony could also facilitate linking between cells with an alignment difference of up to 80 degrees (Samonds et al. 2006). Here we demonstrate synchrony's strong dependence on orientation (Figure 8D), which was enhanced by the close proximity of receptive fields. Synchrony may allow for an adaptive mechanism of contour detection that links cells via short-term enhancement of synaptic effectiveness. A possible mechanism is described by Womelsdorf et al. (2007) who demonstrated that an increase in assembly interactions is more likely when rhythmic activity between assemblies was in phase. As receptive field properties may change with context (Pettet and Gilbert 1992), this plasticity would be beneficial by having a virtually-connected system instead of overcoming hard-wired anatomical restrictions. Synchrony can then identify salient contours, which have the potential to be integrated at subsequent locations in the extrastriate hierarchy.

Temporal Dynamics of Larger Assemblies with the PSP Algorithm

While array technology allows for the simultaneous single-unit recording of dozens of neurons, current analysis methods are insufficient to completely describe cooperative population activity. Perkel et al. (1967) introduced the cross-correlation histogram (CCH) method to quantify cooperative relationships between pairs of neurons. However, CCHs and other techniques such as the Joint Peri-Stimulus Time Histogram (JPSTH; Aertsen et al. 1989) cannot characterize the synchrony between more than two cells. The CCH has been extended to include cooperation among three cells (Gerstein and Perkel 1972; Perkel et al. 1975; Abeles and Goldstein 1977), but the resulting display is limited to triangular coordinates and cannot be applied practically to larger assemblies. Other techniques such as gravitational clustering (Gerstein and Aertsen 1985; Gerstein et al. 1985) identify cells that fire together, but the results are qualitative, do not allow for dynamic grouping, and are still based on pair-wise distance calculations.

However, one important feature of the JPSTH and gravitational clustering methods is that cooperative activity can be tracked over time. We introduced the PSP algorithm, which tracks synchronous events and includes the added capability of analyzing any arbitrary number of neurons. In the PSP algorithm, synchrony is computed as a fraction of total activity within an assembly and can be monitored dynamically throughout the stimulus presentation. Like firing rate, averaging synchrony across the entire presentation masks any information that is time-dependent and may be strongly affected by events such as the stimulus onset. On the other hand, examining the temporal evolution of synchronous activity may aid in understanding the neural substrate of synchrony, e.g., feedforward or feedback influences.

Investigating Natural Stimulation

While natural images are the most practical way of stimulating an army of cells, they are also fundamentally necessary for understanding the role of synchrony. The historic use of spatially or spectrally pure stimuli (lines, gratings) allowed controlled and systematic manipulation of the visual environment. This was founded on the presumptions that responses to simple stimuli could be used to describe the processing of more complex stimuli. However, more recent descriptions of previously unsuspected interactions such as receptive field reorganization due to stimulation of the non-classical periphery (Pettet and Gilbert 1992) suggest that we may not yet have a realistic model for cell behavior in the context of behavioral vision. For instance, David et al. (2004) found that natural tuning properties are not well-predicted from responses to grating sequences. This could be due in part to the reduced effectiveness of simple stimuli (as opposed to natural scenes) in driving cortical cells (Rieke et al. 1995). Since responses of V1 neurons to natural stimuli are both qualitatively and quantitatively different from those to simple stimuli (Baddeley et al. 1997; Kayser et al. 2003), progress in understanding the cellular support of behavioral vision must rely on natural image stimulation.

References

Abeles M and Goldstein M Jr. Multiple spike train analysis. *Proceedings of the IEEE*, 65, 762-773, 1977.

Aertsen AMHJ, Gerstein GL, Habib MK, and Palm G. Dynamics of neuronal firing correlation: Modulation of "effective connectivity". *Journal of Neurophysiology*, 61, 900-917, 1989.

Azouz R and Gray CM. Adaptive coincidence detection and dynamic gain control in visual cortical neurons in vivo. *Neuron,* 37, 513-523, 2003.

Baddeley R, Abbott LF, Booth MC, Sengpiel F, Freeman T, Wakeman EA, and Rolls ET. Responses of neurons in V1 and IT to natural scenes. *Proceedings of the Royal Society of London B Biological Sciences,* 264, 1775-1783, 1997.

Barlow HB. Possible principles underlying the transformation of sensory messages. In *Sensory Communication*, ed. WA Rosenblith, Cambridge, MA: MIT Press, 217-234, 1961.

Barlow HB. Single units and sensation: a neuron doctrine for perceptual psychology? *Perception*, 1(4), 371-394, 1972.

Born RT and Tootell RB. Spatial frequency tuning of single units in macaque supragranular striate cortex. *Proceedings of the National Academy of Sciences of the United States of America*, 15:88(16), 7066-7070, 1991.

Bosking WH, Zhang Y, Schofield B, and Fitzpatrick D. Orientation selectivity and the arrangement of horizontal connections in tree shrew striate cortex. *Journal of Neuroscience,* 17, 2112-2127, 1997.

David SV, Vinje WE, and Gallant JL. Natural stimulus statistics alter the receptive field structure of V1 neurons. *Journal of Neuroscience,* 24, 6991-7006, 2004.

Eckhorn R, Bauer R, Jordan W, Brosch M, Kruse W, Munk M, and Reitboeck HJ. Coherent Oscillations: A mechanism of feature linking in the visual cortex? *Biological Cybernetics*, 60, 121-130, 1988.

Elder JH and Goldberg RM. Ecological statistics of Gestalt laws for the perceptual organization of contours. *Journal of Vision,* 2, 324-353, 2002.

Field DJ. Relations between the statistics of natural images and the response properties of cortical cells, *Journal of the Optical Society of America A,* 4, 2379-2394, 1987.

Field DJ, Hayes A, and Hess RF. Contour integration by the human visual system: evidence for a local "association field". *Vision Research,* 33, 173-193, 1993.

Geisler WS, Perry JS, Super BJ, and Gallogly DP. Edge co-occurrence in natural images predicts contour grouping performance. *Vision Research,* 41, 711-724, 2001.

Gerstein GL and Aertsen AMHJ. Representation of cooperative firing activity among simultaneously recorded neurons. *Journal of Neurophysiology,* 54, 1513-1528, 1985.

Gerstein GL and Perkel DH. Mutual temporal relationships among neuronal spike trains: Statistical techniques for display and analysis. *Biophysical Journal,* 12, 453-473, 1972.

Gerstein GL, Perkel DH, and Dayhoff JE. Cooperative firing activity in simultaneously recorded populations of neurons: Detection & measurement. *J Neurosci* 5, 881-889,1985.

Gray CM, Konig P, Engel AK, and Singer W. Oscillatory responses in cat visual cortex exhibit inter-columnar synchronization which reflects global stimulus properties. *Nature*, 338, 334-337, 1989.

Hess RF, Hayes A, and Field DJ. Contour integration and cortical processing. *Journal of Physiology (Paris)*, 97, 105-119, 2003.

Hubel DH and Wiesel TN. Receptive fields, binocular interaction and functional architecture in the cat's visual cortex. *Journal of Physiology,* 160, 106-154, 1962.

Kapadia MK, Ito M, Gilbert CD, and Westheimer G. Improvement in visual sensitivity by changes in local context: parallel studies in human observers and in V1 of alert monkeys. *Neuron*, 15(4), 843-856, 1995.

Kayser C, Salazar RF, and Konig P. Responses to natural scenes in cat V1. *Journal of Neurophysiology,* 90, 1910-1920, 2003.

Kelly RC, Smith MA, Samonds JM, Kohn A, Bonds AB, Movshon JA, and Lee TS. Comparison of recordings from microelectrode arrays and single electrodes in the visual cortex. *Journal of Neuroscience*, 10:27(2), 261-264, 2007.

Kersten D. Predictability and redundancy of natural images. *Journal of the Optical Society of America A*, 4, 2395-2400, 1987.

Maffei L and Fiorentini A. The visual cortex as a spatial frequency analyser. *Vision Research,* 13(7), 1255-1267, 1973.

Malach R, Amir Y, Harel M, and Grinvald A. Relationship between intrinsic connections and functional architecture revealed by optical imaging and in vivo targeted biocytin injections in primate striate cortex. *Proceedings of the National Academy of Sciences of the United States of America*, 90, 10469-10473, 1993.

Nishimoto S, Arai M, and Ohzawa I. Accuracy of subspace mapping of spatiotemporal frequency domain visual receptive fields. *J Neurophysiology,* 93, 3524-3536, 2005.

Perkel DH, Gerstein GL, and Moore GP. Neuronal spike trains and stochastic point processes, II. Simultaneous spike trains. *Biophysical Journal,* 7, 419-440, 1967.

Perkel DH, Gerstein GL, Smith MS, and Tatton WG. Nerve-impulse patterns: a quantitative display technique for three neurons. *Brain Research,* 00, 271-296, 1975.

Pettet MW and Gilbert CD. Dynamic changes in receptive field size in primary visual cortex. *Proceedings of the National Academy of Sciences of the United States of America*, 89, 8366-8370, 1992.

Rieke F, Bodnar DA, and Bialek W. Naturalistic stimuli increase the rate and efficiency of information transmission by primary auditory afferents. *Proceedings of the Royal Society of London B Biological Sciences,* 262, 259-265, 1995.

Rousche PJ and Normann RA. Chronic recording capability of the Utah Intracortical Electrode Array in cat sensory cortex. *Journal of Neuroscience Methods,* 82, 1-15, 1998.

Rousche PJ and Normann RA. A method for pneumatically inserting an array of penetrating electrodes into cortical tissue. *Annals of Biomedical Engineering*, 20, 413-422, 1992.

Samonds JM, Allison JD, Brown HA, and Bonds AB. Cooperation between Area 17 neuron pairs enhances fine discrimination of orientation. *Journal of Neuroscience,* 23, 2416-2425, 2003.

Samonds JM, Zhou Z, Bernard MR, and Bonds AB. Synchronous activity in cat visual cortex encodes collinear and cocircular contours. *Journal of Neurophysiology,* 95, 2602-2616, 2006.

Schneidman E, Berry MJ 2nd, Segev R, and Bialek W. Weak pairwise correlations imply strongly correlated network states in a neural population. *Nature,* 440:1007-1012, 2006.

Schmidt S, Horch K, and Normann RA. Biocompatibility of silicon-based electrode arrays implanted in feline cortical tissue. *Journal of Biomedical Materials Research*, 27, 1393-1399, 1993.

Schwartz O and Simoncelli EP. Natural signal statistics and sensory gain control. *Nature Neuroscience*, 4, 819-825, 2001.

Shadlen MN and Movshon JA. Synchrony unbound: a critical evaluation of the temporal binding hypothesis. *Neuron*, 24(1):67-77, 111-125, 1999;

Shoham S, Fellows MR, and Normann RA. Robust, automatic spike sorting using mixtures of multivariate t-distributions. *Journal of Neuroscience Methods*, 127, 111-122, 2003.

Sigman M, Cecchi GA, Gilbert CD, and Magnasco MO. On a common circle: natural scenes and Gestalt rules. *Proceedings of the National Academy of Sciences of the United States of America,* 98, 1935-1940, 2001.

Simoncelli EP. Vision and the statistics of the visual environment. *Current Opinion in Neurobiology*, 13,144-149, 2003.

Singer W and Gray CM. Visual feature integration and the temporal correlation hypothesis. *Annual Review of Neuroscience*, 18, 555-586, 1995.

Skottun BC, De Valois RL, Grosof DH, Movshon JA, Albrecht DG, and Bonds AB. Classifying simple and complex cells on the basis of response modulation. *Vision Research*, 31(7-8), 1079-1086, 1991.

Strehler BL and Lestienne R. Evidence of precise time-coded symbols and memory of patterns in monkey cortical neuronal spike trains. *Proceedings of the National Academy of Sciences of the United States of America,* 83, 9812-9816, 1986.

Touryan J, Felsen G, and Dan Y. Spatial structure of complex cell receptive fields measured with natural images. *Neuron*, 3:45(5), 781-791, 2005.

Ts'o DY, Gilbert CD, and Wiesel TN. Relationships between horizontal interactions and functional architecture in cat striate cortex as revealed by cross-correlation analysis. *Journal of Neuroscience.* 6, 1160-1170, 1986.

Victor JD. How the brain uses time to represent and process visual information. *Brain Research*, 886, 33-46, 2000.

Vinje WE and Gallant JL. Sparse coding and decorrelation in primary visual cortex during natural vision. *Science,* 287, 1273-1276, 2000.

von der Malsburg C. The what and why of binding: the modeler's perspective. *Neuron*, 24(1):95-104, 111-125, 1999.

Womelsdorf T, Schoffelen JM, Oostenveld R, Singer W, Desimone R, Engel AK, and Fries P. Modulation of neuronal interactions through neuronal synchronization. *Science*, 316(5831), 1609-1612, 2007.

CHAPTER V

SYNCHRONOUS ACTIVITY IN CAT VISUAL CORTEX DETECTS COMPLEX
CONTOURS IN NATURAL IMAGES

Introduction

In striate cortex, the spatiotemporal filter characteristics of individual neurons and

the localization of their classical receptive fields limit their responses to a restricted range

of information contained within the input. More specifically, the emergence of enhanced

specialization for certain stimulus parameters such as spatial frequency, orientation, and

direction allow cells to respond selectively to local contrast patches (Hubel and Wiesel

1962). In natural images, contrast gradients can exist for object boundaries, texture

patterns, surface shading, and shadows. As simple edge detection mechanisms (Marr and

Vaina 1982), V1 neurons parse images into their basic structural elements. However,

many of these candidate edges reflect spurious contrast information from uninteresting

properties of the stimulus that do not necessarily contribute to the description of salient

visual features. Relevant contrast segments that define important stimulus structures are

grouped together by the visual system to give the perception of global elements such as

complex contours and complete figures, but the mechanism supporting this grouping (the

binding problem; Treisman 1996) is poorly understood.

The temporal binding theory (Milner 1974; von der Malsburg 1981) postulates

that the firing of neurons which identify related contour segments are linked through

neuronal synchronization. The first neurophysiological experiments linking synchrony

and feature integration used drifting light bars (Eckhorn et al. 1988; Gray et al. 1989).

This type of coherent collinear stimulation yielded synchrony between pairs of neuron

clusters with similar orientation preferences and collinear receptive fields. However, if synchrony is involved in feature integration, then it should be observed between cells with different orientation preferences given the appropriate stimulation. In fact, collinearity among receptive fields is a special case of the more general property of cocircularity (Parent and Zucker 1989) in which receptive fields have orientation preferences that are tangent to the same circle. Cocircular structures are ubiquitous in natural scenes (Geisler et al. 2001; Sigman et al. 2001; Elder and Goldberg 2002) and the predictable relationship between cocircular segments has been proposed as the foundation of contour integration (Field et al. 1993). Inspired by psychophysical studies, Field et al. (1993) introduced the *association field* framework which describes the perception of contours and continuity. In this paradigm, contour segments are grouped depending on proximity and the similarity of their orientations. Applying these concepts to neurophysiology, association field theory predicts linking between orientation-tuned cells that is dependent on their joint relative orientation and spatial position.

By using an experimental protocol consisting of drifting sinusoidal gratings and concentric rings, we tested synchrony's adherence to association field rules by seeing if it predictably existed for pairs of cells with different orientation preferences, but whose receptive fields still had cocircular alignments (Samonds et al. 2006). Using a 10x10 microelectrode array, we simultaneously recorded from multiple single-units in areas 17 and 18 of anesthetized cats and found that neuron pairs synchronized based on an appropriate match between stimulus curvature and receptive field configuration. Furthermore, synchronous responses were more reliable than changes in average firing rate in discriminating between concentric ring and grating stimuli. Group membership

was found to be dynamic in that individual cells could belong to more than one functional group, which assembled based on the spatiotemporal properties of the stimulus.

Analyses of electrode distance, receptive field overlap, and synchronous lag times show that the magnitude and probability of observing synchrony among cell pairs matched the fundamental prediction of the association field theory. Extending collinear synchrony results (Eckhorn et al. 1988; Gray et al. 1989) to cells with cocircular receptive field properties is vital in establishing synchrony's role in complex feature integration. In this paper, we measured synchrony's dependence on the proximity, orientation, and alignment of assembly receptive fields during natural stimulation and used these parameters to create an index of association. Synchrony was moderately correlated with this index showing adherence to the association field rules for larger neural assemblies and complex natural features. By quantitatively correlating synchronous activity to local contrast structure, we found that cooperative activity is driven by a continuous, well-defined contour. Furthermore, synchrony measured between assemblies driven by different contours on the same or different objects was inhibited. These findings suggest a more global and purposeful function in which synchrony detects related contour segments, which have the ability to be integrated at higher processing centers throughout the visual system.

Materials and Methods

Data Recording and Acquisition

Four adult cats (2.5-4.0 kg) were prepared for electrophysiological recordings in the primary visual cortex. All procedures were performed in accordance with guidelines

129

set forth by the American Physiological Society and the Institutional Animal Care and Use Committee at Vanderbilt University and are described in Chapter 2. Simultaneous single-unit recordings were made from cells in the visual cortex via the Utah Intracortical Electrode Array (UIEA; Cyberkinetics Neurotechnology Systems, Foxborough, MA). The UIEA recordings have good signal to noise ratios and have been shown to have qualities comparable to those from single-electrode recordings (Kelly et al. 2007). The implant is a square 10x10 silicon array (electrode length of 1.0 mm), which is inserted to a depth of 0.6 mm with a pneumatic implantation tool (Rousche and Normann 1992) that minimizes tissue damage (Schmidt et al. 1993; Rousche and Normann 1998). The insertion depth concentrates the electrodes in layers II/III and avoids impact to the cortical surface by the electrode base. The wires from the array to the amplifier are flexible, which enhances stability and allows for reliable recording sessions of more than thirty hours. Thresholds are dynamic and set to 3.25x the mean activity on each electrode and waveforms are sampled at 30 kHz for 1.5 ms windows. Viable channels are processed with a MATLAB-based spike-sorting program to remove noise and artifact (Shoham et al 2003). Approximately 5% of channels with multi-unit activity were discarded. Channels with isolated single-unit activity were used only if the activity was $\geq$ 5 spikes per second and showed clear orientation tuning (signal to noise $\geq$ 2:1) when viewing drifting sinusoidal gratings. We recorded from 134 single units, 125 of which were complex cells (Hubel and Weisel 1962; Skottun et al. 1991) with a median relative modulation, F_1/F_0, of 0.06 (n = 125 cells). All cells were used for analysis.

Stimulation

We tested two different types of stimuli: drifting sinusoidal gratings and a natural

130

image sequence. In order to estimate receptive field properties during the experiment, we used the grating protocol to reveal orientation tuning preferences (Nishimoto et al. 2005), which were subsequently used during manual mapping of receptive field extent and location. The center of the aggregate activity was determined and used to align the stimuli to maximize neuronal responses from the majority of the recorded population. All stimuli were displayed on a gamma-corrected SONY Trinitron 21" monitor with a resolution of 800 x 600 pixels (22.6 pixels per visual degree) driven either by a Cambridge Research Systems VSG2/3F controller board (for gratings) or a video controller using the WinVis software package (for the natural image sequence). Displays were refreshed at 120 Hz, which avoided entrainment artifact (Wollman and Palmer 1995; Snider et al. 1996). The natural stimulus protocol (Figure 5.2A) contained a sequence of 336 natural, grayscale images from www.imageafter.com, each rotated at 9 angles (40° to 360°, in 40° increments) for an effective stimulus set of 3024 pictures, presented for 500 ms followed by a mean luminance (73 cd/m^2) interval of 500 ms. In addition, there were two null stimuli during which only the mean luminance was shown. Each presentation was static, images were randomly interleaved, and the entire sequence was repeated 8, 9, 10, or 13 times for reliability. All stimuli spanned 18°x18° and were scaled to have a global contrast of 0.32 (see Touryan et al. 2005).

Data Processing

Since previous measures quantify correlation among pairs of cells (Perkel et al. 1967; Aertsen et al. 1989), we have developed a method that detects and quantifies the amount of synchronous activity in a neuronal assembly of arbitrary size. As a hypothetical neural substrate for encoding salient stimulus properties, synchrony

enhances the probability of eliciting postsynaptic action potentials (PSPs) when neurons behave as coincident detectors (Azouz and Gray 2003). Our basic algorithm (described in detail in Chapter 2) is designed to reflect the relevance of group synchrony to postsynaptic neurons by modeling the temporal summation of postsynaptic potentials. The steps in the algorithm are as follows: (Step 1) Convert spike waveforms to point-process spike trains. (Step 2) Convolve point-process spike trains with an alpha function to create PSP trains. (Step 3) Determine the time windows (t_s) during which all PSP trains exhibit activity. (Step 4) Add PSP trains from all cells to get PSP activity for the entire assembly. (Step 5) Integrate the assembly activity over t_s and t then divide to compute the Raw Score. (Step 6) Compute Chance Score by shifting 1 or more stimulus periods and repeating Steps 1-5. (Step 7) Compute statistical significance and normalize the magnitude of synchrony.

By convolving a point-event spike train with a truncated (10 ms) alpha waveform, we derive a similarity measure that is conscious of time. PSP trains for a group of cells can be summed and compared to identify spike times that are coincident. The magnitude of synchrony is computed as the ratio of the area under coincident waveforms to the total area under all waveforms in the assembly. Unlike other approaches, this can be applied to neural assemblies of arbitrary size, not just pairs. Also, the temporal dynamics of synchrony can be monitored throughout the stimulus presentation. By using the shift predictor (Step 6; Perkel et al. 1967), we can resolve and separate sources of synchrony in order to normalize our results for the effects of firing rate. However, the uncertainties of normalization and firing rate dependence are minimized due to the very low probability of chance events as group sizes grow.

Results

To examine the specific relationships between complex natural stimulus structure and synchronous activity in assemblies of 2-8 cells, we used a sequence of natural images to elicit responses. The receptive fields of the synchronously-driven cells were then compared to the image to identify the local contrast structure driving each interaction. Using a broad selection of natural images offers an efficient approach for analyzing the complex spatial organization of larger assemblies. We determined the relevance of association field concepts (Field et al. 1993) to the grouping of cooperative members by studying how the magnitude of synchrony was affected by the orientation, proximity, and continuity of neighboring receptive fields. Data from these dependency studies were integrated to create a Contour Index, which described how well an aggregate receptive field conformed to a well-associated contour configuration. Together with a Contrast Index, which estimates the expected firing rate response, these measures quantified the relationship between synchronous assembly and contour structure in natural scenes. Finally, we investigated the viability of inter-assembly linking as a binding mechanism for multiple related contours.

Using a 10x10 microelectrode array, we simultaneously recorded from 134 cells in the visual cortex of four paralyzed and anesthetized cats. The number of candidate grouping possibilities offered by the size of our moderate recording population is exhaustive and cannot be analyzed in its entirety. Instead, we sampled these combinations by choosing assemblies of 2-8 neurons with an assortment of receptive field layouts. Assemblies with a range of orientation preferences, proximities, and alignments were chosen to optimize responses to the variety of structural information in the natural image sequence. We used different thresholds for each parameter to find over

one thousand assemblies in each size group (N = 1399, 1166, 1379, 1432, 1394, 1422, and 1373 for assembly sizes 2-8, respectively). Because of the broad range of spatial structures contained within the sequence, each identified assembly synchronized beyond the chance level (significance was measured with the PSP Method using $\alpha = 0.01$) to at least one image and usually to several images with similar features.

Resolution of Trigger Features for an Assembly

We have previously shown that synchrony between cell pairs can represent cocircular contours (Samonds et al. 2006), suggesting that synchrony within larger assemblies may be involved in encoding more complex contours. To investigate the role of synchrony as a contour-encoding mechanism in natural vision, we measured the synchronous responses of larger neural assemblies to a sequence of 3024 natural images. In a previous study (Chapter 4), we found that the degree of synchrony depended on the coherence of visual structure and was negatively influenced by spatial modifications like noise addition and frequency filtering. While those results yield information on how assemblies respond to global image manipulations, they do not address the particular spatial structure that might provide ideal stimulation for the group. In a method adapted from Smyth et al. (2003) and Weliky et al. (2003), we presented the natural image sequence and identified images that elicited strong synchrony and firing rate responses in a given group. Orientation and spatial frequency components filtered by the measured selectivity and spatial localization of each cell in the assembly were extracted from each image (see Appendix), summed together and weighted by the magnitude of the response. The resulting composite synthesized a stimulus attribute seen in each picture or combined different structural features to create a new attribute that was ideal for the group.

134

For each assembly, synchrony responses were measured across the image set and normalized by the maximum response. The firing rate of each cell was normalized by its maximum response and responses from each cell in the assembly were averaged together to compute the group response. The firing rate response for each assembly was measured for each image in the sequence and normalized by the maximum group response across all stimulus conditions. On the same scale, the synchrony and firing rate responses were then averaged to calculate a combined response for each stimulus. We combined these quantities because we wanted to investigate synchrony when all cells were being optimally driven. The top ten images with the largest combined responses were selected for feature extraction. The orientation preference, spatial frequency tuning, and location of each receptive field in the assembly were used to filter the image for the local contrast information to which the cell is responding. The contrast segments from each neuron were summed together to produce filtered visual information for the entire assembly. The extracted features from the top ten images were weighted by their combined response and summed to produce a composite element that embodied preferred features for the assembly.

Figure 5.1 shows trigger features for two assemblies of four neurons. In Figure 5.1A, the best images elicit large synchrony and firing rate responses and the synthesized features resembles a well-defined contour. A similar contour from different images was reliably and consistently signaled by the assembly activity and this selectivity has been manifested by the composite of extracted features. In Figure 5.1B, a different assembly shows an enhanced selectivity for an acute corner feature seen across multiple images. This feature generated the highest combined response, but overall synchrony levels were low when compared to the first assembly. In both cases, the firing rate responses
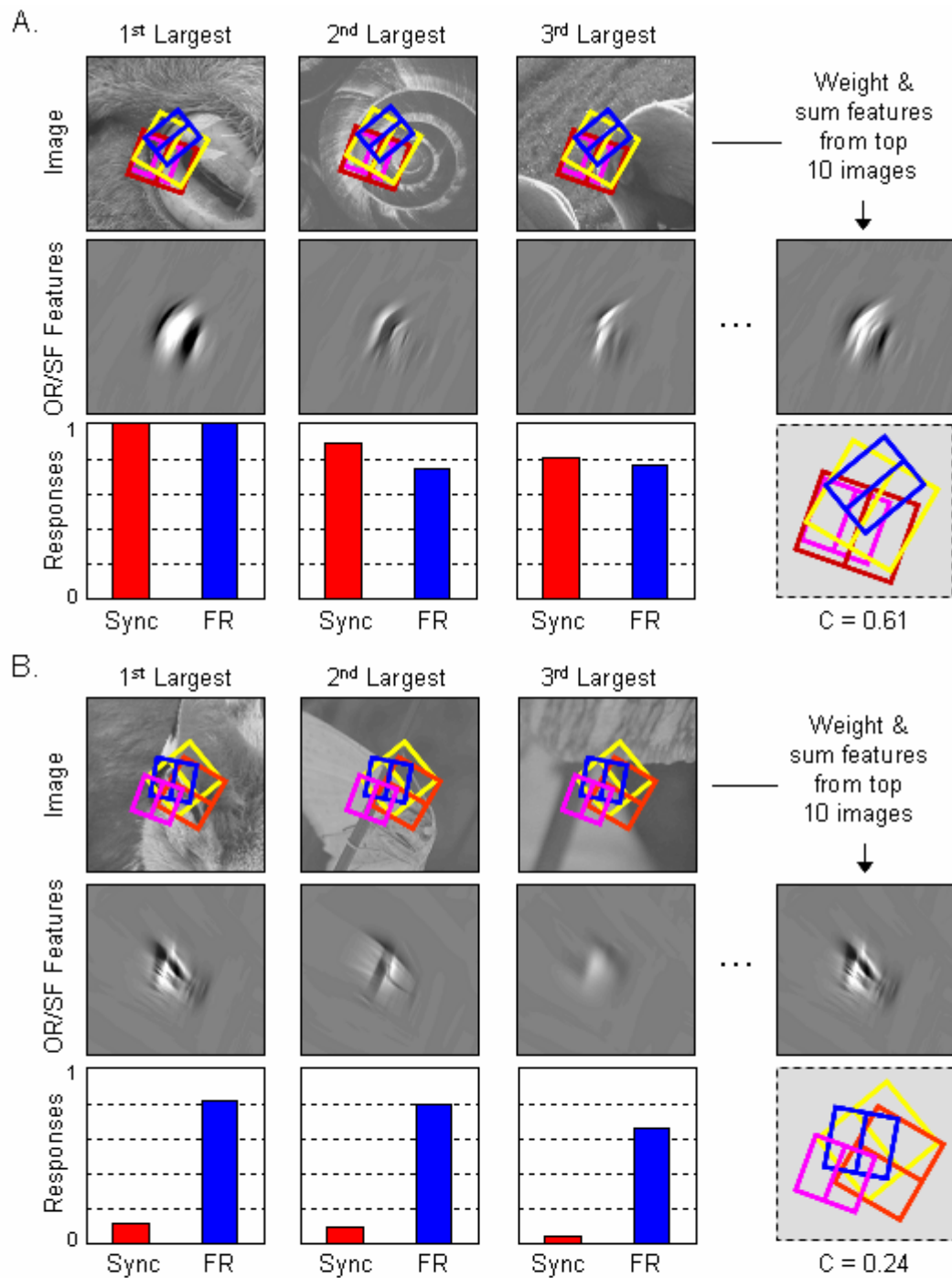
Figure 5.1. (A) Assembly of 4 neurons with large firing rate and synchrony responses (bar graphs) to the natural images shown. These images generated the highest combined responses. Under each picture are the extracted orientation and spatial frequency features (contrast enhanced 5x) to which the assembly is responding. The top 10 extracted images were summed and weighted by the magnitude of the combined response to produce the final image. (enhanced 5x). (B) Assembly of 4 neurons with large firing rate responses, but poor synchrony responses, to the images with the largest combined responses.

136

suggested each assembly was driven adequately by the stimulus, but some property of the first assembly was more conducive to cooperation. We hypothesize that this property was related to the spatial relationship between receptive fields. In Figure 5.1A, receptive fields from each cell had similar orientations, closer proximities, and better alignment as compared to the assembly in Figure 5.1B.

Association Field Correlations

Unlike simple stimuli, natural scenes have complex high-order spatial correlations (Schwartz and Simoncelli 2001). In an image, neighboring locations have similar color and intensity values and line segments tend to be arranged in a collinear or cocircular fashion (Geisler et al. 2001; Sigman et al. 2001; Elder and Goldberg 2002). First-order image statistics describe individual pixel intensities, whereas second-order statistics describe correlations between pairs of pixel values. Higher-order statistics are needed to describe local features such as contours, surfaces, and textures. To psychophysically investigate how the visual system codes contour continuity, Field et al. (1993) studied the integration of contours made from spatial frequency narrowband elements. By using Gabor patch segments, the investigators systematically varied the spatial properties relating adjacent elements to understand the perceptual discrimination of grouped segments from random background constituents. These results formed the foundation of a theory known as the association field, which describes the perception of contours based on continuity. In this model, the probability of perceptual grouping is higher when neighboring contour segments are close and have similar orientation and alignment.

Numerous studies suggest the visual system may be optimized for processing the statistics of natural scenes (Barlow 1961; Kersten et al. 1987; Simoncelli 2003). A neurophysiological correlate of the association field using orientation-tuned cells in V1 would provide a direct link between physiology and perceptual behavior. This theory predicts linking between neurons that is dependent on their joint relative orientation and spatial position. The results of our previous study (Samonds et al. 2006) suggest that synchronous activity in the primary visual cortex is consistent with the association field. Pairs of cells synchronized to drifting sinusoidal concentric rings as long as their orientation preference and separation varied predictably by association field rules. To extend these findings to larger assemblies viewing more complex contours, we tested the hypothesis that synchrony would depend on the degree of association among assembly member receptive fields (see Figure 5.2B). We measured the synchrony from the image with the highest combined response for each assembly and plotted it against the receptive field parameters of proximity, orientation, and continuity (the next section describes how each measure was computed). Figure 5.2C shows the correlation between synchrony and each property for 399 assemblies of four cells observed during the same experiment. The magnitude of synchrony is moderately dependent on each property ($R = -0.48$ for proximity, $R = -0.56$ for orientation, and $R = -0.57$ for continuity), suggesting adherence to the association field predictions for larger assemblies and complex contours.

Contour Quantification Analysis

The results from Figure 5.1 suggest that the specific feature that best drives a synchronous assembly is a continuous, well-defined contour. We wish to quantitatively describe the contour content in natural images, but this is a challenging task. Contour
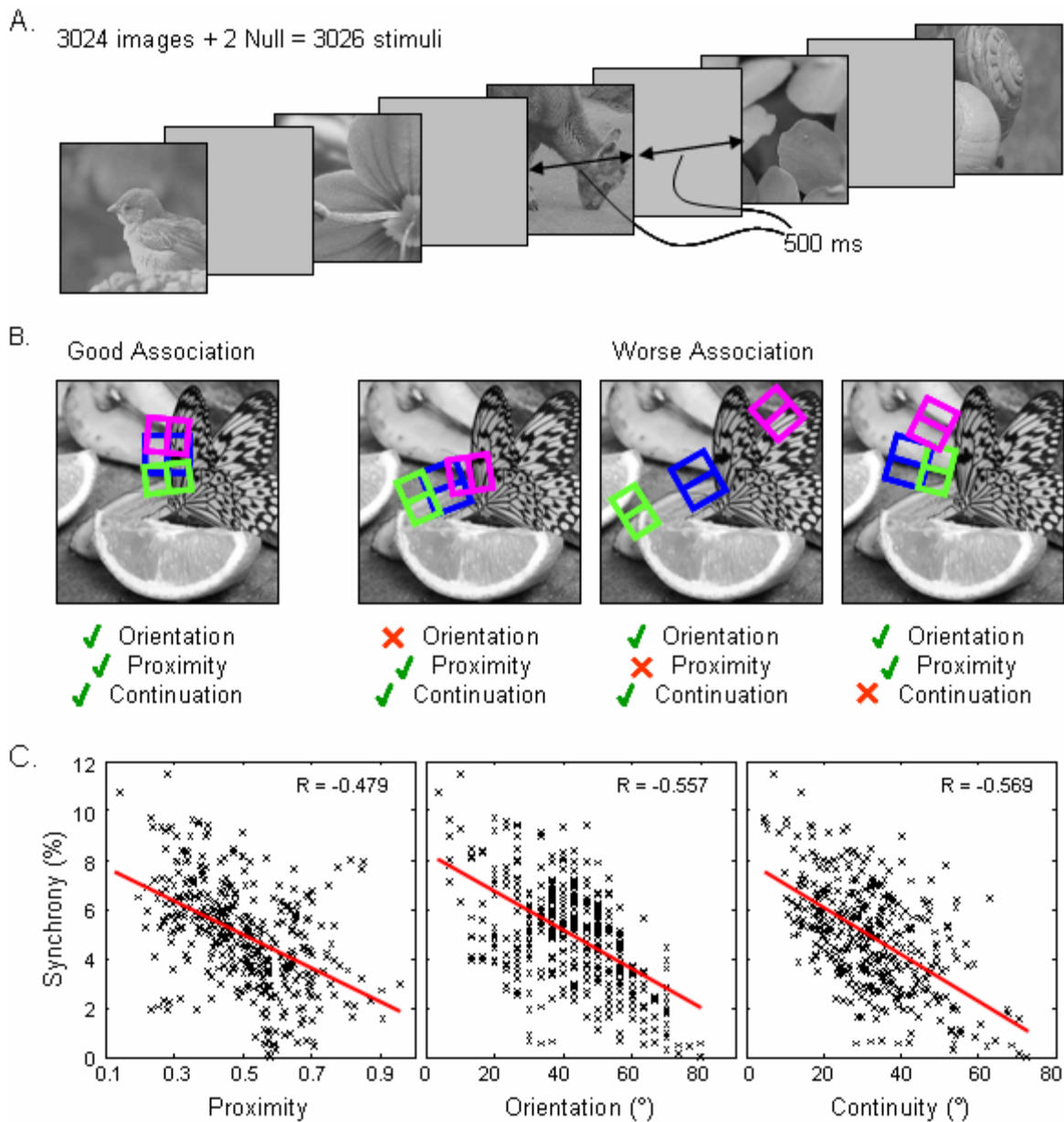
Figure 5.2. Association Field Properties. (A) Example images from the stimulus sequence (www.imageafter.com). Two null stimuli were added to the sequence of 3024 images to make 3026 total stimuli. (B) Properties of the Association Field model (Field et al. 1993). Contour segments are grouped more easily when they have similar orientations, close proximities, and good continuation. As a neurophysiological correlate, the model predicts linking between V1 neurons whose receptive fields have good associations according to the same principles. (C) Synchrony dependence on average distance between receptive field centers (normalized by the width of each receptive field), average assembly orientation difference, and continuation as measured by the average directional difference angle between a line drawn through the center of each receptive field and the orientation preference.

presence depends on contrast, blur, occlusions, and numerous other qualities that make identifying contours a subjective matter. Detection is also dependent on which assembly is viewing the image as contours will be "present" only if they fall within the assembly's aggregate receptive field. In order to quantitatively measure whether synchronous activity within assemblies is signaling contours in natural images, we have created a two-part measure based on the rules of implication (Figure 5.3). The first measure relates how well a contour structure fits an assembly's receptive field configuration and the second measures how well the assembly's receptive field configuration fits an image. Together, these measures describe how well a contour structure fits the part of the image the assembly is viewing. Good matches for each measure imply that the contrast structure eliciting a response from the assembly is arranged as a contour.

Here we will quantitatively relate the contour content of images to the spatial organization of the cells composing the synchronous assembly. The association field theory (Field et al. 1993; Hess et al. 2003) describes three properties of contour association: proximity, orientation, and continuity. In this paper, delta (δ) is the distance metric and represents the Euclidean distance between the centers of two neighboring receptive fields. This measure is normalized by the average width of the receptive fields in order to control for eccentricity. Distance values less than unity reflect overlapping receptive fields and those above unity are spatially distinct. In assemblies with more than two cells, this metric is computed as the average distance between consecutive neighboring receptive fields in a directed manner such that proximity is minimized within the assembly. Theta (θ) is the orientation metric and represents the difference in preferred orientations between neighboring cells. In assemblies with more than two neurons, this value is computed as the average difference in preferred orientation between

140
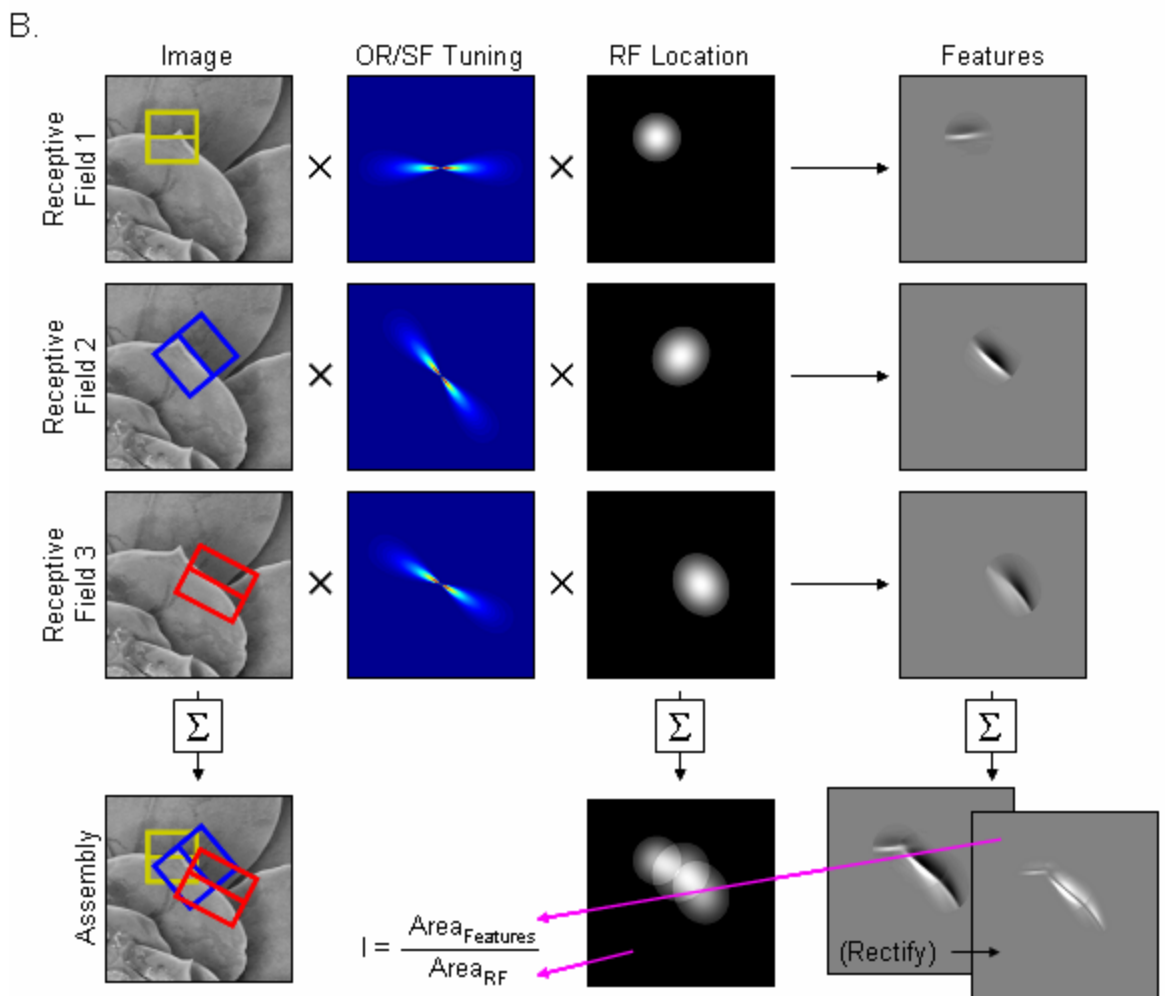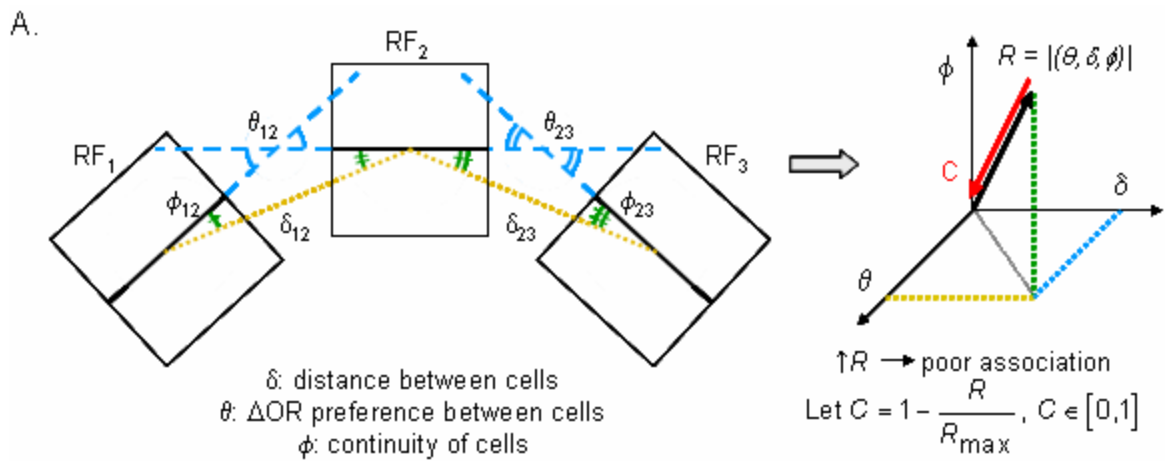
Figure 5.3. Contour quantification. (A) Assembly proximity, orientation, and continuity are integrated into a 3-D vector and reversed to compute the *Contour Index, C.* (B) The *Contrast Index, I,* is calculated by computing the area after rectifying the sum of extracted orientation and spatial frequency components for each cell and dividing by the area subtended by the assembly receptive field.

consecutive neighboring receptive fields and is an indication of curvature. Again, this follows the same direction as distance and has a maximum value of 90°. Phi (φ) is the continuity variable and is computed as the minimum difference between the orientation preferences of neighboring cells and the angle of a vector drawn between their receptive field centers. For assemblies with more than two cells, this metric is computed as the average continuity in directed neighboring cells and represents the degree of receptive field alignment (Field et al. 1993; May and Hess 2007).

Although Hess et al. (2003) described a more prominent perceptual discrimination effect for continuity than proximity and our results from Figure 5.2 suggest that synchrony is slightly less correlated with proximity, the three metrics described above are normalized (which gives equal weighting to each property) and integrated into one variable as the elements of a three-dimensional vector in "association space." However, this vector scales with an increase in these properties and thus represents and indication of poor association. Therefore, we have defined a new variable, C, which is termed the *contour index*:

$$C = 1 - \frac{R}{R_{max}} \tag{5.1}$$

The contour index is a number between 0 and 1 and represents the degree to which an assembly's receptive field properties fit a contour configuration as described by the association field theory. Receptive fields arranged with good association (distance, orientation, and continuity) will resemble a contour structure and have a contour index near one. Assemblies with poor receptive field associations will have a contour index near zero.

142

For the second measure, we needed to relate how well the receptive fields of an assembly match an image. A good indication of how well receptive field tuning is matched to the contrast structure in an image is the firing rate. A similar measure can be computed by measuring the local contrast information in the image in the area covered by the receptive fields of the assembly. Pooled cell activity is directly linked to local contrast structure (Weliky et al. 2003), so these measures are correlated (see Figure 5.4A). To compute the amount of contrast information in an image, we used a procedure modified from Weliky et al. (2003). We first created a feature matrix by extracting the orientation and spatial frequency components in the image matching the tuning properties of each cell in the assembly and summing them together (Figure 5.3B; see Appendix). Next, we computed the absolute value of the feature matrix, computed the area ($Area_{Features}$), and normalized it by the area subtended by the receptive fields ($Area_{RF}$, where areas covered by more than one receptive field are counted multiple times). This creates a measure, I, called the *contrast index* which describes the degree of fit between an assembly and an image:

$$I = \frac{Area_{Features}}{Area_{RF}} \tag{5.2}$$

The contrast index can be used to estimate the firing rate response of an assembly in order to avoid using variable responses from different stimulus trials or evaluate images for testing.

Using the same assemblies as in Figure 5.2C, Figures 5.4A-F display the different correlations for synchrony, firing rate, contour index, and contrast index. As mentioned above, firing rate and contrast index are highly correlated since the contrast index is an estimator of firing rate. Synchrony computed with the PSP algorithm is normalized for
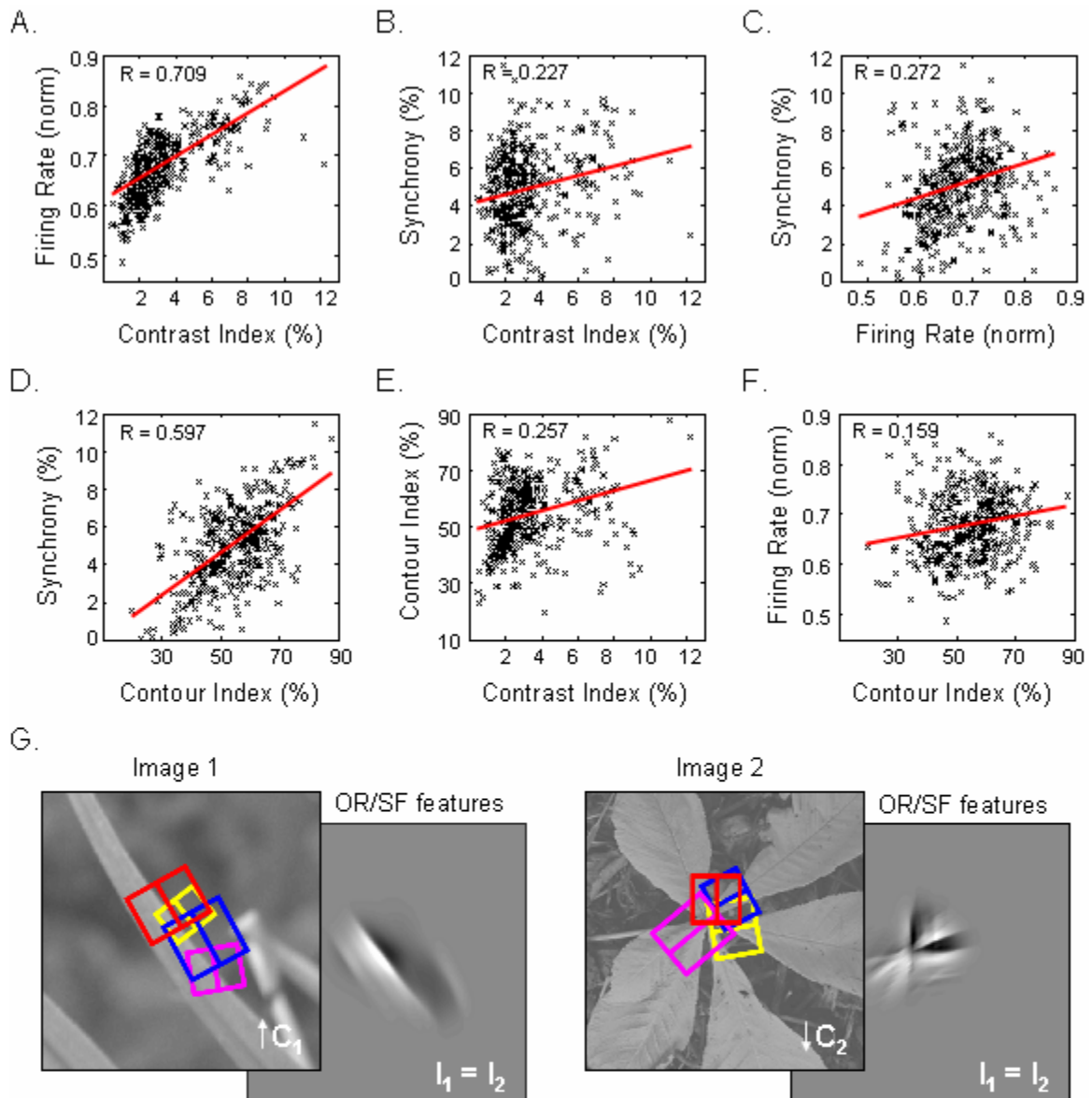
Figure 5.4. Synchrony and firing rate dependence on contour and contrast indices. Responses were measured for 399 groups of 4 cells to the image for each assembly that generated the highest combined firing rate and synchrony response (responses were configured to the same scale). Firing rate was normalized to the maximum response for each cell and then averaged across all cells in the assembly. Scatter plots showing the correlation between (A) firing rate and contrast index, (B) synchrony and contrast index, (C) synchrony and firing rate, (D) synchrony and contour index, (E) contour index and contrast index, and (F) firing rate and contour index. (G) In this example, each assembly has a high degree of expected response (similar contrast indices: $I_1 = I_2$), but the configuration of assembly 1 is more similar to a contour (higher contour index), which means the contrast structure to which it is responding is more likely to be arranged in a contour as compared to assembly 2.

firing rate effects, but these quantities (and synchrony vs. contrast index) show a slight correlation because we imposed one by looking at the stimuli with the largest combined response. The small correlation coefficient suggests that the images with the largest synchrony response were often not the ones with the largest firing rate response. On the other hand, synchrony is moderately correlated with the contour index, suggesting that cooperative activity depends on the spatial configuration of the assembly when there is an appropriate match between assembly and image structure. This means that when assemblies have a good association, they synchronize to contrast segments that also have a good association, i.e. a contour. There is a weak correlation between firing rate and contour index (contrast index vs. contour index), which may be due to the abundance of contour structure in natural images. Figure 5.4G shows an example of four neurons viewing stimuli in which the contrast indices are matched, but the contour index is higher for the group on the left. These metrics work together by showing that the contrast structure to which the assembly is responding has a higher probability of being arranged in a contour as compared to the assembly on the right.

Dynamic Grouping

A coding strategy involving dynamic synchronization of neuronal responses offers tremendous advantages in terms of coding capacity. The physical mechanism underlying synchrony would allow for neurons to be effectively connected and form dynamic local circuits to efficiently transmit information about the visual environment. Dynamic grouping also provides a way to multiplex visual information within a neuronal spike train while allowing neurons to participate in multiple functional assemblies to recover all the structure represented in a visual scene. Organization of assemblies could

145

result from changes in the precise temporal structure of spikes trains, which produces a short-term enhancement of synaptic effectiveness (Hayek 1952). In this manner, groups of cells could assemble and disassemble during certain tasks and individual cells could belong to more than one functional group. Furthermore, uncorrelated groups could coexist without interference.

We investigated whether synchronous activity between assemblies may constitute the foundations of a linking mechanism for features of the same object. We found thirty-eight instances of dynamic grouping in which two pairs of cells synchronized with a third neuron, but did not synchronize with each other (Figure 5.5A). These different functional groups signaled different objects (image on left) or different features of the same object (image on right). The magnitude of synchrony was significant within each group (N = 76 3-cell assemblies, N = 76 cooperative pairs, and N = 152 uncooperative pairs), but synchrony was inhibited between groups by 31.9%. The magnitude of synchrony between uncooperative assemblies was significantly below that expected by chance correlations from firing rate effects (p < 0.004). These results suggest that different functional groups do not interact at this stage of processing. However, synchrony is involved in signaling contours and is consistent with a detection mechanism.

Concerning the role of synchrony in the visual cortex, several neurophysiological studies have been unable to find unambiguous relationships between synchrony and specific visual tasks designed around segmentation or figure-ground discrimination (Lamme and Spekreijse 1998, Thiele and Stoner 2003, Roelfsema et al. 2004, Palanca and DeAngelis 2005). Perhaps the definition of synchrony is too narrow for these tasks. Since synchrony strength decreases with increasing distance between electrodes (Singer and Gray 1995; Eckhorn 1994; Das and Gilbert 1999), we should consider recruitment of

146

A.

Pair 1 (A,B) syncs Cell C

Pair 2 (D,E) syncs Cell C

Pair 1 🚫 Pair 2

A or B 🚫 D or E

X: Average synchrony in 3-cell assemblies

Y: Average synchrony in cooperative pairs

Z: Average synchrony in uncooperative pairs

B.
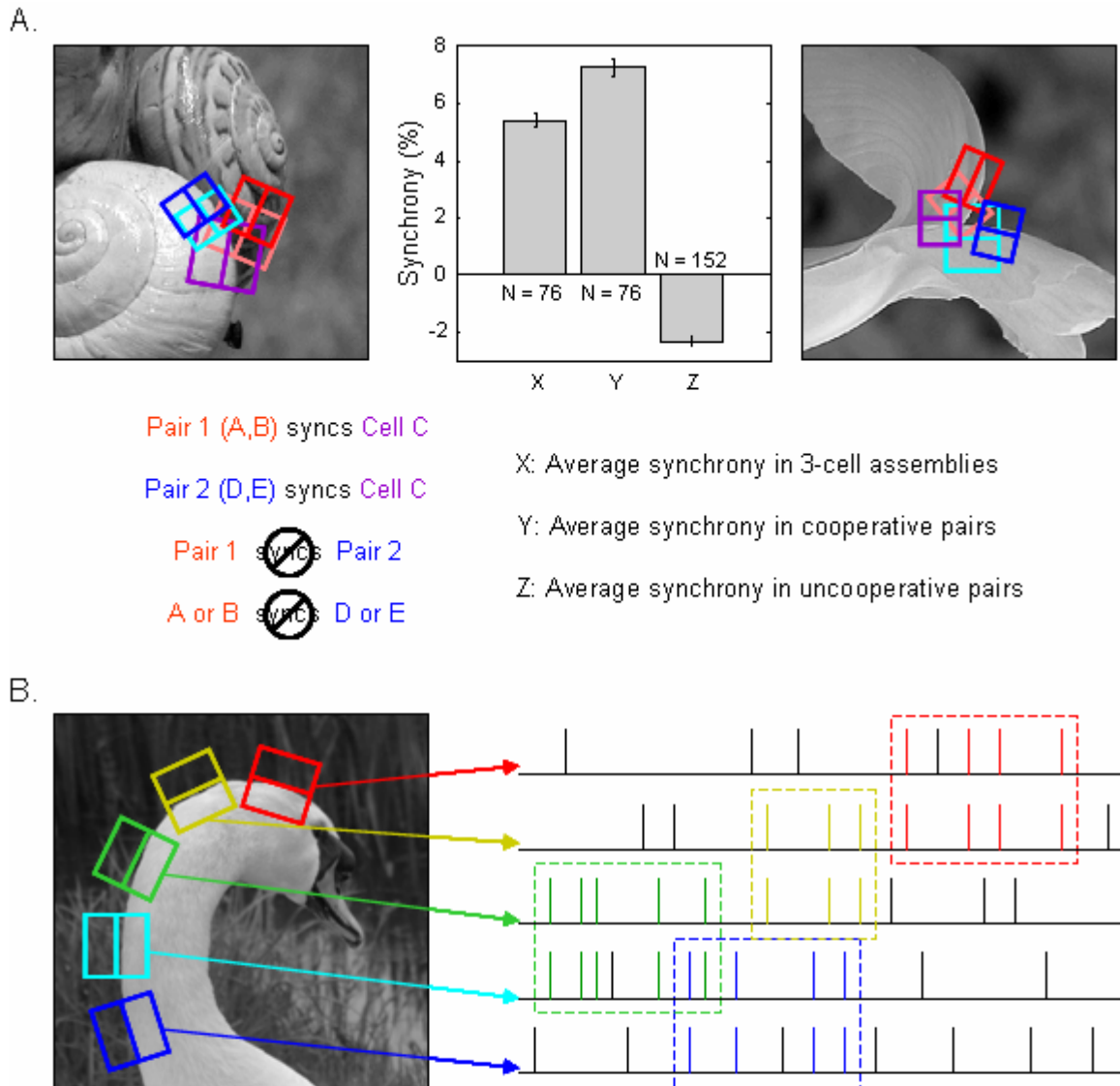
Figure 5.5. Inter-assembly linking and recruitment. (A) We found 38 instances of dynamic grouping in which 2 pairs of cells (red and blue) synchronize with a third cell (purple), but do not synchronize with each other to represent an assembly of 5 neurons. These different functional groups signaled different objects (image on left) or different features of the same object (image on right). The magnitude of synchrony was significant within each group (N = 76 3-cell assemblies, N = 76 cooperative pairs, and N = 152 uncooperative pairs), but synchrony was inhibited between groups by 31.9%. The magnitude of synchrony between uncooperative assemblies was significantly below that expected by chance correlations from firing rate effects (p < 0.004). (B) We looked for evidence of recruitment in which neurons may synchronize with each other in a delayed fashion to represent extended features, but did not find any assemblies that exhibited this property. Dynamic grouping was observed as in (A), but the cooperation was concurrent (not delayed) and did not exist for segments of the same feature.

147

neurons across the cortex. Our definition of synchrony requires all members of a selected

assembly to contribute to overall cooperation, but does not consider assemblies in which

delayed synchrony (i.e., not present at stimulus onset, but developing throughout the

presentation) may link small assemblies, especially across large distances in the visual

field. Such a mechanism (Figure 5.5B) could recruit neurons over a broad cortical

distance using top-down influences from feedback or lateral connections. Unfortunately,

although we found dynamic grouping as in Figure 5.5A, the cooperation was concurrent

(not delayed) and did not exist for segments of the same feature. Our inability to find

examples of recruitment support psychophysical results that suggest linking is not

iterative (Hess et al. 2001).

Discussion

The importance of synchrony in the process of natural vision remains unknown

and natural images offer an efficient approach for analyzing the complex spatial

organization of larger assemblies. We presented broad selections of natural stimuli and

identified the appearance of repeatable and reliable cooperative interactions within the

cell population. Using concepts from the association field theory (Field et al. 1993; Hess

et al. 2003), we quantitatively correlated synchronous interactions with unique visual

features in the scene to determine how synchrony is governed by the specific association

among cells. We found that the magnitude of synchrony correlated moderately with the

spatial relationships (proximity, orientation, and alignment) of receptive fields in the

assembly. These parameters were combined into one metric that described how well the

assembly organization fits an association-defined contour. Synchrony was moderately

correlated with this index ($R = 0.597$), which quantitatively showed that the receptive

fields of cells within an assembly tended to be aligned on a complex contour in the image with the highest combined (synchrony and firing rate) response. Preferred contours are reliably detected across multiple images. We propose that higher-order features found in natural images (e.g., complex contours) are responsible for the high selectivity of synchrony because adequate descriptions of high-order spatial correlations require the coordinated response of multiple cells. This process is cumulative, in that more complex structures require larger neural assemblies for accurate description. This most likely reflects the need to combine more elemental image features represented by individual cells in order to represent the complex features.

Neural Mechanisms Underlying the Association Field

The consistency of synchronous activity with the predictions made by the association field suggests that the two may be inherently related and served by the same underlying cortical machinery. Results such as those in Figures 5.1 demonstrate an enhancement of synchrony for well-associated neurons viewing continuous contours, but little or no synchrony is observed for incoherent contour segments. The responses of neurons in the primary visual cortex change depending on surrounding information in the visual field (Knierim and van Essen 1992; Kapadia et al. 1995). For example, neurons increase their response when stimulated by edge segments that are aligned with similar elements outside their classical receptive fields (Kapadia et al. 1995). Similarly, psychophysical results show that humans demonstrate increased sensitivity to certain edge segments when they are aligned with other edges (Polat and Sagi 1994; Kapadia et al. 1995). Horizontal connections in the primary visual cortex could account for this phenomenon and represent neural connections that link cells with similar receptive field

properties (Rockland and Lund 1983; Gilbert 1992). The underlying anatomical mechanism for the surround effect could be facilitated by the long-range horizontal connections linking cells with a separation of more that 4 mm (Kapadia et al. 1995; Gilbert 1992). These connections extend from excitatory pyramidal neurons and reach postsynaptic cells that can be excitatory or inhibitory (Gilbert 1992; Hirsch and Gilbert 1991; Weliky et al. 1995). Furthermore, horizontal connections are asymmetrical extending for a longer distance along the axis of the receptive field (Rockland and Lund 1983; Gilbert and Wiesel 1983; Fitzpatrick 1996; Bosking et al. 1997).

Network Oscillations

Horizontal connections may also be linked to the coherence of gamma oscillations in neural responses (Gray et al. 1989; Gray and Singer 1989; Eckhorn et al. 1988). Gray et al. (1989) used multiple electrodes to record the activity of collinear neuron clusters in the primary visual cortex of anesthetized cats to bar stimuli. Using cross correlation analysis, they examined the correlated timing of firing between pairs of clusters when stimulated with 1) two light bars moving in opposite directions; 2) two light bars moving in the same direction; and 3) a long light bar moving across the receptive fields instead of two short light bars. When a long light bar was used to stimulate the receptive fields, the magnitude of synchrony observed was highest.

We have shown that synchrony between single units can be observed for neurons with wholly different preferred orientations, but still mainly follow association field rules (Samonds et al. 2006). With this information and findings from Chapter 3 and Zhou et al. 1998, we propose that synchrony is initiated during the onset response and correlates with the contour information in the stimulus. This activity is then maintained by network

oscillations (Samonds and Bonds 2005) via lateral connections, which shapes synchrony to conform to association field rules.

Appendix: Extracting Orientation and Spatial Frequency Components from an Image

To aid in the investigation of whether synchronous responses of assemblies in the primary visual cortex encode contours in natural images, we used the objective measure described by Weliky et al. (2003) to quantify two-dimensional contrast structure in the image falling within each cell's classical receptive field (Figure 5.A1). Any image (A) is comprised of an intensity value at two given spatial coordinates and can be transformed into an equivalent Fourier representation in the frequency domain (D). Jean Baptiste Fourier showed that any signal could be reconstructed by summing a series of sine waves with appropriate phase and frequency. In our case, the signal is two-dimensional and each point in the Fourier transform reflects the magnitude of a two-dimensional sine wave with a specific orientation and spatial frequency. Most neurons in the primary visual cortex respond selectively to simple sinusoidal stimuli restricted in the Fourier domain and therefore have tuning preferences that are sensitive to specific ranges of orientations and frequencies (B). These tuning properties, in their Fourier representation (E), are multiplied by the Fourier representation of the image to create an estimate of the contrast components in the image that match a neuron's tuning preferences (F). The inverse Fourier transform is applied to this result to produce an image filtered by a cell's tuning characteristics (C), which is spatially filtered by the receptive field mask of the cell (G) to obtain an estimate of the two-dimensional contrast structure in the image to which the cell's classical receptive field is responding.
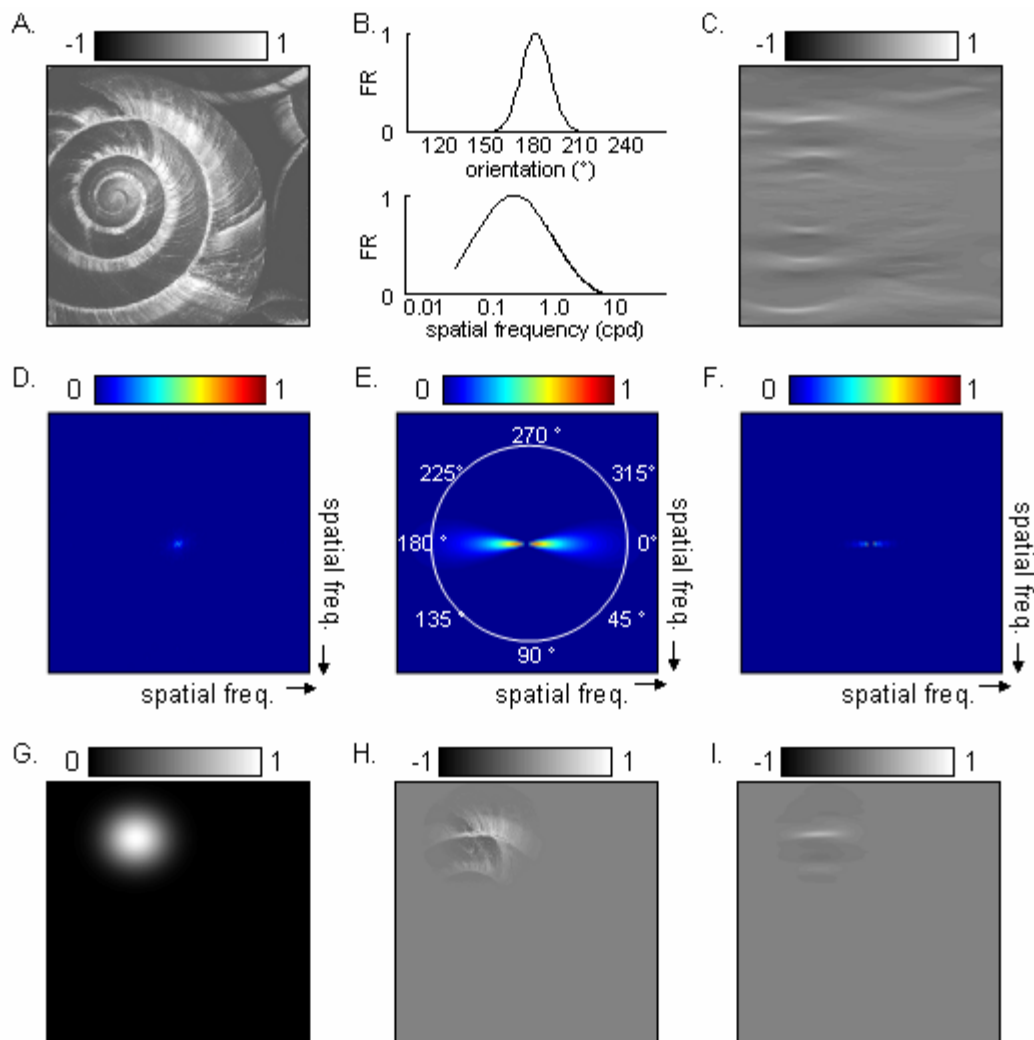
Figure 5.A1. Extraction of orientation and spatial frequency components in an image for quantifying the two-dimensional contrast structure falling within a cell's classical receptive field. (A) Natural scene image. (B) Orientation and spatial frequency tuning curves obtained for one neuron estimated from responses to drifting sinusoidal gratings and fitted with normal distributions. (C) The natural scene image shown in (A) filtered by the orientation and spatial frequency tuning properties in (B). (D) The two-dimensional spatial frequency content of the natural scene image in (A) derived from its Fourier transform. (E) The two-dimensional spatial frequency content of the orientation and spatial frequency tuning curves in (B). (F) The two-dimensional spatial frequency content of the natural image bandpass filtered by the tuning properties (DxE). (G) Measured classical receptive field (fitted with a bivariate normal distribution) of the neuron whose properties are shown in (B), normalized from 0.0 to 1.0. (H) Extraction of the region of the original natural scene falling within the receptive field (AxG). (I) Extraction of the orientation and spatial frequency components of the natural scene falling within the measured classical receptive field (CxG). Adapted from Weliky et al. (2003).

152

In our analysis, orientation tuning curves were fitted with normal distributions. In the interest of time during the experiment, spatial frequency tuning was not measured, and instead the filter was estimated by using a normal distribution with $\mu = \log_{10}(0.45)$ and $\sigma = 0.6$ cycles/$^\circ$. Classical receptive fields were estimated as bivariate normal distributions where μ was the measured receptive field center and σ_1 (σ_2) was the measured height (width) of the receptive field divided by 3 (since >99% of values drawn from a standard normal distribution are within 3 standard deviations of the mean). Finally, this method was extrapolated for an assembly of cells by repeating the process for each cell in the assembly to quantify the specific arrangement of two-dimensional contrast structure lying within their aggregate receptive field.

References

Aertsen AMHJ, Gerstein GL, Habib MK, and Palm G. Dynamics of neuronal firing correlation: Modulation of "effective connectivity". *J. Neurophysiol.*, 61:900-917, 1989.

Azouz R and Gray CM. Adaptive coincidence detection and dynamic gain control in visual cortical neurons in vivo. *Neuron,* 37:513-523, 2003.

Barlow HB. Possible principles underlying the transformation of sensory messages. In *Sensory Communication*, ed. WA Rosenblith, Cambridge, MA: MIT Press, 217-234, 1961.

Bosking WH, Zhang Y, Schofield B, and Fitzpatrick D. Orientation selectivity and the arrangement of horizontal connections in tree shrew. *J Neurosci* 17: 2112–2127, 1997.

Das A and Gilbert CD. Topography of contextual modulations mediated by short-range interactions in primary visual cortex. *Nature* 399: 655–661, 1999.

Eckhorn R. Oscillatory and non-oscillatory synchronizations in the visual cortex and their possible roles in associations of visual features. *Prog Brain Res*.102:405-26, 1994.

Elder JH and Goldberg RM. Ecological statistics of Gestalt laws for the perceptual organization of contours. *J. Vis.* 2:324-353, 2002.

Eckhorn R, Bauer R, Jordan W, Brosch M, Kruse W, Munk M, and Reitboeck HJ. Coherent Oscillations: mechanism of Feature Linking? *Biol. Cybern.*, 60:121-130, 1988.

Field DJ, Hayes A, and Hess RF. Contour integration by the human visual system: evidence for a local "association field". *Vision Res.* 33:173-193, 1993.

Fitzpatrick D. Seeing beyond the receptive field in primary visual cortex. *Curr. Opin. Neurobiol.*10:438-443, 2000.

Geisler WS, Perry JS, Super BJ, and Gallogly DP. Edge co-occurrence in natural images predicts contour grouping performance. *Vision Res.* 41:711-724, 2001.

Gilbert CD. Horizontal integration and cortical dynamics. *Neuron*. Jul;9(1):1-13, 1992.

Gilbert CD and Wiesel TN. Clustered intrinsic connections in cat visual cortex. *J Neurosci*. May;3(5):1116-33, 1983.

Gray CM, Konig P, Engel AK, and Singer W. Oscillatory responses in cat V1 exhibit synchronization which reflects global stimulus properties. *Nature*, 338:334-337, 1989.

Gray CM. and Singer W. Stimulus-specific neuronal oscillations in orientation columns of cat visual cortex. *Proc. Nat. Acad. Sci.* USA, 86:1698-1702, 1989.

Hayek FA. *The Sensory Order*. Chicago: University of Chicago Press, 1952.

Hess RF, Barnes G, Dumoulin SO, and Dakin SC. How many positions can we perceptually encode, one or many? *Vision Res*. Jun;43(14):1575-87, 2003.

Hess RF, Beaudot WH, and Mullen KT. Dynamics of contour integration. *Vision Res*. Apr;41(8):1023-37, 2001.

Hirsch JA and Gilbert CD. Synaptic physiology of horizontal connections in the cat's visual cortex. *J Neurosci*. Jun;11(6):1800-9, 1991.

Hubel DH and Wiesel TN. Receptive fields, binocular interaction and functional architecture in the cat's visual cortex. *J Physiol* 160: 106–154, 1962.

Kapadia MK, Ito M, Gilbert CD, and Westheimer G. Improvement in visual sensitivity by changes in local context: parallel studies in human observers and in V1 of alert monkeys. *Neuron.* Oct;15(4):843-56, 1995.

Kelly RC, Smith MA, Samonds JM, Kohn A, Bonds AB, Movshon JA, and Lee TS. Comparison of recordings from microelectrode arrays and single electrodes in the visual cortex. *J Neurosci.* Jan 10;27(2):261-4, 2007.

Kersten D. Predictability and redundancy of natural images. *J. Opt. Soc. Am. A* 4:2395 – 2400, 1987.

Knierim JJ and van Essen DC. Neuronal responses to static texture patterns in area V1 of the alert macaque monkey. *J Neurophysiol.* Apr;67(4):961-80, 1992.

Lamme VAF and Spekreijse H. Neural synchrony does not represent texture segregation. *Nature*, 396:362-366, 1998.

Marr D and Vaina L. Representation and recognition of the movements of shapes. *Proc R Soc Lond B Biol Sci.* Mar 22;214(1197):501-24, 1982.

May KA and Hess RF. Dynamics of snakes and ladders. *J Vis.* Sep 28;7(12):13.1-9, 2007

Milner P. A model for visual shape recognition. *Psychol. Rev.,* 81: 521-535, 1974.

Nishimoto S, Arai M, and Ohzawa I. Accuracy of subspace mapping of spatiotemporal frequency domain visual receptive fields. *J Neurophysiol.* 93:3524-3536, 2005.

Parent P and Zucker SW. Trace inference, curvature consistency, and curve detection. *IEEE Trans Pattern Anal Machine Intell* 11:823-839, 1989.

Palanca BJ and DeAngelis GC. Does neuronal synchrony underlie visual feature grouping? *Neuron.* 46:333-346, 2005.

Perkel DH, Gerstein GL, and Moore GP. Neuronal spike trains and stochastic point processes, II. Simultaneous spike trains. *Biophys. J.* 7:419-440, 1967.

Polat U and Sagi D. The architecture of perceptual spatial interactions. *Vision Res.* Jan;34(1):73-8, 1994.

Rockland KS, Lund JS. Intrinsic laminar lattice connections in primate visual cortex. *J Comp Neurol.* May 20;216(3):303-18, 1983.

Roelfsema PR, Lamme VA, and Spekreijse H. Synchrony and covariation of firing rates in the primary visual cortex during contour grouping. *Nat. Neurosci.* 7:982-991, 2004.

Rousche PJ and Normann RA. Chronic recording capability of the Utah Intracortical Electrode Array in cat sensory cortex. *J. Neurosci. Methods* 82:1-15, 1998.

Rousche PJ and Normann RA. A method for pneumatically inserting an array of penetrating electrodes into cortical tissue. *Annals of Biomed. Eng.*, 20:413-422, 1992.

Samonds JM, Zhou Z, Bernard MR, and Bonds AB. Synchronous activity in cat V1 encodes collinear and cocircular contours. *J. Neurophysiol.* 95:2602-2616*,* 2006.

Samonds JM and Bonds AB. Gamma oscillation maintains stimulus structure-dependent synchronization in cat visual cortex. J. Neurophysiol. *93*, 223-236, 2005.

Schmidt S, Horch K, and Normann RA, Biocompatibility of silicon-based electrode arrays implanted in feline cortical tissue. *J. Biomed. Mater. Res*. 27:1393-1399, 1993.

Schwartz O and Simoncelli EP. Natural signal statistics and sensory gain control. *Nature Neuroscience*. 4:819-825, 2001.

Shoham S, Fellows MR, and Normann RA. Robust, automatic spike sorting using mixtures of multivariate t-distributions. *J Neurosci Methods*. 127:111-122, 2003.

Sigman M, Cecchi GA, Gilbert CD, and Magnasco MO. On a common circle: natural scenes and Gestalt rules. *Proc. Natl. Acad. Sci. USA*. 98:1935-1940, 2001.

Skottun BC, De Valois RL, Grosof DH, Movshon JA, Albrecht DG, and Bonds AB. Classifying simple and complex cells on the basis of response modulation. *Vision Res*. 31(7-8):1079-86, 1991.

Simoncelli EP. Vision and the statistics of the visual environment. *Curr. Opin. Neurobiol.* 13:144-149, 2003.

Singer W and Gray CM. Visual feature integration and the temporal correlation hypothesis. *Annu. Rev. Neurosci.*, 18:555-586, 1995.

Smyth D, Willmore B, Baker GE, Thompson ID, and Tolhurst DJ. The receptive-field organization of simple cells in primary visual cortex of ferrets under natural scene stimulation. *J. Neurosci.* 23:4746-4759, 2003.

Thiele A and Stoner G. Neural synchrony does not correlate with motion coherence in cortical area MT. *Nature*, 421:366-370, 2003.

Touryan J, Felsen G, and Dan Y. Spatial structure of complex cell receptive fields measured with natural images. *Neuron*. Mar 3;45(5):781-91, 2005.

Treisman A. The binding problem. *Curr Opin Neurobiol*. Apr;6(2):171-8, 1996.

von der Malsburg C. The correlation theory of brain function. *Internal Report, Max-Planck Institute for Biophysical Chemistry*. Goettingen, Germany, 1981.

Weliky M, Fiser J, Hunt RH, and Wagner DN. Coding of natural scenes in primary visual cortex. *Neuron*. 37:703-718, 2003.

Weliky M, Kandler K, Fitzpatrick D, Katz LC. Patterns of excitation and inhibition evoked by horizontal connections in visual cortex share a common relationship to orientation columns. *Neuron*. 1995 Sep;15(3):541-52.

Zhou Z. Spatial characteristics of cooperative interactions in the striate cortex. Ph.D. dissertation. Vanderbilt University, 2008.

CHAPTER VI

SYNCHRONOUS ACTIVITY IN CAT VISUAL CORTEX IMPLEMENTS A SPARSE
CODING STRATEGY FOR NATURAL IMAGES

Introduction

How can neuronal responses represent contours, surfaces, and textures in natural

scenes? This is dependent on the more general question of how information about the

natural environment is encoded by the early visual system. While the traditional model

involving cells acting as independent filters (Barlow 1972) doubtless contributes to this

process, it fails to account for any interactions between the filters making up the

population and the dynamic nature of the filters. Due to the dynamic nature of grouping,

the combinatorial possibilities of a population code offer a vastly increased

dimensionality for encoding visual information (Sherrington 1941, Hebb 1949).

Employing a population code, in which subsets of the neural population form dynamic

assemblies to accomplish tasks, enhances robustness and contributes to learning and

plasticity. Although current recording technology allows us to monitor the interactions of

hundreds of neurons simultaneously, we cannot understand their contribution to visual

perception without a conceptual framework that describes their information processing

strategy. Two competing theories within this general approach include *compact coding*

and *sparse coding*, both of which take advantage of redundancy in natural scenes to

produce more efficient representations of the environment (Field 1994).

In a compact coding strategy, the goal of visual coding is to reduce the

redundancy in natural scenes by creating a representation with the minimum number of

cells. This idea is closely related to Barlow's theories of redundancy reduction (Barlow

1961) as well as dimensionality reduction using Principal Components Analysis (PCA). Neurons in a target assembly are differentiated from others by having higher activation levels. Different objects are then represented by the different firing patterns of the same subset of cells. Although a number of studies have suggested that spatial coding by the visual system is consistent with a compact code (e.g. Atick and Redlich 1990, 1992; Daugman 1988, 1991; Linsker 1988; Sanger 1989), there are several inconsistencies in its ability to account for receptive field properties of cells in the retina and primary visual cortex. The absence of phase information due to the stationarity of natural scenes (i.e. features do not prefer any specific spatial location) means that compact coding cannot account for the localized nature of receptive fields (Field 1994). Furthermore, this criterion may confound coactivated assemblies since the identification of members to particular assemblies is lost (von der Malsburg 1986, Sakurai 1999).

In a sparse coding strategy, different objects are represented by firing patterns from different subsets of cells in the population. Willmore and Tolhurst (2001) define two different sparseness properties for encoding the depth and breadth of information in the cortex. *Population sparseness* describes the response probability of the cell population at one instance in time (e.g. for one stimulus condition). The distribution of responses is leptokurtic with a large peak at zero (or chance), indicating that most of the population is inactive for any given stimulus. *Lifetime sparseness* describes the activity of one neuron (or assembly) across time (e.g. responses to the set of all input images), also yielding a leptokurtic response distribution with a peak at zero (or chance). Across all input images, all cells have an equal response probability, but have a low response probability for any single image. With sparseness, the dimensionality is not reduced, but the redundancy in the input is transformed into the redundancy in the firing pattern of the

158

cells (Field 1994). In this manner, information about the environment is distributed

across all cells and objects are represented by which cells are active and not by the

relative activity or overall amount of activity of a specific subset.

Sparse coding has been observed in the visual system and has been found to be

consistent with the representations of natural scenes (Field 1987, 1989, 1994; Zetzsche

1990). The degenerate mapping of highly correlated stimuli to a sparse representation is

described as a fault-tolerant method of reliably learning and discriminating closely-

related patterns (Leonardo 2005). In the primary visual cortex of primates, neurons

produce (lifetime) sparse responses when stimulated with natural image sequences (Vinje

and Gallant 2000, 2002) and high lifetime and population sparseness is found in V1 of

ferrets (Weliky et al 2003). Furthermore, responses are most sparse when the non-

classical receptive field is stimulated, implying that sparseness (and possible learning) is

modulated by context. Lifetime sparseness has been shown to exist in the auditory

system of rats (DeWeese et al. 2003), the somatosensory system of rats (Brecht and

Sakmann 2002), and the olfactory system of insects (Perez-Orive et al. 2002; Laurent

2002; Theunissen 2003). Kenyon cells in the mushroom body of the locust olfactory

system have sparse odor identity-specific responses (Stopfer et al. 2003). In the

inferotemporal cortex of monkeys, neuronal responses to faces have shown high

population sparseness (Young and Yamane 1992). Population sparseness has also been

exhibited in the hippocampus (Thompson and Best 1989) and in computational models

on auditory speech processing (Coath et al. 2005). Similar to sensory modalities,

(lifetime) sparseness is also evident in the motor systems of rabbits (Beloozerova et al.

2003), rats (Brecht et al. 2004), and the zebra finch (Hahnloser et al. 2002; Fiete et al.

2004).

Previous studies that have investigated the sparse coding capabilities of the visual cortex have focused on the average firing rate of independent neurons and found that the encoding of visual information is in fact sparse and distributed across small populations of cells. In the previous chapter, we demonstrated that synchrony among neuronal assemblies is correlated with local contour information in natural scenes. We would like to compare firing rate results from previous studies to results generated for a synchrony-based coding strategy in order to determine how consistent synchrony is with a sparse coding representation and determine its efficiency for encoding contours in natural images.

Using a 10x10 microelectrode array, we measured the simultaneous response of single cells to thousands of natural images and analyzed the sparseness and dispersal of synchrony and firing rate response distributions. We found that synchrony response distributions increased in sparseness across assembly size as compared to firing rate response distributions, which led to a more efficient coding capability, but that firing rate response distributions were more distributed when considering additional members. Field (1994) suggested that the phase spectrum of natural images provided the foundation for sparse coding, so we wanted to see if synchrony was correlated with natural phase information. We measured synchrony and firing rate responses of assemblies viewing hybrid images with natural or random phase spectra. We found that images with natural phase spectra generated more synchrony than images with random phase spectra and that firing rates for each condition showed less sensitivity. These results suggest that synchrony among visual cortical neurons is implementing a sparse code for contours in natural images.

Materials and Methods

Preparation and Data Acquisition

Six adult cats (2.3-4.0 kg) were prepared for electrophysiological recordings in the primary visual cortex. All procedures were performed in accordance with guidelines set forth by the American Physiological Society and the Institutional Animal Care and Use Committee at Vanderbilt University. Details on the preparation are described in Chapter 2. Simultaneous single-unit recordings were made from cells in the visual cortex of anesthetized cats via the Utah Intracortical Electrode Array (UIEA; Cyberkinetics Neurotechnology Systems, Foxborough, MA). The UIEA recordings have good signal to noise ratios and have been shown to have qualities comparable to those from single-electrode recordings (Kelly et al. 2007). The implant is a square 10x10 silicon array with a 0.4 mm electrode separation. The electrodes have a length of 1.0 mm and are inserted to a depth of 0.6 mm with a pneumatic implantation tool (Rousche and Normann 1992). Recordings are displayed in real time and the waveform of each neural event is stored for later analysis by a comprehensive software system from Cyberkinetics. When the array is inserted, not every channel records reliable neural activity. Inevitably, the size of the array coupled with the curvature of the brain places some electrodes over a blood vessel or sulcus. However, the majority of electrodes do record neural activity and these channels are processed with a MATLAB-based spike-sorting program to remove noise and artifact (Shoham et al 2003). We did not include multiple units that were recorded and resolved from a single channel. Approximately 5% of channels with multi-unit activity were discarded. Channels with isolated single-unit activity were used only if the activity was $\geq$ 5 spikes per second and showed clear orientation tuning (signal to noise $\geq$

161

2:1) when viewing drifting sinusoidal gratings. In the end, we recorded from 215 single

units, 205 of which were complex cells (Hubel and Weisel 1962; Skottun et al. 1991)

with a median relative modulation, F_1/F_0, of 0.06 (n = 205 cells). Unless otherwise

stated, all cells were used for analysis.

Stimulation

All stimuli were displayed on a gamma-corrected SONY Trinitron 21" monitor

with a resolution of 800 x 600 pixels (22.6 pixels per visual degree) driven either by a

Cambridge Research Systems VSG2/3F controller board (for gratings) or a video

controller using the WinVis software package (for natural images and sequences).

Displays were refreshed at 120 Hz. All stimuli spanned 18°x18°, appeared against a

mean luminance background (73 cd/m^2), and were scaled to have a global contrast of

0.32 (see Touryan et al. 2005). Two stimulus protocols were used. The first stimulus

protocol (Figure 6.1A) was used on four subjects (described in Chapter 5) and contained

a sequence of 336 natural, grayscale images from www.imageafter.com, each rotated at 9

angles (40° to 360°, in 40° increments) for an effective stimulus set of 3024 pictures,

presented for 500 ms. There were two null stimuli and a 500 ms delay between each

image, during which only the mean luminance was shown.   Each presentation was

static, images were randomly interleaved, and the entire sequence was repeated 8, 9, 10,

or 13 times for reliability. The second stimulus protocol (Figure 6.5A) was used in two

experiments (similar to that described in Chapter 4) and contained three natural,

grayscale images with hybrid modifications, presented for 2 seconds. Natural images

were separated into their power and phase components in the frequency domain and

swapped with those from a random white noise stimulus. These hybrid images either
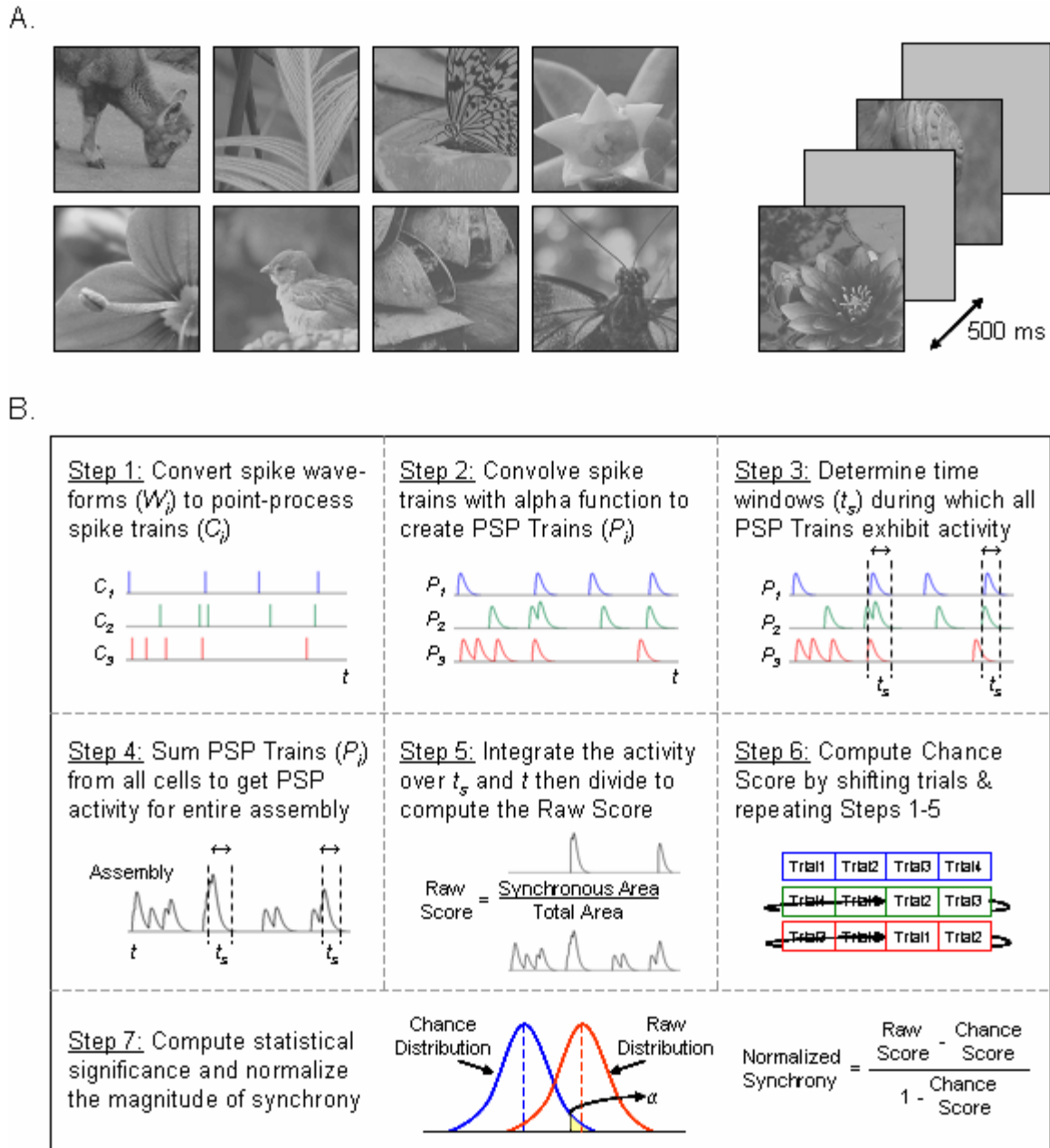
Figure 6.1. Methods. (A) Example stimuli from the natural image sequence. All images were obtained from www.imageafter.com, converted to grayscale, and scaled to have a global contrast on 0.32. Each image was presented for 500 ms followed by a 500 ms interval of mean luminance. (B) Quantification of synchrony using the PSP Method. Analysis was only performed on channels that exhibited good single-unit isolation and clear orientation tuning to drifting sinusoidal gratings. Synchrony is defined as the ratio of overlapping activity among all cells to the total activity in the assembly. The contribution of synchrony due to firing rate effects is estimated with the Shift Predictor (Perkel et al. 1967) and subtracted from the Raw measure. Stimulus trials are concatenated to form one long initial spike train.

contain a natural phase spectrum and random power spectrum or a random phase spectrum and natural power spectrum. Stimuli were jittered 5 pixels (0.22°) in random star fashion (returning to origin) at 60 Hz to provide motion while anchoring features within the receptive field. There was a 1 second delay between each image, during which only the mean luminance was shown, and each presentation was repeated 100 times for reliability.

Data Processing

We have developed a method that detects and quantifies the amount of correlated activity in a neuronal assembly of arbitrary size (Figure 6.1B). As a hypothetical neural substrate for encoding salient stimulus properties, synchrony enhances the probability of eliciting postsynaptic action potentials (PSPs) when neurons behave as coincident detectors (Azouz and Gray 2003). Our basic algorithm (described in detail in Chapter 2) is designed to reflect the relevance of group synchrony to postsynaptic neurons by modeling the temporal summation of postsynaptic potentials. In this measure, synchrony is computed as a fraction of total activity within an assembly and can be monitored dynamically throughout the stimulus presentation. The steps in the algorithm are as follows:

Step 1: Convert spike waveforms to point-process spike trains

>The activities recorded simultaneously from all neurons in a target assembly are preprocessed to retain only spike initiation times, creating point-event spike trains. Stimulus repetitions are concatenated to form one long spike train

Step 2: Convolve point-process spike trains with an alpha function to create PSP trains

Convolve a point-event spike train with a truncated (10 ms) PSP waveform, yielding a PSP train. We modeled the PSP waveform with an alpha function, $a(t) = Ate^{-1/\tau}$, where $\tau = 1$ ms.

Step 3: Determine the time windows during which all PSP trains exhibit activity

Determine the timing of coincident events by noting the time periods (t_s) in which *all* trains exhibit spiking activity, i.e., intervals in which all PSP trains have a value greater than zero.

Step 4: Sum PSP trains from all cells to get PSP activity for the entire assembly

To visualize the total amount of activity within an assembly, add PSP trains from all neurons.

Step 5: Integrate the assembly activity over t_s and t then divide to compute the Raw Score

The Raw Score is computed as the ratio of the area under the overlapped portion of coincident waveforms to the total area under all waveforms in the assembly. The total area is found by summing all PSP trains and then integrating the resulting waveform over all time (t). The synchronous area results from integration of the summed trains over just the time periods found in Step 3 (t_s). The Raw Score is the ratio of synchronous area to total area and represents the percentage of assembly activity that is synchronous.

Step 6: Compute Chance Score by shifting 1 or more stimulus periods and repeating Steps 1-5

The Chance Score estimates the amount of stimulus-locked activity generated by the coactivation of each cell and is computed by completing Steps 1-5 with spike trains that are shifted in time by the length of at least one stimulus trial compared

to all other trains. This step is repeated 100 times with different shift orders and combinations to build a distribution with which to statistically compare the Raw Score.

Step 7: Compute statistical significance and normalize the magnitude of synchrony

We use a one-tailed student's t-test ($\alpha = 0.01$) to compare scores from the Raw and Chance distributions. A Normalized Score can be computed by subtracting the Chance Score from the Raw Score and renormalizing the resulting value so that Chance is assigned a value of 0 and synchrony among identical spike trains has a value of 1.

Results

Using a 10x10 microelectrode array, we recorded the responses of hundreds of neurons in the striate cortex of six paralyzed and anesthetized cats. Using the PSP algorithm, we quantified the amount of synchronous activity generated among the neurons in response to each stimulus and compared it to the combined average firing rate response. In the first protocol, we tested and compared six sparseness metrics that can be alternatively computed for population or lifetime analysis by changing two variable definitions. The degree of distribution for synchrony-based and firing rate-based strategies was quantified using dispersal (Willmore et al. 2000). In the second protocol, the phase spectra of three images were modified and the effects on synchrony and firing rate were measured to evaluate the dependence on power and phase components. In order to examine trends across assembly size, we evaluated the collective responses of hundreds of assemblies for each size group ($n = 2$ to 8 cells).

Natural Image Sequence

We simultaneously recorded single-unit activity from 18, 32, 39, and 45 channels in four cats. Since computation of all combinatorial arrangements of cells from the recorded population is exhaustive, and the probability of randomly testing a successful assembly of cells with individual sparse response properties (Vinje and Gallant 2000, 2002) is low, we needed an intelligent way to identify members of larger assemblies that were likely to synchronize. In Chapters 3 and 4, this was accomplished by computing a relatively low number of small assembly scores and progressively clustering cells that synchronize well to create an assembly of arbitrary size that has a high probability of synchronizing. However, this method was only practical because of the small number of stimuli shown. Our natural image sequence contains over three thousand images and would require a considerable amount of computational resources to complete this step for each image.

Fortunately, in Chapter 5 we found that specific receptive field organizations were conducive to synchrony. Cells that had receptive field configurations consistent with the association field model (Field et al. 1993; Hess et al. 2003) often matched local contrast structure throughout the natural image sequence. We therefore organized assemblies based on their receptive field layouts (similar orientation preferences, close proximity, and good continuity), but still used a variety of configurations (e.g. larger proximities to examine neurons with separate receptive fields) to optimize responses to the variety of structural information in the sequence. We used various orientation, proximity, and continuity thresholds to find over one thousand assemblies in each size group (N = 1399, 1166, 1379, 1432, 1394, 1422, and 1373 for assembly sizes 2-8, respectively). Because of the assortment of spatial structure throughout the sequence, each assembly

synchronized beyond that expected by chance (significance was measured with the PSP Method using $\alpha = 0.01$) to at least one and usually to multiple images with similar features.

Sparseness

Traditionally, selectivity is expressed by tuning functions for individual cells, but the dimensionality of spatial factors leading to synchrony in large groups does not allow selectivity to be expressed by simple filter functions. Instead we assessed selectivity on the basis of the probability distribution of such synchrony (and firing rate) across presentation of numerous natural images. As there is no standard measure of sparseness, we tested and compared six sparseness metrics that can be alternatively computed for population or lifetime analysis by changing two variable definitions. S_1 is the Treves and Rolls (1991) measure as modified by Willmore and Tolhurst (2001), S_2-S_4 are three metrics defined by Olshausen and Field (1997), S_5 is the "activity (or response) sparseness" measure (Willmore and Tolhurst 2001), and S_6 is kurtosis of the response distribution. In each equation, x_i is the response of one assembly to N stimuli (lifetime) or the response for one image from N assemblies (population). The mean and standard deviation of the responses are *xbar* and *s*, respectively. For each measure, the value for a Gaussian distribution (mesokurtic) has been subtracted so that a number above zero reflects a leptokurtic distribution while a number less than zero reflects a platykurtic distribution.

$$S_1 = 1 - \left(\frac{1}{N} \sum_{i=1}^{N} |x_i| \right)^2 \Big/ \left(\frac{1}{N} \sum_{i=1}^{N} x_i^2 \right) \tag{6.1}$$

$$S_2 = \frac{1}{N}\sum_{i=1}^{N} e^{-\left(\frac{x_i - \bar{x}}{s}\right)^2} - \frac{1}{\sqrt{3}} \tag{6.2}$$

$$S_3 = -\frac{1}{N}\sum_{i=1}^{N} \ln\left(1 + \left(\frac{x_i - \bar{x}}{s}\right)^2\right) + 0.5331 \tag{6.3}$$

$$S_4 = -\frac{1}{N}\sum_{i=1}^{N} \left|\frac{x_i - \bar{x}}{s}\right| + \sqrt{\frac{2}{\pi}} \tag{6.4}$$

$$S_5 = \frac{1}{N}\sum_{i=1}^{N} \left(x_i \leq Threshold\right) \tag{6.5}$$

$$S_6 = \frac{1}{N}\sum_{i=1}^{N} \left(\frac{x_i - \bar{x}}{s}\right)^4 - 3 \tag{6.6}$$

All of these metrics reflect how strongly peaked a distribution is, with many zero (or chance) values and long tails as compared to less peaked distributions of the same variance. The peakedness of a response distribution reflects how infrequently an assembly responds significantly above expectation. Across numerous stimulus conditions, an assembly that responds sparsely would only produce strong responses to a few stimuli and the response distribution would have a sharp peak at zero. On the other hand, if the assembly produced all responses with equal frequency, then the distribution of responses would be flat and have no peak. However, the peakedness of the response distribution does not always reflect sparseness and may be due to trivial properties of the visual stimulus. Baddeley (1996) showed that exaggerated kurtosis could result from local luminance variances between images, which could be caused by daily changes in illumination or indoor vs. outdoor settings. This phenomenon occurs between images, so it affects measures of lifetime kurtosis and not population kurtosis. Similarly, preprocessing of images such as pseudo-whitening or log-transformations can affect

169

measures of sparseness. In our study, all images were scaled to have the same global contrast and all sparseness metrics are compared relatively for different response types.

The fifth metric is a measure that is derived from the definition of sparseness and represents the number of images (response sparseness – lifetime) or assemblies (activity sparseness – population) that are "off" in a given distribution (Willmore and Tolhurst 2001). To calculate response sparseness, a threshold set to one standard deviation above the mean response over all images is used to divide the distribution. Any assembly response above this line is considered "on" and all others are considered "off." This binary measure directly counts the number of images to which the assembly does not respond. Similarly, for activity sparseness, the threshold is set for the distribution of responses to one image and responses below this line are counted and represent the number of assemblies that do not respond to a particular stimulus. Any threshold can be chosen for these measures, but one based on the standard deviation of the response distribution effectively standardized these measures similar to the other metrics.

The last metric is kurtosis, which is the fourth moment of the response distribution. As it measures the peakedness of a distribution, kurtosis seems like an obvious choice for sparseness metric, but it has certain limitations. For instance, it is more accurate for unimodal distributions that are approximately symmetrical about zero. Since cell responses do not often have symmetric distributions, kurtosis should be used with caution for these data (see Vinje and Gallant 2000).

In this study, we wanted to compare sparseness metrics for average firing rate-based and synchrony-based information. Average firing rate is quantified as the mean firing rate over all neurons in the assembly and is normalized to the maximum response from each distribution. This action effectively behaves like a logic OR operation. The

firing rate responses of each assembly are summed together (and divided by the number of neurons), which expands the response with each additional member. The entire assembly responds to an image if any one neuron increases its firing frequency to that image. On the other hand, our definition of synchrony requires all members in the assembly to be active, which behaves like an AND operation. In this manner, the assembly response is dependent on the activation of all members and will happen more rarely as compared to the firing rate case. Although this discrepancy helps to highlight synchrony's role as a sparse code, to even the playing field we also measured the firing rate responses after introducing a threshold above which all members must comply. We set this value to chance. All firing rate responses were normalized for chance firing, which is the average background activity level for each neuron as measured during the two null stimuli.

Figure 6.2 shows the results of each metric for synchrony, firing rate, and thresholded firing rate response distributions computed for lifetime sparseness. As mentioned above, this quantity refers to the sparseness of the response distribution from one assembly over all stimulus conditions. This figure shows plots from one subject and represents the average response from hundreds of assemblies for assemblies of size 2, 4, 6 and 8. All results were similar and displayed the same trend between subjects. Figure 6.2A-C show the average distributions for synchrony, firing rate, and thresholded firing rate responses. Synchrony response distributions increase in peakedness with assembly size while firing rate distributions depress slightly and shift to the right. The six sparseness metrics (Figure 6.2D-I) indicate that synchrony and thresholded firing rate distributions increase in sparseness as assemblies are more selective across the image sequence while the sparseness of firing rate distributions decreases slightly as each group

Figure 6.2. Lifetime sparseness. This quantity refers to the sparseness of the response distribution from one assembly over all stimulus conditions. In this case, each plot represents the average response from hundreds of assemblies for each size group. (A) Average synchrony, (B) firing rate, and (C) thresholded firing rate response distributions for assemblies of 2, 4, 6, and 8 cells. (D)-(I) Sparseness metrics S_1-S_6, respectively, for the synchrony (blue), firing rate (green), and thresholded firing rate (red) distributions measured across assembly size (2-8 neurons). The increase in sparseness for synchrony and thresholded firing rate response distributions indicate that as assembly size increases, each assembly becomes more selective and responds to fewer and fewer images in the sequence (like an AND logic operation). On the other hand, average firing rate response distributions become less sparse, which means each assembly responds to more images as assembly size increases because each group now responds to all of the images that trigger each additional member (OR operation).

172

responds to all of the images that trigger each additional member. Similar trends observed across the metrics suggest they are consistent with one another and are measuring the same quantity.

Figure 6.3 shows the same plots recomputed for population sparseness. This quantity refers to the sparseness of the responses to one stimulus condition over all assemblies and each plot represents the average response for 3026 images in each size group. Again, the top three plots (Figure 6.3A-C) show the average response distributions for one image over four different assembly sizes. All traces show similar sparseness trends compared to the lifetime values. The firing rate traces again indicate a decreased selectivity across assembly size meaning that more and more assemblies respond to each image. The sparseness of synchrony and thresholded firing rate distributions increases for larger assemblies. All metrics again show similar trends to each other.

Variance and Dispersal

The variance of an assembly response distribution measures the spread of activity over the natural image sequence. Since each response is normalized by chance (for synchrony, the number of synchronous events expected to occur from increased activation, or for firing rate, the background activity level monitored during null stimulation), an assembly can produce a range of responses from strongly positive to strongly negative. If responses along this entire axis are produced during the image set, then each assembly has a large response variance. This means that the assembly can discriminate between members of the image set and can serve as an appropriate encoder of this information. An ideal encoder would have a widely different response for each
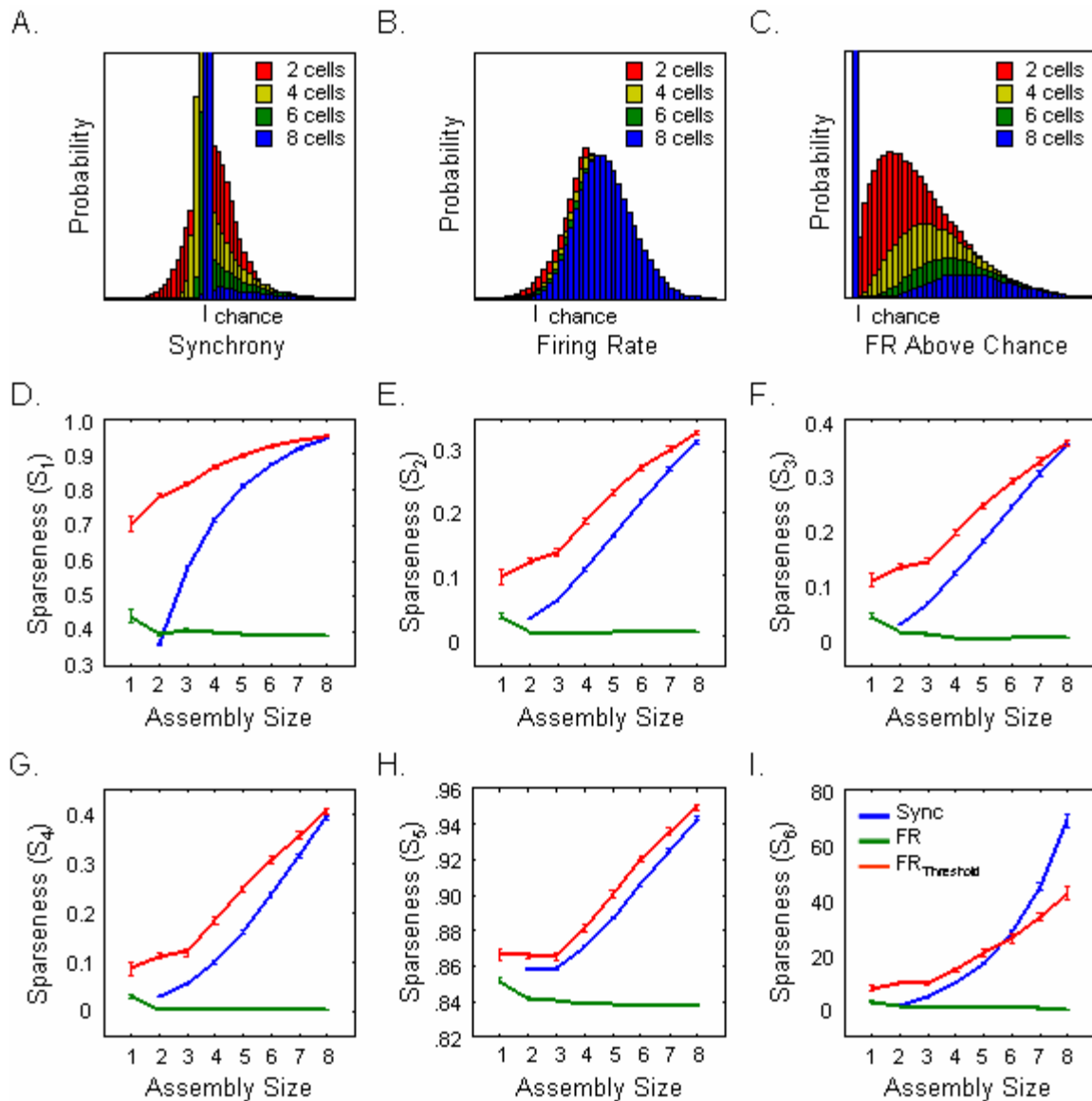
173
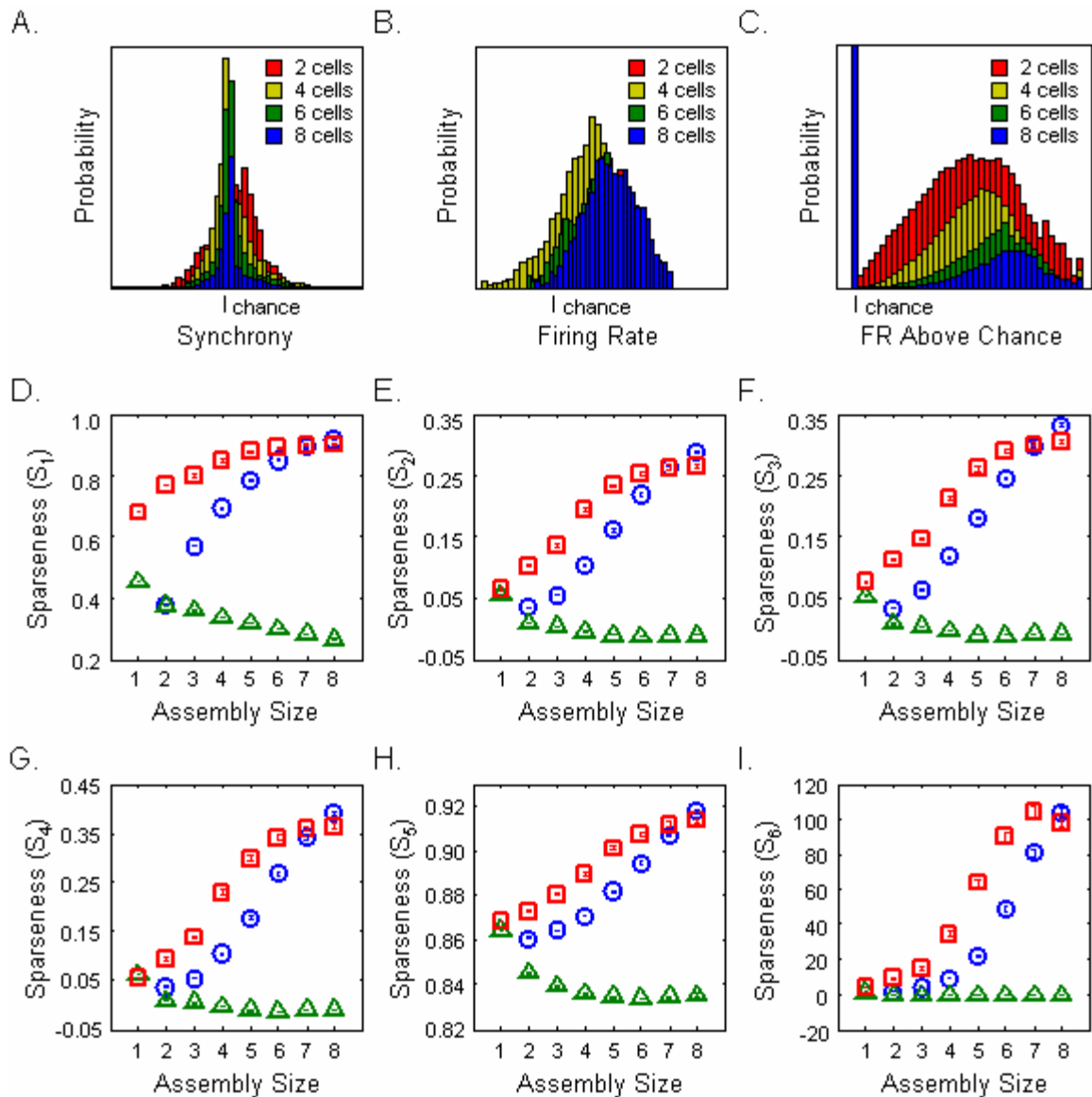
Figure 6.3. Population sparseness. This quantity refers to the sparseness of the response distribution over one stimulus condition for all assemblies. In this case, each plot represents the average response for 3026 images from each size group. (A) Average synchrony, (B) firing rate, and (C) thresholded firing rate response distributions for assemblies of 2, 4, 6, and 8 cells. (D)-(I) Sparseness metrics S1-S6, respectively, for the synchrony (blue), firing rate (green), and thresholded firing rate (red) distributions measured across assembly size (2-8 neurons). The increase in sparseness for synchrony and thresholded firing rate response distributions indicate that as assembly size increases, fewer and fewer assemblies respond to each image. Alternatively, average firing rate response distributions become less sparse, which means that as assembly size increases, more and more assemblies respond to each image. This is because for each image, larger assemblies are more likely to contain a member that responds to that image.

image, yielding a one-to-one correspondence between stimulus and response. On the other hand, an assembly with a small response variance is a poor encoder of this information. Too few responses or similar responses may be able to discriminate between broadly different stimuli, but images with similar properties may be lumped together and effectively indistinguishable by response alone.

The degree of distribution of each code can be quantified using dispersal (Willmore et al. 2000). The variance of each assembly to all natural images is computed and normalized by the maximum value and rank-ordered in a scree plot. This plot quantifies the distribution of variance across the assemblies and also indicates the distribution of assembly responses across the natural images. Plots with high plateaus indicate that each assembly is a good encoder of the stimulus set and this code is distributed across all assemblies. In contrast, scree plots that resemble a decaying exponential indicate that only a few assemblies encode the images, while the others give little or no response across all stimulus conditions (as in PCA when the first few principal components cover the largest variance). Figures 6.4A-C show the scree plots for each response type (synchrony, firing rate, thresholded firing rate where all cells in the assembly fire above their background levels) across assembly size (2-8 neurons for synchrony, and 1-8 for both firing rate response distributions). Figure 6.4D shows the dispersal of each code computed from the area under each curve. Across assembly size, firing rate responses show an increased level of distribution, signifying that larger assemblies are better at discriminating between images in the sequence. In contrast, synchrony and thresholded firing rate scree plots show decreased levels of dispersal across the population of assemblies for larger assemblies, decaying for groups of 2-4 and stabilizing for groups with 5 or more cells. This suggests that the inclusion of more
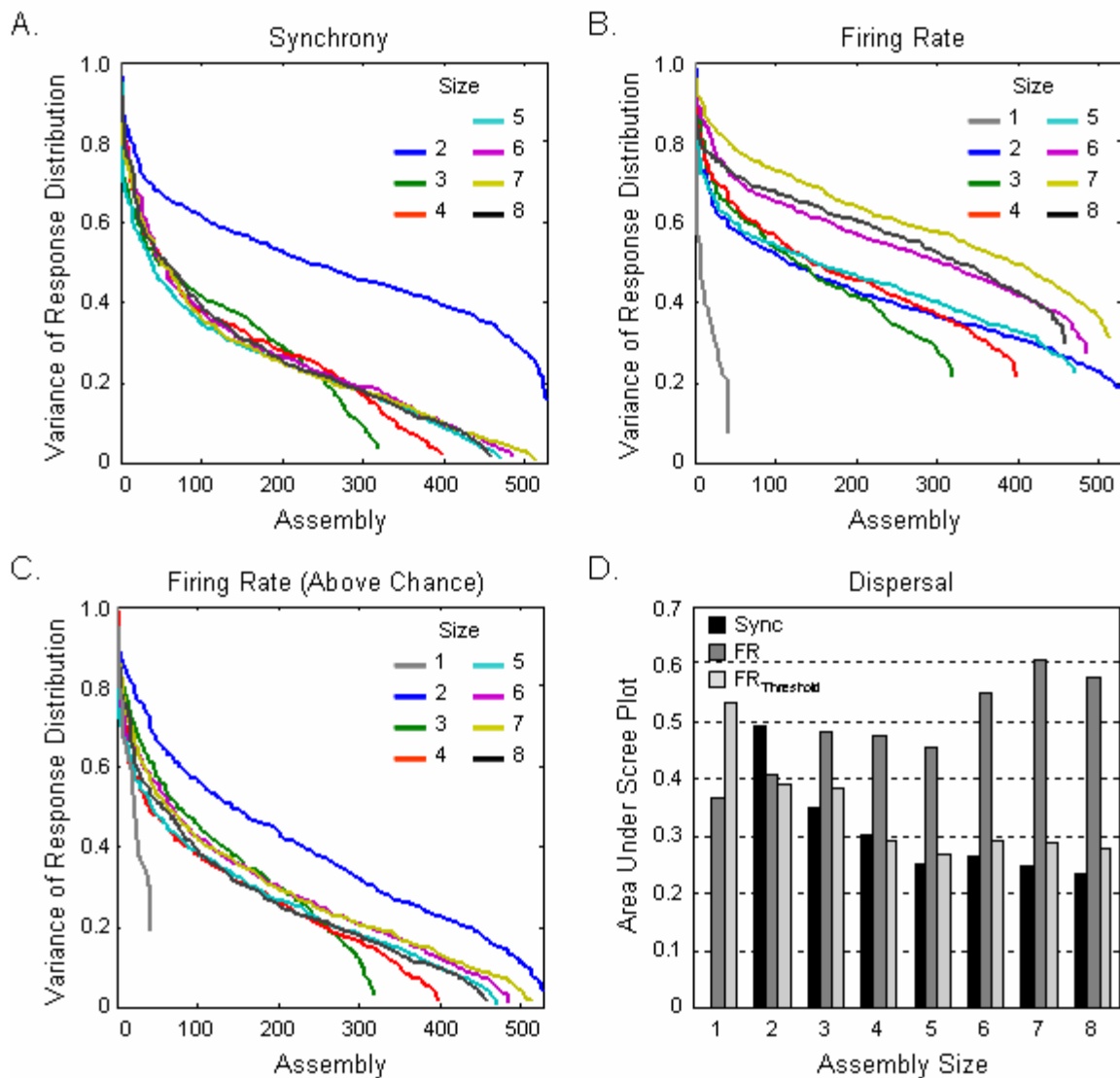
Figure 6.4. Dispersal. (A)-(C) Variance of response distributions normalized to unity and rank-ordered in a scree plot across all assemblies and assembly sizes for synchrony, average firing rate, and thresholded firing rate, respectively. As synchrony can only be measured between two or more cells, scree plots are shown for assembly sizes 2-8 for synchrony and 1-8 for average firing rate and thresholded firing rate response distributions. These plots show the distribution of assembly responses across the set of images. (D) Bar graph showing the dispersal of each average response distribution, which is calculated by taking the area under each scree plot, and quantifies how evenly coding is distributed across the assemblies (Willmore et al. 2000).

members reduces the variance of responses to the entire image set, but the reduction in dispersal could be a result of sampling from a sparse assembly population.

Hybrid Image Protocol

For the second protocol, we simultaneously recorded single-unit activity from 39 and 42 cells in two cats. Since assemblies were chosen for only three images (see Images 1, 2, and 3 in Figure 6.5) and those same assemblies were analyzed for each image modification, choosing which assemblies to analyze was based on the clustering of smaller assemblies (see Chapter 4). We used the fact that all subsets of a synchronous assembly must also synchronize to narrow the possibility of finding successful assemblies with significant synchronous activity among all possible assemblies for a certain size group. Likely assemblies built based on pairwise scores were identified and then processed with the PSP algorithm to determine if, in fact, their grouping was significant (to build larger assemblies from smaller ones, synchrony must exist *between* groups as well as *within* groups). This shortcut is only used to predict members of synchronous assemblies because scores from subgroups do not necessarily correlate with the overt behavior of the entire assembly (see Chapter 5). We used the PSP algorithm to compute the amount of synchronous activity among all pair-wise combinations of cells (N = 1602; 741 pairs from cat 1 and 861 pairs from cat 2) and found a total of 266 pairs that had significant activity ($\alpha = 0.01$) for Image 1, 275 pairs for Image 2, and 214 pairs for Image 3. These pairs were clustered to suggest larger assemblies (n = 2-8) which were then tested with the PSP algorithm to determine statistical significance until 50 assemblies of each size were identified.

Phase Spectrum Analysis

Since the brain shows a considerable amount of adaptation and plasticity, it has been suggested that the visual system may be optimized for processing the statistics of natural scenes (Barlow 1961; Kersten et al. 1987; Simoncelli 2003). Using spike-triggered covariance analysis, Felsen et al. (2005) found that complex cells had an enhanced sensitivity to natural images as compared to random stimuli and that this high feature sensitivity was due to the spatial characteristics of the stimuli. Exploring this phenomenon one step further, the investigators parsed natural images into power and phase components and switched them with those from a random white noise stimulus to create synthetic hybrid stimuli and investigate the effect on complex cell response. The power spectrum of natural images falls off inversely with spatial frequency, approximately as $1/f^2$ (Field 1987; Tolhurst et al 1992; van der Schaaf and van Hateren 1996), and nearby frequencies tend to have similar phases. Phase alignment allows for the formation of edges and surfaces and accounts for the localized nature of image features. In contrast, a white noise stimulus has a flat power spectrum and random phase structure. Using their synthetic stimulus ensembles, the investigators determined that the observed cortical feature sensitivity was related more closely to natural phase regularities and not the spatial power spectra.

Field (1994) suggested that the phase spectrum of a natural image describes the redundancy necessary for sparse coding. The structure of complex image features is preserved in the phase information and the presence of certain features is rare across the set of natural scenes. In a previous study, we found that synchronous activity among pairs of cells could discriminate between collinear and cocircular contours (Samonds et al. 2006) and that this activity was more predictable than changes in average firing rate.

178

Cells synchronized dynamically depending on their joint tuning preferences relative to the spatial configuration of the stimulus. Similarly, we showed in Chapter 5 that synchronous activity in larger assemblies with receptive fields organized according to the association field model (Field et al. 1993; Hess et al. 2003) consistently signaled complex contours in natural images. If synchrony reflects the implementation of a sparse code, we would expect to find that synchronized activity is stronger when viewing hybrid images with natural phase spectra than when stimulated with images that have random phase spectra. Since the phase spectrum captures structural information, this finding would support our hypothesis that synchrony may function as a contour-encoding mechanism in the primary visual cortex.

We can determine whether synchrony depends on the phase spectrum of an image by altering it. We separated three natural images into their power and phase components in the frequency domain. By swapping components with a random white noise stimulus, hybrid images were produced that had a natural phase spectrum and random power spectrum (natural hybrid) or a random phase spectrum and natural power spectrum (random hybrid; Figure 6.5A). We measured the synchrony and firing rate responses (averaged across all neurons) in assemblies of 2-8 cells over each stimulus condition and found that while synchrony decreased to approximately 60% of its original value after removal of the natural power spectrum, almost all activity was obliterated when the phase spectrum was eliminated (Figure 6.5C). Firing rate decreased in a similar fashion, but the rate of change was less severe (Figure 6.5D). Consistent with an earlier finding that synchrony signals fine, but not coarse, changes in orientation (Samonds et al. 2003), we suggest that synchrony is more sensitive to fine structure in the natural hybrid stimulus than firing rate.

179
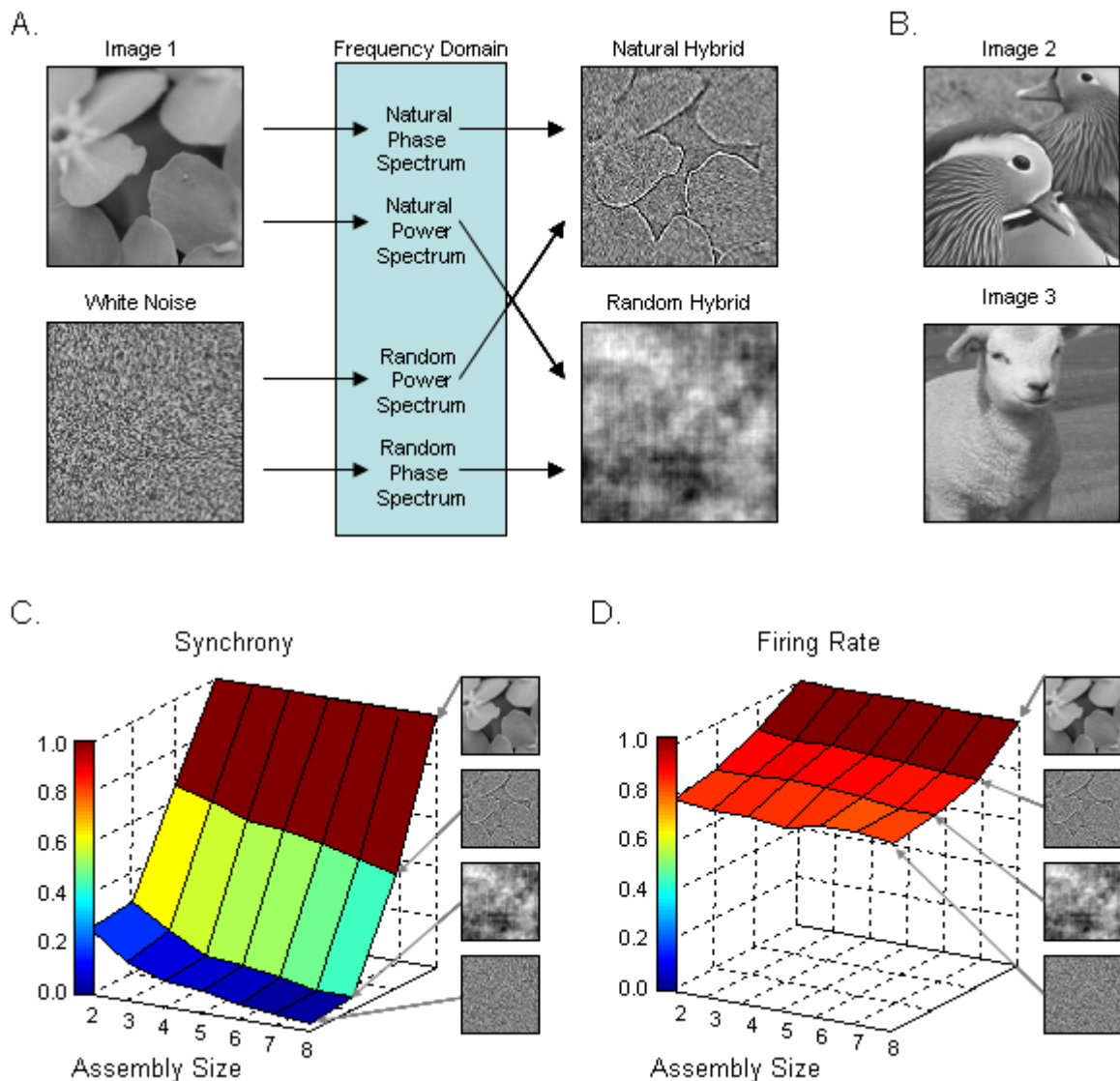
Figure 6.5. Phase spectrum analysis. (A) Process of creating hybrid images. Natural and white noise images are converted into their frequency domain counterparts and separated into power and phase components. The phase spectra are swapped and each image is recombined so that a natural hybrid image has a natural phase spectrum and random power spectrum. Alternatively, the random hybrid has a random phase spectrum and natural power spectrum. (B) Two other natural images investigated during this protocol. (C) Synchrony and (D) average firing rate responses to each original and hybrid image in (A), normalized to unity across each group size. Synchrony drops precipitously as the natural power spectrum is removed and more so when the phase spectrum is lost. On the other hand, firing rate decreases more gradually across conditions. Recall that jitter motion induces spiking activity relative to the static condition and can contribute 71.0% more spikes and 27.1% more synchronous events (from Chapter 4).

Discussion

Field (1994) proposed that the hallmarks of an efficient encoding strategy for the representation of natural scenes are sparseness and distribution. Synchrony was investigated as a viable sparse-dispersed code employed by the visual cortex to represent high-order stimulus features in natural scenes. Using a 10x10 microelectrode array and the PSP algorithm, we recorded from and subsequently analyzed the responses of hundreds of neurons in the striate cortex of cats when viewing a natural image sequence or spectral hybrid stimuli. We found that the definition of synchrony requires increased sparseness across assembly size, which was consistent with an artificially sparsified firing rate code in which all members were forced to exhibit simultaneous coactivation above a chance threshold determined from the background activity of each neuron. Responses were sparse for each assembly across the image set (lifetime) as well as across all assemblies for each condition (population). Average firing rate response distributions decreased in sparseness across assembly size, but had higher dispersal values. Results from the phase spectrum analysis suggest that synchrony is particularly sensitive to structural content in natural images and since neuronal spike trains contain firing rate and synchrony responses, these coding strategies may be simultaneously employed in the primary visual cortex to encode the representation of natural scenes.

Sparse-Dispersed Coding

Previous studies report that firing rate-based codes are sparse and distributed (Willmore et al. 2000; Willmore and Tolhurst 2001), but we expected to find that a synchrony-based code also has high population sparseness, lifetime sparseness, and dispersal and that these properties grew with assembly size. As synchrony is a subset of

firing rate and is by definition less frequent, our results came as no surprise when we found that synchrony response distributions are sparser than average firing rate. Across all six metrics, we found a drastic increase in selectivity when considering a synchrony-based code than one based on average firing rate. And although there was a similar trend for lifetime and population analyses implying that assembly responses to natural scenes are uncommon events, these quantities do not measure the same property and are not always correlated (Willmore and Tolhurst 2001). Sparseness statistics measure the infrequency of assembly responses, but recall that our probability of response was enhanced by the selection of assemblies with receptive field organizations conducive to synchronous activity. This suggests that our results actually underestimate sparseness, but the selection criteria were necessary in order for assemblies to be evaluated with a sample of 3026 images.

In choosing specific assemblies, we tried to find groups that responded to numerous elements in the stimulus sequence. However, synchrony responses were found to be less distributed across assembly size. This could be due to two reasons. First, as synchrony signals higher-order structure, increasingly complex features become rarer in the image set and the assembly responses become less variable. Second, the assemblies chosen for analysis do not necessarily form a representative sample of all possible assemblies that could be chosen from the primary visual cortex as the combinatorial possibilities lead to an endless amount of feature selectivity. With their orientation preferences and locations, two cells can be used to identify a circle (Samonds et al. 2006). Pairs of cells in our analysis showed the most dispersal because cocircularity is a ubiquitous structure in natural scenes (Geisler et al., 2001; Sigman et al., 2001; Elder and

Goldberg, 2002). On the other hand, larger assemblies can encode more highly-figured stimuli, which become more and more uncommon.

Across assembly size, firing rate responses show an increased level of distribution, signifying that larger assemblies are better at discriminating between images in the sequence. This is due to the successive inclusion of neurons with different spatiotemporal properties which, together, represent an aggregate encoder with the superposition of all response variations produced by its members. Parameter specificities allow individual cells to act as spatiotemporal filters by responding to a limited range of spatial and temporal information in the visual field. By sampling a continuum of spatial frequency, orientation, direction, and/or disparity, visual cortical cells behave as filters for different stimulus dimensions. And because these cells cover the range of parameter values to which the visual system is sensitive, their average firing rate activity is sufficient to encode each stimulus attribute. With respect to orientation preference, a group of approximately forty neurons can sufficiently sample the full range of orientations. Because tuning bandwidths for this property is sufficiently wide, the variance of firing rate responses for each cell across a set of stimuli will be high and encoding will be dispersed across the population of cells (or assemblies that combine these cells).

Advantages of a Sparse Code

Evidence from numerous studies suggest that cells in the visual cortex perform a sparse-dispersed coding of the spatial information of natural scenes (Field 1994; Olshausen and Field 1996, 1997; Bell and Sejnowski 1997). Basis functions produced when the visual system is optimized to process the statistics of natural scenes (Barlow

1961; Kersten et al. 1987; Simoncelli 2003) resemble the receptive fields of simple cells (Olshausen and Field 1996; Bell and Sejnowski 1997; van Hateren and van der Schaaf 1998; van Hateren and Ruderman 1998; Hyvarinen and Hoyer 2000). In addition, sparse coding models have been shown to learn complex cell receptive fields and topography from natural images (Hyvarinen and Hoyer 2001). Outside of the visual system, this approach has been extended to represent natural sounds as sparse events and the resulting receptive fields have similar spectro-temporal properties of auditory nerve cells (Lewicki 2002; Olshausen and O'Connor 2002).

There are several biological advantages for employing a sparse coding strategy. For instance, by utilizing a small number of neurons during any one task, sparse codes are energy efficient. Estimates of the energy required for signaling in cortical neurons suggest that less than 2% of the population can be significantly active at any given time (Attwell and Laughlin 2001; Lennie 2003). Experimental evidence has shown that average firing rates are low for natural images compared to that from optimal grating stimulation, which reduces the metabolic demands of visual processing (Baddeley et al. 1997; Guo et al. 2005). Also, several theoretical and computational studies have shown that sparse representations are most effective for storing patterns in associative memory models (Willshaw et al. 1969) and they are advantageous for learning associations in neural networks (Palm 1980; Baum et al. 1988; Zetsche 1990; Field 1994; Sommer and Palm 1999). Since the response of any one cell (assembly) is relatively rare, tasks that require matching or detecting corresponding features are more successful. As a code becomes more sparse (i.e. lowered probability of one cell or assembly responding), the probability of detecting a correct correspondence increases. Higher-order relations requiring large neural assemblies are increasingly rare and thus more informative when

present. High-order features in nature can then be represented by a unique subset of cells. In fact, Hoyer and Hyvarinen (2002) have shown that a multi-layer sparse coding network is capable of learning contour coding from natural images in an unsupervised fashion.

Sparse coding networks have been shown to exhibit continuous generalization across changing input, smooth degradation if the network is incomplete or damaged, and can store large numbers of representations (Rolls and Tovee 1995). Sakurai (1999) suggested that continuous generalization, functional compensation, and information-encoding capabilities are all qualities of a dynamic population code that utilizes the temporal coordination of neuronal firing. A population code requires specific rules for the association among cells. While sparse coding requires a subset of cells to be active for any given input, what properties of the input define the subsets formed? Is formation guided by intrinsic properties such as anatomical connections among cells with similar tuning preferences, extrinsic properties such as features within the stimulus, or both? Furthermore, how is this property represented by the subset? Since a given subset is particular to certain inputs, this property may be stimulus-dependent and relatively rare across the population of inputs. As mentioned above, higher-order features (contours, surfaces, textures) may be represented in a sparse code. Our previous results suggest that synchrony may be encoding contours in natural images (Samonds et al. 2006). Like Sakurai (1999), we propose that this representation is reflected in the cooperative activity of the subset. In other words, synchrony is a way to implement a sparse coding strategy where higher-order stimulus information preserved in the phase spectrum is represented in the precise temporal pattern of a neural assembly. Precise temporal coordination

among neurons preserves the requirements for sparse coding in that information is transmitted efficiently (through cooperation) and by a few neurons (assembly).

Dual Coding Strategy

By introducing a method whose output is relevant to the postsynaptic neuron, the magnitude of synchrony is also a measure of efficiency. Higher scores reflect more efficient transmission in that threshold can be reached more quickly than with assemblies with lower scores. Synchrony, itself, represents an efficient coding strategy since dynamic grouping allows for the formation of transient functional groups during different stimuli or separate functional groups during the same stimulus. Victor (2000) suggested that stimulus information is multiplexed at different temporal resolutions of the interspike interval histogram, but we suggest that cells can multiplex information in their spike trains by forming separate assemblies to encode all objects in a scene. Therefore, synchrony allows for multitasking so that visual information can be processed with a minimum number of cells. Conversely, a larger number of cells can process more complicated stimuli.

To increase encoding capabilities, the brain probably takes advantage of multiple supplemental coding strategies. Just as synchrony may behave as a sparse code to identify assemblies, there may also be a firing rate compact code within each assembly that optimizes not only on which cells are active, but also information can be revealed from the amount of activity generated by each neuron or assembly. Dual coding with assemblies and single neuron functions (Eichenbaum 1993; Sakurai 1999) would maximize sparseness as well as dispersal creating the ideal sparse-dispersed code. Stopfer et al. (2003) showed evidence for the dual coding of odor concentration and

identity in the locust olfactory system. In the motor cortex, Riehle et al. (1997)

demonstrated that synchrony within an assembly reliable encodes cognitive processes

like expectation while the magnitude of single unit activity encoded external events. In

Chapter 4, we showed that synchrony can be used to identify contour structure and the

amount of synchrony correlated with the degree of structural integrity. Both firing rate

and synchrony are stimulus-dependent (e.g. see Figure 6.5C and D), but may reflect this

in different proportions to encode different stimulus attributes. Although firing rate

correlates with local contrast structure (Weliky et al. 2003) and can signal coarse stimulus

properties (Samonds et al. 2003), synchrony defines specific relationships between the

figural elements detected, which can be interpreted at higher cognitive levels in the visual

system.

References

Atick J.J. and Redlich A.N. What does the retina know about natural scenes? *Neural Comp*. 4:449-572, 1992.

Atick J.J. and Redlich A.N. Towards a theory of early visual processing. *Neural Comp*. 4: 196-210, 1990.

Attwell D and Laughlin SB. An energy budget for signaling in the grey matter of the brain. *J Cereb Blood Flow Metab.* Oct;21(10):1133-45, 2001.

Azouz R and Gray CM. Adaptive coincidence detection and dynamic gain control in visual cortical neurons in vivo. *Neuron,* 37:513-523, 2003.

Baddeley R, Abbott LF, Booth MC, Sengpiel F, Freeman T, Wakeman EA, and Rolls ET. Responses of neurons in primary and inferior temporal visual cortices to natural scenes. *Proceedings of the Royal Society of London B Biological Sciences,* 264, 1775-1783, 1997.

Baddeley R.Visual perception. An efficient code in V1? *Nature.* Jun 13;381(6583):560-1, 1996.

Barlow HB. Single units and sensation: a neuron doctrine for perceptual psychology? *Perception*, 1:371-394, 1972.

Barlow HB. Possible principles underlying the transformation of sensory messages. In *Sensory Communication*, ed. WA Rosenblith, Cambridge, MA: MIT Press, 217-234, 1961.

Baum EB, Moody J, and Wilczek F. Internal representations for associative memory. *Biol. Cybern.* 59:217-228, 1988.

Bell AJ and Sejnowski TJ. The "independent components" of natural scenes are edge filters. *Vision Res*. Dec; 37(23): 3327-38. 1997.

Beloozerova IN, Sirota MG, and Swadlow HA. Activity of different classes of neurons of the motor cortex during locomotion. *J Neurosci.* Feb 1;23(3):1087-97, 2003.

Brecht M, Singer W, and Engel AK. Amplitude and direction of saccadic eye movements depend on the synchronicity of collicular population activity. *J Neurophysiol*. Jul;92(1):424-32, 2004.

Brecht M and Sakmann B. Dynamic representation of whisker deflection by synaptic potentials in spiny stellate and pyramidal cells in the barrels and septa of layer 4 rat somatosensory cortex. *J Physiol*. Aug 15;543(Pt 1):49-70, 2002.

Coath M, Brader JM, Fusi S, and Denham SL. Multiple views of the response of an ensemble of spectro-temporal features support concurrent classification of utterance, prosody, sex and speaker identity. *Network.* Jun-Sep;16(2-3):285-300, 2005.

Daugman JG. Self-similar oriented wavelet pyramids: Conjectures about neural non-orthogonality. In A. Gorea, ed., *Representations of Vision*. Cambridge University Press, Cambridge, 1991.

Daugman JG. Complete discrete 2-D Gabor transforms by neural networks for image analysis and compression. *IEEE Transact. Acoustics, Speech, Signal Process.* 36(7):1169-1179, 1988.

Eichenbaum H. Thinking about brain cell assemblies. *Science.* 261:993–994, 1993.

Elder JH and Goldberg RM. Ecological statistics of Gestalt laws for the perceptual organization of contours. *J. Vis*. 2:324-353, 2002.

Felsen G, Touryan J, and Dan Y. Contextual modulation of orientation tuning contributes to efficient processing of natural stimuli. *Network.* Jun-Sep;16(2-3):139-49, 2005.

Field DJ. What is the goal of sensory coding? *Neural Comp.* 6:559-601, 1994.

Field DJ, Hayes A, and Hess RF. Contour integration by the human visual system: evidence for a local "association field". *Vision Res.* 33:173-193, 1993.

Field DJ. Relations between the statistics of natural images and the response properties of cortical cells, *Journal of the Optical Society of America A,* 4, 2379-2394, 1987.

Field DJ. What the statistics of natural images tell us about visual coding. *Proc. SPIE.* 1077:269-276, 1989.

Fiete IR, Hahnloser RH, Fee MS, and Seung HS. Temporal sparseness of the premotor drive is important for rapid learning in a neural network model of birdsong. *J Neurophysiol.* Oct;92(4):2274-82, 2004.

Geisler WS, Perry JS, Super BJ, and Gallogly DP. Edge co-occurrence in natural images predicts contour grouping performance. *Vision Res.* 41:711-724, 2001.

Guo K., Robertson RG., Mohamoodi S., and Young MP. Centre-surround interactions in response to natural scene stimulation in the primary visual cortex. *Eur. J. Neurosci.* 21:536-548, 2005.

Hahnloser RH, Kozhevnikov AA, and Fee MS. An ultra-sparse code underlies the generation of neural sequences in a songbird. *Nature.* Sep 5;419(6902):65-70, 2002.

Hebb DO. *The Organization of Behavior: a Neuropsychological Theory.* New York: Wiley, 1949.

Hess RF, Barnes G, Dumoulin SO, and Dakin SC. How many positions can we perceptually encode, one or many? *Vision Res.* Jun;43(14):1575-87, 2003.

Hoyer PO. and Hyvarinen A. A multi-layer sparse coding network learns contour coding from natural images. *Vision Res.* 42(12):1593-1605, 2002.

Hubel DH and Wiesel TN. Receptive fields, binocular interaction and functional architecture in the cat's visual cortex. *J Physiol* 160: 106–154, 1962.

Hoyer PO and Hyvarinen A. Independent component analysis applied to feature extraction from colour and stereo images. *Network: Computation in Neural Systems.* 11(3):191-210, 2000.

Hyvarinen A and Hoyer PO. A two-layer sparse coding model learns simple and complex cell receptive fields and topography from natural images. *Vision Res.* Aug;41(18):2413-23, 2001.

Kelly RC, Smith MA, Samonds JM, Kohn A, Bonds AB, Movshon JA, and Lee TS. Comparison of recordings from microelectrode arrays and single electrodes in the visual cortex. *J Neurosci.* Jan 10;27(2):261-4, 2007.

Kersten D. Predictability and redundancy of natural images. *Journal of the Optical Society of America A*, 4, 2395-2400, 1987.

Laurent G. Olfactory network dynamics and the coding of multidimensional signals. *Nat Rev Neurosci*. Nov;3(11):884-95, 2002.

Lennie P. The cost of cortical computation. *Curr. Biol.* 13:493-497, 2003.

Lewicki MS. Efficient coding of natural sounds. *Nat Neurosci.* Apr;5(4):356-63, 2002.

Linsker R. Self-organization in a perceptual network. *Computer*. 21:105-117, 1988.

Olshausen BA and O'Connor KN. A new window on sound. *Nat Neurosci.* Apr;5(4):292-4, 2002.

Olshausen BA and Field DJ. Emergence of simple-cell receptive field properties by learning a sparse code for natural images. *Nature* 381:607–609, 1996.

Olshausen BA and Field DJ. Sparse coding with an overcomplete basis set: a strategy employed by V1? *Vision Res.* 37:3311-3325, 1997.
Palm G. On associative memory. *Biol. Cybern.* 36:19-31, 1980.

Perez-Orive J, Mazor O, Turner GC, Cassenaer S, Wilson RI and Laurent G. Oscillations and sparsening of odor representations in the mushroom body. *Science*. 297:359-365, 2002.

Riehle A, Grun S, Diesmann M, and Aertsen A. Spike synchronization and rate modulation differentially involved in motor cortical function. *Science.* 278:1950–1953, 1997.

Rolls ET and Tovee MJ. Sparseness of the neuronal representation of stimuli in the primate temporal visual cortex. *J Neurophysiol*. Feb;73(2):713-26, 1995.

Rousche PJ and Normann RA. A method for pneumatically inserting an array of penetrating electrodes into cortical tissue. *Annals of Biomed. Eng.*, 20:413-422, 1992.

Sakurai Y. How do cell assemblies encode information in the brain? *Neurosci Biobehav Rev.* 23(6):785-96, 1999.

Samonds JM, Zhou Z, Bernard MR, and Bonds AB. Synchronous Activity in Cat Visual Cortex Encodes Collinear and Cocircular Contours. *J. Neurophysiol.* 95:2602-2616, 2006.

Samonds JM, Allison JD, Brown HA, and Bonds AB. Cooperation between Area 17 neuron pairs enhances fine discrimination of orientation. *Journal of Neuroscience,* 23, 2416-2425, 2003.

Sanger TD. Optimal unsupervised learning in a single layer network. *Neural Networks*. 2:459-473, 1989.

Sherrington CS. *Man on His Nature*. London: Cambridge University Press, 1941.

Shoham S, Fellows MR, and Normann RA. Robust, automatic spike sorting using mixtures of multivariate t-distributions. *J Neurosci Methods*. 127:111-122, 2003.

Sigman M, Cecchi GA, Gilbert CD, and Magnasco MO. On a common circle: natural scenes and Gestalt rules. *Proc. Natl. Acad. Sci. USA*. 98:1935-1940, 2001.

Simoncelli EP. Vision and the statistics of the visual environment. *Current Opinion in Neurobiology*, 13,144-149, 2003.

Skottun BC, De Valois RL, Grosof DH, Movshon JA, Albrecht DG, and Bonds AB. Classifying simple and complex cells on the basis of response modulation. *Vision Res*. 31(7-8):1079-86, 1991.

Sommer FT and Palm G. Improved bidirectional retrieval of sparse patterns stored by Hebbian learning. *Neural Netw*. Mar;12(2):281-297, 1999.

Stopfer M, Jayaraman V, and Laurent G. Intensity versus identity coding in an olfactory system. *Neuron*. Sep 11;39(6):991-1004, 2003.

Theunissen FE. From synchrony to sparseness. *Trends Neurosci*. 26:61-64, 2003.

Thompson LT and Best PJ. Place cells and silent cells in the hippocampus of freely-behaving rats. *J Neurosci.* Jul;9(7):2382-90, 1989.

Tolhurst DJ, Tadmor Y, and Chao T. Amplitude spectra of natural images. *Ophthalmic Physiol Opt*. Apr;12(2):229-32, 1992.

Touryan J, Felsen G, and Dan Y. Spatial structure of complex cell receptive fields measured with natural images. *Neuron*. Mar 3;45(5):781-91, 2005.

Treves A and Rolls ET. What determines the capacity of autoassociative memories in the brain? *Network: Comput. Neural Syst.* 2 371–97, 1991.

van der Schaaf A and van Hateren JH. Modelling the power spectra of natural images: statistics and information. *Vision Res.* Sep;36(17):2759-70, 1996.

van Hateren JH and van der Schaaf A. Independent component filters of natural images compared with simple cells in primary visual cortex. *Proc Biol Sci.* Mar 7;265(1394):359-66, 1998.

van Hateren JH and Ruderman DL. Independent component analysis of natural image sequences yields spatio-temporal filters similar to simple cells in primary visual cortex. *Proc Biol Sci.* Dec 7;265(1412):2315-20, 1998.

Victor JD. How the brain uses time to represent and process visual information. *Brain Res.*, 886:33-46, 2000.

Vinje WE and Gallant JL. Sparse coding and decorrelation in primary visual cortex during natural vision. *Science,* 287, 1273-1276, 2000.

Vinje WE and Gallant JL. Natural stimulation of the nonclassical receptive field increases information transmission efficiency in V1. *J. Neurosci.* 22:2904-2915, 2002.

von der Malsburg C. Am I thinking assemblies? In: Palm G, Aertsen A, editors. Brain theory, Berlin: Springer, pp. 161, 1986.

Weliky M., Fiser J., Hunt R.H., and Wagner D.N. Coding of natural scenes in primary visual cortex. *Neuron*. 37:703-718, 2003.

Willmore B, Watters PA and Tolhurst DJ. A comparison of natural-image-based models of simple-cell coding. *Perception* 29:1017-1040, 2000.

Willmore B and Tolhurst DJ. Characterizing the sparseness of neural codes. *Network* 12:255-270, 2001.

Willshaw DJ, Buneman OP, Longuet-Higgins HC. Non-holographic associative memory. *Nature*. Jun 7;222(5197):960-2, 1969.

Young MP and Yamane S. Sparse population coding of faces in the inferotemporal cortex. *Science* 256:1327-1331, 1992.

Zetsche C. Sparse coding: The link between low level vision and associative memory. In *Parallel Processing in Neural Systems and Computers*, R. Eckmiller, G. Hartmann, and G. Hauske, eds. North-Holland, Amsterdam, 1990.

CHAPTER VII

SUMMARY AND FUTURE DIRECTIONS

Summary

The work presented here investigates the dynamic associations among small populations of neurons during natural stimulation and seeks the form of the neural code for representation of visual structures. Microelectrode array technology allows the simultaneous sampling of neurons with a variety of spatiotemporal preferences, which can be used to explore complex intercellular interactions. This recording paradigm and a novel algorithm for quantifying synchrony were used to study the timing relationships among neurons in the primary visual cortex of cats to evaluate synchrony's role as a possible neural substrate for contour detection.

Chapter 1 discussed relevant history of the problem of neural coding. A review of the temporal binding theory (Milner 1974; von der Malsburg 1981) and evidence that synchrony may be involved in contour detection (Gray et al. 1989; Samonds et al. 2006) provided the motivation for our current research. In Chapter 2, we described our experimental protocol. Our multielectrode array technology allows the recording of dozens of single units, which can be analyzed simultaneously with the PSP algorithm. Based on modeling postsynaptic potential integration, this method quantifies the amount of synchronous activity in an assembly of arbitrary size and provides measures for direct statistical comparison.

In Chapter 3, we studied the spatial and temporal evolution of synchronous activity across the striate cortex and found that cooperation between pairs of cells

decreased linearly with a separation distance of up to 3 mm. The average magnitude of synchrony decreased with the difference in joint orientations, but could still be found in significant quantities between cells with wholly different orientation preferences ($< 80°$) similar to the findings in Samonds et al. (2006). We measured the effects of stimulus presentation style and found that firing rate responses were more sensitive to motion effects. We also found that jittering stimuli in random directions about the origin produced the same amount of synchrony as that obtained during the drift presentation with the largest response. Furthermore, moderate amounts of synchrony were still observed during presentation of static stimuli. These results have important implications for the use of natural images in similar paradigms since the use of natural stimuli is vital in understanding sensory processing in the early visual pathway (Felsen and Dan 2005). Analysis of the time course of synchrony during stimulus presentations showed that large amounts of synchrony are generated during the onset response transient and reach a stable level after approximately 800 ms. This result and the finding that synchrony is minimally affected by stimulus motion suggest that cooperative activity is initiated by the spatial properties of the image. Finally, an assessment of raw synchrony compared to stimulus-locked events reveals that normalization is irrelevant for assemblies with four or more cells.

In Chapter 4, we used a difference method to study systematically the effects of structural degradation in natural images by measuring responses to stimuli before and after noise, frequency, and contrast manipulations. We found that synchronous activity, unlike firing rate, is sensitive to the degree of image degradation when added noise and removing spatial frequency bands. This reduction in synchrony was attributed to the generation of fewer synchronous events rather than a shortening of existing events. A

194

quantitative analysis of receptive field layout showed that assemblies with good associations as described by the association field model (Field et al. 1993; Hess et al. 2003), with similar preferred orientations and close receptive field proximity, tended to generate more synchrony than assemblies with poorer associations. As in Chapter 3, these results suggest that synchrony signals spatial elements in the stimulus and reflects the presence of coherent structural information.

The results from Chapter 4 were extended into Chapter 5 where we specifically measured synchrony's dependence on the proximity, orientation, and alignment of assembly receptive fields. Using a large natural image sequence with a variety of visual features to optimize stimulation of the entire recorded population, we showed that synchronous activity was moderately correlated with the properties of association. We used these properties to create a contour index, which quantitatively described how well an assembly's configuration matched a contour structure. Synchrony was well-correlated with this measure, which, along with a measure of the corresponding contrast information to which the assembly is responding, indicates that cooperation may be selective for local contrast structure arranged in continuous, well-defined contours. Synchronous activity measured between assemblies representing different contours on the same or different object was severely reduced and found in amounts much lower than expected by chance.

Finally, Chapter 6 describes synchrony in the context of a sparse coding strategy used to encode contour information in natural scenes. We measured the simultaneous response of assemblies to thousands of natural images and analyzed the sparseness and dispersal of synchrony and firing rate distributions. We found that the definition of synchrony requires increased sparseness across assembly size as groups become more selective for stimulus features. This was consistent with an artificially sparsified firing

rate code in which the activities of all members were forced to exhibit simultaneous coactivation above a change threshold. Synchronous responses were sparse for each assembly across the image set (lifetime) and well as across all assemblies for each condition (population). In contrast, average firing rate response distributions were less sparse for larger assemblies, but represented a more distributed code. An analysis of the phase spectrum suggests that synchronous activity is particularly sensitive to structural content in natural images, which is preserved in the phase regularities in the image and not the power spectrum.

Large amounts of synchrony during the stimulus onset response emphasize that synchrony is stimulus-dependent. Although it is unlikely that the large assembly response (50% of the population) signals features of the same object, an initial synchronization may ready the cortex for incoming information, which is then parsed out among smaller assemblies. We have been concerned with the binding problem, assuming that the visual input is effectively in pieces and must be put together. However, another view is that incoming information is initially represented as a complete picture that must be resolved into individual components. In Chapter 6, we mentioned that the brain may take advantage of firing rate and synchrony coding capabilities to implement a dual coding strategy for the representation of natural scenes. While synchrony initially signals all salient features, firing rates of individual neurons respond to local contrast information and these two paths may combine to describe coherent features and can be modulated by feedback. Although this field started with the measuring of single neurons, which described pieces of the visual scene, the brain may start with a complete representation (although not immediately meaningful) that must be broken down.

Analytical stimuli applied to the receptive fields of single cells have produced a

solid foundation for understanding the cellular processes of vision, but elaboration of vision at a more holistic level must rely on more global approaches. Here we combine simultaneous recordings from dozens of cells with natural image stimulation and a novel method for identification of cellular assemblies defined by synchrony. By analyzing responses to natural images, we found that synchronous activity was able to discriminate changes in structural integrity and overcome the ambiguity of firing rate to identify contour structure. The time course of synchrony suggests that it is directly related to spatial stimulus properties. Our results demonstrate that synchrony has the potential to encode image properties not apparent from changes in firing rate and, in that capacity, may serve as a neural substrate for contour detection. Orientation linking appears to operate prior to feature extraction (Dakin and Hess 1999). As a fundamental mechanism of sensory cognition, synchrony may act as a sparse code to help facilitate the detection of contour information for integration and processing in higher visual areas.

Future Directions

Understanding Synchrony with Visual Illusions

As described in earlier chapters and in Samonds et al. (2006), we have demonstrated that synchrony is stimulus-dependent and corresponds to the appropriate match between stimulus features and the spatiotemporal preferences of the assembly. These conclusions are based on studies that have examined natural scenes or simple analytical stimuli that have explicit perceptual relationships between objects. However, a greater understanding of visual neurophysiology may be obtained through the use of unconventional stimulation in which content is enigmatic. A more complete

understanding of synchrony and its underlying neural mechanisms may follow from an investigation of stimuli in which the incoming visual information is perceptually ambiguous. Whether assembly membership and synchronous activity modulates with actual stimulus structure or perceived content may reveal if synchrony plays a role in perception or simply behaves as a signal transmission mechanism. Our prediction is that synchrony correlates with actual stimulus structure at the onset of the response, but may evolve to signal perceived structure after the influences of feedback from network interactions and higher processing centers.

Visual illusions are false percepts induced by the precise arrangement of elements in a visual scene that create emergent and not necessarily existing features. Illusions can be created with real lines such as in the tilt effect (Roncato and Casco 2006) or Ponzo, Hering, and Zollner illusions. Figure 7.1A-C shows variations of an Ehrenstein illusion in which the apparent curvature of real contours change with context. Straight lines can take an apparent concave or convex direction depending on the placement of a pattern of concentric rings. On the other hand, illusory contours can be perceived in images in which there is no physical stimulation for that feature. Contour interpolation exists for amodal completion such as when the visual system connects contours under occlusion and for modal completion, which is experienced with the Kanizsa square (Kanizsa 1976). Figure 7.1D-F shows variations of the Kanizsa square whose apparent curvature changes with context similar to Figure 7.1A-C. Stimuli such as The Window by Sandro del Petre (Figure 7.1I) demonstrate figure-ground ambiguity in which the incoming visual information produces two different percepts.

A number of neurophysiological experiments have investigated illusory contour formation in the visual system. Responses to stimuli that produce illusory contours in
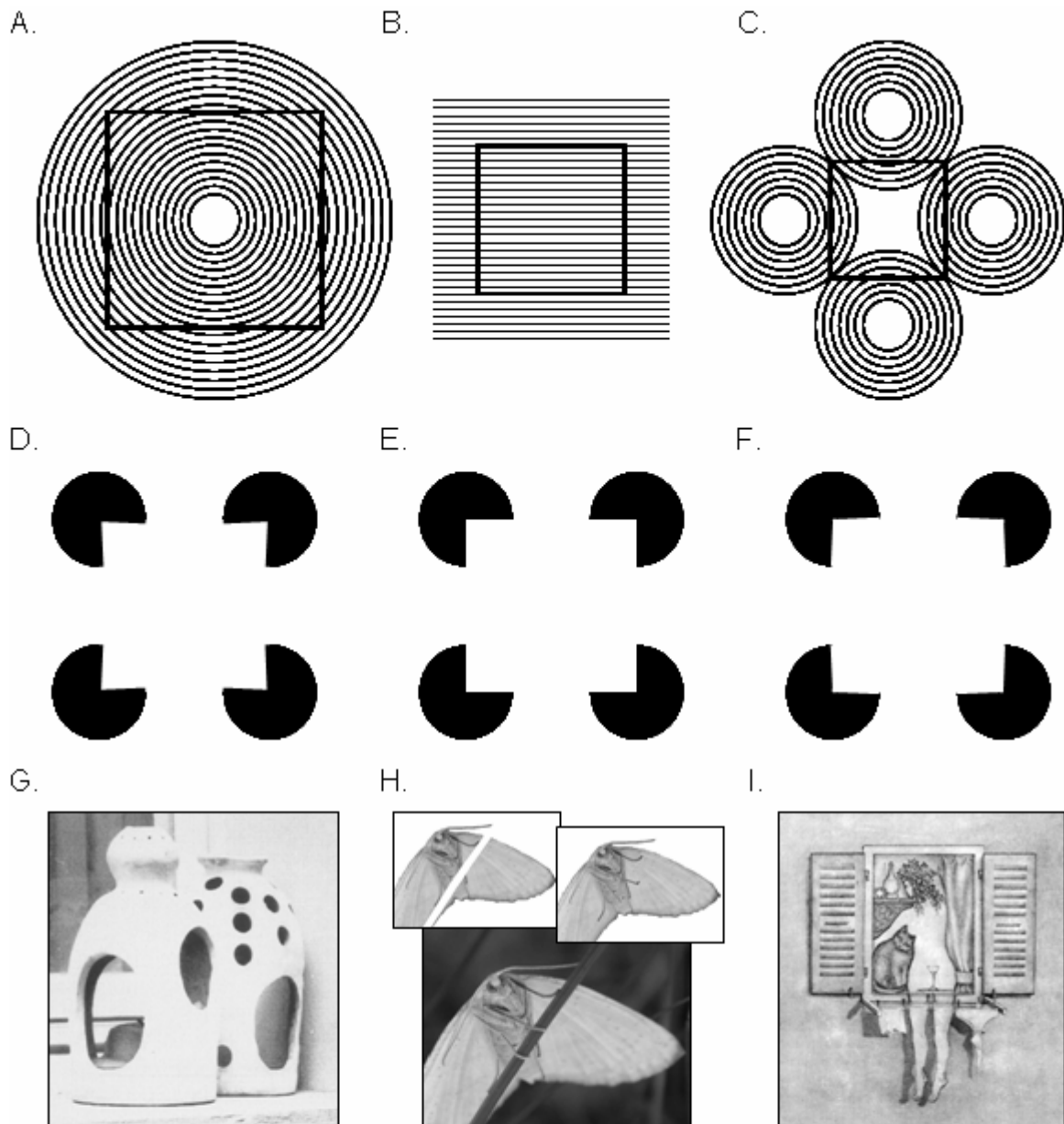
Figure 7.1. Example stimuli for future research. (A)-(C) Real contours whose apparent curvature changes with context. (A) Ehrenstein illusion in which a square placed inside a pattern of concentric rings take an apparent concave shape. (B) The square appears regular. (C) Ehrenstein illusion in which the square appears convex. (D)-(F) Illusory contours in a Kanizsa square whose apparent curvature change with context similar to (A)-(C). (G) Natural image with illusory contours (www.psych.stanford.edu/~lera/psych115s/notes/lecture9/figures2.html). (H) Natural image with a figure and occluding object. The insets depict two possible figures in the image. (I) Figure/ground ambiguity in "The window" by Sandro del Petre. The picture shows a pair of stockings, cat, glass, curtain, shelf, and plant. The woman is part of your Freudian imagination (www.doc.gold.ac.uk/~ffl/MSC101/Vision/Gestalt.html).

humans were found in V2 neurons of monkeys (von der Heydt and Peterhans 1989; Ramsden et al. 2001) and less often in V1 (Lee and Nguyen 2001). Although cognitive factors influence the perception of illusory contours (Bradley and Petry 1977; Rock and Anson 1979; Wallach and Slaughter 1988), findings from early visual areas suggest higher processing centers may not be needed for illusory contour formation (Coren 1972; Gregory 1972; Kanizsa 1976; Rock and Anson 1979). In fact, many psychophysical studies have implicated real and illusory contours in several processes of early vision such as the tilt aftereffect (Smith and Over 1975, 1979), apparent motion (von Grunau 1979; Ramachandran 1985), orientation discrimination (Vogels and Orban 1987), and motion aftereffect (Smith and Over 1979; Weisstein et al. 1977).

Neurons in V2 demonstrate similar orientation selectivity for real and illusory contours while the selectivity of V1 neurons is reversed (Ramsden et al. 2001). Psychophysical evidence suggests that real and illusory contour processes in these visual areas may be competitive rather than supportive (Ringach and Shapley. 1996). Speculation on the boundary completion process that underlies illusory contour formation has provided opposing viewpoints. While some researchers suggest a comparable contour integration process to real contours involving the linking of neural activity with similar orientations along the direction of the inducing elements (Grossberg and Mingolla 1985, 1987), others postulate a different relationship between the perceived contour and inducing units (Kellman and Shipley 1991; Finkel and Edelman 1989; Peterhans et al. 1986). Illusory contour formation may not necessarily be a component of the integration process (Field et al. 2000). In order to understand synchrony's role in the process of visual illusions, we suggest an in depth investigation of real and illusory contour stimuli, including the effects of occlusion and figure-ground ambiguity (Figure 7.1). Our

previous results suggest synchrony may behave as a contour detection mechanism for real

contours and these results would give insight into whether illusory contours may be

detected by a similar mechanism or be produced by some alternate process.

Neuroethological Experiments

Traditional approaches to the study of vision have involved recording from an

anesthetized animal during presentations of pure spatial frequency grating or light bar

stimuli. This "systems identification" approach uses non-natural stimuli with adjustable

properties to analyze the operation of the system in an attempt to understand the

metaphorical black box of the brain. This technique may yield a partial understanding for

early processing centers that function in a quasi-linear fashion, but by and large give

inaccurate descriptions of brain function in the numerous nonlinear components

throughout the visual system. Subsequently, the field of neuroethology emerged as a

branch of neuroscience that focuses on the study of neural mechanisms in the context of

natural behavior. The foundation for the neuroethological method stems from the idea

that over time, an animal's nervous system has evolved to behave and react in a particular

environmental niche. As it would not make sense to study a fish out of water, so would it

not be appropriate to study an animal's neural basis of behavior outside of its natural

surroundings.

The research detailed in the previous chapters investigated the role of neural

coding mechanisms in the context of natural vision. Although progress was made in

understanding the information encoding capacity of neuronal synchronization, our novel

approach was still hampered by the subject and relative immaturity of the experimental

protocol. For practical and often necessary considerations, our protocol was dependent

on laboratory conditions to control certain aspects of the environment. Besides controlling for elements such as electrical noise that could confound our measurements, we had to keep our subjects stable under general anesthesia in order to map the receptive field extent and location of dozens of cells. In this manner, the eyes were in a fixed position during mapping and viewed the same localized space for all stimulus presentations. Mapping this many cells in an awake, behaving animal would have been impractical due to the time required. Controlling eye movements was necessary for this reason and also critical to reflect a one-to-one correspondence between cell responses and stimulus features.

Critics have suggested that synchrony could be a byproduct of anesthesia and not actually exist as a natural phenomenon in the awake brain (Kulli and Koch 1991). However, synchronization of multi-unit activity, oscillations, and local field potentials has been observed in several visual areas of anesthetized cats (Eckhorn et al. 1988; Gray et al. 1989; Engel et al. 1991; Schwarz and Bolz 1991), in the primary visual cortex of awake cats (Raether et al. 1989), in visual areas of anesthetized (Livingstone 1996) and awake monkeys (Krieter and Singer 1992; Eckhorn et al. 1993), and in the optic tectum of awake pigeons (Neuenschwander and Varela 1993; see review in Singer and Gray 1995). In all instances, the synchronized activity had similar properties. In fact, identical experiments from anesthetized cats (Engel et al. 1991) have been repeated in awake monkeys (Krieter and Singer 1996) and the replication of results suggests that synchrony is a general property of the visual cortex.

Besides using awake preparations, our protocol could be improved by recording from larger populations of neurons. Although our measurements focused on moderate-sized assemblies of 2-8 neurons, a more realistic view of assembly function would be

obtained from larger groups. We have the ability to record from dozens of neurons

simultaneously, but can only find robust assemblies on a smaller scale (i.e., we have yet

to find stimulation that will induce synchronization in the entire recorded population).

The recordings sample multiple functional groups that organize around contour structure

in natural images. Up to approximately 50% of the recorded population has

demonstrated synchronization during the stimulus onset response transient (see Chapter

4), predicting that larger recorded samples could yield larger assemblies. For now, we

are limited by the size of the microelectrode array, which has 100 electrodes with 0.4 mm

spacing. Future studies should investigate arrays with a finer resolution and greater

recording capacity. Also, studies linking this single-unit activity with population studies

such as fMRI could provide significant insight into the role of synchrony in natural

vision.

Other Roles for Synchrony and Cooperation Beyond the Visual System

As synchrony allows for the formation of dynamic functional assemblies to

encode information in a visual scene, cooperative activity may serve more than one

purpose. In the visual cortex, most studies on neuronal synchrony and oscillations

contend that these mechanisms are involved in contour integration or figure-ground

discrimination (for review, see Singer and Gray 1995). However, synchronous activity

could carry out multiple functions in different visual areas (or on different time scales)

and other possible functions have been hypothesized. Poppel and Logothetis (1986)

studied human reaction times during pursuit eye movements and speculated that gamma

oscillations could operate as a clock, organizing temporal events. Sleep studies suggested

synchrony was related to cognitive experience and could reflect the state of

consciousness (Llinas and Ribary 2001; Madler et al. 1991; Kulli and Koch 1991; Crick and Koch 1990). Iwabuchi and Shimizu (1997) used flickering stimuli to conclude that synchrony may place objects in different depth planes, which is consistent with the temporal binding theory (Milner 1974; von der Malsburg 1981). Other hypotheses implicate cooperative activity in multi-modal integration (Damasio 1990), discrimination of tactile structure (Ahissar and Vaadia 1990), and selective attention (Crick 1984).

When investigating possible roles for synchrony, many investigators looked between visual areas and beyond the visual system (for a complete review, see Iwabuchi 1998; Singer and Gray 1995). Synchronous activity has been observed in many visual sectors including areas 17, 18, 19, and PMLS (Eckhorn et al. 1993; Engel et al. 1990, 1991; Gray et al. 1990), between visual areas such as between areas 17, 18, and 19 (Eckhorn et al. 1988; Nelson et al. 1992), between area 17 and PMLS (Engel et al. 1991a), and between area 17 in both hemispheres (Engel et al. 1991b). Correlated activity has also been observed in other sensory areas such as the somatosensory cortex (Ahissar and Vaadia 1990), motor cortex (Murthy and Fetz 1992), prefrontal cortex (Vaadia et al. 1995), and lateral geniculate nucleus of the thalamus (Ghose and Freeman 1992; Podvigin et al. 1992; Neuenschwander and Singer 1996; Sillito et al. 1994). Roelfsema et al. (1997) also showed robust synchronous activity between areas of the visual and parietal cortex and between areas of the parietal and motor cortex in awake cats. To gain a comprehensive understanding of synchrony for future studies, we suggest an investigation of the synchronous activity across all layers of organization in the cortex: within and between cortical layers, cortical areas, sensory systems, and brain hemispheres.

Clinical Applications and the Role of Synchrony in Neurological Disorders

The research in this dissertation studies synchronous activity in neural assemblies during natural stimulation to determine the role of such cooperation in the normal brain. However, malfunctioning processes and their overt system effects can also contribute to the understanding of normal brain functions. Abnormalities in the synchronization of neuronal oscillations have been implicated in the cognitive dysfunctions of brain disorders such as schizophrenia, epilepsy, autism, Alzheimer's disease, and Parkinson's disease (Uhlhaas and Singer 2006). By examining clinical results with electroencephalography, magneto-encephalography, and magnetic resonance imaging, these techniques revealed deficiencies in tasks designed around perceptual grouping, attention-dependent stimulus selection, routing of signals across cortical networks, sensory-motor integration, working memory, and perceptual awareness (for a review see Singer 1999; Schnitzler and Gross 2005).

For example, schizophrenia is a mental disorder characterized by psychotic symptoms, negative symptoms, and disorganization of thought and behavior (Uhlhaas and Singer 2006). Speculation on the pathophysiological mechanisms leading to the manifested behavior of schizophrenia suggests that deficits in the coordination of distributed processes may be linked to the synchronization of firing oscillations (Friston 1999). Visual binding tasks have been shown to reduce non-stimulus-locked oscillatory activity (Spencer et al. 2003). In epilepsy, increases in local synchrony and decreases in long-range synchronization have been correlated with specific dysfunctions in the area where a seizure occurred (Niedermeyer 2005). In autism, reduced functional connectivity and neural synchrony correlate with impairments in perception, social cognition, and attention (Belmonte et al. 2004; Hill and Frith 2003). In Alzheimer's

disease, reduced synchronization of oscillatory activity during the resting state

corresponds to deficits in working memory, attention, and executive processes (Stam et

al. 2003, 2005, 2006). Studies of synchrony in Parkinson's disease show an increase in

oscillations in the basal ganglia and between subcortical structures that are linked to

deficits in motor functioning (Boroud et al. 2005).

Research on many of these neurological disorders showed evidence for reduced

anatomical connectivity, which may contribute to the observed deficiencies in

synchronous activity. A comprehensive investigation of synchrony and oscillations

including studies of anatomical connections, long-range synchrony, and related

perceptual processes will provide medically relevant information that can possibly be

used in the diagnosis and treatment of these and other neural pathologies.

References

Ahissar E and Vaadia E. Oscillatory activity of single units in a somatosensory cortex of an awake monkey and their possible role in texture analysis. *Proc Natl Acad Sci U S A*. Nov;87(22):8935-9, 1990.

Belmonte MK, Allen G, Beckel-Mitchener A, Boulanger LM, Carper RA, and Webb SJ. Autism and abnormal development of brain connectivity. *J Neurosci*. Oct 20;24(42):9228-31, 2004.

Boroud T, Brown P, Goldberg JA, Graybiel AM, and Magill PJ. Oscillations in the Basa Ganglia: The good, the bad, and the unexpected. In: J.P. Bolam, C.A. Ingham and P.J. Magill, Editors, *The Basal Ganglia VIII*, Springer, New York, pp. 3–24, 2005.

Bradley DR and Petry HM. Organizational determinants of subjective contour: the subjective Necker cube. *Am J Psychol*. Jun;90(2):253-62, 1977.

Coren S. Subjective contours and apparent depth. *Psychol Rev*. Jul;79(4):359-67, 1972 .

Crick F and Koch C. Some reflections on visual awareness. *Cold Spring Harb Symp Quant Biol*.55:953-62, 1990.

Crick F. Memory and molecular turnover. *Nature*. Nov 8-14;312(5990):101, 1984.

Dakin SC and Hess RF. Contour integration and scale combination processes in visual edge detection. *Spat Vis*.;12(3):309-27, 1999.

Damasio AR. Category-related recognition defects as a clue to the neural substrates of knowledge. *Trends Neurosci.* Mar;13(3):95-8, 1990.

Eckhorn R, Frien A, Bauer R, Woelbern T, and Kehr H. High frequency (60-90 Hz) oscillations in primary visual cortex of awake monkey. *Neuroreport.* Mar;4(3):243-6, 1993.

Eckhorn R, Bauer R, Jordan W, Brosch M, Kruse W, Munk M, and Reitboeck HJ. Coherent Oscillations: A mechanism of Feature Linking in the Visual Cortex? *Biol. Cybern.*, 60:121-130, 1988.

Engel AK, König P, Gray CM, and Singer W. Stimulus-Dependent Neuronal Oscillations in Cat Visual Cortex: Inter- Columnar Interaction as Determined by Cross-Correlation Analysis. *Eur J Neurosci.*2(7):588-606, 1990.

Engel AK, Konig P, Kreiter AK, and Singer W. Interhemispheric synchronization of oscillatory neuronal responses in cat visual cortex, *Science* 252, pp. 1177–1179, 1991.

Engel AK, Fries P, and Singer W. Dynamic predictions: oscillations and synchrony in top-down processing, *Nat. Rev. Neurosci.* 2, pp. 704–716, 2001.

Felsen G and Dan Y. A natural approach to studying vision. *Nat Neurosci.* Dec 8(12): 1643-6, 2005.

Field DJ, Hayes A, and Hess RF. The roles of polarity and symmetry in the perceptual grouping of contour fragments. *Spat Vis*.13(1):51-66, 2000.

Field DJ, Hayes A, and Hess RF. Contour integration by the human visual system: evidence for a local "association field". *Vision Res.* 33:173-193, 1993.

Finkel LH and Edelman GM. Integration of distributed cortical systems by reentry: a computer simulation of interactive functionally segregated visual areas. *J Neurosci.* Sep;9(9):3188-208, 1989.

Friston KJ. Schizophrenia and the disconnection hypothesis, *Acta Psychiatr. Scand.* 395, pp. 68–79, 1999.

Ghose GM and Freeman RD. Oscillatory discharge in the visual system: does it have a functional role? *J Neurophysiol.* Nov;68(5):1558-74, 1992.

Gray CM, Engel AK, König P, and Singer W. Stimulus-Dependent Neuronal Oscillations in Cat Visual Cortex: Receptive Field Properties and Feature Dependence. *Eur J Neurosci*.2(7):607-619, 1990.

Gray CM, Konig P, Engel AK, and Singer W. Oscillatory responses in cat visual cortex exhibit inter-columnar synchronization which reflects global stimulus properties. *Nature*, 338:334-337, 1989.

Gregory RL. Comments on L. E. Krueger's "disconfirming evidence" of R. L. Gregory's theory of illusions. *Psychol Rev.* Nov;79(6):540-1, 1972.

Grossberg S and Mingolla E. Neural dynamics of form perception: boundary completion, illusory figures, and neon color spreading. *Psychol Rev*. Apr;92(2):173-211, 1985.

Grossberg S and Mingolla E. Neural dynamics of perceptual grouping: textures, boundaries, and emergent segmentations. *Percept Psychophys.* Aug;38(2):141-71, 1987 .

Hess RF, Barnes G, Dumoulin SO, and Dakin SC. How many positions can we perceptually encode, one or many? *Vision Res*. Jun;43(14):1575-87, 2003.

Hill EL and Frith U. Understanding autism: insights from mind and brain, *Philos. Trans. R. Soc. Lond. B Biol. Sci.* 358, pp. 281–289, 2003.

Iwabuchi A. Dynamic binding of visual features by neuronal/stimulus synchrony. *Appl Human Sci.* May;17(3):97-108, 1998.

Iwabuchi A and Shimizu H. Antiphase flicker induces depth segregation. *Percept Psychophys*. Nov;59(8):1312-26, 1997.

Kanizsa G. Subjective contours. *Sci Am*. Apr;234(4):48-52, 1976.

Kellman PJ and Shipley TF. A theory of visual interpolation in object perception. *Cognit Psychol.* Apr;23(2):141-221, 1991.

Kreiter AK and Singer W. Stimulus-dependent synchronization of neuronal responses in the visual cortex of the awake macaque monkey. *J Neurosci*. Apr 1;16(7):2381-96, 1996.

Kreiter AK and Singer W. Oscillatory Neuronal Responses in the Visual Cortex of the Awake Macaque Monkey.*Eur J Neurosci*.4(4):369-375, 1992.

Kulli J and Koch C. Does anesthesia cause loss of consciousness? *Trends Neurosci.* Jan;14(1):6-10, 1991.

Lee TS, Nguyen M. Dynamics of subjective contour formation in the early visual cortex. *Proc Natl Acad Sci U S A*. Feb 13;98(4):1907-11, 2001.

Livingstone MS. Oscillatory firing and interneuronal correlations in squirrel monkey striate cortex. *J Neurophysiol.* Jun;75(6):2467-85, 1996.

Llinás R and Ribary U. Consciousness and the brain. The thalamocortical dialogue in health and disease. *Ann N Y Acad Sci*. Apr;929:166-75, 2001.

Madler C, Keller I, Schwender D, and Pöppel E. Sensory information processing during general anaesthesia: effect of isoflurane on auditory evoked neuronal oscillations. *Br J Anaesth.* Jan;66(1):81-7, 1991.

Milner P. A model for visual shape recognition. *Psychol. Rev.,* 81: 521-535, 1974.

Murphy VN and Fetz EE. Oscillatory activity in sensorimotor cortex of awake monkeys: synchronization of local field potentials and relation to behavior, *J. Neurophysiol.* 76, pp. 3949–3967, 1996.

Nelson JI, Salin PA, Munk MH, Arzi M, and Bullier J. Spatial and temporal coherence in cortico-cortical connections: a cross-correlation study in areas 17 and 18 in the cat. *Vis Neurosci.* Jul;9(1):21-37, 1992.

Neuenschwander S and Singer W. Long-range synchronization of oscillatory light responses in the cat retina and lateral geniculate nucleus. *Nature.* Feb 22;379(6567):728-32, 1996.

Neuenschwander S and Varela FJ. Visually triggered neuronal oscillations in the pigeon: an autocorrelation study of tectal activity. *Eur J Neurosci.* Jul 1;5(7):870-81, 1993.

Niedermeyer E, Epileptic Seizure Disorders. In: E. Niedermeyer and F. Lopes Da Silva, Editors, *Electroencephalography: Basic Principles, Clinical Applications, And Related Fields* (Fifth Edition), Lippincott Williams and Wilkins, Philadelphia, pp. 505–621, 2005.

Podvigin NF, Jokeit H, Pöppel E, Chizh AN, and Kiselyeva NB. Stimulus-dependent oscillatory activity in the lateral geniculate body of the cat. *Naturwissenschaften.* Sep;79(9):428-31, 1992.

Pöppel E and Logothetis N. Neuronal oscillations in the human brain. Discontinuous initiations of pursuit eye movements indicate a 30-Hz temporal framework for visual information processing. *Naturwissenschaften.* May;73(5):267-8, 1986.

Raether A, Gray CM, and Singer W. Intercolumnar interactions of oscillatory neuronal responses in the visual cortex of alert cats. *Eur Neurosci Assoc.* 12:72.5, 1989.

Ramachandran VS. The neurobiology of perception. *Perception.*14(2):97-103, 1985.

Ramsden DB. Themed issue: neurodegenerative diseases. *Mol Pathol.* Dec;54(6):361, 2001.

Ringach DL and Shapley R. Spatial and temporal properties of illusory contours and amodal boundary completion. *Vision Res.* Oct;36(19):3037-50, 1996.

Rock I and Anson R. Illusory contours as the solution to a problem. *Perception.* 8(6):665-81, 1979.

Roelfsema PR, Engel AK, Konig P, and Singer W. Visuomotor integration is associated with zero time-lag synchronisation among cortical areas, *Nature* 385, pp. 157–161, 1997.

Roncato S and Casco C. Illusory boundary interpolation from local association field. *Spat Vis.*19(6):581-603, 2006.

Samonds JM, Zhou Z, Bernard MR, and Bonds AB. Synchronous Activity in Cat Visual Cortex Encodes Collinear and Cocircular Contours. *J. Neurophysiol.* 95:2602-2616, 2006.

Schnitzler A and Gross J. Normal and pathological oscillatory communication in the brain, *Nat. Rev. Neurosci.* 6 pp. 285–296, 2005.

Schwarz C and Bolz J. Functional specificity of a long-range horizontal connection in cat visual cortex: a cross correlation study. *J Neurosci.* Oct;11(10):2995-3007, 1991.

Sillito AM, Jones HE, Gerstein GL, and West DC. Feature-linked synchronization of thalamic relay cell firing induced by feedback from the visual cortex. *Nature*. Jun 9;369(6480):479-82, 1994.

Singer W. Neuronal synchrony: A versatile code of the definition of relations?, *Neuron* 24, pp. 49–65, 1999;

Singer W and Gray CM. Visual feature integration and the temporal correlation hypothesis. *Annu. Rev. Neurosci.*, 18:555-586, 1995.

Smith AT and Over R. Motion aftereffect with subjective contours. *Percept Psychophys*. Feb;25(2):95-8, 1979.

Smith A and Over R. Tilt aftereffects with subjective contours. *Nature.* Oct 16;257(5527):581-2, 1975.

Spencer KM, Nestor PG, Niznikiewicz MA, Salisbury DF, Shenton ME and McCarley RW. Abnormal neural synchrony in schizophrenia, *J. Neurosci.* 23, pp. 7407–7411, 2003.

Stam CJ, van der Made Y, Pijnenburg YA, and Scheltens P. EEG synchronization in mild cognitive impairment and Alzheimer's disease, *Acta Neurol. Scand.* 108, pp. 90–96, 2003.

Stam CJ, Montez T, Jones BF, Rombouts SA, van der Made Y, Pijnenburg YA, and Scheltens P. Disturbed fluctuations of resting state EEG synchronization in Alzheimer's disease, *Clin. Neurophysiol.* 116, pp. 708–715, 2005.

Stam CJ, Jones BF, Nolte G, Breakspear M, and Scheltens P. Small-world networks and functional connectivity in Alzheimer's disease, *Cereb. Cortex* in press, 2006.

Uhlhaas PJ and Singer W. Neural synchrony in brain disorders: relevance for cognitive dysfunctions and pathophysiology. *Neuron.* Oct 5;52(1):155-68, 2006.

Vaadia E, Haalman I, Abeles M, Bergman H, Prut Y, Slovin H, and Aertsen A. Dynamics of neuronal interactions in monkey cortex in relation to behavioural events. *Nature.* Feb 9;373(6514):515-8, 1995.

Vogels R and Orban GA. Illusory contour orientation discrimination. *Vision Res.*27(3):453-67, 1987.

von der Heydt R and Peterhans E. Mechanisms of contour perception in monkey visual cortex. I. Lines of pattern discontinuity. *J Neurosci.* May;9(5):1731-48, 1989.

von der Malsburg C. The correlation theory of brain function. *Internal Report, Max-Planck Institute for Biophysical Chemistry.* Goettingen, Germany, 1981.

von Grünau MW. The involvement of illusory contours in stroboscopic motion. *Percept Psychophys.* Mar;25(3):205-8, 1979.

Wallach H and Slaughter V. The role of memory in perceiving subjective contours. *Percept Psychophys*. Feb;43(2):101-6, 1988.

Weisstein N, Maguire W, and Berbaum K. A phantom-motion aftereffect. *Science*. Dec 2;198(4320):955-8, 1977.